The Gran Sasso National Laboratory

The Gran Sasso National Laboratory (LNGS) is the largest underground laboratory in the world for experiments in particle and astroparticle physics. It is one of four INFN national laboratories and it is used as a worldwide facility by scientists (presently 900 in number) from 24 countries.

Its location is near the town of L'Aquila, about 120 km from Rome. The underground facilities are located on a side of the ten kilometres long freeway tunnel crossing the Gran Sasso Mountain. They consist of three large experimental halls, each about 100 m long, 20 m wide and 15 m high and service tunnels for a total volume of about 180,000 cubic metres.

The average 1400 m rock coverage gives a reduction factor of one million in the cosmic ray flux; moreover, the neutron flux is thousand times less than on the surface, thanks to the smallness of the Uranium and Thorium content of the dolomite rocks of the mountain.

The headquarters and the support facilities including the general electric and safety service, library and meeting halls, canteen, computing and networking services, mechanical, electronic and chemical shops, low radioactivity service, assembly halls, offices and administration department are located on the surface.

The mission of the Laboratory is to host experiments that require a low background environment in the field of astroparticle physics and nuclear astrophysics and other disciplines that can profit of its characteristics and of its infrastructures.

The geographical location (inside the National Park of Gran Sasso - Monti della Laga) and the special operating conditions (underground, near a highway tunnel and in close proximity to a large water basin) demand that special attention is paid to the safety and environmental aspects of the activities.

Main research topics of the present scientific programme are: neutrino physics with neutrinos naturally produced in the Sun and in Supernova explosion and neutrino oscillations with a beam from CERN (CNGS program), search for neutrino mass in neutrinoless double beta decays, dark matter search, nuclear reactions of astrophysical interest.

The year 2006 has seen the end of the heavy safety works by the Government Commissioner. Thanks to a strong inter-coordination effort of the Commissioner’s and the Laboratory staff the unavoidable problems and delays were minimized.

The 2006 scientific activity was characterized by arrival of the first neutrino beam from CERN. Let us summarize the activity of the main research lines.

Solar neutrino physics is one of the traditional research sectors of the laboratory. After the glorious life of GALLEX and GNO, the focus is now on Borexino, which is dedicated mainly to the measurement of the Be line component of the solar neutrino spectrum. The experiment has been successfully completed and is now ready for the data taking.

The solar models are based on data and extrapolations; in particular the thermonuclear cross sections of the involved reactions are not measured in the relevant energy range but rather extrapolated from higher energies. The direct measurements are made very difficult by the very low values of the cross sections. Using the new 400 kV accelerator, LUNA continued its activity for the measurements of the cross section of nuclear reaction of astrophysical interest.

The detection of low energy neutrinos from the gravitational collapse of galactic objects is the major purpose of the LVD (Large Volume Detector) experiment. The experiment is

continuosly monitoring the galaxies with its 1000 tons of liquid scintillator and was able to detect the first events induced by the CNGS neutrino beam.

LVD participates to the Supernovae Early Warning System of detectors.

Elementary particles are different from their antiparticles because their charges - not only the electric one, but all of them - are opposite. The standard model assumes that neutrinos have only one charge, the lepton number. But, if this charge is not conserved, neutrinos and antineutrinos can be two states of the same particle. In this case well-specified nuclides would decay through the neutrino-less double beta channel. The Laboratory hosts today experiments searching for these very rare decays, employing different and complementary techniques, and is preparing new important activities.

CUORICINO, which employs TeO_2 bolometers for a total of 42 kg and started taking data data in 2003, has continuously operated in 2006. It is the most sensitive running experiment today.

In this field the Laboratory approved two new experiments representing the state of the art: CUORE, which brings the CUORICINO technique to a mass of more than 400 kg of TeO_2 bolometers, and GERDA planning to employ 500 kg of enriched ^{76}Ge. The preparatory works for the installation of these experiments is in progress.

From astronomical observations, we know that most of the matter in the Universe is not made of nuclei and electrons as normal matter. It is called dark matter, because it does not emit light, and its nature is unknown. Probably, its constituents, elementary particles that interact only very weakly with the rest (they are called WIMPs,) have not been discovered yet; they are around us, invisible, waiting to be discovered. The search for WIMPs is very difficult and requires a very low background environment and the development of advanced background reduction techniques. The search is going on in many experiments worldwide. At Gran Sasso several experiments, using different techniques, are active and new experiments have been approved and started operating in 2005.

DAMA/LIBRA employs NaI crystals to detect the WIMPs by means of the flash of light produced in the detector by a Iodine nucleus recoiling after having been hit by a WIMP, a very rare phenomenon. To distinguish these events from the background, DAMA searches for an annual modulation of the rate, a behaviour that has several aspects that are peculiar of the searched effect and not of the main backgrounds. With its about 100 kg sensitive mass DAMA was the only experiment world wide sensitive to the annual modulation signature. After the conclusion of the experiment, results were published confirming a signal of annual modulation.

The larger experiment LIBRA, with 250 kg sensitive mass, continued regularly to take data along all the year.

CRESST searches for WIMPs with a cryogenic technique, looking for a very tiny temperature increase in the detector, due to the energy deposited by nuclei hit by the WIMPs. Activity of the new CRESST2 $CaWO_2$ detector has continued.

Two new dark matter experiments, WARP and XENON are preparing their activity underground. They are based on the simultaneous detection of the ionization and scintillation signals in, respectively, liquid argon and liquid xenon. WARP and XENON performed interesting measurements underground with a 2.3 l and a 10 l prototype, respectively.

One of the major committments of the Gran Sasso laboratory in the next five years will be the search of τ neutrino appearance on the artificial μ neutrino beam being built at CERN in Geneva,

the CERN Neutrinos to Gran Sasso (CNGS) project. The beam, directed through the Earth crust to Gran Sasso at 732 km distance, was ready in the summer of 2006.

The OPERA experiment is designed for the direct observation of τ neutrinos resulting from oscillations of the μ neutrino of the beam. This search requires both micrometer scale resolution, obtained with modern emulsion techniques and large sensitive mass (1800 t) obtained with 200 000 bricks cosisting in Pb sheets interleaved by emulsion layers. In 2006 the installation in Hall C has continued regularly, as well as the start of the realization of the bricks with the brick assembly machine. The first events induced by the CNGS neutrino beam were detected by OPERA with its RPC and scintillator detectors.

ICARUS is a general-purpose detector, with a broad physics programme, based on the novel concept of the liquid Argon time-projection chamber. The 600 ton module was transported from Pavia to our underground Laboratory in december 2004. During 2006 the construction of the new insulation panel by Air Liquide and the preparation of the Hall B infrastructure have continued.

The main activity of the theory group, staff and visitor scientists, has been focused on astroparticle physics, including solar and Supernova neutrinos, massive neutrinos, ultra high energy cosmic rays, topological defects and relativistic astrophysics. Important activity took place also in particle phenomenology and computer simulations of Lattice Field Theories.

The Gran Sasso laboratory is recognized by Europe as a large scientific infrastructure. An EU contract is involving LNGS as one of the leader paricipants in the Integrated Infrastructure Initiative (I3) called ILIAS within Framework Program 6 (contract RII3-CT-2003-505818).

The main goal of ILIAS (Integrated Large Infrastructures for Astroparticle Physics) is to pull together all of Europe's leading infrastructures in Astroparticle Physics to produce a focused, coherent and integrated project to improve the existing infrastructures and their operation as well as to organise and structure the scientific community to prepare the best infrastructures for the future.

Gran Sasso, July 3 2007

The Director of the Laboratory
Prof. Eugenio Coccia

BOREXINO. Solar Neutrino Physics

H. Back[n], M. Balata[b], G. Bellini[a], J. Benziger[c], S. Bonetti[a], B. Caccianiga[a], F.P. Calaprice[d], D. D'Angelo[h], A. de Bellefono, H. de Kerret[o], A. Derbin[m], A. Etenko[s], R. Ford[b], D. Franco[a], C. Galbiati[d], S. Gazzana[b], M.G. Giammarchi[a], A. Goretti[a], C. Grieb[n], E. Harding[d], G. Heusser[j], A. Ianni,[d], A.M. Ianni[c], G. Korga[a], Y. Kozlov[s], D. Kryn[o], M. Laubenstein[b], C. Lendvai[h], M. Leung[d], E. Litvinovich[s], P. Lombardi[a], I. Machulin[s], D. Manuzio[i], G. Manuzio[i], F. Masetti[g], U. Mazzucato[g], K. McCarty[d], E. Meroni[a], L. Miramonti[a], V. Muratova[m], L. Niedermeier[h], L. Oberauer[h], M. Obolensky[o], F. Ortica[g], M. Pallavicini[i], L. Papp[a], L. Perasso[i], R.S. Raghavan[l], G. Ranucci[a], A. Razeto[i], A. Sabelnikov[s], C. Salvo[i], S. Schönert[j], T. Shutt[d], H. Simgen[j], M. Skorokhvatov[s], O. Smirnov[m], A. Sotnikov[m], S. Sukhotin[s], Y. Suvorov[s], V. Tarasenkov[s], R. Tartaglia,[b], G. Testera[i], D. Vignaud[o], B. Vogelaar[n], F. von Feilitzsch[h], V. Vyrodov[s], W. Wojcik[q], O. Zaimidoroga[m], G. Zuzel[q]

[a]Dip. di Fisica dell'Università and Infn Milano - Italy
[b]Laboratori Nazionali del Gras Sasso, Assergi (Aq) - Italy
[c]Dept. of Chemical Engineering, Princeton University - NJ USA
[d]Dept. of Physics, Princeton University - NJ USA
[e]Dip. di Fisica dell'Università and Infn Pavia - Italy
[f]Dept. of Physics, Massachusetts Institute of Technology - MA USA
[g]Dip. di Chimica dell'Università and Infn Perugia - Italy
[h]Technische Universität München - Germany
[i]Dip. di Fisica dell'Università and Infn Genova - Italy
[j]Max Planck Inst. für Kernphysik, Heidelberg - Germany
[l]Bell Laboratories, Lucent Technologies, Murray Hill - NJ USA
[m]J.I.N.R. Dubna - Russia
[n]Dept. of Physics, Virginia Polytechnic Institute - VA USA
[o]Laboratoire de Physique Corpusculaire et Cosmologie, Paris - France
[q]Institute of Physics, Jagellonian University, Kracov - Poland
[r]Dept. of Physics, Queen's University, Ontario - Canada
[s]RRC Kurchatov Institute, Moscow - Russia

Abstract

Borexino is a solar neutrino detector in start-up phase in Hall C of LNGS. We summarize here the status of the project and the main technical achievements obtained in these years of development.

1 Introduction

Borexino is a real time experiment to study low energy (sub-MeV) solar neutrinos. The main experimental goal is the detection of the 0.862 MeV ^{7}Be solar neutrino line through

the neutrino-electron elastic scattering reaction. The maximum energy of the recoiling electron is 664 KeV and the experimental design threshold will be at 250 keV. The detection reaction will be observed in a large mass (100 tons fiducial volume) of well shielded liquid scintillator.
The main problem of a real time experiment with such a low energy threshold is the natural radioactivity which is present in any environment and in any material. For these reasons an intense R&D program has been carried out in the last ten years to develop methods for selecting low radioactivity materials and/or purify them. An effort in this field has to be complemented by a comparably thorough research in the field of detection and measurement of very low radioactivity levels.
The development of purification methods has been focused on the costituents of the liquid scintillator. Four main methods have been developed: distillation, water extraction, stripping with ultrapure N_2, solid gel column (Si gel, Al gel) adsorption. Significant results have been achieved by the Collaboration as for example: $10^{-16} - 10^{-17}$ (g of contaminants/g of material) for ^{232}Th and ^{238}U family and a few microBq of Rn-222 sensitivity in gases and liquids.
In addition the organic solvent selected by the collaboration has been shown to have a ^{14}C presence not exceeding 10^{-18} in its ratio to ^{12}C. This impurity is particularly important because it cannot be removed by chemical purification methods.
For the measurements of these ultralow radioactivity levels, dedicated methods were developed. In addition to small-scale techniques (Ge underground detectors installed in Rn free environment, Inductively Coupled Plasma Mass Spectometer, high sensitivity Neutron Activation, Atomic Absortion Spectroscopy etc...), a Counting Test Facility (CTF), has been constructed on purpose and operated in the Hall C of LNGS. The Counting Test Facility features 4 tonnes of liquid scintillator viewed by 100 photomultipliers and shielded by 1000 tons of ultrapure water.
The sensitivities reached are summarized below and correspond to the lowest radioactivity levels obtained by the Borexino Collaboration, in preparation of the experiment:

- Bulk material radiopurities of 10^{-10} g/g for ^{238}U and ^{232}Th, $\sim 10^{-5}$ for ^{nat}K, few tenths of mBq/kg for ^{60}Co, have been measured with Ge detectors in construction materials such as stainless steel, photomultipliers, metal and plastic gaskets, products for PMT sealing, piping, filters...
- Radon emanations of 10 μBq/m^2 from plastic materials, 0.1 mBq/m^3 for Rn-222 and 1 mBq/m^3 for Ra-226 in water, 1 mBq/m^3 for the N_2 used for scintillator stripping.
- Radiopurity levels of a few times 10^{-15} g/g ^{238}U, ^{232}Th and ^{40}K have been reached with ICMPS in measuring the Borexino shielding water.
- few ppt for ^{238}U and ^{232}Th have been obtained in Nylon bulk measurements.
- The radiopurity of the scintillator itself was measured to be at the level of few 10^{-16} g/g for ^{238}U, ^{232}Th and $\sim 10^{-18}$ for ^{14}C/^{12}C in the Counting Test Facility.
- Bulk radiopurity levels of $10^{-13} - 10^{-14}$ g/g for Au, Ba, Ce, Co, Cr, Cs, Ga, Hg, In, Mo, Rb; less than few 10^{-15} g/g for Cd, Sb, Ta, W; $10^{-16} - 10^{-17}$ g/g for La, Lu, Re, Sc, Th; less than 1x10^{-17} g/g for U, have been reached by mean of Neutron Activation followed by β-γ coincidence analysis selection applied to the scintillator.
- Kr and Ar contamination in nitrogen at 0.005 ppm (for Ar) and 0.06 ppt (for Kr) were

obtained and measured with noble gas mass spectrometry.

These results were a milestone in the development of the Borexino detector and technique. Several of these concepts were incorporated in the construction of the high purity systems for the treatment of the most critical liquid, the scintillator of the experiment.

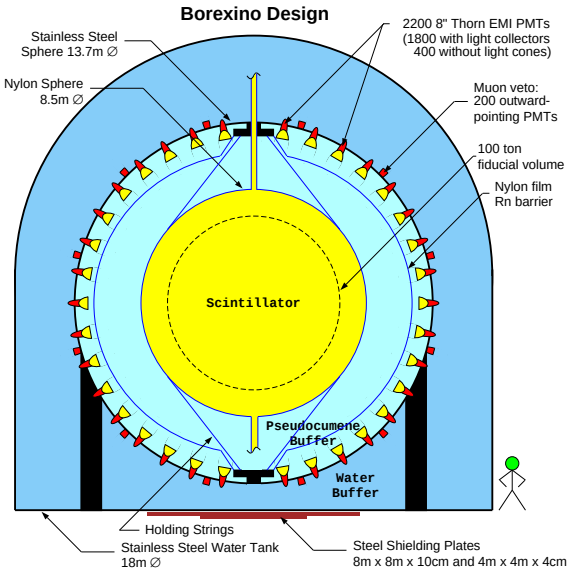

Figure 1: Schematic view of the Borexino detector.

2 The Borexino Detector

Borexino is an unsegmented scintillation detector featuring 300 tonnes of well shielded liquid ultrapure scintillator viewed by 2200 photomultipliers (fig. 1). The detector core is a transparent spherical vessel (Nylon Sphere, 100μm thick), 8.5 m of diameter, filled with 300 tonnes of liquid scintillator and surrounded by 1000 tonnes of high-purity buffer liquid. The scintillator mixture is PC and PPO (1.5 g/l) as a fluor, while the buffer liquid will be PC alone (with the addition of DMP as light quencher). The photomultipliers are supported by a Stainless Steel Sphere, which also separates the inner part of the detector from the external shielding, provided by 2400 tonnes of pure water (water buffer).
An additional containment vessel (Nylon film Radon barrier) is interposed between the Scintillator Nylon Sphere and the photomultipliers, with the goal of reducing Radon diffusion towards the internal part of the detector.
The outer water shield is instrumented with 200 outward-pointing photomultipliers serving as a veto for penetrating muons, the only significant remaining cosmic ray background at the Gran Sasso depth (about 3500 meters of water equivalent). The innermost 2200 photomultipliers are divided into a set of 1800 photomultipliers equipped with light cones (so that they see light only from the Nylon Sphere region) and a set of 400 PMT's without

light cones, sensitive to light originated in the whole Stainless Steel Sphere volume. This design greatly increases the capability of the system to identify muons crossing the PC buffer (and not the scintillator).
The BOREXINO design is based on the concept of a graded shield of progressively lower intrinsic radioactivity as one approaches the sensitive volume of the detector; this culminates in the use of 200 tonnes of the low background scintillator to shield the 100 tonnes innermost Fiducial Volume. In these conditions, the ultimate background will be dominated by the intrinsic contamination of the scintillator, while all backgrounds from the construction materials and external shieldings will be negligible.
BOREXINO also features several external systems and conceived to purify the experimental fluids (water, nitrogen and scintillator) used by the experiment.

3 Status of the project

The Borexino detector and the associated purification and ancillary plants are completed. The whole system is now in filling phase and the detector will be fully operational by June 2007.
While filling is taking place, the CTF is taking data to complete tests on purification strategies to be used in the experiment.

4 Borexino and Neutrino Physics

Borexino will be studying solar neutrino physics below the 1 MeV threshold, where the Large Mixing Angle suppression pattern becomes vacuum dominated. This is in contrast with the "matter dominated" situation of the B-8 neutrinos, the only component observed in real-time up to now.
The expected Be-7 solar neutrino rates is close to 30 counts/day. With a sizeable number of real-time expected events, Borexino can also study several time-dependences of the solar neutrino signal, including day-night and seasonal variations.
Finally, a 10% accuracy measurement of the Be-7 line will be of great relevance when compared to solar model predictions.

Other physics topics can be investigated with high sensitivity with the Borexino detector, such as Supernova neutrinos, neutrino magnetic moment, terrestrial neutrinos and other rare events.

5 List of articles published in year 2006

1. M. Balata et al., *Search for electron antineutrino interactions with the Borexino Counting Test Facility at Gran Sasso.* European Physical Journal C, 47 (2006) 21.

2. H. Back et al., *CNO and pep neutrino spectroscopy in Borexino: Measurement of the deep underground production of cosmogenic* ^{11}C *in an organic liquid scintillator.*

Physical Review C, 74 (2006) 045805.

References

[1] G. Alimonti et al., *Science and technology of Borexino: a real-time detector for low energy solar neutrinos*, Astroparticle Physics 16 (2002) 205.

[2] C. Arpesella et al., *Measurements of extremely low radioactivity levels in BOREXINO*, Astroparticle Physics 18 (2002) 1.

COBRA

University of Sussex: J.V. Dawson, C. Reeve, J.R. Wilson, K. Zuber*
Universität Dortmund: D. Dobos, C. Gößling, H. Kiel, D. Münstermann, S. Oehl
University of Warwick: P.F. Harrison, B. Morgan, Y. Ramachers, D. Stewart
University of Liverpool : A. Boston, P. Nolan, S. Rigby
University of Birmingham: T. Bloxham, M. Freer
University of York: S.P. Fox, B. Fulton, J. McGrath, R. Wadsworth
Laboratori Nazionali del Gran Sasso : M. Junker
University of Bratislava: F. Simkovic
University of Washington in St. Louis: I. Jung, H. Krawczynski
(* Spokesperson)

Abstract

The aim of COBRA is to search for neutrino-less double beta decay events in a large array of Cadmium Zinc Telluride (CZT) semiconductor detectors. As a semiconductor, CZT offers the low radioactivity levels and good energy resolution required for a rare decay search, with the added advantage that it can be operated at room temperature. It contains a number of double beta decay candidates, the most promising of which is ^{116}Cd, which has a high Q-value (2.8 MeV) above many of the possible background contributions from natural radioactivity. Currently, a prototype apparatus is being established in LNGS to investigate the major experimental issues of operating CZT detectors in low background mode, whilst additional studies into the detector technology are proceeding in surface laboratories.

1 Introduction

Over the last 10 years various neutrino experiments have proved that neutrinos oscillate between flavour states and therefore have a non-vanishing rest mass. However, as neutrino oscillation experiments probe the difference between neutrino mass states, the absolute mass scale is still unknown. Another important unknown is the fundamental nature of the neutrino which could be either Dirac or Majorana. A golden channel for answering both the question of neutrino nature and neutrino mass is neutrinoless double beta decay. The COBRA experiment aims to provide answers to these fundamental questions by searching for these rare decays of ^{116}Cd isotopes in a large array of Cadmium Zinc Telluride (CZT) semiconductor detectors.

1.1 Neutrinoless Double Beta Decay

Double beta decay ($2\nu\beta\beta$), as expressed in equation 1, is a rare process that is allowed as a second order process in the Standard Model of particle physics for 35 known nuclei that cannot decay via single beta-decay.

$$(Z, A) \rightarrow (Z + 2, A) + 2e^{-} + 2\bar{\nu}_e \qquad (2\nu\beta\beta\text{-decay}) \tag{1}$$

In neutrinoless double beta decay ($0\nu\beta\beta$), as expressed in equation 2, no neutrinos are emitted so lepton number conservation is violated by 2 units and the two electrons carry away the entire Q-value of the decay.

$$(Z, A) \rightarrow (Z + 2, A) + 2e^- \qquad (0\nu\beta\beta\text{−decay}) \tag{2}$$

The rate of this process is related to the Majorana neutrino mass through a phase space factor and a nuclear matrix element.

The largest mass difference measured in neutrino oscillations suggests that the neutrino mass could be of the order $\sim 50\,\text{meV}$. A number of experiments searching for $0\nu\beta\beta$ have not observed the predicted signals, resulting in upper limits on the neutrino mass of order 0.2–0.5 eV. In 2002 observational evidence for $0\nu\beta\beta$–decay of ^{76}Ge[16] ,which infers a neutrino mass of 0.2–0.6 eV, was published (and confirmed in 2006[17]) but resulted in much debate in the field. Further searches for this decay are planned with large scale experiments and exploration of other isotopes is vital to rule out any unconsidered Ge-specific backgrounds and will give more information on the absolute neutrino mass scale since conversion from half-life to neutrino mass depends on nuclear matrix element calculations which are subject to a high degree of uncertainty. COBRA will provide the isotope ^{116}Cd for this study.

1.2 Other Physics Mechanisms

The Schechter-Valle theorem will guarantee that there is a massive Majorana neutrino if $0\nu\beta\beta$–decay occurs, however, there are several other physics processes which could be involved. The relative contributions of these different physics processes must be understood in order to derive the absolute neutrino mass value from the rate of $0\nu\beta\beta$–decay. Other mechanisms that would realise zero neutrino double beta decay include right handed weak currents and R-parity violating supersymmetry. Right handed currents play a more important role in $\beta^+\beta^+$-decays where two positrons are emitted from the same nuclei.

$$(Z, A) \rightarrow (Z - 2, A) + 2e^+ \ (+2\nu_e) \qquad (\beta^+\beta^+) \tag{3}$$

$$e_B^- + (Z, A) \rightarrow (Z - 2, A) + e^+ \ (+2\nu_e) \qquad (\beta^+/\text{EC}) \tag{4}$$

$$2e_B^- + (Z, A) \rightarrow (Z - 2, A) \ (+2\nu_e) \qquad (\text{EC/EC}) \tag{5}$$

This mode is always accompanied by EC/EC or β^+/EC-decay (equations 3–5). The Coulomb-barrier causes a reduction of the Q-value by $2m_ec^2$ for each produced positron, the rate for $\beta^+\beta^+$ is therefore small and energetically only possible for six nuclides. As has been shown in Ref. [14] β^+/EC decays have an enhanced sensitivity to right handed weak currents hence their measurement, alongside $\beta^-\beta^-$ decays will help to probe the underlying physics mechanism. Experiments with tracking capabilities will also be able to measure individual β energies and the angle between them which may help to distinguish between different physics processes.

CZT also contains 4 isotopes that can undergo $\beta^+\beta^+$ and electron capture decays. ^{106}Cd is particularly interesting with a Q-value of 2771 keV that allows it to emit two β^+s.

With the modular array, and even better with a pixellated array, COBRA will be able to study these interesting decay modes, which produce events with distinct characteristics, and could help to interpret the underlying physics mechanism.

2 COBRA

The idea of COBRA is to use a large quantity of CdZnTe (CZT) semiconductor material which contains a number of isotopes that can undergo double beta decay[25]. The main focus will be on ^{116}Cd and ^{130}Te, which are well suited for a double beta search due to their high Q-values (2805 and 2529 keV respectively). Calculations show that the theoretical rates of $0\nu\beta\beta$–decay for ^{116}Cd and ^{130}Te are favourably high.

COBRA follows the strategy that source and detector are identical, a method proven to be successful in various other double beta decay approaches. As a semiconductor, CZT crystals can be produced with good energy resolution and low levels of intrinsic radioactivity. Due to a large bandgap the detectors can be operated at room temperature avoiding extensive cooling operations.

A large scale version of COBRA would aim for a total of $40\times40\times40$ 1 cm^3 detectors, enriched to 90 % in ^{116}Cd. This would result in 420 kg of CZT detectors to achieve a neutrino mass sensitivity of 50 meV and below. The predicted half-life sensitivity is shown in Fig. 1 for three different scenarios. To obtain sensitivity to $T_{1/2} = 10^{26}$ y in 5 years of operation, a resolution of $\Delta E < 2\%$ (FWHM), and a background rate in the signal region of < 0.001 counts/keV/kg/year are required.

The modular design allows for easy extension and direct access to separate detector regions and is also advantageous for physics analysis. Simulations have shown that the background contribution from naturally occurring radioactivity in and around the crystals can be reduced significantly by selecting only single-crystal events since high energy photons are more likely to deposit energy in multiple detectors than double beta events. Further reductions in background can be achieved if the individual crystals are pixellated, giving the detector tracking capabilities. This will provide additional information to discriminate between alpha, beta and gamma interactions in the crystals, and allows positive identification of double beta events.

3 R&D Activities

The experiment is currently in an R&D phase, operating a proto-type low-background apparatus in the LNGS laboratory in order to investigate the instrumentation and background issues critical to the rare decay search. Studies into detector properties are being performed simultaneously at a number of member institutions. Details of the experimental set-up and recent progress are given in this section.

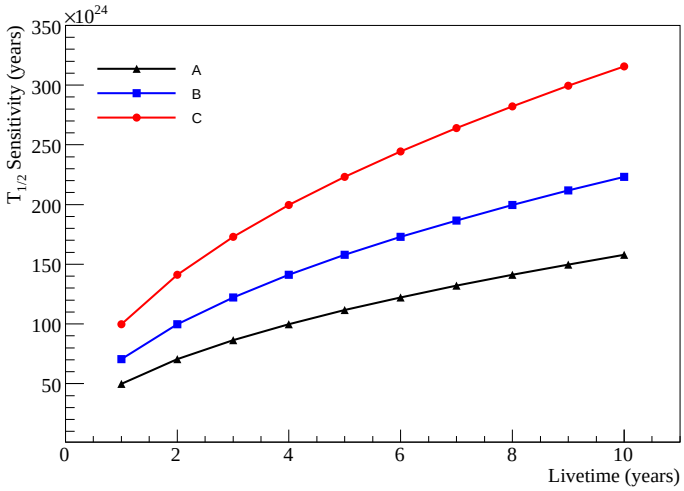

Figure 1: The expected half-life sensitivity for $0\nu\beta\beta$–decay of ^{116}Cd in an array of 64,000 1 cm^3 detectors, enriched to 90% in ^{116}Cd for three scenarios: A $= 10^{-3}$ background counts/keV/kg/year, $\Delta E = 2\%$ at 2.8 MeV. B $= 10^{-3}$ background counts/keV/kg/year, $\Delta E = 1\%$ at 2.8 MeV. C $= 5 \times 10^{-4}$ background counts/keV/kg/year, $\Delta E = 1\%$ at 2.8 MeV.

3.1 Low Background Proto-type

A proto-type COBRA detector, consisting of 64 1 cm^3 CZT crystals is being installed in LNGS. This small array will provide valuable information on the background levels of various components of the set-up and will be used to test methods of instrumentation and construction that would also be applicable to a larger array.

The crystals currently used in the low background experiment are 1 cm×1 cm×1 cm CZT semiconductor detectors, each of mass ∼6.5 g, provided by eV-PRODUCTS. They utilise coplanar grid technology to ensure that only the electron signal is read out [19] and hence symmetric energy peaks are obtained.

The detectors are mounted in four 4×4 layers, held in a Delrin support. The first layer of detectors is shown in Fig. 2. The four holders are mounted in a copper casing (Fig. 2), surrounded by 10 cm of pure copper shielding and 20 cm of low radioactivity lead. Supply of bias voltages, and signal readout occurs via copper traces on kapton foils which feed through this shielding. The custom built preamplifier electronics are ∼25 cm from the crystals. This apparatus is all mounted inside a copper Faraday cage, surrounded by 5 cm of polypropylene and 20 cm of borated paraffin to shield the apparatus from neutrons. Location in the Gran Sasso laboratory provides a further ∼3500 mwe of shielding against cosmic ray sources.

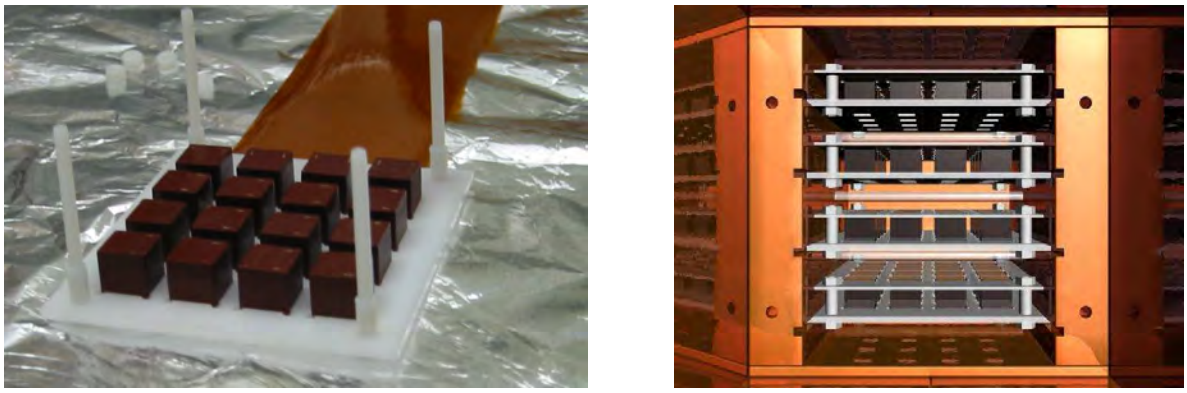

Figure 2: A photograph of the first layer of the 64-crystal proto-type (left) and an engineering model of the whole array in the copper mounting structure (right).

3.1.1 Monitoring and Control

To allow for easy and regular calibration of the detectors, there are five teflon tubes which feed into the central copper casing. Wire mounted ^{22}Na, ^{232}Th and ^{57}Co sources can be fed down these tubes into the central detector cavity without opening the shielding structure.

The signals are processed by a VME-based data acquisition system with a number of custom-built, peak sensing, 4 channel, 14-bit ADC channels. In the past year, equipment has been installed to allow full remote control of the apparatus through the VME interface. A custom made 64-channel high voltage supply allows independent control and read-back of the voltage supplied to each crystal. In addition, a grid bias supply was designed and constructed so that the grid bias voltage for each crystal could be controlled in a similar fashion.

Initial data showed that the detectors were responding to environmental factors such as sound and vibrations in the laboratory and temperature and humidity variations. A series of monitoring tools were developed to monitor these factors which are now recorded in the data stream. This additional information can be used to understand and monitor the data quality and to veto spurious events in the detectors.

3.1.2 Background Studies

Prior to the installation of the 64 crystal array, a smaller proto-type consisting of just 4 crystals was installed inside the same shielding structure. All materials used in the underground apparatus were measured for contaminants in the LNGS Ge-detector facility. As a consequence of those measurements, the pertinax holders and lemo cables were replaced by delrin holders and kapton foils. A further upgrade was performed at a later date to replace an old CAMAC based data acquisition system with the VME-based system described in the previous section. The summed data from these separate periods are shown in Fig. 3. Period A comprises data from all 4 detectors and has slightly less events in the high energy regions as the background levels in detectors 3 and 4 are lower. Periods B and C only contain data from detector 1 but show less events at low energies due to

improvements in the cleanliness of mounting materials.

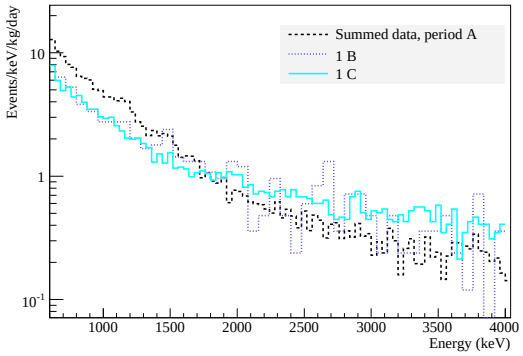

Figure 3: The prepared data sets from the 4-crystal prototype for the three data-collecting periods: A, B and C.

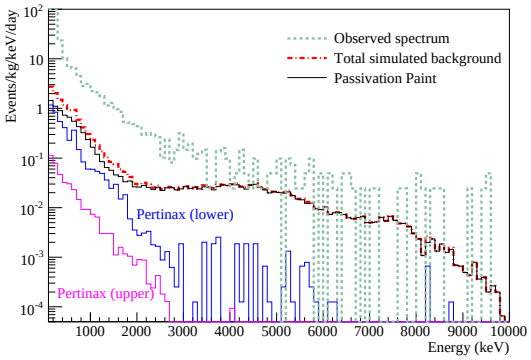

Figure 4: Measured spectrum for subset 4A, compared to simulated activities of the individual components.

No contamination of the CdZnTe could be detected with the Ge facility. With the known activities of contaminants in the individual components, extensive Monte Carlo modelling based on GEANT4 was performed to describe the observed spectrum (Fig. 4). This clearly shows that events from the passivation paint on the detector surfaces are a significant background contribution to the range of interest (2–3 MeV). The excess of events below 3 MeV is thought to be due to backgrounds associated with the lemo cables and solder.

The largest background in the 2–3 MeV region was found to evolve from a passivation paint on the detector surface. The precise prediction of this contribution varies slightly due to uncertainty in the paint mass and the inhomogeneous paint thickness, which affects the alpha-particle simulation in particular. However, there is a slight advantage associated with the contaminated paint as the detector effectively acts as a self-calibrating device. The installation of the VME system at the start of period C significantly increased the timing resolution achieved for event read-out (from $\sim$1 ms to $\leq 10\,\mu$s) permitting the observation of $\beta - \alpha$ coincidence events from ^{214}Bi. This isotope originates from the Th-decay chain, present in the passivation paint, and beta-decays with an endpoint of 3.3 MeV; the daughter isotope, ^{214}Po, alpha-decays with a half-life of 164.3 μs, releasing a 7.7 MeV α.

Fig. 5 shows the time difference between each pair of events satisfying selection criteria based on the timing and energy of the two events. The exponential fitted to this distribution represents a decay half-life of $T_{1/2} = 162 \pm 19\,\mu$s, which is in excellent agreement with the half-life of ^{214}Po, confirming that the source of these events is correctly identified. The rate of event pairs observed in the period C data-set was consistent with the measured activity of a paint sample. Furthermore, it shows that any possible dead layer at the detector surface is insignificant, otherwise the alpha-particles would not be detected.

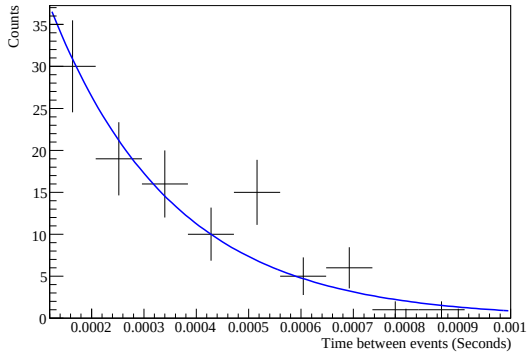

Figure 5: The time difference between pairs of events satisfying criteria for ^{214}Bi $\beta - \alpha$ coincidences.

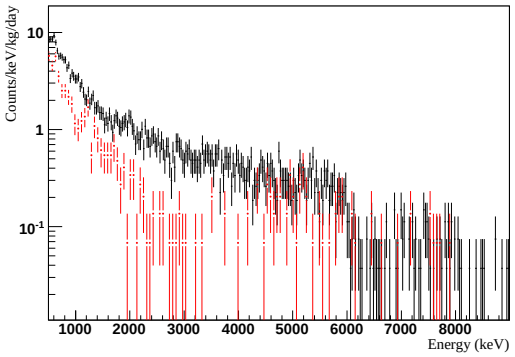

Figure 6: Data collected with a crystals with coloured passivation (black crosses) and colourless paint (red squares).

Having identified this dominant source of background events, an alternative passivation coating was sourced from eV-PRODUCTs. Four crystals with a colourless coating were installed into the low-background proto-type set-up[1]. Fig. 6 compares data collected with one of these new crystals to one with the original coloured passivation paint. In the region of interest for $0\nu\beta\beta$ searches (2–3 MeV) the reduction in events is a factor of ~ 10. This clearly shows that a major background has been correctly identified and work is now proceeding to source and test other passivation materials to further reduce this background contribution.

3.2 Analysis

A total of 3.82 kg·days of data were collected with the small 4-crystal proto-type detector, which were used to perform a number of physics analyses.

3.2.1 $\beta\beta$-Decay Half-life Limits

A search was performed for rare decays of all the double beta candidate isotopes in CdZnTe that produce peaks above 600 keV. A maximum likelihood analysis was used to determine the most likely number of signal and background events in the data sample, taking into account variations in background levels and resolution functions between the different crystals and data-collecting periods. An exponential parameterisation of the form,

$$y = A + B\exp(-C.x) \tag{6}$$

was selected to describe the background based on studies of the simulated background components.

[1]Installation of the second and subsequent layers of the 64-array proto-type were delayed in order to make this measurement.

The 90% upper confidence limit on half-life is derived from the fitted number of signal events, $\theta_s \pm \delta_s$:

$$T_{\rm half} \geq \frac{N_{\rm iso} \ln 2\epsilon}{\theta_s + 1.28\delta_s} \tag{7}$$

where $N_{\rm iso}$ is the number of candidate nuclei for the given decay per crystal and ϵ is the efficiency for observing the peak, as determined from Monte Carlo simulations of the decay in question. The factor 1.28 is for one-sided 90% confidence limits.

A limit calculated with equation 7 only includes the statistical uncertainty from the likelihood fit. A comprehensive review of possible systematic effects identified two dominant uncertainties. An uncertainty in the size of the active volume of each crystal could be as much as 10% and the zinc content in the CdZnTe material could vary between 7 and 11%.[2] Therefore, to account for these possible systematic effects the limiting parameters which give the least candidate isotopes for each decay were used in calculating the half-life limits.[3]

Where possible, each conceivable signal peak was fitted separately, however, in some cases the proximity of peak energies required multiple peaks to be treated together in the likelihood function. The fit performed for the 2.805 and 2.529 MeV peaks of ^{116}Cd and ^{130}Te respectively are shown in Fig. 7.

For each double beta fit performed, the fitted number of events was found to be consistent with zero. Therefore, the 90% C.L. upper limit on the number of signal events was used to calculate a minimum half-life for each decay process. The results with the dominant systematic uncertainties included are summarised in table 1. Note that new world-best limits are achieved for the decays of ^{64}Zn and ^{120}Te.

3.2.2 ^{113}Cd β Decay

In addition to the double beta decay search, the single beta decay of ^{113}Cd was studied. The transition ^{113}Cd $\rightarrow$ ^{113}In is characterised as a $1/2^+ \rightarrow 9/2^+$ transition. Hence it is a 4-fold forbidden non-unique decay ($\Delta I = 4$ and no change in parity). Only three isotopes of this type are known, ^{50}V, ^{113}Cd and ^{115}In. As shown in Fig. 8, ^{113}Cd spectra with an endpoint energy of about 320 keV can be seen consistently in all four detectors. The final data sample for this analysis comprised 0.86 kg·days due to the lower threshold requirements for this analysis.

The measurements of ^{113}Cd decay yielded a half-life of

$$T_{1/2} = (8.2 \pm 0.2({\rm stat.})^{+0.2}_{-1.0}({\rm sys.})) \times 10^{15}{\rm yrs} \tag{8}$$

which is in good agreement with the values quoted in [1, 10]. A comparison with the electron energy spectrum from the 'Table of Isotopes' web-page is shown in Fig. 8 with the spectra normalised to the total number of events in the range 100–320 keV. This spectral shape is clearly not supported by the data. For more details see Ref. [13].

[2] These are conservative limits provided by eV-PRODUCTS.

[3] Work is underway to measure both the zinc content and crystal active volumes more accurately in the near future.

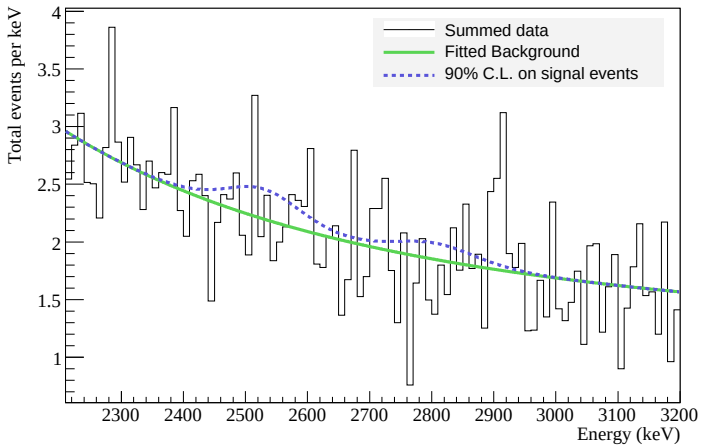

Figure 7: Data and fits, summed over all data sets, for fits to $\beta^-\beta^-$ decay of ^{116}Cd and ^{130}Te to the ground state.

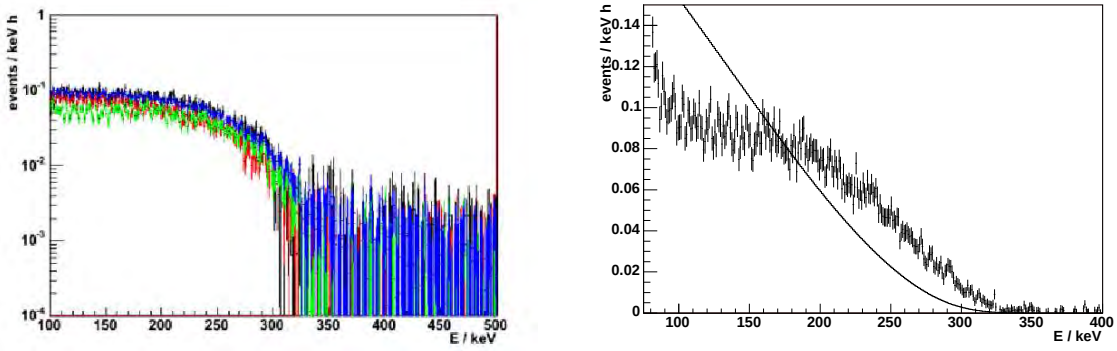

Figure 8: Left: Low energy range of all four CdZnTe detectors. As can be seen they all result in a consistent spectrum below 320 keV due to ^{113}Cd decay. Right: Measured energy spectrum of the summed detectors (histogram) compared to the expected shape from the Table of Isotope Web-page (line) indicating poor agreement. The spectra are normalised to the number of events between 100–320 keV.

3.3 COBRA Shielding Development

The design task of creating an efficient radiation shield for the new COBRA double-beta decay experiment led to a comprehensive study of commercially available shielding materials in order to find the most efficient combination under the constraints of an extreme low-background experiment. All existing shield configurations for this type of experiment have been found to perform sub-optimally[22].

CdZnTe detectors will be particularly sensitive to thermal neutron capture reactions on ^{113}Cd which produce γ-radiation in the relevant signal energy region. This study therefore focused first on this external background source.

Isotope	Decay	$T_{1/2}$ limit (years)	
		This work	World Best
$\beta^-\beta^-$ decays			
^{116}Cd	to g.s	3.14×10^{19}	1.7×10^{23} [11]
^{130}Te	to g.s	9.92×10^{19}	1.8×10^{24} [4]
^{130}Te	to 536 keV	3.73×10^{19}	9.7×10^{22} [2]
^{116}Cd	to 1294 keV	4.92×10^{18}	2.9×10^{22} [11]
^{116}Cd	to 1757 keV	9.13×10^{18}	1.4×10^{22} [11]
^{70}Zn	to g.s	2.24×10^{17}	9.0×10^{17} [12]
^{128}Te	to g.s	5.38×10^{19}	1.1×10^{23} [3]
^{116}Cd	to 2112 keV	1.08×10^{19}	6.0×10^{21} [11]
^{116}Cd	to 2225 keV	9.46×10^{18}	$1.0\times10^{20\dagger}$ [5]
$\beta^+\beta^+$ decays			
^{64}Zn	$0\nu\beta^+$EC to g.s.	2.78×10^{17}	2.4×10^{18} [12]
^{64}Zn	0νECEC to g.s.	$\mathbf{1.19\times10^{17}}$	7.0×10^{16} [12]
^{120}Te	$0\nu\beta^+$EC to g.s.	$\mathbf{1.21\times10^{17}}$	2.2×10^{16} [15]
^{120}Te	0νECEC to g.s.	$\mathbf{2.68\times10^{15}}$	-
^{120}Te	0νECEC to 1171keV	$\mathbf{9.72\times10^{15}}$	-
^{106}Cd	$0\nu\beta^+\beta^+$ to g.s.	4.50×10^{17}	2.4×10^{20} [7]
^{106}Cd	$0\nu\beta^+$EC to g.s.	7.31×10^{18}	3.7×10^{20} [7]
^{106}Cd	0νECEC to g.s.	5.70×10^{16}	1.5×10^{17} [20]
^{106}Cd	$0\nu\beta^+\beta^+$ to 512keV	1.81×10^{17}	1.6×10^{20} [7]
^{106}Cd	$0\nu\beta^+$EC to 512keV	9.86×10^{17}	2.6×10^{20} [7]

Table 1: Obtained 90% confidence limits with conservative systematic uncertainties applied, compared to the world best limits. New world best values from COBRA are shown in bold. †Quoted limit is 68% not 90%.

Several recent studies for underground experiments quantified design criteria for shielding, in particular neutron shielding was a target due to interest of new dark matter search experiments [21, 9, 24]. However, none of those aimed at a complete description including (n,γ)-reactions and shielding effects on the combined neutron and photon population.

For this study, commercially available shielding materials were selected. Most of them are specialised neutron shielding materials (the hydrocarbon class) but a few pure metals were also included. As a representation of typical neutron fluxes as a function of energy in a deep underground laboratory, the measured neutron flux from Gran Sasso was used[6] (see also the updated discussion about Gran Sasso neutron fluxes [23]).

The main tool for this research is computational dosimetry using Monte-Carlo codes. The results are based mainly on the MCNPX code package [18] and on VENOM, a GEANT4 based simulation code custom written for COBRA.

The total observable neutron number is not always the most important for experiments

interested in energy measurements. Nevertheless, it appears that studies focusing on total neutron number have served to define design criteria for shields so far. The flux energy dependence is at least as important as the number of counts and, in addition, build-up factors from neutron inelastic reactions either in terms of neutron multiplication or γ-production are other important factors to consider.

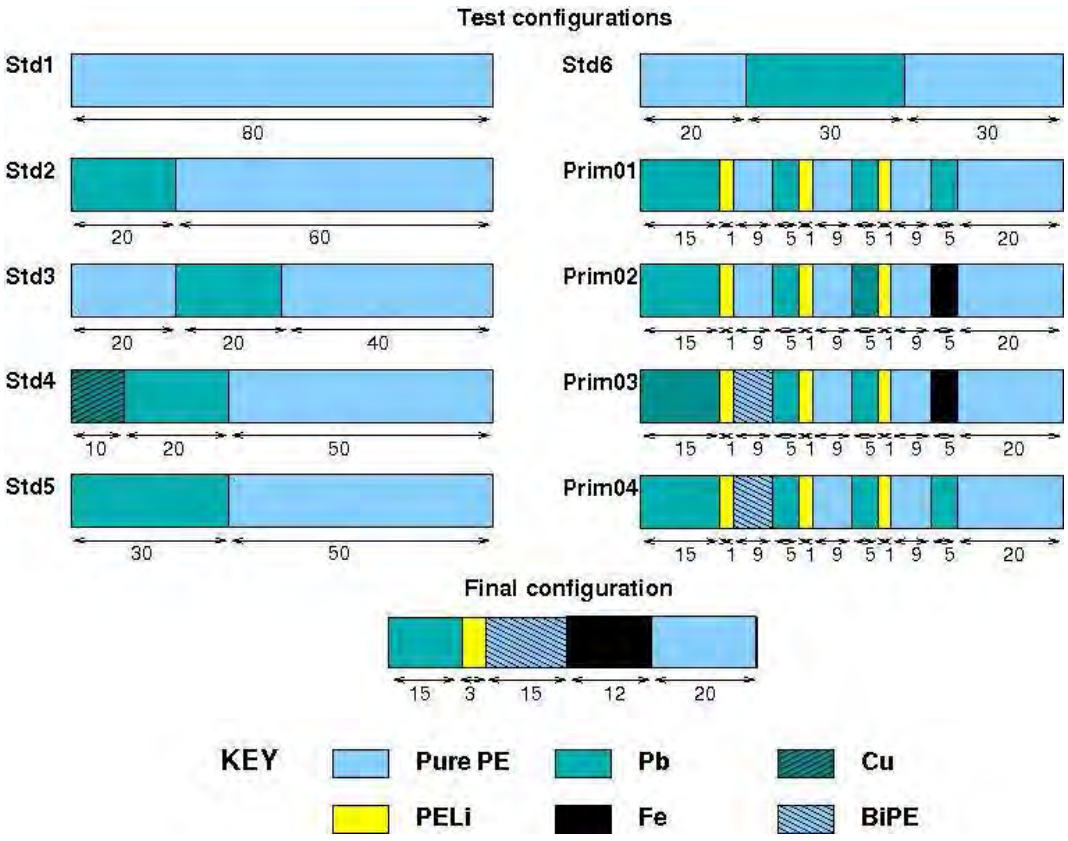

Figure 9: Shown is the summary of simulated test configurations for shielding structures and the final configuration. Tests have been calculated for a fixed shield thickness of 80 cm. The final configuration has a passive layer thickness of 65 cm. The main efforts of these simulations went into understanding the effects of multilayer shield configurations and their comparison to six standard shields, labelled 'std' here. Many more multilayer structures have been surveyed than indicated here. From this study it was concluded that existing shields perform sub-optimally.

The extensive survey was used to develop an optimal radiation shield for COBRA, shown in Fig. 9. The multilayer structure turns out to be more efficient in dealing with neutron flux evolution. Thermal neutron absorbers have been shown to be very efficient when used as thin sheets rather than as significantly more expensive bulk material. For pure moderation purposes, simple PE is sufficient. Metals are necessarily present for γ-ray attenuation but they are also interesting due to their influence on neutron fluxes.

The current design for a specific COBRA shielding includes a muon veto and an active

inner veto, 20 cm thick, made of a safe liquid scintillator which would be located inside the Lead. With an anticipated threshold of 100 keV (muon veto at 1 MeV), the following contributions were obtained for several important external background sources:

- Muons: Simulated 506.4 days lifetime at Gran Sasso which yields a total background index of 1.3×10^{-5} counts/keV/year/kg. Main background contribution is from delayed (cut at 100 μs) reaction events, i.e. inelastic muon–nucleon reactions. This contribution depends critically on the active veto presence (both vetoes).

- Spallation Neutrons (high-energy neutrons from hadronic cascades): Simulated 104.55 years lifetime at Gran Sasso which yields a total background index of 3.7×10^{-7} counts/keV/year/kg. This contribution depends on the inner active veto presence but not significantly.

- Low-energy neutrons (from (α, n)-reactions in cavern walls mainly): Simulated 378.1 days lifetime at Gran Sasso which yields a limit on the total background index of $< 5.4 \times 10^{-6}$ counts/keV/year/kg. The inner active veto is not critical for this assessment.

- External γ–radiation: Simulated 738.05 days lifetime of ^{232}Th and 803.56 days lifetime of ^{238}U at Gran Sasso. The resulting background indices, which both rely on the inner active veto presence, are: 6.1×10^{-5} counts/keV/year/kg for ^{232}Th and 8.1×10^{-6} counts/keV/year/kg for ^{238}U.

3.4 Pixellated Detector Studies

The development of pixellated detectors offers the possibility for enhancing the performance of COBRA in two key areas; (i) background suppression, and (ii) providing a unique signal for double beta-decay. It is the different characters of beta, alpha and gamma-radiation compared to that of double beta decay, within the CZT material, which provides the potential for event identification. For example, a beta of energy 2.8 MeV will travel 1–1.5 mm in CZT, whilst an alpha of a similar energy has a range of only $\sim$15 μm. A detector with pixellization of the order of 100–200 μm would yield a sample of 5–10 points along the track of the beta particle, but the alpha-decay would be largely confined to single-pixel. In this way, combined with timing criteria, pixellization would allow the elimination of all background processes which precede, or follow, alpha decay. This includes many of the beta-decay components of the natural thorium and uranium chains which can be problematic for low-background experiments. Simulations of the response of a 200 μm detector indicate that it is possible to suppress such background by almost three orders of magnitude[8].

Further background reduction can be achieved by discriminating against events in which non-adjacent pixels are activated. This occurs for Compton scattering of gamma-rays, or pair-production where the produced gamma-rays propagate through the crystal, where they re-interact.

The second strand is that it is highly desirable to uniquely identify the double-beta decay as opposed to the single beta events, or high energy electrons from photoelectric gamma-ray interactions. This provides a signal enhancement which potentially via track reconstruction could permit the characteristics of the decay process to be determined, e.g. angular distributions, etc. The present simulations indicate that the distributions of the single and double-electron events are characteristically different and these may be used to substantially enhance the sensitivity to the decay mode of interest. The present simulations suggest that for a 200 μm detector it is possible to uniquely identify double-beta events (as opposed to single electrons) with a 70% efficiency.

Work into characterisation of pixellated detectors has commenced. Although simulations indicate that the required pixellation is of order 100–200 μm pitch, initial measurements are being performed on 2 types of detector with a coarser pitch: a 16 pixel (4×4) detector with 2×2 mm^2 pixels, and a 256 (16×16) detector with 1.6×1.6 mm^2 pixels. The experimental programme is targeted at evaluating the response of these two detector types, including resolution as a function of shaping time, temperature and bias voltage. These results will then be compared with detailed GEANT4 based simulations to establish a simulation package that can be extrapolated to detectors with finer pixellisation.

In addition, the detectors are also being scanned at Liverpool University using a system that allows sources of various energies to be aimed at well defined points. The apparatus digitises the pulse shape, which reveals information on the depth of the interaction within the crystal as well as the energy deposited. The pulse shape analysis aims to improve upon the attainable energy resolution of the pixellated detectors and to use the depth information to reconstruct the event in 3D rather than 2D. The parameters T30 and T50 (the time to reach 30% of total pulse height and 50% of total pulse height respectively) show a good linear depth dependence and tests indicate that the depth can be deduced with close to 1 mm accuracy.

The high number of readout channels for pixellated detectors requires more sophisticated processing electronics. The detectors currently being tested are interfaced to an ASIC supplied by IDEAS, but alternative ASIC solutions, tuned to COBRA's experimental requirements are being explored. In particular the contributed activity to the local detector environment will be carefully assessed since mounting the ASICS in close proximity to the detectors produces significant improvements in detector energy resolution.

4 Conclusions

The COBRA experiment aims to search for neutrinoless double beta decay of ^{116}Cd with a sensitivity to half-lives greater than 10^{26} years with a large array of CdZnTe crystals. The background in the signal region will be minimised through careful selection of materials, a comprehensive shielding with active veto, and the use of timing and spatial coincidences to reject radioactive decay events. A proto-type experiment is operating in the Gran Sasso laboratory to investigate the experimental requirements, in particular the low background issues for a large array, whilst further R&D work to optimise the detector properties is

also proceeding.

5 List of Publications in 2006

- *Radiation Shielding for Underground Low-background Experiments*, D.Y. Stewart, P.F. Harrison, B. Morgan, Y.A. Ramachers, accepted for publication in NIM volume A (2006) nucl-ex/0607032
- *Evaluation of Pixellated CZT Detectors for Neutrinoless Double Beta-decay Measurements*, T.R. Bloxham & M. Freer, accepted for publication in NIM volume A (2006)
- *First Results on Double Beta Decay Modes of Cd, Te and Zn Isotopes with the COBRA Experiment*, T. Bloxham *et al*, Submitted to Phys. Rev. C. (2006)
- *The COBRA Double Beta Decay Experiment*, J.V. Dawson, submitted to LRT 2006, AIP Conference Proceedings (2006)
- *The COBRA Double Beta Decay Search Experiment*, D.Y. Stewart, proceedings of the 9th Conference on the Intersections of Particle and Nuclear Physics, AIP publishing (2006)
- *Double Beta Decay Measurement with COBRA*, J.R. Wilson, submitted to Journal of Physics Conference Series, Nu2006, IoP publishing (2006)
- *The COBRA Double Beta Decay Experiment*, B. Morgan, Particles and the Universe Proceedings of the 20th Lake Louise Winter Institute to be published by World Scientific (2006)

References

[1] A. Alessandrello et al. Bolometric measurement of the beta spectrum of ^{113}cd. *Nucl. Phys. B (Proc. Suppl.)*, 35:394, 1994.

[2] A. Alessandrello et al. New experimental results on double beta decay of ^{130}te. *Phys. Lett. B*, 486:13, 2000.

[3] C. Arnaboldi et al. A calorimetric search on double beta decay of ^{130}te. *Phys. Lett.*, B557:167–175, 2003.

[4] C. Arnaboldi et al. A new limit on the neutrinoless double beta decay of 130te. *Phys. Rev. Letters*, 95:142501, 2005.

[5] A.S. Barabash, A.V. Kopylov, and V.I. Cherehovsky. Search for double beta-decay of ^{100}mo and ^{116}cd to the excited states of ^{100}ru and ^{116}sn. *Phys. Lett. B*, 249:186–190, 1990.

[6] P. Belli et al. *Nuov. Cim.*, 101A:959, 1989.

[7] P. Belli et al. New limits on 2beta+ decay processes in ^{106}cd. *Astropart. Phys.*, 10:115, 1999.

[8] T. Bloxham and M. Freer. *Nucl. Instr. Meth. A*, 2006. Accepted for publication.

[9] M.J. Carson et al. *Nucl. Instr. Meth. A*, 546:509, 2005.

[10] F. Danevich et al. Beta decay of ^{113}cd. *Phys. Atom. Nucl.*, 59:1, 1996.

[11] F. A. Danevich et al. Search for 2β decay of cadmium and tungsten isotopes: Final results of the slotvina experiment. *Phys. Rev.*, C68:035501, 2003.

[12] F. A. Danevich et al. $Znwo_4$ crystals as detectors for 2β decay and dark matter experiments. *Nucl.Instrum.Meth.*, A544:553–564, 2005.

[13] C. Goessling et al. Experimental study of ^{113}cd beta decay using cdznte detectors. *Phys. Rev. C*, 72:064328, 2005.

[14] M Hirsch et al. Nuclear structure calculations of beta+ beta+, beta+/ec and ec/ec decay matrix elements. *Zeit. f. Physik*, A347:151–160, 1994.

[15] H. Kiel, D. Munstermann, and K. Zuber. A search for various double beta decay modes of cd, te and zn isotopes. *Nucl. Phys.*, A723:499–514, 2003.

[16] H.V. Klapdor-Kleingrothaus et al. Evidence for neutrinoless double beta decay. *Mod. Phys. Lett.*, A16:2409–2420, 2001.

[17] H.V. Klapdor-Kleingrothaus et al. *Mod. Phys. A*, 21:1547, 2006.

[18] Los Alamos National Lab. Mcnpx user's manual. 2002. publication LA-CP-02-408, version 2.4.0; http://mcnpx.lanl.gov/.

[19] P. Luke. Unipolar charge sensing with coplanar electrodes - application to semiconductor detectors. *IEEE Transactions on Nuclear Science*, 42:207, 1995.

[20] E. B. Norman and M. A. DeFaccio. Searches for double β^+, β^+/ec and double electron-capture decays. *Physics Letters*, B148:31–34, 1984.

[21] P.F. Smith et al. *Astropart. Phys.*, 22:409, 2004.

[22] D.Y. Stewart et al. *Nucl. Instr. and Meth. A*, in press, 2007.

[23] H. Wulandari et al. *Astropart. Phys.*, 22:313, 2004.

[24] H. Wulandari et al. Neutron background studies for the cresst dark matter experiment. 2004. Preprint archive (http://arxiv.org/) hep–ex/0401032.

[25] K. Zuber. Cobra - double beta decay searches using cdte detectors. *Phys. Lett. B*, 519:1–7, 2001.

CRESST. Dark Matter Search

G. Angloher [a], I. Bavykina [a], C. Bucci [d], C. Coppi [c], F. von Feilitzsch [c], D. Hauff [a], S. Henry [b], P. Huff [a], J. Jochum [e], M. Kimmerle [e], H. Kraus [b], J.C. Lanfranchi [c], R. Lang [a], B. Majorovits [a], M. Malek [b], R. McGowan [b], V. Mikhailik [b], E. Pantic [a], F. Petricca [a], S. Pfister [c], W. Potzel [c], F. Pröbst [a], M. Razeti [c], C. Rottler [e], S. Scholl [e], W. Seidel [a, +], M. Stark [c], L. Stodolsky [a], B. Tolhurst [b], W. Westphal [c],

[a] *MPI für Physik, Föhringer Ring 6, 80805 Munich, Germany*
[b] *University of Oxford, Department of Physics, Oxford OX1 3RH, U.K.*
[c] *Technische Universität München, Physik Department, D-85747 Garching, Germany*
[d] *Laboratori Nazionali del Gran Sasso, I-67010 Assergi, Italy*
[e] *Eberhard-Karls-Universität Tübingen, D-72076 Tübingen, Germany*
[+] *Spokesperson E-mail address: seidel@mppmu.mpg.de*

Abstract

The aim of CRESST (**C**ryogenic **R**are **E**vent **S**earch with **S**uperconducting **T**hermometers) is to search for particle Dark Matter and to contribute to the elucidation of its nature. The experiment is located at the 'Laboratori Nazionali del Gran Sasso' (LNGS), Italy, and it uses low background cryogenic detectors with superconducting phase transition thermometers for the direct detection of WIMP-nucleus scattering events.

1 The Dark Matter Problem

The search for Dark Matter and the understanding of its nature is of central interest for particle physics, astronomy and cosmology. There is strong evidence for its existence on all scales, ranging from dwarf galaxies, through spiral galaxies like our own, to large scale structures. The history of the universe is difficult to reconstruct without Dark Matter, be it Big Bang Nucleosynthesis or structure formation.

Particle physics provides a well motivated candidate with the lightest SUSY-particle, the "neutralino". Generically, such particles are called WIMPs (Weakly Interacting Massive Particles). WIMPs are expected to interact with ordinary matter by elastic scattering on nuclei. All direct detection schemes have focused on this possibility.

Conventional methods for direct detection rely on the ionization or scintillation caused by the recoiling nucleus. This leads to certain limitations connected with the low ionization or scintillation efficiency of the slow recoil nuclei. The cryogenic detectors developed for the first phase of CRESST (CRESST-I) measure the deposited energy calorimetrically, independent of ionization, and allow a detection of much smaller recoil energies. When the cryogenic measurement of the deposited energy is combined with a measurement of scintillation light an extremely efficient discrimination of the nuclear recoil signals from radioactive background signals can be obtained. This type of detectors is beeing used in the upcoming phase CRESST-II.

2 Detection Principle

The low temperature calorimetric detectors consist of a target crystal, the so-called absorber, an extremely sensitive superconducting phase transition thermometer, and a weak thermal coupling to a heat bath to allow thermal relaxation of the system after an interaction. The thermometer is made of a tungsten film evaporated onto the absorber crystal. Its temperature is stabilized in the transition region from the superconducting to the normal conducting state, which occurs at termeratures of about 10 mK. A typical width of the transition region is about 1 mK. A small temperature rise (typically some μK), e.g. from a WIMP nucleus scattering event, leads to an increase of resistance, which is measured with a SQUID based readout. For the first phase of CRESST, which ended in Feb. 2001, 262 g sapphire detectors have been developed at the institute. These detectors provided an excellent energy resolution of 133 eV at 6 keV and a very low energy threshold of 600 eV.

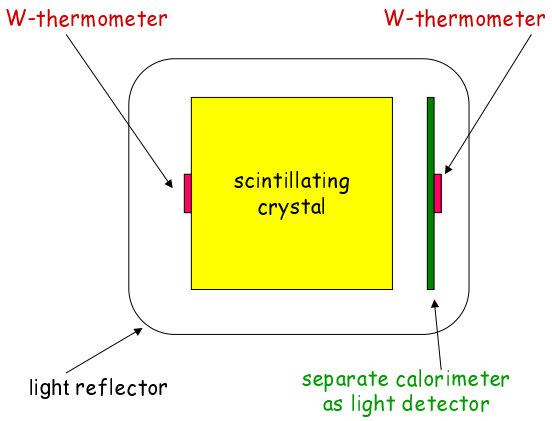

Figure 1: Sketch of the detector setup for the coincident detection of phonons and scintillation light. This novel concept will be used in CRESST-II. It allows to effieciently discriminate nuclear recoils signals from radioactive backgrounds.

In the upcoming second phase CRESST-II, we are using 300 g scintillating $CaWO_4$ crystals as absorbers. The scintillating crystal is equipped with a superconducting tungsten phase transition thermometer for the detection of the phonons created by particle interactions in the scintillating crystal. The scintillation light is measured in coincidence with a separate cryogenic detector, optimized for light detection. Fig. 1 schematically shows the setup of this composite detector. Starting with a proof of principle experiment in 1998, the technique of simultaneous measurement of phonons and scintillation light has been developed at the institue.

The important advantage of the simultaneous detection of phonons and scintillation light is that it offers an extremely efficient suppression of the radioactive background. The ratio of the energy in the phonon channel and the energy in the light channel depends on the type of interaction. Nuclear recoils, such as WIMP or neutron scattering events, emit substantially less scintillation light than fully ionizing interactions, e.g. γ or β interactions do. As the overwhelming part of the backgroud consists of β and γ interactions, this phonon/light technique provides a very effective method of background suppression. Fig. 2 illustrates this novel detection method. With this proof of

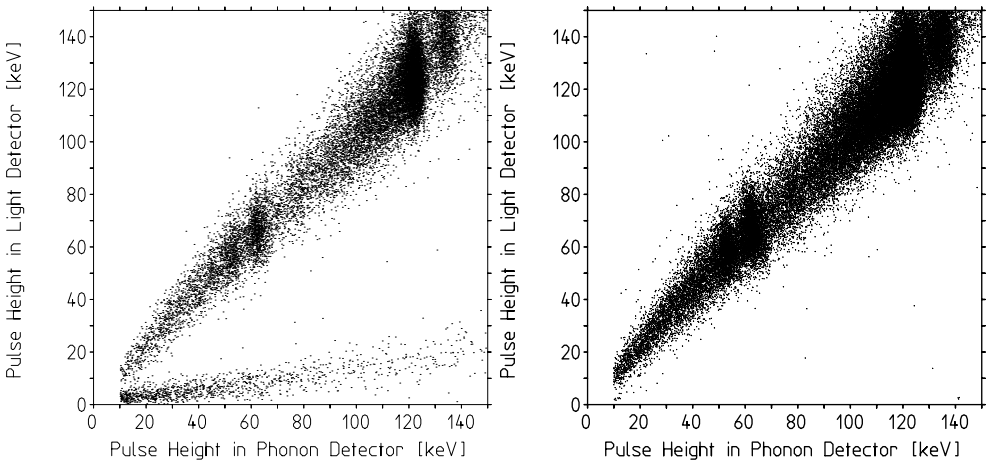

Figure 2: Coincident detection of phonons and scintillation light with a 6 g proof of principle $CaWO_4$ detector. Left fig.: The upper band of events is due to irradiation of the $CaWO_4$ crystal with electrons and gammas, whereas the lower band with lower light yield, is from nuclear recoils caused by a neutron source. Removing the neutron source (right fig.), confirms that there is no leakage of ionizing events into the nuclear recoil region.

principle device, a 99.7 % suppression of ionizing background in the energy range from 15 and 25 keV , and 99.9 % at energies above 25 keV has been demonstrted.

Compared to the alternative approach of simultaneous measurement of phonons and charge in a semiconductor crystal, which is applied in the experiments CDMS and Edelweiss-II, the method developed for CRESST-II has the important advantage that it does not suffer from dead layers at the surface. A reduced charge collection for ionizing events occurring close to the surface in semiconducting crystals may lead to a false identification of low energetic γ's and β's as nuclear recoils. The result in Fig. 2, which was obtained with a gamma and beta source, confirms that the supression also works for low energy electrons impinging onto the crystal surface.

3 The CRESST Setup in Gran Sasso

The central part of the CRESST installation is the cryostat, sketched in figure 3. The low temperature generated in the mixing chamber of the dilution refrigerator is transferred into the radiopure cold box, which houses the detectors, via a 1.5 m long cold finger, protected by thermal radiation

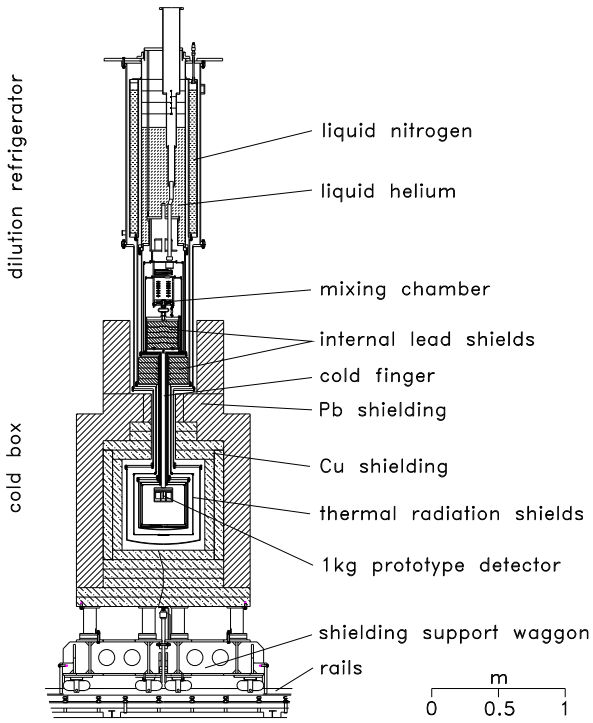

Figure 3: Layout of the CRESST ^{3}He/^{4}He dilution refrigerator and low background cold box with its shielding.

shields, all fabricated of low background copper. Two internal cold shields consisting of low level lead are attached to the mixing chamber and to a thermal radiation shield at liquid N_2 temperature, respectively, in order to block any line-of-sight from the non-radiopure parts of the dilution refrigerator to the detectors inside the cold box. The design completely avoids potentially contaminated cryogenic liquids inside the cold box.

An extensive passive shielding of low background copper and lead surrounds the cold box and serves to shield radioactivity from the surrounding rock. The entire shilding is inclosed inside a gas-tight radon box, that is flushed with boil of N_2 gas and maintained at a small overpressure. Special care has been taken to minimize above ground exposure of the construction materials of the cold box and the shielding to cosmic rays, in order to avoid activation.

Figure 4 schematically shows the CRESST experimental building. The cryostat is installed in a two level faraday cage to shield electromagnetic interference. The ground level inside the faraday cage is equipped as a class-100 clean room, in order to minimize contamination of the detectors and

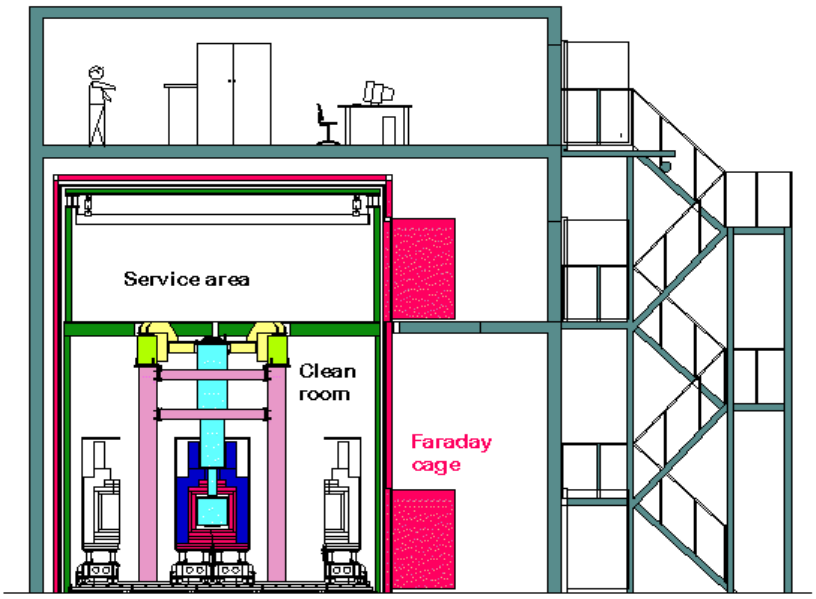

Figure 4: Schematic drawing of the three level CRESST building in hall B of the Gran Sasso Underground Laboratory.

cold box during mounting. The head of the cryostat extends into the first floor of the farady cage, which is outside the clean room to simplify servicing of the cryostat. The first floor also houses the sensitive analog electronics. The gas handling system of the cryostat and the DAQ is outside the faraday cage. In the top floor, of the experimantal building a laminar flow work place is installed which serves to assemble and rebond detectors under clean conditions.

4 Preparations for CRESST-II

Until 2004 different prototype detector modules were teted in the cryostat A final run with two detectors was performed in 2004 with a net exposure of 20.5kg days. Form factor effects effectively limit the energy transfer to the heavy tungsten nuclei in elastic WIMP nucleus scattering to energies below 40 keV. We obtained 16 events in the nuclear recoil acceptance band in the relevant energy region between 12 keV and 40 keV. The cryostat is still without neutron shield and this rate of 0.87 events per kg and day is consistent with the predicted neutron background. Moreover, most of

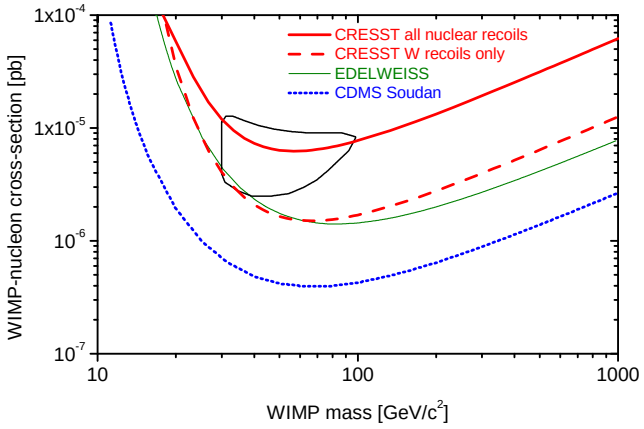

Figure 5: Exclusion plot for spin independent WIMP interaction, derived from 8.11 kg days of data from one 300 g CRESST-II detector module. The area above the curve is excluded at 90% c.l. For comparison, the DAMA positive evidence is shown and also the limits from other cryogenic experiments, CDMS and EDELWEISS.

this recoil events have a clear light signal associated with the phonon signal as expected for neutron generated recoils. Neutron events in this energy range are dominantly oxyxgen recoils, whereas WIMPs with spin independent interaction almost exclusively ($\sigma \propto A^2$) recoil off tungsten nuclei. We have measured a very large quenching factor of $Q \approx 40$ for W-recoils, whereas the quenching factor for oxygen recoils is $Q = 7.3$ at mK temperatures and $Q \approx 10$ at room temperature. If a similar quenching factor applies for the tungsten recoils at low temperature, there should be no light emission observed in the 12 to 40 keV region within the detection limit. The exclusion plot derived from this run is shown infig. 5.

The detector was calibrated with external ^{57}Co (122 keV γ's) and ^{60}Co (1.1 MeV and 1.3 MeV γ's) sources. With electric heater pulses the energy calibration is extended over the complete energy range of interrest. Periodically injected heater pulses also serve to confirm the stability of the calibration and to measure the trigger efficiency close to threshold. The phonon channel had a detection threshold for reoils of 3 keV at 100% efficiency and the threshold of the light channel was 8 keV for γ andβ interactions. As shown in fig. 6, the phonon channel exhibited an energy resolution of 1 keV at a 46.53 keV peak from an external ^{210}Pb contamination during the whole measuring period.

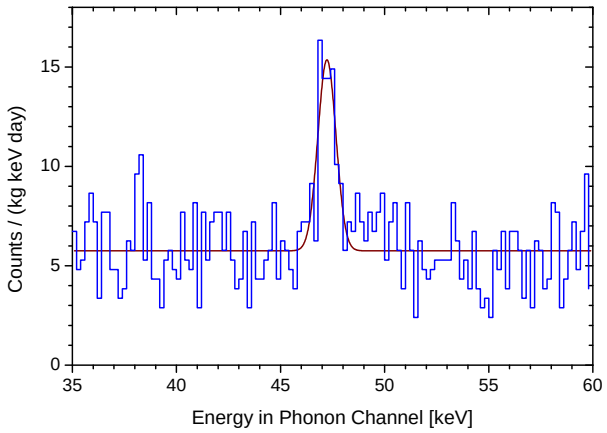

Figure 6: Energy spectrum of the phonon channel of a 300 g $CaWO_4$ detector. The peak at 46.53 keV, with a rate of 3.2 counts/day, is from an external ^{210}Pb contamination. The agreement with the nominal decay energy and the good resolution confirms the energy calibration and its stability.

Since this detectors can clearly discriminate background from alpha particles and pgamma background one can obtain a background free alpa spectrum. In this spectrum we could unambigously detect the natural α-decay of ^{180}W.A half-life of $T_{1/2} = (1.8 \pm 0.2) \times 10^{18}$ y and an energy release of Q = (2516.4 $\pm$ 1.1 (stat.) $\pm$ 1.2 (sys.)) keV have been measured. The limits on the decay of other Tungsten isotopes could be improved by more than a foactor 50 over present limits.

After these measurements the setup has been upgraded for the experimental program of CRESST-II, which will use 33 of such 300 g phonon/light detector modules. The upgrade includes the installation of a 66 channel SQUID readout system in the existing cryostat, a new wiring running (in total 432 wires)from room temperature to 7 mK, a new detector holder support structure able to hold 33 modules, the installation of a neutron shield and a muon veto, a new multichannel electronics and DAQ. The cryostat with the upgraded shielding is shown schematically in fig. 7. The upgrade was completed in 2006.

Nine Detector modules with a total mas of 2.7 kg were installed fig. 8 and a comissioning run started which will go until spring 2007.

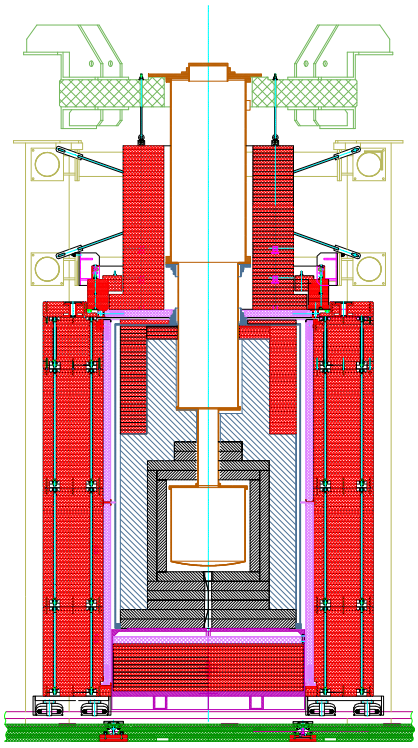

Figure 7: Dilution refrigerator and low background cold box with its shielding upgraded for CRESST-II. The gas tight radon box enclosing the Cu (shown in grey) and Pb (blue) shielding will be completely covered by a plastic scintillator μ-veto (pink) and 50 cm of polyethylen (red).

Figure 8: Installation of the first 9 detector modules in CRESST II.

5 Publications

Limits on WIMP dark matter using scintillating CaWO cryogenic detectors with active background suppression G.Angloher et al. Journal of Astroparticle Physics 23 , 325-339 (2005)
Detection of Natural Alpha Decay of Tungsten C. Cozzini et al. Phys. Rev. C 70 (2004)
CRESST-II: dark matter search with scintillating absorbers G. Angloher et al. NIM A Vol. 520 Nos. 1-3
Light detector development for CRESST-II, F. Petricca et al. , NIM A Vol. 520 Nos. 1-3

CUORICINO and CUORE

F. Alessandria[b], E. Andreotti[i], R. Ardito[a,c], C. Arnaboldi[a], F. T. Avignone III[d], M. Balata[e], I. Bandac[d], M. Barucci[f], J.W. Beeman[s], F. Bellini[q], B. Berger[g,l], C. Brofferio[a], A. Bryant[g,l], C. Bucci[c], S. Capelli[a], L. Carbone[a], S. Cebrian[h], M. Clemenza[a], C. Cosmelli[p], S. Cuneo[j,k], O. Cremonesi[a], R. J. Creswick[d], I. Dafinei[p], M.P. Decowski[g,l], S. Di Domizio[j,k], M. Diemoz[p], M.J, Dolinski[g,l,o], R. Faccini[p], H. A. Farach[d], F. Ferroni[p], E. Fiorini[a], L. Foggetta[i], S.J. Freedman[g,l], C. Gargiulo[p], A. Giachero[c,j], L. Gironi[a], E. Guardincerri[g], A. Giuliani[i], P. Gorla[c], T.D. Gutierrez[q], E. E. Haller[m,s], K.M. Heeger[r], I. G. Irastorza[h], R. Kadel[g], K. Kazkaz[o], L.Koogler[g,l], Yu.G.Kolomensky[g,l], E. Longo[p], G. Maier[c], R.H. Maruyama[r], C. Martinez[d], S. Morganti[p], S. Nisi[e], C. Nones[a], E. B. Norman[o], A. Nucciotti[a], M. Olcese[j,k], P. Ottonello[j,k], M. Pallavicini[j,k], V. Palmieri[n], M. Pavan[a], M. Pedretti[i], G. Pessina[a], S. Pirro[a], E. Previtali[a], L. Risegari[f], C. Rosenfeld[d], S. Sangiorgio[i], N.D. Scielzo[o], M. Sisti[a], A. R. Smith[g], L. Torres[a], C. Tomei[p], G. Ventura[f] M. Vignati[p], N. Xu[g], C. Zarra[c], and L. Zanotti[a]

[a] Dip. di Fisica dell'Univ. di Milano-Bicocca e Sez. INFN di Mi-Bicocca, Milano I-20126 -Italy
[b] INFN - Sez. di Milano, Milano I-20133 - Italy
[c] Dip. di Ingegneria Strutturale del Politecnico di Milano, Milano I-20133 - Italy
[d] Dept.of Phys. and Astron., Univ. of South Carolina, Columbia, South Carolina 29208 - USA
[e] Laboratori Nazionali del Gran Sasso, I-67010, Assergi (L'Aquila) - Italy
[f] Dip. di Fisica dell'Univ. di Firenze e Sez. INFN di Firenze, Firenze I-50125 - Italy
[g] Nuclear Science Division, Lawrence Berkeley National Lab., Berkeley, CA 94720 - USA
[h] Lab. de Fisica Nuclear y Altas Energias, Univ. de Zaragoza, 50009 Zaragoza - Spain
[i] Dip. di Fisica e Matematica dell'Univ. dell'Insubria e Sez. INFN di Milano, Como I-22100 - Italy
[j] Dip. di Fisica dell'Università di Genova - Italy
[k] Sez. di Genova dell'INFN, Genova I-16146 - Italy
[l] Dept. of Physics, Univ. of California, Berkeley, CA 94720 - USA
[m] Dept. of Materials Sc. and Engin., Univ. of California at Berkeley, Berkeley, CA 94720 - USA
[n] Laboratori Nazionali di Legnaro, I-35020 Legnaro (Padova) - Italy
[o] Lawrence Livermore National Laboratory, Livermore, California, 94550 - USA
[p] Dip. di Fisica dell'Univ. di Roma La Sapienza e Sez. INFN di Roma, Roma I-00185 - Italy
[q] California Polytechnic State Univ., San Luis Obispo, CA 93407 - USA
[r] Univ. of Wisconsin, Madison, Wisconsin - USA
[s] Materials Sc. Division, Lawrence Berkeley National Lab., Berkeley, CA 94720 - USA

Abstract

CUORE R&D and Cuoricino results achieved in 2006 will be presented.

1 Cuoricino 2006

Besides being a sensitive experiment on $\beta\beta(0\nu)$ of ^{130}Te CUORICINO is a conclusive test of CUORE. Installed at LNGS during 2002 and cooled down for the first time in January 2003, CUORICINO is providing important results concerning both the technical performances of the bolometric tower (CUORE will be made of 19 such towers), the $\beta\beta(0\nu)$ background level and origin, and the $\beta\beta(0\nu)$ of ^{130}Te .

CUORICINO is a tower of 13 planes containing 62 crystals of TeO_2; 44 of them are cubes of 5 cm on a side while the dimensions of the others are 3×3×6 cm^3 (the two 9 crystal 3×3×6 cm^3 planes are the only relevant difference between the CUORICINO and CUORE towers). The total mass of TeO_2 in CUORICINO is 40.7 kg, the largest by more than an order of magnitude than any cryogenic detector.

The performances recorded for the detectors are excellent: the average FWHM resolution measured during the periodic (once a month) exposition to a ^{232}Th source of the detectors is $\sim$ 7 keV for the 5x5x5 cm^3 crystals and $\sim$ 9 keV for the 3x3x6 cm^3 crystals. Both these values are measured on the ^{208}Tl gamma line at 2615 keV. Similar values are measured on the ^{208}Tl line visible in the sum background spectra of 5×5×5 cm^3 and 3×3×6 cm^3 crystals: no deterioration of the FWHM is observed when summing long measurements and all the detectors together. The statistics collected up to May 2006 for the $\beta\beta(0\nu)$ measurement corresponds to 8.38 kg(^{130}Te) y and it is fully analyzed. Other $\sim$3 kg(^{130}Te) y collected during 2006 will be added soon to the total statistic. No evidence of a 2530 keV peak is found in the analyzed data. A Maximum Likelihood procedure is used to establish the maximum number of $\beta\beta(0\nu)$ events compatible with the measured background. Performing the Likelihood relative to the spectra collected in the two runs three kind of detectors (big, small natural and enriched crystals) are combined together, allowing for different background levels in the two runs for the 3 detector types. The FWHM is fixed to the measured values and the efficiencies to the MonteCarlo evaluated ones. A lower bound for the ^{130}Te $\beta\beta(0\nu)$ half-life of 2.4× 10^{24} years at 90% C.L. results, with a weak dependence on the used background function (linear or flat), and on the assumed $\beta\beta(0\nu)$ peak position (allowing it to span over the 1 sigma error quoted for the Q-value) and peak shape (symmetric or asymmetric gaussian). The corresponding upper bound on the Majorana effective mass ranges from 0.18 and 0.9 eV (using the NME from [1]). CUORICINO will run until the completion of CUORE, foreseen for 2010. Assuming a 60% live time efficiency in May 2010 Cuoricino would have added 2.4 years of statistics reaching therefore 28 kg(^{130}Te) y and resulting in a sensitivity of about 6 10^{24} years on the $\beta\beta(0\nu)$ half-life.

Table 1: Estimate of the relative contributions of the different sources responsible for the background measured in CUORICINO.

Source	^{208}Tl	$\beta\beta(0\nu)$	3-4 MeV
TeO_2 ^{238}U and ^{232}Th surf. contam.	-	10± 5%	20± 10%
Cu ^{238}U and ^{232}Th surf. contam.	$\sim$15%	50± 20%	80± 10%
^{232}Th contam. of cryostat Cu shields	$\sim$85%	30± 10%	-

2 Background contributions in CUORICINO

Figures 1 and 2 show the background measured by $5\times5\times5$ cm^3 crystals in CUORICINO. The two histograms plotted in each figure are the spectrum of events collected operating the CUORICINO array in anticoincidence (therefore selecting events where just one crystal is hit within the time coincidence window of about 50 ms) and the spectrum obtained operating the array in coincidence (here the coincidence is obtained selecting events where two and only two crystals are contemporary hit, spectra requiring higher multiplicity per event can also be plotted even if they show a by far lower counting rate). In both cases the energy spectra collected by each single (independent) detector of the array are summed toghether to produce the "sum energy spectra" plotted in the two figures. The $\beta\beta(0\nu)$ peak should appear as a gaussian line at about 2530 keV in the anticoincidence spectrum (the efficiency with which the two electrons are completely contained within one $5\times5\times5$ cm^3 crystal is $\sim$86%). The capability of operating the detectors in anticoincidence (that is made possible thanks to the independence of the detector read-out, trigger and acquisition) allows to reduce the background in the $\beta\beta(0\nu)$ region. In CUORICINO this reduction is not much relevant (see fig. 3) but in the thight-packed structure of CUORE it will play a fundamental role. Finally from the differences between coincidence and anticoincidence spectra important informations concerning the background origin and location are obtained as it will be clear in the following.

In a preliminar analysis of CUORICINO background, included in CUORE Proposal, we temptatively quantified the different contributions to the $\beta\beta(0\nu)$ background as shown in table 1. More detail on this analysis are presented in the next paragraphs of this section.

2.1 ^{232}Th bulk contribution and the 3-4 MeV continuum.

As shown in fig.1 the background measured by CUORICINO on the left side of the 2615 keV ^{208}Tl line and on its right side differs by about 30%.

The ^{208}Tl line is the highest natural γ line due to environmental contamination (indeed no higher energy gamma lines are observed in any of our TeO_2 bolometers background spectra, including CUORICINO ones) and appears as the only possible γ contribution (through Compton events) to the $\beta\beta(0\nu)$ background. The other two peaks appearing in fig. 1 are the 2448 keV, due to ^{214}Bi, and the 2505 keV sum line due to the interaction, in the same crystal, of the two γ 's contemporary emmitted by ^{60}Co in its beta decay. Both peaks have an energy definetely too low to give any contribution to the $\beta\beta(0\nu)$ background. The ^{208}Tl line originates from contaminations relatively far from detector, as proved by the reduced intensity of the low energy gamma lines coming from the ^{232}Th chain. The contamination is more likely in the refrigerator itself, a possible guess for its exact position is some thermal shield or the superinsulation itself (the source is appearently seen in the same way by all the crystals of the tower). From this guess on the source position, it was possible to extrapolate - on the basis of a MonteCarlo simulation - the contribution gave from ^{208}Tl to the $\beta\beta(0\nu)$ background.

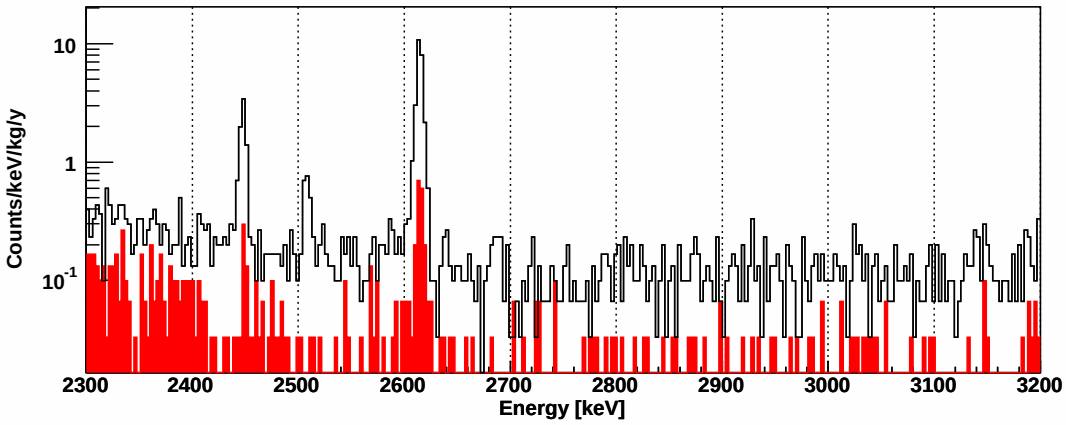

Figure 1: CUORICINO background in the $\beta\beta(0\nu)$ region: the black line refers to the anticoincidence events spectrum (only one detector hit) the red filled histogram refers to coincidence events (two detectors contemporary hit). The 2448 keV ^{214}Bi, the 2505 ^{60}Co and the 2615 keV ^{208}Tl line are clearly visible. The $\beta\beta(0\nu)$ decay should appear as a gaussian peak in the anticoincidence spectrum at 2530 keV (without any corresponding line in the coincidence spectrum). Above the 2615 keV line a flat continuous background, attributed to degraded alpha particles, is visible. The low contribution of coincidence event proves that only a small fraction of the continuum can be ascribed to crystal contaminations. This background extends clearly even below the ^{208}Tl peak and partake to the counting rate measured in the $\beta\beta(0\nu)$ region.

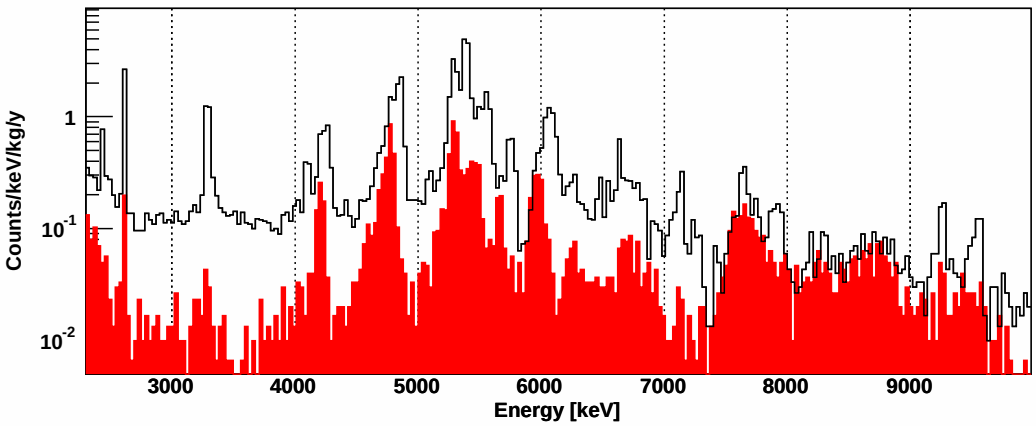

Figure 2: CUORICINO background above 2.3 MeV: the black line refers to the anticoincidence events spectrum (only one detector hit) the red filled histogram refers to coincidence events (two detectors contemporary hit). Most of the peaks appearing in the region above 4 MeV are ascribed to U and Th surface contamination of the crystals: in the anticoincidence spectrum the peaks have their high energy side centered at the transition energy of the decay (α+recoil completely contained in the crystal) and have a long, low energy tail (either α or recoil exit from the crystal depositing part of its energy outside). A similar pattern is observed in the coincidence events spectrum, in this case to give rise to a coincidence two crystals have to partake to the event. Therefore the maximum energy of the peak correspond to the α energy (i.e. the case in which the α is completely contained in one crystal and the recoil in the other one). The α peak centered at $\sim$ 3200 keV is ascribed to an internal contamination of the TeO_2 crystals in the long living isotope ^{190}Pt: the shape of the peak is gaussian (no low energy tail) no peak appears in the coincidence spectrum, the energy of the peak is compatible with the transition energy of ^{190}Pt.

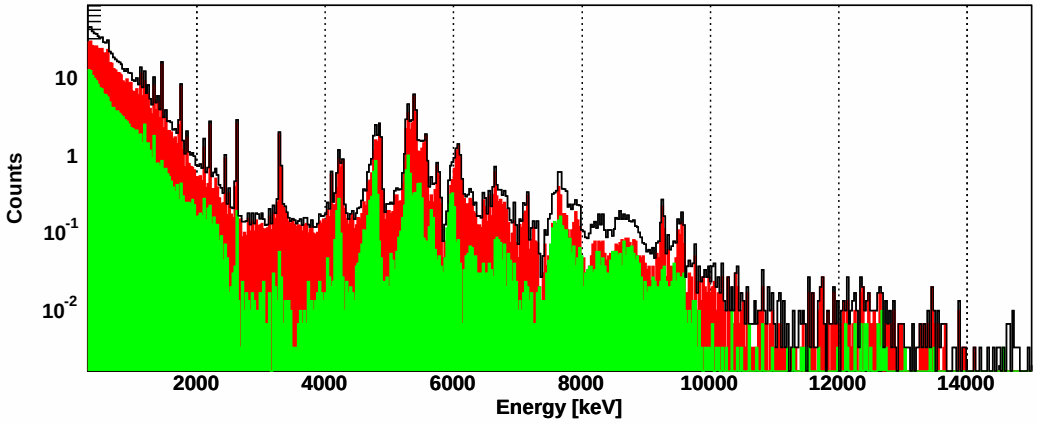

Figure 3: CUORICINO background: the black line refers to the total spectrum (all the events are counted) the red filled histogram refers to anticoincidence events (one detector contemporary hit) and the green filled histogram refers to coincidence events (two detectors hit per event). While in CUORICINO the fraction of coincidence events is relatively small in CUORE the large mass and the high granularity of the array will allow to have a relevant reduction of the counting rate by applying an anticoincidence cut.

2.2 The flat continuum between 3 and 4 MeV.

The background measured on the right side of the ^{208}Tl line is ascribed mainly to degraded alphas coming from U and Th radioactive chains and due to surface contamination of the crystals or of the inert material facing them. This continuum clearly extends below the ^{208}Tl line thus partecipating to the to the $\beta\beta(0\nu)$ background counting rate. While the heavy shielding forseen for CUORE will guarantee a deep reduction of the γ background (and therefore of the ^{208}Tl contribution), for α background (that comes only from the very inner part of the detector, i.e. the crystal themselves and the material directely facing the crystals) only a severe control of bulk and surface contaminations can guarantee the fulfillment of the sensitivity requirements for CUORE. To do that a correct identification and localization of the sources of the continuous α background is mandatory. Finally other contribution to the 3-4 MeV background could come from sources different from surface contamination, as it will be discussed later. As it will be disussed in the next section it is on this flat background that we focoused all our efforts in view of CUORE. This because:

1. it is clearly evident that its reduction would mean also a reduction of the $\beta\beta(0\nu)$ counting rate;

2. in our Hall C experimental measurements we can easly reach in this energy region a sensitivity similar to that of CUORICINO whereas the $\beta\beta(0\nu)$ region is dominated by an unavoidable ^{208}Tl background, generally higher than in CUORICINO;

2.3 Surface contaminations.

Alpha peaks can be identified very clearly in bolometers spectra. The peak position and shape give strong indication on the location of the contamination: sharp gaussian peaks indicate contamination of either the crystal bulk, if the energy corresponds to the transition energy of the decay (i.e. α+recoil), or of an extremely thin surface layer (could it be on the crystals surface or on the inert material surface facing the crystal) if the energy corresponds to the alpha energy. On the contrary asimmetric, "long-tailed" peaks are produced by thick contamination of surfaces. Finally a bulk or a deep surface contamination of an inert material facing the detector should produce just a continuum without any α peak (but several, visible γ peaks). Examples of the characteristic features resulting from the different location of the contamination are shown in fig. 4.

Side information, useful in this study, come from the analysis of coincidence events in the array and from the study of gamma peaks. Indeed when the background is dominated by α particles a coincidence between two crystals is produced only if the α emitter is on the surface of one crystal and the α or the recoiling nucleus exits from one crystal and enters into one other, producing a characteristic pattern clearly visible in fig. 4 bottom right.

Unfortunately while α peaks are clearly evident and their origin rather easly understood the continuous background underlying the peaks and extending toward the $\beta\beta(0\nu)$ region cannot be easly correlated to the one or the other peak (i.e. to the one or the other contamination). Hypotesis can be done on the basis of MonteCarlo simulations that however require as input a contamination intensity and a density profile, both unknown.

In CUORICINO (fig. 2) most of the peaks appearing in the region above 4 MeV are ascribed to U and Th surface contamination of the crystals. Indeed these peaks are visible in both coincidence and anticoincidence spectra, moreover they have a large low energy tail that once more is (as discussed) a prove that the contamination is at the crystal surface. Finally they are clearly identified also in the scatter plot of coincident events (fig. 5). Four peaks do not belong to this category:

- the α peak centered at $\sim$ 3200 keV. It is ascribed to an internal contamination of the TeO_2 crystals in the long living isotope ^{190}Pt: indeed the shape of the peak is gaussian (no low energy tail) and no peak appears in the coincidence spectrum, the energy of the peak is compatible with the transition energy of ^{190}Pt. The contamination is probably due to inclusions of fragments of the Pt crucible used in TeO_2 crystal growth;

- the α peak centered at $\sim$ 4080 keV. It grows on the low energy tail of a surface contamination peak but, as it will be discussed in next the section, it is attributed to a bulk contamination in Th;

- the α peak centered at $\sim$ 5300 keV. It is centered at the α (and not α+recoil) emitted by ^{210}Po . The peak is stable in time and is therefore attributed to a ^{210}Pb contamination (^{210}Pb has a half-life of 22 years while that of ^{210}Po is 138 days). The position of the peak indicates that the contamination has to be on a very thin layer

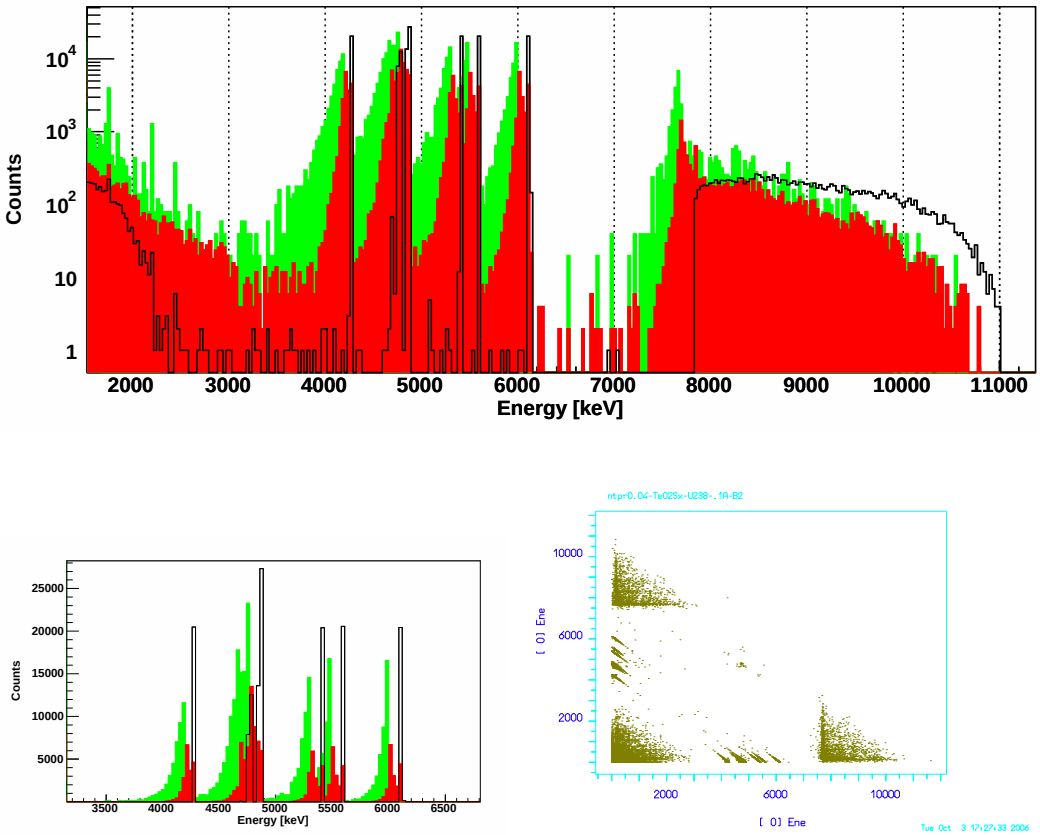

Figure 4: Top: MonteCarlo simulation of the anticoincidence spectra produced in CUORICINO by a ^{238}U contamination in crystal bulk (black line), crystal surface (red filled histogram) and copper mounting surface (green filled histogram). Surface contaminations has been simulated with an exponential density profile and a thikness of 0.1 micron. Bottom left: a detail of the top histograms showing the different shapes of α peaks. Bottom right: the scatter plot of coincident events for the ^{238}U crystal surface contamination shown in red in the histograms, the other two simulated contamination do not contribute to the scatter plot.

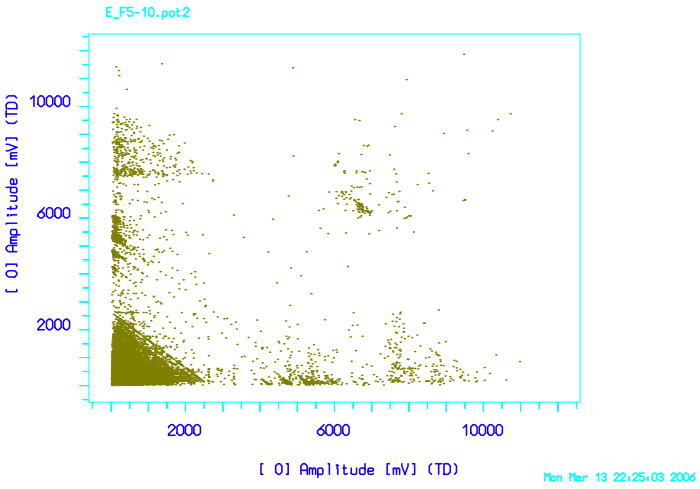

Figure 5: CUORICINO background: the scatter plot of coincident events.

(much thinner than the U crystal surface contamination described above) either on the crystal surface or on the mounting surface. From the coincidence spectra and scatter plots it is then possible to conclude that at least part (probably not all) of the peak has to be due to a contamination of the crystal surface. If this is the case also part of the 5.4 MeV peak has to be attributed to a such contamination;

- the α peak centered at $\sim$ 5400 keV. It has an intensity clearly decreasing with time in agreement with ^{210}Po half-life. The ^{210}Po contamination, usually observed in recently grown TeO_2 crystals, is ascribed to a bulk contamination (no coincidences are observed). Part of the peak is however attributed to the U and ^{210}Pb surface contamination discussed above. When CUORICINO was started the 5.4 MeV peak was by far dominated by the bulk contamination ^{210}Po peak (with an intensity as high as 0.2 c/h/crystal), now the peak has a much reduced intensity ($\sim$0.03 c/h/crystal) where the surface contamination seems to dominate.

Finally the small amount of coincidences in the 3-4 MeV range as well as the extrapolation (based on MonteCarlo simulations) of the counts attributable to crystal surface contaminations, indicate that a large fraction of the flat continuum between 3 and 4 MeV has its source outside the crystals. Degraded α could come either form surface or bulk contamination of the mounting components, however the reduced rate of low (hundred keV) energy gamma peaks allow to exclude that this continuum could be due to U and Th bulk contaminations of copper mounting.

Excluding important contribution from the bulk contamination of the small parts of the detector (thermistors, heaters, bonding wires, PTFE parts ...) on the basis of the radioactive measurements made before the construction of CUORICINO and excluding neutrons on the basis of both MonteCarlo simulation and experimental results

(MiDBD experiment didn't see any change in the $\beta\beta(0\nu)$ background rate when the borated polyethylene shield was mounted) we have concluded that most of the background measured by CUORICINO should come from crystal and copper surfaces. The surface background contribution extrapolated in Table 1 was obtained on the basis of this model.

It is however worth to note that minor contribution from small parts and neutrons cannot be excluded, and cannot be neglected in CUORE.

To get rid of this puzzle two main solutions were devised:

- reduction of surface contamination;
- development of bolometers able to identify and reject events originated at the detector surface.

These two solution are not mutually exclusive, and their developement runs in parallel toghether with a further check of the radioactive contamination of the small parts of the detector structure and the investigation of neutron background.

3 CUORE 2006

The CUORE Project [2] foresees the realization of a $\beta\beta(0\nu)$ experiment with an active mass of the order of 1 ton. CUORE will employ 988 natural TeO_2 bolometers each made of a cubic $5\times5\times5$ cm^3 TeO_2 crystal with a mass of about 750 g. The goal of the CUORE collaboration is to reach, in the energy region of interest, a background level lower than 10^{-2} counts/keV/kg/y obtaining hence a sensitivity on the effective Majorana mass of neutrino of the order of 50 meV.

The CUORE array is designed in order to have the most compact structure reducing to a minimum the distance between the crystals and the amount of inert material interposed between them. The 988 bolometers of the array are arranged in a cylindrical matrix organized into 19 "towers", each made of 13 planes. Every plane contains four crystals supported inside a copper frame. The entire array, surrounded by a 6 cm thick lead shield, will be operated at about 10 mK in a He^3/He^4 dilution refrigerator. A further thickness of 30 cm of low activity lead will be used to shield the array from the dilution unit of the refrigerator and from the environmental activity. A borated polyethylene shield and an air-tight cage will surround externally the cryostat. The experiment will be installed underground in the Laboratori Nazionali del Gran Sasso(LNGS) at a depth of 3400 m.w.e.

Despite operating a 1000 bolometer array at 10 mK could look rather challenging, the technical feasibility of CUORE has been extensively proved by the good performances of the CUORICINO experiment, while the possibility of cooling large masses in dilution refrigerators have been proved, for example, by the gravitational antenna experiments. The true challenge in CUORE - as in all the next generation $\beta\beta(0\nu)$ experiments - will be the background achievement. Up to now - thanks to the background knowledge acquired through CUORICINO and dedicated radioactive measurements of various type (NAA, ICMPS, HPGe ...) - the limiting factor appears to be the background coming from contamination of the detector surfaces (TeO_2 crystals and Cu mounting structure surfaces). With the present know-how the background in CUORE would be between 2 and 4 10^{-2} counts/keV/kg/y. New techniques are however under development and will be applied to

a test array consisting in a CUORE-like small tower (two or three planes instead of 13) that is used to evaluate background achievements in view of CUORE.

3.1 CUORE Hut and Shields

During year 2006 the design of the Hut that will host the CUORE experimental apparatus was completed and it construction begun. Also the design of the external shields have been finalized after a careful study of environmental background. The cryostat will be surrounded by a gamma shield made of 25 cm of Lead. According to our MonteCarlo simulations the measured environmental gamma flux will be reduced by such a shield to a level - in the $\beta\beta(0\nu)$ region - of 10^{-6} counts/keV/kg/y.

Outside the Lead shield a 20 cm thickness of Polyethylene will be added in order to thermalise environmental neutrons that will be then absorbed by the 3 cm of H_3BO_3 powder contained in the hollow space between the Lead and the Polyethylene itself. MonteCarlo simulation indicate that such a shield will limit neutron induced background to a rate far below the required level for CUORE. The opportunity of mounting a muon veto to avoid possible muon induced background is under study. The Hut and the experimental apparatus are however projected in order to eventually mount a detector array operated as muon veto.

3.2 CUORE Detectors

The design of the array structure (toghether with its exact dimension) have been definitively fixed. Moreover in year 2006 the study of materials to be used in array construction was completed for what concerns Copper and TeO_2 crystals requirements. Still open questions are the choice of the cabling and of the the spacers that are used in crystal mounting. For wires and connectors the problem is their radiopurity while for spacers the definition of the exact shape and material could still require some cryogenic and radioactive test. The crystal growing procedure has been agreed with the SICCAS (the crystal provider in China), this including the material selection and treatment protocols. The more delicate question of crystal surface treatment is still on the table. The technique succesfully optimized in LNGS and verified with the RAD array (see following sections) has been codified and transmitted to SICCAS: 8 newly grown crystals will be treated with such technique in China and tested within year 2007. If succesfull all CUORE crystals will be directely treated in China and will be therefore provided us just ready for mounting.

3.3 CUORE Background achievement

In year 2006 the activity dedicated to background reduction for CUORE continued. Once again the focus was on the flat background rate that characterizes all our detectors in the region between 3 and 4 MeV. This background clearly extends below the 2.6 MeV peak and partake in the $\beta\beta(0\nu)$ region counting rate. It is worth to note that the background reachable in the $\beta\beta(0\nu)$ region cannot be directly measured because of the unavoidable Tl contribution coming from the experimental set-up ^{232}Th contamination. (Only Cuore with its specially built refrigerator and with its heavy internal and external lead shield will

achieve the required low level of ^{232}Th). As a consequence it is the 3-4 MeV region which is used to check the background achievements. Two different detectors have been realized in the past year for test purposes: the two cryogenic test have been RAD detector and the CAW detector. The former was specially built for background studies, the latter for technical studies regarding the crystal mounting system for CUORE. Both these detectors have been employed in year 2006 to check background achievements and further investigate background sources. A summary of the results obtained so far is presented in the next two chapters.

4 The RAD detector

The "Radioactivity Array Detector" or RAD was built at the end of summer 2004. The RAD consists in a 2-plane array made of 8 5×5×5 cm^3 TeO_2 crystals, with a structure almost identical to that of CUORICINO (fig. 9). A nice feature of the RAD is that it can be mounted inside the hall C cryostat, as a standalone system, together with other detectors housed in an independent mounting structure. In this manner it is possible to exploit the hall C facility simultaneously for different CUORE measurements.

4.1 RAD1

The preparation of the first run of the RAD started in June 2004 (RAD1). The crystals were etched with nitric acid (removing about 10 micron on the surfaces) and then polished with a SiO_2 powder. The copper mounting structure was etched and successively treated through electroerosion removing from 10 to 30 microns on the surfaces.

The result of RAD1 was quite successful from the point of view of crystal cleaning (fig. 6): the TeO_2 surface contamination in U and Th was drastically reduced as proved by the disappearance of the U and Th alfa peaks. The extremely low background reached so far allowed us for the first time to disentangle the bulk vs. surface contamination of the crystals: once the large spread peaks due to surface contamination disappeared the gaussian sharp peaks of the internal contamination of TeO_2 were visible. Appearently the crystals are contaminated in Th isotopes (^{232}Th in secular equilibrium and long living ^{230}Th isotope belonging to the U chain) while no evidence of U contamination in secular equilibrium is obtained.

The only other alpha peaks visible in RAD1 are the two 5.3 and 5.4 peaks due to ^{210}Po decay (as discussed usually the contamination is not in ^{210}Po that has a very short lifetime but in its father ^{210}Pb , indeed only in the case of TeO_2 crystals we have found in the years that a bulk contamination of ^{210}Po and not in ^{210}Pb is present). When compared to CUORICINO the intensity of these two lines results to be: comparable in the case of the line due to the deposition of the entire transition energy (α+recoil = 5.4 MeV), 3 times higher in the case of the line due to the deposition of the only α particle energy (5.3 MeV). Finally, despite the strong reduction of the U and Th crystal contamination, no improvement is observed in the flat background spanning the 3-4 MeV region.

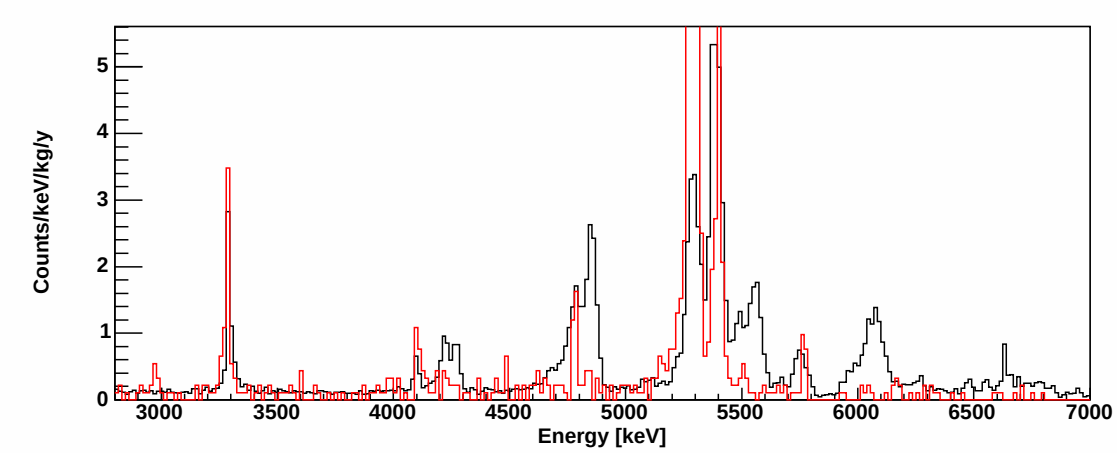

Figure 6: CUORICINO background (black) compared with RAD1 (red): the disappearance of crystal surface contamination peaks (visible in CUORICINO spectra as large asymmetric peaks) is evident. The only peak that remain in RAD1 are the doublet of ^{210}Po and the gaussian sharp peaks ascribed to a bulk contamination of the crystals in long living Th isotopes (to a level of about 10^{-13} g/g).

4.2 RAD2

RAD2 was intended to test the background contribution coming from the so-called "small parts" of the detector. The detetor is made not only by the TeO_2 crystals and the Cu structure but also by small parts like the PTFE clams, the NTD Ge thermistor, the Si heater, the gold bonding wires and finally glue and pins. In RAD2 the top and bottom plates of the Cu mounting structure were covered with samples of these small parts. These were: a PTFE slab covering the top plate (i.e. facing 4 crystals), a set of heaters facing two crystals on the bottom plane (169 heater for each crystal) and a set of gold wires facing the other two crystals on the bottom plane. In this way the amount of PTFE, heater and gold wires seen by the interested crystal was increased by a factor respectively of 6, 80 and 169. The 3-4 MeV rates measured by the RAD2 proved that the three materials have a maximum contribution to RAD1 and to CUORICINO background in the 3-4 MeV region of: heaters 1%, wires 3% and PTFE 50%.

4.3 RAD3 and RAD4

RAD3 was operated at the end of 2005, the only change with respect to RAD1 was the almost complete coverage of the copper faced to the crystals with a polyethylene film. The result was the dramatic reduction of the 5.3 MeV peak (by more than a factor 3) that has now the same intensity as measured in CUORICINO. The 5.4 peak on the other hand appears unchanged (proving that it is due to ^{210}Pb and not directely ^{210}Po). A second run with this same detector started at the beginning of year 2006, after a changement in the cryostat external shielding (now including a neutron shield).

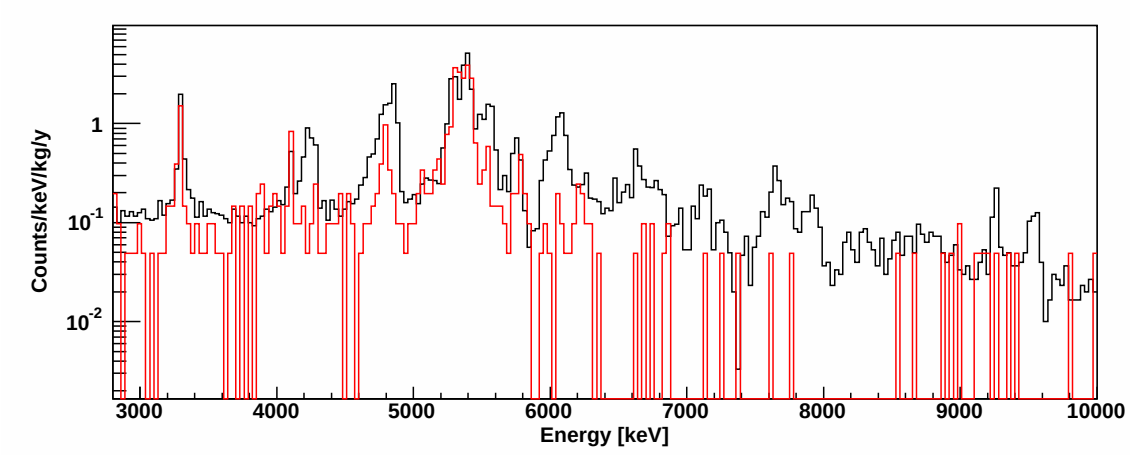

Figure 7: CUORICINO background (black) compared with RAD3+RAD4 (red): the 5.3 MeV peak due to ^{210}Po has here a much reduced intensity with respect to that of RAD1, now compatible with CUORICINO. The continuum background between 3 and 4 MeV appears reduced with respect to CUORICINO (the reduction factor is (38+/-7) %).

The results of RAD4 are completely compatible with those of RAD3, as expected for what concerns the alpha contribution because the detector is untouched. This further proved that environmental neutrons should not influence appreciably our background counting rate. In order to check the neutron absorbtion capability of the shield installed for RAD4 measurement we have performed dedicated measurement with a neutron source (an AmBe source yielding ~2200 n/s) both with and without neutron shielding (see Fig. 8 left panel). The results of the measurements either with the naked source as well as with the source embedded in an acrylic moderator were compared with MonteCarlo simulations in order to check simulation reliability. Finally the environmental neutron flux was simulated for the RAD3 (no neutron shield) and RAD4 configuration and compared with experimental results. Fig. 8 (right panel) shows the background predicted by our MonteCarlo simulation for the RAD4 measurements. The simulation was realized using FLUKA for the evaluation of the neutron and gamma flux impinging on the RAD array and GEANT4 for the evaluation of the energy spectrum measured by the detectors. Simulations and experimental results agree within a factor 3. Similar results (an agreement within a factor 2) have been obtained when comparing n source measurement performed with a shielded/unshielded portable Ge diodes.

Finally the environmental neutron background predicted for RAD3 and RAD4 shielding configuration is more than one order of magnitude lower than what measured. This, toghether with the results achieved in MonteCarlo validation, rules out neutron as a relevant background source.

Once summed, in order to increase the statistic significance of the measurement, the results of this final version of the RAD detector can be summarized as follows:

- crystal surface contaminations in ^{232}Th and ^{238}U are reduced by a factor ~ 4 with respect to CUORICINO;

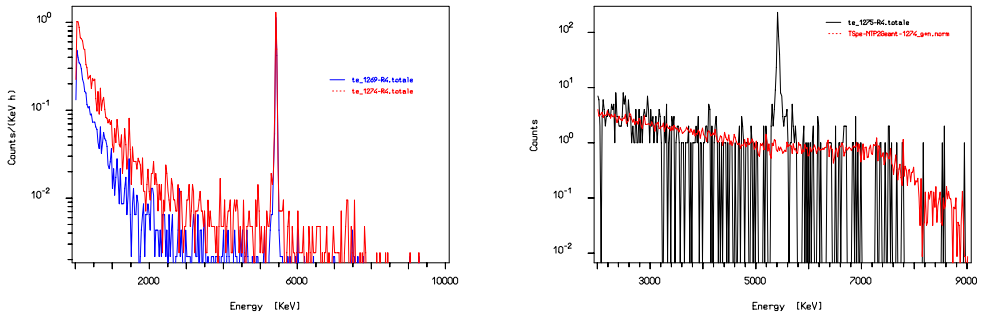

Figure 8: Left: comparison of the spectra obtained with the neutron source measurements performed with (blue) and without (red) neutron shielding. Right: Comparison between measurement with naked neutron source (black) and Montecarlo simulation (red).

Table 2: TeO_2 bulk contaminations as identified in RAD3+RAD4.

isotope	concentration	α lines	origin	comments
^{190}Pt		3290	nat. Pt	α decays on a stable isotope - no γ or β
^{232}Th	$2\pm1\ 10^{-13}$ g/g	4080	^{232}Th	appearently in sec. eq.
^{230}Th	$2\pm1\ 10^{-18}$ g/g	4750	^{238}U	not in sec. eq. with ^{238}U
^{210}Po	$< 1\ 10^{-5}$ Bq/kg	5407	^{238}U	not in sec. eq. with ^{238}U but with ^{210}Pb
^{238}U	$< 2\ 10^{-14}$ g/g	-	^{238}U	upper limit for ^{238}U in sec. eq.

- crystal bulk contaminations have been measured with a sensitivity much higher than in CUORICINO (where α bulk lines were partially covered by the surface contamination peaks) the results are summarized in table 2;
- the 5.4 MeV ^{210}Po peak is stable in time, therefore can be ascribed to a ^{210}Pb contamination;
- the 5.3 MeV ^{210}Po peak, quite high in RAD1, was due to a contamination of the copper surface and it is efficiently reduced, to a level compatible to the CUORICINO one, by means of the polyethylene film used in RAD3 and RAD4. The 5.3 and 5.4 MeV peaks have almost the same intensity and could be both ascribed to the same surface contamination of the crystals;
- the surface treatment plus the polyethylene coverage of the copper have reduced the 3-4 MeV counting rate by a factor 2.0 +/- 0.4 (i.e. to 0.06±0.0116 c/keV/kg/y, to be compared with the 0.122±0.003 c/keV/kg/y of CUORICINO in the region just above the Tl line);

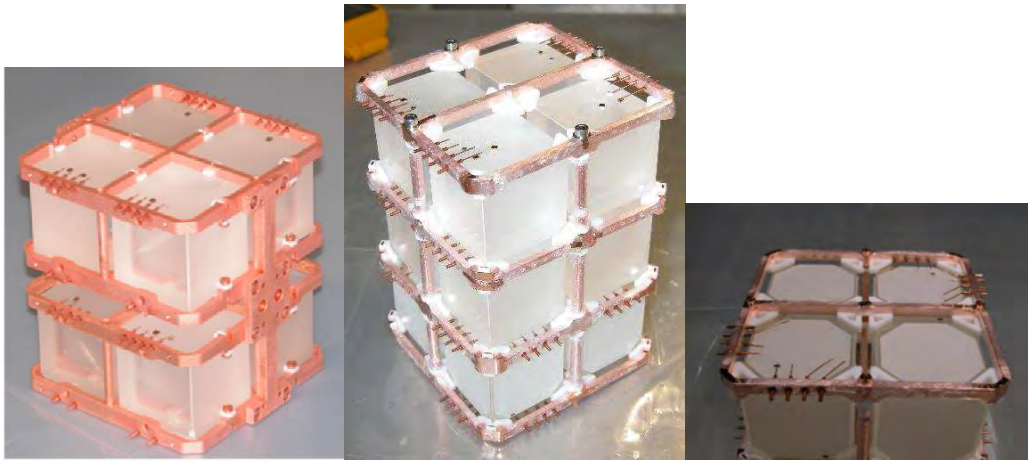

Figure 9: The RAD1 detector (left) and CAW2 detector (center) tested in hall C. The top and middle planes host four 5×5×5 cm^3 crystals while the bottom plane (in detail at the left) hosts four 5×5×5 cm^3 crystals coupled with SSB detectors.

5 The CAW detector

The CAW detector is a 3 plane array having a structure a little bit different from that of RAD and of CUORICINO. This new design is the result of an intense program of optimization of the CUORE detector structure started in 2004, involving all aspects of the single module structure and of its assembly procedure in the final CUORE towers. The new structure should guarantee a high degree of reproducibility in its mechanical features as well as a simply assembly and a reduced amount of inert material (i.e. Copper) in between the detectors. Assuming that a large fraction of the background is due to surface contamination of the mounting structure the reduction by about a factor 2 of the copper surface interposed between the detectors is particularly relevant. The CAW detector is a prototype constructed and succesfully tested in 2005 from the technical point of view (i.e. detector performances). At the beginning of 2006 this same array was used for a background test.

The copper of the mounting structure was treated as for RAD1 and was covered with polyethylene as in RAD3. The 12 crystals were treated also with a surface cleaning procedure similar to the one applied to RAD1 crystals. In the top plane of the array four CTI 5×5×5 cm^3 TeO_2 crystals were mounted. These crystals, bought from CTI (Crystal Technology Incorporated - CA - USA), had to be examined since CTI is a possible provider for CUORE detectors. In the middle and bottom planes eight 5×5×5 cm^3 TeO_2 crystals, bought as usual from SICCAS (China), were mounted. Each of the four crystals in the bottom plane were coupled to six SSB. An SSB is a thin TeO_2 slab glued with four spot to the 5×5×5 cm^3 crystal surface and covering almost completely that surface. The SSB is an "active" detector if it is provided with a thermal sensor while it is a passive shield if it is not (more on SSB in [3]). On two crystals all the SSB were provided with a NTD Ge thermistor ("active" slabs) while on the other two only one of the six slabs had a sensor, the other being "passive" (the effect of a passive slab is to produce a deformation

of pulses originated at the crystal surface and sharing energy between crystal and slab). The purpose of this measurement were:

- check performances and radioactivity of CTI crystals
- check the background achievement obtained with RAD3+RAD4 in a different structure and with different crystals, proving therefore the reproducibility of the cleaning technique
- check the SSB performaces with active and passive TeO_2 slabs
- compare SSB coupled crystal background with RAD in order to understand better the background origin

The results obtained so far were:

- the CTI crystals show a huge ^{210}Po contamination and a ^{232}Th contamination slightly higher that the one typical of the chinese crystals;
- the RAD3+RAD4 results are confirmed, proving that the surface cleaning procedure of crystals and copper are reproducibile;
- either active and passive TeO_2 slabs produce a deformation of surface events;

The only uncertainty in this run was the conclusion about the 3-4 MeV flat background source. The answer should have come by the comparison of the rates measured by the two lowest planes: both with chinese crystals, one with SSB the other without SSB. With SSB perfectly working this would have given a strong indication in favour or against the hypotesis of a copper origin of the background source. Unfortunately one SSB detached from its crystal, for two we lost the electrical contact and finally all the SSB showed an excess alpha surface contamination (SSB were not surface treated as the 1ciccio crystals). As a result the rejection capability of SSB could not be exploited to their best and the background rate only slighlty lower than the one measured by the crystals without SSB made difficult to draw any conclusion concerning copper.

6 Summary, future plans and conclusions

In conclusion while we appearently have a technique that can get rid of the U and Th surface contamination of the crystals, we have not yet find a completely satisfactory solution for the contaminations responsible of the major fraction of that flat continuous background that extends from 4 MeV down to the $\beta\beta(0\nu)$ region. We have however proved that, as predicted by the CUORICINO background model, surface contamination of the copper play a relevant role in 3-4 MeV background. This is clearly evident by comparing RAD1 and RAD3+RAD4 counting rates: RAD1 had a rate comparable with CUORICINO while RAD3+RAD4 (the only change was the polyethylene coverage of copper) had a rate lower by a factor 2. The residual contamination we are presently measuring - if attributed once again to the surfaces (this time of polyethylene mainly) -

would produce a background rate in CUORE that, extrapolated to the $\beta\beta(0\nu)$ region, is of about 0.03 c/keV/kg/y (this because the total amount of copper facing the crystals in much reduced in CUORE). However the low level of background we are presently measuring (0.06 ± 0.01) could make contribution coming from other sources not negligible, particularly if more than one "small" contribution sum up to produce the measured rate. The possible sources we plan to investigate in the future are:

1. PTFE radioactive contribution (indeed according to RAD2 can give a not negligible fraction of the counting rate);
2. glue (the one used for thermistor and heater);
3. thermal signals coming from PTFE relaxation of internal stresses;
4. environmental neutrons
5. environmental muons
6. new Copper surface treatment including the Plasma cleaning

The neutron source calibration performed during CAW2 run allowed us to check our MonteCarlo simulation. This was the fundamental necessary step toward a reliable evaluation of the background induced by environmental neutrons. We plan to reproduce the same measurement in the next future collecting a larger statistic for a more quantitative validation of MonteCarlo on both continuum an peaks. In the next future the RAD detector will be used to test the possibility that part of the background comes from PTFE parts, either due to their radioactivity or to their thermal signals.

7 List of 2006 Publications

1. P. Gorla, R. Ardito, C. Arnaboldi et al., *Cuoricino and Cuore detectors: developing big arrays of large mass bolometers for rare event physics*, Nucl Phys B-Proc Sup 150 (2006) 214-218. Elsevier Science, Amsterdam, Paesi Bassi. Proceedings of the "9th Topical Seminar on Innovative Particle and Radiation Detectors", 23 - 26 May 2004, Siena, Italy

2. R. Ardito et al., *The Cuoricino and Cuore Double Beta Decay experiments*, Prog Part Nucl Phys 57 (2006) 203-216. Elsevier Science, Amsterdam, Paesi Bassi. Proceedings of the International Workshop of Nuclear Physics, 27th course - Neutrinos in Cosmology, in Astro, Particle and Nuclear Physics, Erice, Sicily, Italy, 16-24 September 2005

3. C. Nones, L. Foggetta, A. Giuliani, M. Pedretti, C. Salvioni and S. Sangiorgio, *Developement of new bolometers for rare events with background active discrimination*, Prog. Particle and Nuclear Physics, 57 (2006) 269-271, Elsevier Science, Amsterdam, Paesi Bassi. Proceedings of the International Workshop of Nuclear Physics, 27th course - Neutrinos in Cosmology, in Astro, Particle and Nuclear Physics, Erice, Sicily, Italy, 16-24 September 2005

4. S. Pirro et al., *Further developements in the Cuoricino experiment*, Nuclear Inst. and Methods in Physics Research A 559 (2006) 352-354. Elsevier Science, Amsterdam, Paesi Bassi. Proceedings of the "11th Intenational Workshop on Low temperature Detectors", Tokyo, Japan, 31 July - 5 August, 2005.

5. C. Nones et al., *A new method for background rejection with surface sensitive bolometers*, Nuclear Inst. and Methods in Physics Research A 559 (2006) 355-357. Elsevier Science, Amsterdam, Paesi Bassi. Proceedings of the "11th Intenational Workshop on Low temperature Detectors", Tokyo, Japan, 31 July - 5 August, 2005.

6. C. Arnaboldi, G. Pessina and S. Pirro, *The cold preamplifier set-up of Cuoricino: towards 1000 channels*, Nuclear Instruments and Methods in Physics Research A 559, (2006) 826-828, Elsevier Science, Amsterdam, Paesi Bassi. Proceedings of the "11th Intenational Workshop on Low temperature Detectors", Tokyo, Japan, 31 July - 5 August, 2005.

7. S. Pirro, *Further developements in mechanical decoupling of large thermal detectors*, Nuclear Instruments and Methods in Physics Research A 559, (2006) 361-363, Elsevier Science, Amsterdam, Paesi Bassi. Proceedings of the "11th Intenational Workshop on Low temperature Detectors", Tokyo, Japan, 31 July - 5 August, 2005.

8. C. Nones, L. Foggetta, A. Giuliani, M. Pedretti, C. Salvioni, S. Sangiorgio, *A "must" for a Double Beta Decay experiment: the reduction of the background*, AIP Conference Proceedings 870 (2006) 591-593, Proceedings of the "9th Conference on the Intersections of Particle and Nuclear Physics (CIPANP2006)", Westin Rio Mar Beach, Puerto Rico (USA), 30 May-3 June 2006

9. M. Pedretti et al., *The road to the inverted hierarchy region for neutrino mass: the Cuoricino and Cuore experiments*, AIP Conference Proceedings 870 (2006) 525-528, Proceedings of the "9th Conference on the Intersections of Particle and Nuclear Physics (CIPANP2006)", Westin Rio Mar Beach, Puerto Rico (USA), 30 May-3 June 2006

10. S.Capelli, *Cuoricino latest results and background analysis*, Neutrino 2006 Conference Proceedings, in press., 2006

11. S .Capelli et al., *Cuoricino and Cuore R&D*, Proceedings of the "XXXIII International Conference on High Energy Physics (ICHEP06)", 26 July - 2 August 2006, Moscow, Russia, in press., 2006

12. J. Beeman et al., *CUORE: an experiment to investigate Neutrinoless Double Beta Decay by cooling 750 kg of TeO2crystals at 10 mK*, AIP Conference Proceedings 850 (2006) 1623-1626. Proceedings of the "24th International Conference on Low Temperature Physics - LT24", 10 - 17 August 2005, Orlando, Florida, USA

13. P. Gorla et al., *New Cuoricino results on the way to Cuore*, Phys. Scr. T127 (2006) 49-51

14. S. Sangiorgio et al., *Neutrinoless Double Beta Decay Search for Te-130: Cuoricino status and Cuore prospects*, Proceedings of the "5th Conference on Nuclear and Particle Physics (NUPPAC05)", Cairo, Egitto, 19-23 November 2005.

References

[1] C. Arnaboldi et at., Phys. Lett. B 584 (2004) 260.

[2] C. Arnaboldi et al., NIM A518 (2004) 775, R. Ardito et al, hep-ex/0501010.

[3] CUORE Collaboration, LNGS Annual Report 2005.

DAMA. Dark Matter Search

P. Belli[a], R. Bernabei[a,@], A. Bussolotti[a,*], F. Montecchia[a], F. Nozzoli[a], A. d'Angelo[b], F. Cappella[b], A. Incicchitti[b], A. Mattei[b,*], D. Prosperi[b], S. Castellano[c], R. Cerulli[c], C.J. Dai[d], H.L. He[d], H.H. Kuang[d], J.M. Ma[d], X.D. Sheng[d], Z.P. Ye[d,e]

in neutron measurements: M.Angelone[f], P.Batistoni[f], M.Pillon[f]

in some by-product results and small scale experiments: R.S. Boiko[g], F.A. Danevich[h], V.V. Kobychev[h], S.S.Nagorny[h], D.V. Poda[h], V.I. Tretyak[h], S.S. Yurchenko[h]

in some studies on $\beta^+\beta^+$, EC/β^+, EC/EC decay modes (under the joint Indo-Italian DST-MAE project): P.K. Raina[i], A.K. Singh[i], P.K. Rath[i], A. Shukla[i]

[a]Dip. di Fisica, Università di Roma "Tor Vergata" and INFN-Roma Tor Vergata, 00133 Roma, Italy;
[b]Dip. di Fisica, Università di Roma "La Sapienza" and INFN-Roma, 00185 Roma, Italy;
[c]Laboratorio Nazionale del Gran Sasso, INFN, 67010 Assergi (Aq), Italy;
[d]IHEP, Chinese Academy, P.O. Box 918/3, Beijing 100039, China;
[e]Physics Dept, Jing Gangshan University 343009, Jiangxi, China;
[f]ENEA - C. R. Frascati, P.O. Box 65, 00044 Frascati, Italy;
[g]Chemical Dept., Kiev National Taras Shevchenko University, MSP 01033 Kiev, Ukraine.
[h]Institute for Nuclear Research, 252650 Kiev, Ukraine.
[i]Indian Institute of Technology, Kharagpur, India.
@ Spokesperson
* technical staff

Abstract

DAMA is an observatory for rare processes and it is operative deep underground at the Gran Sasso National Laboratory of the I.N.F.N. (LNGS). The main experimental set-ups are: i) DAMA/NaI ($\simeq$ 100 kg of highly radiopure NaI(Tl)), which completed its data taking on July 2002; ii) DAMA/LXe ($\simeq$ 6.5 kg liquid Kr-free Xenon enriched either in ^{129}Xe or in ^{136}Xe); iii) DAMA/R&D, devoted to tests on

prototypes and to small scale experiments, mainly on the investigations of double beta decay modes in various isotopes; iv) the new second generation DAMA/LIBRA set-up ($\simeq$ 250 kg highly radiopure NaI(Tl)) in operation since March 2003. Moreover, in the framework of devoted R&D for radiopure detectors and photomultipliers, sample measurements are carried out by means of the low background DAMA/Ge detector (installed deep underground since more than 10 years) and, in some cases, by means either of mass spectrometers or of other facilities. In some measurements on rare processes also the four-Ge facility of LNGS is used. In the following main arguments on the activity during 2006 are summarised.

1 DAMA/NaI

The highly radio-pure DAMA/NaI set-up [1, 2, 3, 4] has been a pioneer Dark Matter experiment of suitable exposed mass, sensitivity and stability of the running conditions, taking data at LNGS over seven annual cycles. The data taking has been completed in July 2002 and still results are produced by various kinds of studies.

The main aim of DAMA/NaI has been the investigation of the presence of Dark Matter (DM) particles in the galactic halo by exploiting the model independent annual modulation signature (see refs. [2, 3, 4, 5, 6, 7, 8, 9, 10, 11, 12] and in the 2006 publication list), originally suggested by [13, 14] in the middle of 80's. In addition, profiting by its low-background features and by the high collected exposure, several results have been achieved both on Dark Matter particle investigations with other approaches and on several other rare processes (see refs. [15, 16, 17, 18, 19, 20, 21, 22] and the 2006 publication list).

The DAMA/NaI set-up has pointed out the presence of an annual modulation in the *single-hit* residual rate in the lowest energy interval $(2-6)$ keV (see Fig.1). The observed effect satisfies the many peculiarities of a DM particle induced signature, giving a 6.3 σ C.L. evidence over seven annual cycles (total exposure: 107731 kg $\times$ day) for the presence of DM particles in our Galaxy (see refs. [2, 3, 4, 5, 6, 7, 8, 9, 10, 11, 12] and in 2006 publication list). Neither systematic effects nor side reactions able to account for the observed effect have been found.

This result is model-independent. It represents the first experimental evidence of the presence of DM particles in the halo independently on their nature. At present, apart from DAMA/LIBRA, no other experiment is sensitive, for mass, radiopurity and control of the stability, to such a model independent signature; thus, no other activity is available whose result can directly be compared with the one of DAMA/NaI.

Additional corollary investigations have also been pursued on the nature of the DM candidate particle and on the astrophysical scenarios. These corollary investigations are instead model-dependent and, due to the poor knowledge on the astrophysical, nuclear and particle physics needed assumptions and on the related parameters, they have no general meaning (as well as e.g. the exclusion plots in direct and indirect detection experiments). Thus, these investigations should be handled in the most general way (see e.g. [3, 4, 12], in the 2006 publication list and in literature). Various other scenarios have also been addressed in literature.

DAMA/NaI, having both a light (the ^{23}Na) and a heavy (the ^{127}I) target-nucleus, is intrinsically sensitive to Dark Matter particle both of low and high mass. As regards

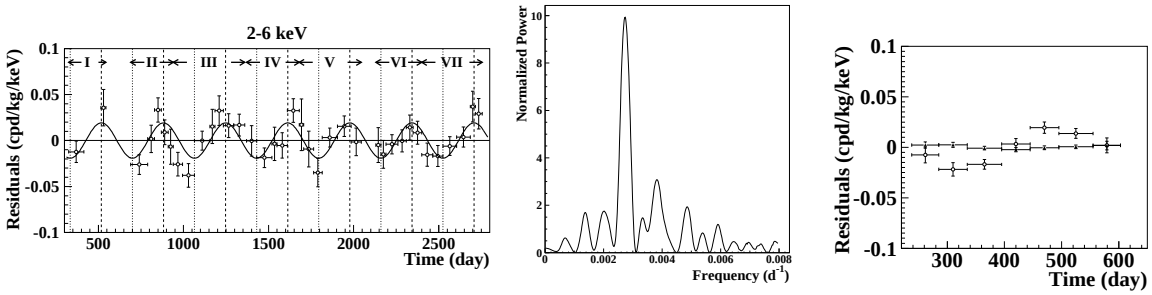

Figure 1: On the left: experimental residual rate for *single-hit* events in the cumulative (2–6) keV energy interval as a function of the time over 7 annual cycles, end of data taking July 2002. The experimental points present the errors as vertical bars and the associated time bin width as horizontal bars. The superimposed curve represents the cosinusoidal function behaviour expected for a Dark Matter particle signal with a period equal to 1 year and phase exactly at 2^{nd} June; the modulation amplitude has been obtained by best fit [3, 4]. Center: power spectrum of the measured *single-hit* residuals for the cumulative (2–6) keV energy interval calculated including also the treatment of the experimental errors and of the time binning. As it can be seen, the principal mode corresponds to a frequency of 2.737×10^{-3} d^{-1}, that is to a period of $\simeq 1$ year. On the right: experimental residual rates over seven annual cycles for *single-hit* events (open circles) – class of events to which DM events belong – and over the last two annual cycles for *multiple-hits* events (filled triangles) – class of events to which DM events do not belong – in the (2–6) keV cumulative energy interval. They have been obtained by considering for each class of events the data as collected in a single annual cycle and using in both cases the same identical hardware and the same identical software procedures. The initial time is taken on August 7^{th}.

the WIMP class of DM candidate particles, it is fully sensitive not only to spin independent (SI) coupling, but also to spin dependent (SD) one, to the SI and SD mixed case, to the preferred inelastic scattering coupling; moreover, it is favoured for several other candidates.

Several (of the many possible) corollary quests for a candidate particle have been carried out on the class of DM candidate particles named WIMPs [3, 4]; in literature several candidates for WIMPs have been considered, all foreseen in theories beyond the Standard Model of particle Physics. In particular in case of a candidate with dominant SI interaction a comparison with the expectations for a neutralino in MSSM can be found in ref. [23] in the framework of models considered in ref. [3, 4]. It is worth to remind that the neutralino itself has both SI and SD coupling and that the basic theory has a very large number of "open" parameters. Moreover, other possibilities exist with a phenomenology similar, but not identical as for the WIMP cases: the mirror Dark Matter particles [24], the self-interacting dark matter particles [25], etc. and in principle even whatever particle with suitable characteristics, even not yet foreseen by theories, can be a good candidate as DM in the galactic halo.

In addition, the corollary quest for the light ($\simeq$ keV mass) bosonic candidate, either with pseudoscalar or with scalar axion-like coupling, already described in the LNGS

annual report 2005, has been published in 2006 [12]. For these candidates, the direct detection process is based on the total conversion in NaI(Tl) crystal of the mass of the absorbed bosonic particle into electromagnetic radiation. Thus, in these processes the target nuclei recoil is negligible and is not involved in the detection process; therefore, signals from these light bosonic DM candidates are detected in DAMA/NaI, but are lost in activities applying rejection procedures of the electromagnetic contribution to the counting rate (such as e.g. Cdms, Edelweiss, Cresst, Warp, etc.) [12]. Despite these particles are unstable, their lifetime can be of cosmological interest and offers valuable candidates for the DM signal, observed in DAMA/NaI. In particular, results for the pseudoscalar case is shown in Fig. 2.

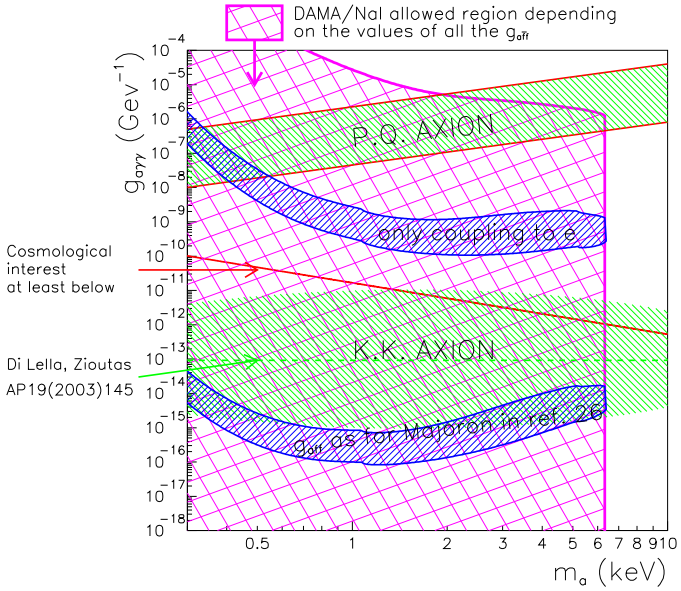

Figure 2: DAMA/NaI allowed region at 3σ C.L. in the plane $g_{a\gamma\gamma}$ vs m_a for a light pseudoscalar candidate (*crossed hatched region*). All the configurations in this region can be allowed depending on the values of all the $g_{af\bar{f}}$. Examples of two of the many possible models: i) *upper black region*: coupling only to electrons; ii) *lower black region*: coupling (proportional to the m_a) through the (weak) isospin to quarks and leptons. For details see ref. [12]. The indicative region of the Kaluza-Klein (K.K.) pseudoscalar axion credited in ref. [26] from the analysis of indirect observations and the region of the DFSZ and KSVZ models (P.Q. axion) are shown as well. The solid line corresponds to a particle with lifetime equal to the age of the Universe; at least all the $g_{a\gamma\gamma}$'s below this line are of cosmological interest. However, in principle, it might be possible that the configurations above this line would also become of interest in case of some exotic mechanism of the a particle production. Thus, a pseudoscalar DM candidate could also account for the DAMA/NaI model independent result as well as the WIMP solutions already discussed elsewhere.

Obviously, these results are not exhaustive of the many scenarios (still possible at present level of knowledge) for these and for other classes of candidates as well as for the astrophysical and nuclear/atomic aspects. In particular, during 2006 we have published

a paper where the effect of the inclusion of the contribution of the SagDEG tidal streams has been investigated considering as example some of the corollary analyses for WIMPs cases already analysed in refs. [3, 4].

1.1 Further corollary investigations during 2006: SagDEG

In 2006 we have investigated the consequences, on the annual modulation result, of the DM stream contribution to the galactic halo due to the SagDEG, the best known satellite galaxy of the Milky Way crossing the solar neighbourhood. In fact, Galaxy hierarchical formation theories [27], numerical simulations [28], the discovery of the Sagittarius Dwarf Elliptical Galaxy (SagDEG) in 1994 [29] and more recent investigations [30] suggest that the dark halo of the Milky Way can have a rich phenomenology containing non thermalized dark matter fluxes. The presence of DM streams would induce a (slightly) variation of the phase value of the modulated component of the signal; such a variation can also depend on the energy.

For simplicity, in this analysis we have investigated these topics just considering some of the candidates belonging to the WIMP class and some of the many possible astrophysical, nuclear and particle Physics scenarios already considered in refs. [3, 4] in order to allow a direct comparison.

Despite the fact that SagDEG is the best known satellite galaxy of the Milky Way crossing the solar neighbourhood, some important quantities such as the value of the mean velocity of the stream, its direction and its velocity dispersion are not yet well known. Thus a large number of related investigations can be found in literature. In particular we have modelized the stream taking into account the different values reported in ref. [32] (derived from the analysis of eight clump stars – from Chiba and Yoshii catalogue [33] – attributed to the SagDEG tail) and in ref. [31] (based on a SagDEG simulation model). For the latter case, the corresponding stream mean velocities have been derived by considering the spherical, the oblate and the prolate halo models selecting for each one of these models the $\simeq 100$ configurations nearest to the Sun within a distance $\lesssim 2.5$ kpc (see Fig. 3; for details see in the 2006 publication list).

In conclusion, we have derived and used the following values for the stream velocity and dispersion: $\vec{V}_{8*} = (V_x, V_y, V_z) = (-65 \pm 22, 135 \pm 12, -249 \pm 6)$ km/s, $(\sigma_x, \sigma_y, \sigma_z)_{8*} =$

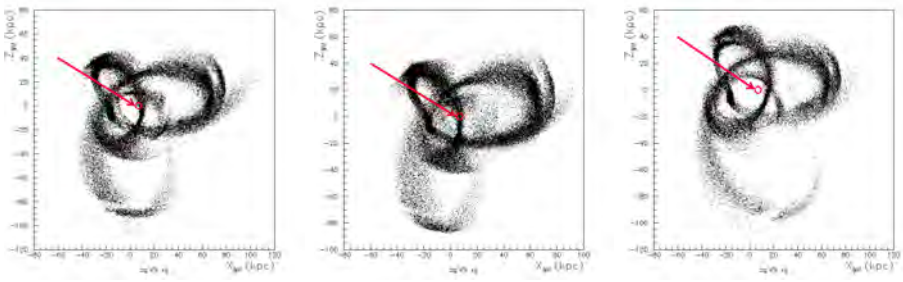

Figure 3: SagDEG simulation models for spherical (left), oblate (center) and prolate (right) halo potentials; data taken from ref. [31]. In each panel the circle pointed by the arrow selects the Earth position and the configurations considered in this paper for the evaluation of the used mean velocity values: $\vec{V}_{sph}$ and $\vec{V}_{obl}$. We note that no configuration is present in the solar neighbourhood for the prolate model.

$(62, 33, 17)$ km/s, to account for [32] reporting 1σ error for each velocity component; $\vec{V}_{sph} = (V_x, V_y, V_z) = (-86 \pm 14, 69 \pm 3, -384 \pm 1)$ km/s, $(\sigma_x, \sigma_y, \sigma_z)_{sph} = (60, 19, 8)$ km/s and $\vec{V}_{obl} = (V_x, V_y, V_z) = (-57 \pm 8, 79 \pm 3, -395 \pm 1)$ km/s, $(\sigma_x, \sigma_y, \sigma_z)_{obl} = (59, 23, 9)$ km/s, to account for [31] calculating velocity dispersions as r.m.s. values of the $\simeq 100$ considered configurations; note that the prolate model has not been considered since it does not provide configurations in the solar neighbourhood.

As regards the phase of the modulation, the net effect of a SagDEG tail contribution to the local halo density is a shift of few days (towards January) in the expected phase of the signal depending on the detected energy. We remind that the DAMA/NaI results (107731 kg $\times$ day exposure) provide $t_0 = (140 \pm 22)$ day averaged in the (2-6) keV energy window; larger exposures, which will be available in near future thanks to the presently running DAMA/LIBRA set-up [34], will offer the possibility of more stringent constraints.

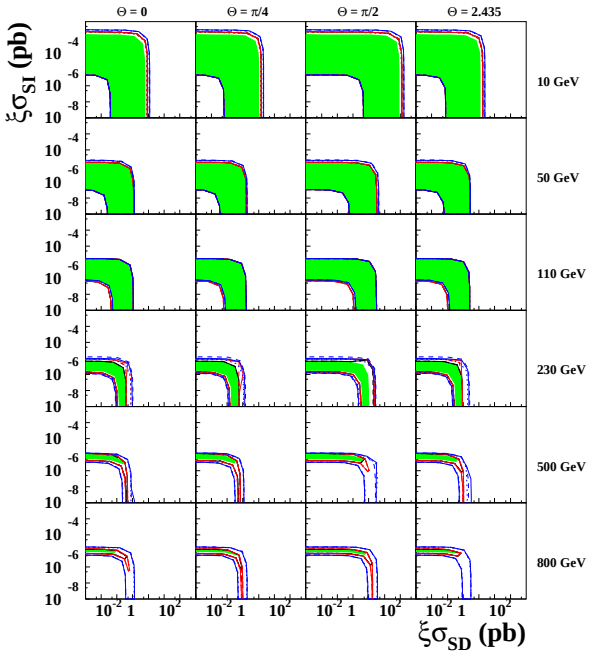

Figure 4: Examples of slices of the four-dimensional allowed volume in the $(\xi\sigma_{SI}, \xi\sigma_{SD})$ plane for some m_W and θ values in the considered scenarios. The shaded regions have been determined for no SagDEG contribution [3], while the areas enclosed by the lines are obtained by introducing in the analysis the SagDEG stream with DM density not larger than 0.1 GeV cm^{-3}. The nine considered possibilities for the SagDEG stream veloctity ($\vec{V}_{8*}$ (blue), $\vec{V}_{sph}$ (black), $\vec{V}_{obl}$ (red)) and $v_{0,sgr}$ dispersion (20 km/s (dashed), 40 km/s (solid) and 60 km/s (dotted)) have been reported. Inclusion of other uncertainties on parameters and models would further extend the regions; for example the use of more favourable form factors and/or of more favourable spin factors would move them towards lower cross-sections.

For simplicity, for the SagDEG stream description we have considered the three possibilities for the velocity ($\vec{V}_{8*}$, $\vec{V}_{sph}$ and $\vec{V}_{obl}$ at their central values) and three possible velocity dispersions ($v_{0,sgr} = 20, 40, 60$ km/s), obtaining nine different cases for each considered halo model (see [3, 4] and in 2006 publication list). In addition, we have also

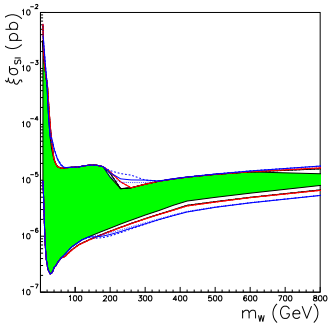

Figure 5: Region allowed in the $(\xi\sigma_{SI}, m_W)$ plane in the considered scenarios for pure SI coupling. The filled region has been determined for no SagDEG contribution [3, 4], while the areas enclosed by lines are obtained by introducing in the analysis the SagDEG stream with DM density not larger than 0.1 GeV cm^{-3}. The nine considered possibilities for the SagDEG stream velocity ($\vec{V}_{8*}$ (blue), $\vec{V}_{sph}$ (black), $\vec{V}_{obl}$ (red)) and $v_{0,sgr}$ dispersion (20 km/s (dashed), 40 km/s (solid) and 60 km/s (dotted)) have been reported. Inclusion of other uncertainties on parameters and models would further extend the regions; for example the use of more favourable form factors would move them towards lower cross-sections.

imposed that the SagDEG density contribution cannot exceed $\sim$0.1 GeV cm^{-3}, as suggested by M/L ratio considerations of ref. [32]. The results of these corollary quests for the candidate particle – reported in Fig. 4, 5 and 6 – are presented in terms of allowed regions obtained as superposition of the configurations corresponding to likelihood func-

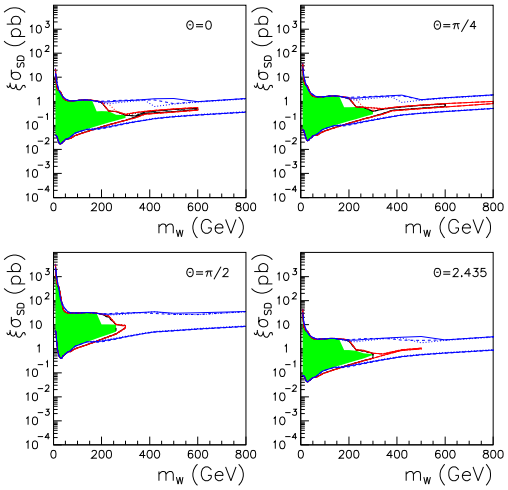

Figure 6: Examples of slices of the three-dimensional allowed volume in the $(\xi\sigma_{SD}, m_W)$ plane for some θ values in the considered scenarios and for pure SD coupling. See Fig. 5 for the meaning of the regions. Inclusion of other uncertainties on parameters and models would further extend the regions; for example the use of more favourable form factors and/or of more favourable spin factors would move them towards lower cross-sections.

tion values *distant* more than 4σ from the null hypothesis (absence of modulation) in each

of the several (but still a limited number) of the possible model frameworks. These results are not exhaustive of the many scenarios possible at present level of knowledge (e.g. for some other recent ideas see [35, 36]) and larger sensitivities than those reported in the following would be reached when including the effect of other existing uncertainties on assumptions and related parameters (see e.g. [3, 4]).

As it can be seen, the SagDEG stream contribution and the related uncertainties significantly modifies the allowed volumes/regions, mainly for larger WIMP masses enlarging as well the sets of best-fit values.

On the other hand, an analysis has also been pursued giving the possibility to set some cautious constraints on the density of the SagDEG stream in the galactic halo and, consequently, on the presence of substructure in the halo, by means of the observed DAMA/NaI annual modulation effect. In fact, by exploiting the likelihood ratio method, the best values for the SagDEG parameters compatible with the annual modulation data have been derived with the respect to all the others quantities involved in the calculation. In this approach, fixing the SagDEG velocity set and velocity dispersion, the WIMP mass (labeled as m_W) and θ, the galactic halo model and all the other needed parameters, a best fit value for ρ_{sgr} has been derived at some C.L.. In this analysis we have investigated for simplicity only the purely SI and the purely SD cases, obtaining, for each considered m_W and stream set velocity, the 90% C.L. allowed intervals on ρ_{sgr}. Fig. 7 shows these intervals as a function of m_W, for pure SD coupling ($\theta = 0, \pi/2, \pi/4$ and 2.435, pure Z_0 coupling). For other cases see 2006 publication list.

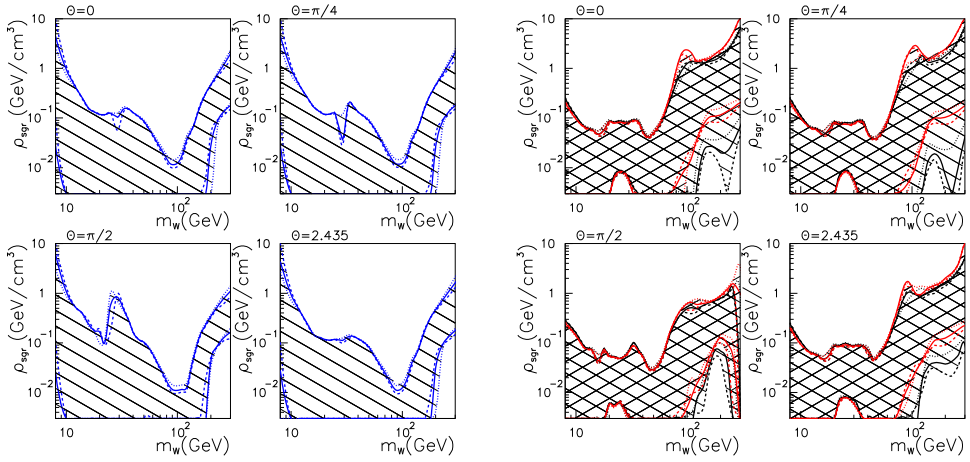

Figure 7: SagDEG density ρ_{sgr} allowed at 90% C.L. (hatched area) for pure SD coupling as function of m_W values for some of the possible θ values. Left 4-box: case of $\vec{V}_{8*}$ velocity set. Right 4-box: case of $\vec{V}_{sph}$ (descending hatched) and $\vec{V}_{obl}$ (ascending hatched) superimposed. The used stream velocity dispersion, $v_{0,sgr}$ values are: 20 km/s (dashed), 40 km/s (solid) and 60 km/s (dotted). For details see 2006 publication list.

It is worth to note that in many of the analyzed configurations the inclusion of the SagDEG contribution improves the data fit. For example, for SI candidate in the case of a stream with velocity set $\vec{V}_{sph}$ and velocity dispersion $v_{0,sgr} = 40$ km/s, about 67% of the configurations have an improvement of the data fit by the inclusion of the SagDEG; in particular, the improvement of about 18% of them is better than 2 σ. Finally, the plot

of the cumulative percentage distribution of ρ_{sgr} best-fit values for the various considered models, providing a C.L. better than 2 σ with the respect to the absence of SagDEG, shows that about 60% of these models gives ρ_{sgr} best-fit values below 0.1 GeV cm^{-3}; in addition, the distribution peaks around $\rho_{sgr} \sim 0.04$ GeV cm^{-3}. These latter values are intriguing considering the expectations on the stream density at Sun position – that is few % of the local dark halo – based on some theoretical studies about the disruption of the satellite galaxies falling in the Milky Way halo [37].

In conclusion this investigation has also pointed out the potentiality of the used approach to study the halo composition as well as to derive experimental bounds on the possible contribution of the SagDEG to the local dark matter density. It is worth to note that, for some of the investigated WIMP masses, the order of magnitude of these bounds, obtained by local measurements, is in agreement with the existing bounds based on non-local M/L ratio observations.

Other streams can potentially play more intriguing roles in the corollary investigations for whatever candidate particle with whatever approach and for comparisons; they will be investigated in near future, such as e.g. the Canis Major [30] and those arising from caustic halo models [36]. In addition, other candidates and other non thermalized substructures will be addressed in near future studies; in particular, the availability of larger exposures by DAMA/LIBRA will offer the possibility of more efficient discrimination capability among – at least some of – the many possible different astrophysical, nuclear and particle physics scenarios.

1.2 Comparisons in the field

No experiment is available - with the exception of the presently running DAMA/LIBRA - whose result can be directly compared in a model independent way with the experimental positive 6.3 σ C.L. evidence for the presence of particle Dark Matter in the galactic halo obtained by DAMA/NaI. Thus, claims for contradictions have intrinsecally no scientific meaning.

In particular, as regards some claimed model-dependent comparisons we just mention – among the many existing arguments – that: i) the other experiments are insensitive to the annual modulation signature; ii) they release just a marginal exposure (orders of magnitude lower than the one by DAMA/NaI) after several/many years underground; iii) they exploit strong data selection and strong and often unsafe rejection techniques of their huge counting rate, becoming at the same time insensitive to several DM candidates; iv) they generally quote in an incorrect/partial/not updated way the DAMA/NaI result (see even in some LNGS web sites and reports); v) they consider a single model fixing all the astrophysical, nuclear and particle Physics assumptions as well as all the theoretical and experimental parameters at a single questionable choice [1]. Thus, e.g. for the WIMP

[1] We note that the naive and partial "prescription" of ref. [38] on some aspects for a single particular WIMP case cannot be defined – on the contrary of what appears in some paper – as a "standard theoretical model". Such a paper summarized a single oversimplified approach adopted at that time. Its use as "unique" reference is obviously uncorrect, since it did not account at all for the level of knowledge on all the involved astrophysics, nuclear and particle physics aspects and parameters, for the many possibilities open on the astrophysical, nuclear and particle physics aspects and for the different existing approaches.

case they do not account for the existing uncertainties on the real coupling with ordinary matter, on the spin-dependent and spin-independent form factors and related parameters for each nucleus, on the spin factor used for each nucleus, on the real scaling laws for nuclear cross sections among different target materials; on the experimental and theoretical parameters, on the effect of different halo models and related parameters on the different target materials, etc. For example, large differences are expected in the counting rate among nuclei fully sensitive to the SD interaction (as ^{23}Na and ^{127}I) with the respect to nuclei largely insensitive to such a coupling (as e.g ^{nat}Ge, ^{nat}Si, ^{nat}Ar, ^{nat}Ca, ^{nat}W, ^{nat}O) and also when nuclei in principle all sensitive to this coupling but having different unpaired nucleon (e.g. neutron in case of the odd spin nuclei, such as ^{129}Xe, ^{131}Xe, ^{125}Te, ^{73}Ge, ^{29}Si, ^{183}W and proton in the ^{23}Na and ^{127}I). Moreover, in case the detection of the DM particles would involve electromagnetic signals (see, for example, the case of the light bosons discussed above, but also the electromagnetic contribution in WIMP detection), all the experiments, such as e.g. Cdms, Edelweiss, Cresst, Zeplin, Warp and their extensions, do lose this signal in their rejection procedures of the e.m. contribution to the counting rate.

For completeness, it is also worth to note that no results obtained with different target material can intrinsecally be directly compared even for the same kind of coupling; in fact, this requires – among others – the knowledge of e.g. the real scaling laws (the situation is much worse than that in the field of double beta decay experiments when different isotopes are used).

Discussions at some extent are also reported in ref.[3, 4, 12], in the 2006 publication list, in literature and in previous reports; these general comments also hold in the substance for more recent data releases.

As regards the indirect searches, a comparison would always require the calculation and the consideration of all the possible DM particle configurations in the given particle model, since it does not exist a biunivocal correspondence between the observables in the two kinds of experiments. However, the present positive hints provided by indirect searches are not in conflict with the DAMA/NaI result.

Finally, it is worth to note that – among the many corollary aspects still open – there is f.i. the possibility that the particle dark halo can have more than one component. The more sensitive NaI(Tl) experiments in progress and in preparation by DAMA will also have this aspect among the arguments to be further investigated.

2 DAMA/LIBRA

In 1996 DAMA proposed to realize a ton set-up and a new R&D project for highly radiopure NaI(Tl) detectors was funded. As a consequence of the results of this second generation R&D, the new experimental set-up DAMA/LIBRA (Large sodium Iodide Bulk for RAre processes), $\simeq$250 kg highly radiopure NaI(Tl) crystal scintillators (matrix of twenty-five $\simeq$ 9.70 kg NaI(Tl) crystals), was funded and realised. This set-up has replaced the previous DAMA/NaI; the experimental site as well as many components of the installation itself have been implemented (environment, shield of the photomultipliers, wiring, High-Purity Nitrogen system, cooling water of air conditioner, electronics and data acquisition sys-

tem, etc.). In particular, all the Copper parts have been chemically etched before their installation following a new devoted protocol and all the procedures performed during the dismounting of DAMA/NaI and the installation of DAMA/LIBRA detectors have been carried out in High-Purity Nitrogen atmosphere [34].

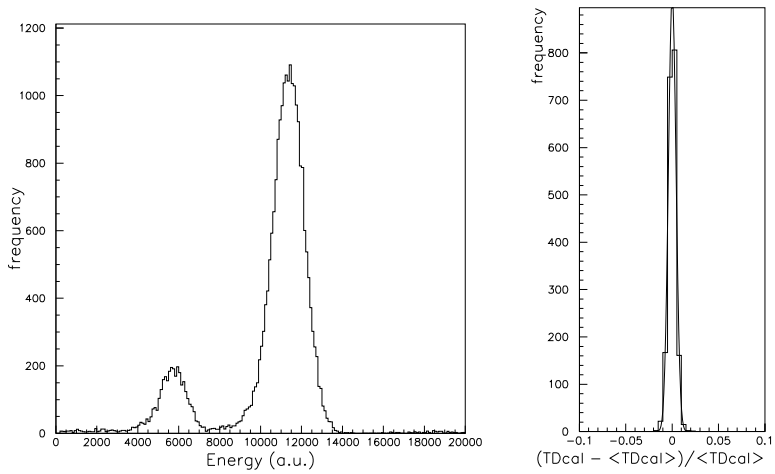

Figure 8: *Left panel*: energy distribution of the ^{241}Am source as measured by one of the new highly radiopure DAMA/LIBRA NaI(Tl) detectors (σ/E = 6.7% at 59.5 keV). *Right panels*: examples of the stability of the calibration factor (*tdcal*) during more than three years of data taking; the standard deviation is 0.5%.

DAMA/LIBRA is continuously taking data since March 2003; for example, up to March 2006, an exposure of about 10^5 kg $\times$ day was already collected. As in the case of the DAMA/NaI experiment we regularly perform routine energy calibration, e.g. in 3 years of measurements we collected about 4×10^7 sources' events. As an example in Fig. 8 – *left* the energy distribution of the ^{241}Am source as measured by one of the new DAMA/LIBRA detectors (σ/E = 6.7% at 59.5 keV) is shown and in Fig. 8 – *right* the stability of the energy scale during more than three years of data taking can be observed.

In 2006 we have also implemented the air conditioning system of the electronic room by installing an additional stand-alone conditioner which can work independently on the water cooling chiller of the underground laboratory. Moreover, we have also prepared an upgraded version of the DAQ system to be ready for the scheduled installation of the new Transient Digitizers, produced by the Acqiris Company; they will replace the Tektronix Waveform Analyzers presently in function, but no more in warranty by the company.

The main aim of the highly radiopure DAMA/LIBRA set-up is to further investigate the model independent evidence pointed out by DAMA/NaI with increased sensitivity. The larger sensitivity will also allow to better study some interesting physical and astrophysical aspects. As an example, we mention the possibility to study with large exposure the contributions of non-thermalized component to the Dark Matter particles in the galactic halo, as expected from tidal streams (from the Sagittarius Dwarf elliptical galaxy and from the Canis Major satellite galaxy), extending the analysis described above.

Moreover, other topics will be further addressed by the highly radiopure DAMA/LIBRA, such as the study (i) on the velocity and spatial distribution of the Dark Matter particles

in the galactic halo (see e.g. [3, 4]); (ii) on other possible non-thermalized components in the galactic halo, as the presence of discrete streams and caustics [36] due to the continuous infall of Dark Matter particles in the galactic gravitational field; (iii) on possible structures as clumpiness with small scale size; (iv) on the gravitational focusing effects of the Sun enhancing the Dark Matter flow ("solar wakes") [36]; (v) on the nature of the Dark Matter particles (SUSY particles in various scenarios, a neutrino of a fourth family, particles from multi-dimensional Kaluza-Klein like theories, Mirror Dark Matter, self-interacting dark matter, axion-like particles, ...); (vi) on different nuclear and particle physics models (such as coupling, inelastic interaction, particle conversion processes, ..., form factors, spin factors, ...); (vii) on scaling laws and cross sections (we remind that, even for the neutralino candidate, the usually adopted scaling laws could not hold [35]); (viii) on possible multi-component dark halo; etc. A large work will be faced by the new DAMA/LIBRA, which will also further investigate with higher sensitivity several other rare processes. The first data release is foreseen not later than 2008.

3 R&D-III towards DAMA/1ton

A third generation R&D effort towards a possible NaI(Tl) ton set-up has been funded by I.N.F.N. and related works on selection of materials for detectors and photomultipliers are in progress. This new low background NaI(Tl) set-up will also act as a "general purpose" experiment (as the previous ones) allowing to investigate not only other approaches for Dark Matter, but also many other interesting topics in underground Physics having the following main advantages: i) well known technology; ii) high radiopurity by selections, chem./phys. purifications, protocols (there is still room for improvements); iii) high duty cycle with the respect to all the experiments available so far; iv) high light response and routine calibrations feasible down to keV range in the same production run conditions; v) well controlled operational condition feasible; vi) no need re-purification procedures (reproducibility ...); vii) absence of microphonic noise; viii) no cryogenic complexities; ix) effective investigation of the annual modulation signature feasible; x) feasibility proved up to the 250 kg stage; xi) large mass feasible; xii) small underground space is needed, xiii) feasible in few years; xiv) pulse shape discrimination feasible at reasonable level in dedicated periods giving a prior for some candidates of the WIMPS class; xv) sensitivity to all the DM particle candidates, including those having interaction not involving nuclear recoils (on the contrary of all the other project based on various techniques of rejection of the electromagnetic component of the counting rate, on the use of different approach and target materials, etc.); xvi) safe and ecological clean set-up; xvii) sensitivity to several rare processes; xviii) cheaper than every other techniques considered in the field; etc.

At present measurements on several materials have been performed by DAMA/Ge and by ICP-MS. New protocols have been set in order to further reduce some trace contaminants both in the powders used for the growth of the Sodium Iodide ingot and in the housing. The production of the first 3" diameter by 3" lenght NaI(Tl) prototypes is going to start. In addition, efforts were, are and will be carried out for the production of photomultipliers with lower traces of radioactive contaminants. In this framework some photomultiplier prototypes without any glass and ceramics have been

produced; their residual contaminations are 1-2 orders of magnitude lower than the previous low-background PMTs. However, improvements in the electronic part as well as the production of larger photocatode PMTs are still necessary.

Finally, in case all the R&D's will give positive results, the already funded RD-IV as a feasibility study of a very low background 1 ton NaI(Tl) (DAMA/1ton) production will be realized. In such a case a possible design can be: i) DAMA/1ton will be realized by four replicas of DAMA/LIBRA; ii) the detectors will have similar size and shape than those already used; iii) the features of low-radioactivity of the set-up and of all the used materials will be assured by many years of experience in the field; iv) the electronic chain and controls will profit by the previous experience and by the use of compact devices already developed, tested and used; v) the new digitizers will offer high expandibility and high performances; vi) the data acquisition system will be a replica of the new one now prepared for DAMA/LIBRA.

DAMA/1ton will allow to further investigate with large exposure and larger sensitivity on the basis of the results of a model independent approach the astrophysical, nuclear and particle physics peculiarities of the DM particles in the galactic halo. Moreover, it will also offer an unique and multi-purpose set-up for the study of many other rare processes with larger sensitivity.

4 DAMA/LXe

We pointed out many years ago (see e.g. ref. [39]) the possible interest in using the liquid Xenon as target-detector material for particle dark matter investigations. Since the end of 80's (former Xelidon experiment of the INFN) we have realized several liquid Xenon (LXe) prototype detectors and, then, we have preliminarily put in measurement the set-up used in the data taking of ref. [40, 41] at LNGS; this set-up (having a Cu inner vessel filled by $\simeq$ 6.5 kg - i.e. $\simeq$ 2 l - of liquid Xenon) was firstly upgraded at fall 1995 [42, 43, 44, 45, 46]. At that time it used Kr-free Xenon enriched in ^{129}Xe at 99.5%. Then, in 2000 the set-up was deeply modified reaching the configuration of ref. [47] in order to handle also Kr-free Xenon enriched in ^{136}Xe at 68.8%. The main features of the set-up, details on the data acquisition, on the cryogenic and vacuum systems and on the running parameters control can be found in refs. [45, 46, 47, 49, 50]. Investigations on several rare processes have been carried out with time passing in the various configurations [40, 41, 42, 43, 44, 45, 46, 47, 48, 49, 51, 52, 53]. In particular, first and/or competing results have been obtained on some approaches for Dark Matter investigations, on double beta decay modes in ^{136}Xe and ^{134}Xe, on possible charge non-conserving processes, on nucleon, di-nucleon and tri-nucleon decay into invisible channels both in ^{129}Xe and in ^{136}Xe.

On the contrary of the NaI(Tl) case, plans for enlarging the exposed mass have never been considered both because of the technical reasons (specific of liquid noble gas detectors and, in particular, of liquid xenon detectors), we pointed out several times in the past (see e.g. [54]), and of the extremely expensive cost of Kr-free and enriched Xenon.

After the forbiddeness of using cryogenic liquids in the underground laboratories, the set-up has taken data just for several months until December 2004; then it has been put in

standby waiting for the restart of LNGS cooling water plant and local water refrigeration system. Its data taking will restart during 2007.

5 DAMA/R&D

The DAMA/R&D installation is a low-background set-up used for measurements on low background prototype scintillators and PMTs realized in various R&D efforts with industries. It is also regularly used to perform small scale experiments also in collaboration with INR Kiev and IIT Kharagpur. This set-up has been upgraded several times and, in particular, during 2006 the calibration facility has been modified. The small scale experiments mainly investigate double beta decay modes in various isotopes. Among the obtained results we remind the search for: i) $\beta\beta$ decay modes in ^{136}Ce and in ^{142}Ce [55]; ii) 2EC2ν decay mode in ^{40}Ca [56]; iii) $\beta\beta$ decay modes in ^{46}Ca and in ^{40}Ca [57]; iv) $\beta\beta$ decay modes in ^{106}Cd [58]; v) $\beta\beta$ and β decay modes in ^{48}Ca [59]; vi) 2EC2ν in ^{136}Ce and in ^{138}Ce and α decay in ^{142}Ce [60]; vii) $2\beta^+0\nu$ and EC$\beta^+0\nu$ decay in ^{130}Ba [61]; viii) cluster decay in ^{138}La and ^{139}La [62]. Both the active and the passive source techniques have been exploited as well as – sometimes – the coincidence technique. Fig. 9 summarizes the many results obtained by DAMA in the searches for double beta decay modes.

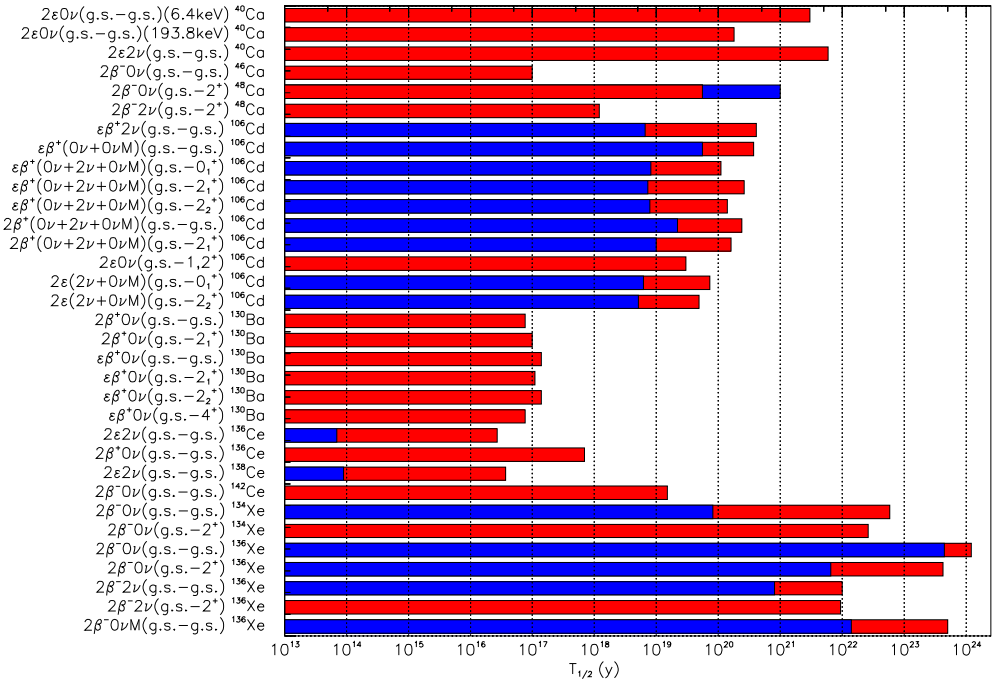

Figure 9: Summary of the $T_{1/2}$ limits obtained by DAMA (light shaded bars) and by previous experiments (dark bars) on various double beta decay processes All limits are at 90% C.L. except the $2\beta^+0\nu$ of ^{136}Ce and $2\beta^+0\nu$ of ^{142}Ce that are at 68% C.L..

5.1 Activities in 2006

In 2006 the activity was focused on:

1. the search for possible CNC decay of ^{139}La into ^{139}Ce (performed for the first time);
2. completion of data analysis of CaF_2(Eu) experiment, performed to observe for the first time the rare α decay of ^{151}Eu;
3. conclusion of the data taking of the $CdWO_4$ experiment;
4. installation of the $ZnWO_4$ detector presently in data taking.
5. a new larger BaF_2 scintillator, available for new measurements in future.
6. the completion of the studies on depletion of the about 150 g of ^{106}Cd from the ^{113}Cd as well as on the possibilities of using it for growing a scintillator; the related works are expected to be completed at end of year 2007 and the data taking is foreseen in 2008/2009.

Here we summarize just the first search for the possible CNC decay of ^{139}La into ^{139}Ce, by exploiting the "source = detector" technique and by using the $LaCl_3$:(8.5±1.0%)Ce crystal (25.4±0.2 mm in diameter by 25.4±0.2 mm length), of (49.7±1.3)g mass, coupled to a low background photomultiplier through a Tetrasil-B light guide (7.6 cm diameter 10 cm long). A detailed description of the used set-up has been given in ref. [62], where the same data have been analysed to investigate the features of the detector and some possible cluster decays modes in La isotopes.

The conservation of the electric charge, which is related with a gauge invariance and masslessness of a photon in accordance with the Weinberg theorem [63], is considered as an absolute law in the standard quantum electrodynamics. Nevertheless, the possibility of charge non-conserving (CNC) phenomena has widely been discussed in the literature (see reviews [64] and references therein) mainly in connection with future unified theories and with the possible existence of extra dimensions [65, 66]; several experimental activities have been performed on this topics.

The approach, we followed, consider the existence of possible β decay process [67] $(A, Z) \rightarrow (A, Z+1) + e^- + \overline{\nu}_e$, where some massless uncharged particle would be emitted instead of the electron (for example, ν_e or γ or Majoron); in this case, an additional 511 keV energy release would occur. Thus, usually forbidden decays to the ground state or to the excited levels of the daughter nuclei would become energetically possible. In our case, following the strategy we have firstly exploited in ref. [68], we search for the presence of ^{139}Ce isotopes, created in the detector after CNC decay of ^{139}La, through their subsequent EC decays into ^{139}La ($T_{1/2}$ = 137.64 d and Q_{EC} = 279 keV [69]). In particular, we look for a peak at $\simeq$ 200 keV due to the γ of $\simeq$ 166 keV and X rays/Auger electrons. The expected response function of the $LaCl_3$(Ce) detector for the EC of ^{139}Ce has been simulated with the help of the EGS4 package [70]. Comparing the experimental energy distribution with the expected response function, no evidence for the presence of ^{139}Ce decay has been been found and a bound on the probability of the investigated process has been extracted

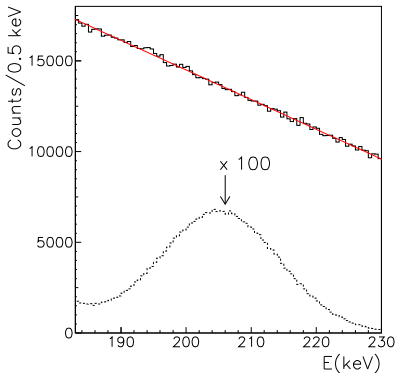

Figure 10: Experimental energy distribution in the energy region 183-230 keV (continuous histogram) with superimposed the best-fit curve obtained for the background. The dashed curve is hundred times the energy distribution expected for τ_{CNC} equal to the 90% C.L. limit reported in the text. For details see in the 2006 publication list.

(see Fig. 10). Note that other data analysis procedures give limits of the same order of magnitude. The obtained most cautious lifetime limit is:

$$\tau_{CNC}(^{139}\mathrm{La}\rightarrow^{139}\mathrm{Ce}) > 1.0 \times 10^{18} \text{ yr at } 90\% \text{ C.L.}$$

This limit holds for whatever CNC ^{139}La decay with emission of massless uncharged particle (γ, Majoron(s), ν, etc., even some other interesting physics which could appear in future).

6 Measurements with DAMA/Ge and LNGS Ge facility

6.1 DAMA/Ge

Various R&D developments to improve low background set-ups and scintillators as well as new developments for higher radiopure PMTs are regularly carried out. The related measurements on samples are usually performed by means of the DAMA low background Ge detector, specially realised with a low Z window. It is operative deep underground in the low background facility of the LNGS since many years. Some selected materials are in addition measured with high sensitivity ICP-MS and mass spectrometers. On 2005 a significant improvement of the DAMA/Ge installation has been performed: a new sealing system, a new system for neutron shielding, an automatic Marinelli and shield opening/closure system have been realised.

During year 2006 samples' measurements have regularly been carried out with particular care to the developments of new low-background PMTs. Moreover, the features of a $Li_6Eu(BO_3)_3$ crystal have also been investigated.

6.2 Measurement of intrinsic radioactivity of $Li_6Eu(BO_3)_3$ crystal

A $Li_6Eu(BO_3)_3$ monocrystal $14.5\varnothing \times 5.6$ mm (corresponding to a mass of about 2.72 g) was inserted in the HP Ge detector (size 408 cm^3) located deep underground at low background Ge facility of LNGS in order to measure its radioactive contaminations. The experimental spectrum measured during 1500 h is reported in Fig. 11 a) and the background spectrum of the HP Ge detector in Fig. 11 b). By analysing these energy spectra the radiative contaminants in the crystal have been derived and the results are summarized in Table 1.

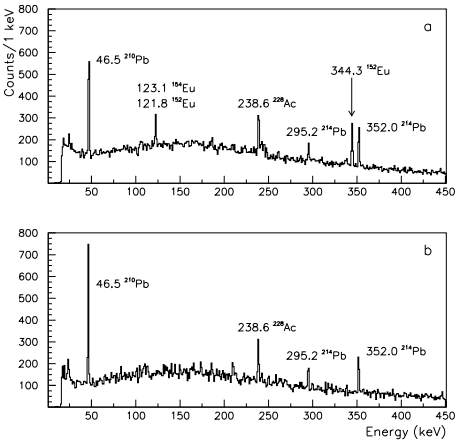

Figure 11: Measured energy distributions: (a) $Li_6Eu(BO_3)_3$ sample during 1500 h; (b) background of the used HP Ge detector during 689 h (normalized to 1500 h). Peaks at 122 keV and 344 keV due to the ^{152}Eu radioactive decay are evident in the $Li_6Eu(BO_3)_3$ spectrum.

As by product, the collected data have also been used to set the first experimental limits on the half lives of the rare alpha decays of ^{151}Eu into the first excited level of ^{147}Pm and of ^{153}Eu into ^{149}Pm. They are, respectively: $T_{1/2} > 2.4 \times 10^{16}$ yr and $T_{1/2} > 1.1 \times 10^{16}$ yr at 90% C.L. Other measurements by using this crystal and some other detectors are foreseen.

Table 1: Measured radioactive contaminations in the $Li_6Eu(BO_3)_3$ crystal. Limits are at 90% C.L.

Chain	Nuclide	Activity, Bq/kg
^{232}Th	^{228}Ac	<0.20
	^{212}Pb	<0.25
	^{208}Tl	<0.13
^{238}U	^{214}Pb	<0.17
	^{214}Bi	<0.07
	^{40}K	<1.5
	^{60}Co	<0.026
	^{137}Cs	<0.081
	^{207}Bi	<0.009
	^{152}Eu	=0.949(48)
	^{154}Eu	=0.212(35)

6.3 Measurement of two-neutrino $\beta\beta$ decay of ^{100}Mo to the first excited 0^+ level of ^{100}Ru

The me*A*su*R*e*M*ent of tw*O*-*N*eutr*I*no $\beta\beta$ dec*A*y of ^{100}Mo to the first excited 0^+ level of ^{100}Ru (for semplicity hereafter named *ARMONIA*) consists of a Molybdenum sample of $\simeq 1$ kg enriched in ^{100}Mo at 99.5%. The sample – in form of metallic powder – is installed in the four low-background HP Ge detectors (about 225 cm^3 each, all mounted in one cryostat) facility located at LNGS. The sample has been purified and compressed to a density of about 6 g/cm^3 before the measurement.

The aim of this high sensitivity experiment is to measure the $2\beta 2\nu$ decay of ^{100}Mo to the first excited 0^+ level of ^{100}Ru ($E(0_1^+) = 1130.5$ keV) either to confirm positive results reported in [71, 72, 73] (with $T_{1/2}$ in the range around $6-9\times10^{20}$ y) or to confirm previous higher limit value of ref. [74] ($T_{1/2} > 1.2\times10^{21}$ y at 90% C.L.).

Preliminary data have been collected deep underground at LNGS during 1927 h. In accordance with the scheme of ^{100}Mo decay two γ of 590.8 keV and 539.6 keV respectively are expected in the de-excitation of the 0_1^+ level. The measured energy distribution in the range of 500-600 keV is reported in Fig. 12 and compared with the background spectrum measured without the ^{100}Mo sample (shaded area). Note that peaks at 511 keV and 583 keV are related with ^{208}Tl decay and annihilation processes.

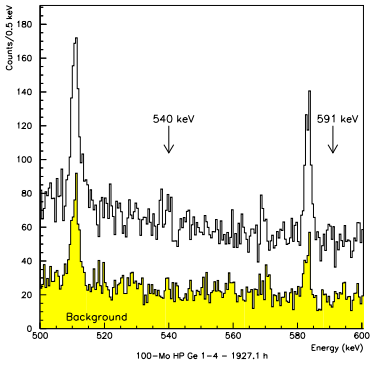

Figure 12: Spectrum of ^{100}Mo sample (mass of 1009 g) measured with 4 HP Ge detectors set-up at LNGS during 1927 h in the range of 500-600 keV. Shaded area is background spectrum (without ^{100}Mo sample) normalised to the same time of measurements. Peaks at 511 keV and 583 keV are related with ^{208}Tl decay and annihilation process (511 keV).

A very modest peak structure seems to be present – but at very low C.L. – around 540 keV, where one γ searched for is expected. If this would be ascribed to the decay searched for, one gets: $T_{1/2} = 3\times10^{20}$ y. However, no significant statistical evidence for the peak at the energy of 591 keV is found and a limit on the half-life can be derived: $T_{1/2} > 6\times10^{20}$ y at 90% C.L.. These measurements have shown that *ARMONIA* is entering in the sensitivity region of interest. Therefore, after that, further chemical purification of the sample has been performed at the LNGS chemical laboratory and the data taking with the new sample has been restarted in order to increase the sensitivity (and exposure) needed for the verification searched for.

7 Conclusions

In conclusion, the main activities during year 2006 can be summarized as in the following:

I. Further corollary investigations on the 6.3 σ C.L. model independent evidence for the presence of a particle Dark Matter component in the galactic halo, obtained by DAMA/NaI over seven annual cycles. Other ones are in progress

II. The new DAMA/LIBRA set-up is regularly in data taking. DAQ modifications for the new Transient Digitizers, which will be installed during 2007, have been completed.

III. The RD-III towards the possible DAMA/1ton is progressing on the various aspects.

IV. The DAMA/LXe set-up is going to restart the data taking as soon as the laboratory will conclude some works.

V. The DAMA/R&D set-up has been used in various small scale experiments; several data analyses are in progress. The data taking is in progress with a new detector and various other relatively small scale experiments are in preparation.

VI. The DAMA/Ge is regularly selecting materials, while a double beta decay experiment is also in progress in the LNGS Ge facility with ^{100}Mo.

8 List of Publications during 2006

1. R. Bernabei, P. Belli, F. Montecchia, F. Nozzoli, F. Cappella, A. d'Angelo, A. Incicchitti, D. Prosperi, R. Cerulli, C.J. Dai, H.L. He, H.H. Kuang, J.M. Ma, Z.P. Ye, Recent DAMA results, in the volume "Astroparticle, Particle and Space Physics, Detectors and Medical Physics Applications", World Sc. pub. (2006), 158.

2. R. Bernabei, P. Belli, F. Montecchia, F. Nozzoli, F. Cappella, A. d'Angelo, A. Incicchitti, D. Prosperi, R. Cerulli, C.J. Dai, H.L. He, H.H. Kuang, J.M. Ma, Z.P. Ye, Physics and astrophysics with dark matter particles, Journal of Physics: Conf. series 39 (2006) 148.

3. R. Bernabei, P. Belli, F. Montecchia, F. Nozzoli, F. Cappella, A. d'Angelo, A. Incicchitti, D. Prosperi, R. Cerulli, C.J. Dai, H.L. He, H.H. Kuang, J.M. Ma, Z.P. Ye, Highlights of DAMA, Journal of Physics: Conf. series 39 (2006) 82.

4. R. Bernabei, P. Belli, F. Montecchia, F. Nozzoli, F. Cappella, A. d'Angelo, A. Incicchitti, D. Prosperi, R. Cerulli, C.J. Dai, H.L. He, H.H. Kuang, J.M. Ma, Z.P. Ye, Particle Dark Matter: from DAMA/NaI to DAMA/LIBRA, Physics of Atomic Nuclei 69 (2006), 2056-2067.

5. R. Bernabei, P. Belli, F. Montecchia, F. Nozzoli, F. Cappella, A. Incicchitti, D. Prosperi, R. Cerulli, C.J. Dai, V.Yu. Denisov, V.I. Tretyak, Search for rare processes with DAMA/LXe experiment at Gran Sasso, Eur. Phys. J. A 27 s01 (2006), 35-41.

6. R. Bernabei, P. Belli, F. Montecchia, F. Nozzoli, F. Cappella, A. d'Angelo, A. Incicchitti, D. Prosperi, R. Cerulli, C.J. Dai, H.L. He, H.H. Kuang, J.M. Ma, Z.P. Ye, From DAMA/NaI to DAMA/LIBRA at LNGS, Eur. Phys. J. A 27 s01 (2006), 57-62.

7. R. Bernabei, P. Belli, F. Montecchia, F. Nozzoli, F. Cappella, A. Incicchitti, D. Prosperi, R. Cerulli, C.J. Dai, H.L. He, H.H. Kuang, J.M. Ma, Z.P. Ye, Investigating pseudoscalar and scalar dark matter, Int. J. Mod. Phys. A 21 (2006) 1445-1469.

8. R. Bernabei, P. Belli, F. Montecchia, F. Nozzoli, F. Cappella, A. Incicchitti, D. Prosperi, R. Cerulli, C.J. Dai, H.L. He, H.H. Kuang, J.M. Ma, Z.P. Ye, Dark Matter investigations, to appear on the Proc. of the 12th Lomonosov Conf. on Elementary Particle Physics, Moscow.

9. R. Bernabei, P. Belli, F. Montecchia, F. Nozzoli, A. d'Angelo, F. Cappella, A. Incicchitti, D. Prosperi, S. Castellano, R. Cerulli, C.J. Dai, V.I. Tretyak, Search for possible charge non-conserving decay of ^{139}La into ^{139}Ce with $LaCl_3$(Ce) scintillator, Ukr. Journal of Physics 51 (2006) 1037-1043.

10. R. Bernabei, P. Belli, F. Montecchia, F. Nozzoli, F. Cappella, A. Incicchitti, D. Prosperi, R. Cerulli, C.J. Dai, H.L. He, H.H. Kuang, J.M. Ma, X.D. Sheng, Z.P. Ye, M.Martinez, G. Giuffrida, Investigating halo substructures by annual modulation signature, Eur. Phys. J. C 47 (2006) 263-271

11. R. Bernabei, P. Belli, F. Montecchia, F. Nozzoli, A. d'Angelo, F. Cappella, A. Incicchitti, D. Prosperi, S. Castellano, R. Cerulli, C.J. Dai, F. Danevich, V.I. Tretyak, Searches for rare processes by DAMA at Gran Sasso, pre-print ROM2F/2006/14, to appear on Nucl. Phys. and Atomic Energy

12. R. Bernabei, P. Belli, F. Montecchia, F. Nozzoli, F. Cappella, A. Incicchitti, D. Prosperi, R. Cerulli, C.J. Dai, H.L. He, H.H. Kuang, J.M. Ma and Z.P. Ye, Results by DAMA at Gran Sasso, pre-print ROM2F/2006/15, to appear on Nucl. Phys. and Atomic Energy

13. P. Belli, R. Bernabei, R.S. Boiko, R. Cerulli, F.A. Danevich, S. d'Angelo, A. Incicchitti, V.V. Kobychev, B.N. Kropivyansky, M. Laubenstein, P.G. Nagornyi, S.S. Nagorny, S. Nisi, D.V. Poda, D. Prosperi, V.I. Tretyak, I.N. Vishnevsky, S.S. Yurchenko (Armonia), Preliminary results on the search for ^{100}Mo 2β decay to the first excited 0_1^+ level of ^{100}Ru, pre-print ROM2F/2006/20, to appear on Nucl. Phys. and Atomic Energy

14. R. Bernabei, P. Belli, F. Montecchia, F. Nozzoli, F. Cappella, A. Incicchitti, D. Prosperi, R. Cerulli, C.J. Dai, H.L. He, H.H. Kuang, J.M. Ma, Z.P. Ye, Dark Matter signals: from underground to space investigation, to appear on the Proc. of Space Part 2006 Conference, Beijing (China), 2006.

15. R. Bernabei, P. Belli, F. Montecchia, F. Nozzoli, F. Cappella, A. Incicchitti, D. Prosperi, R. Cerulli, C.J. Dai, H.L. He, H.H. Kuang, J.M. Ma, X.D. Sheng, Z.P.

Ye, Dark Matter Search: the status of art, to appear on the Proc. of Vulcano 2006 Workshop, Italy, 2006.

16. R. Bernabei, P. Belli, F. Montecchia, F. Nozzoli, F. Cappella, A. d'Angelo, A. Incicchitti, D. Prosperi, R. Cerulli, C.J. Dai, H.L. He, H.H. Kuang, J.M. Ma, X.D. Sheng, Z.P. Ye, Future goals for the possible DAMA/1ton, now at R&D stage, to appear on the Proc. of Vulcano 2006 Workshop, Italy, 2006.

17. R. Bernabei, P. Belli, F. Montecchia, F. Nozzoli, F. Cappella, A. Incicchitti, D. Prosperi, R. Cerulli, C.J. Dai, H.L. He, H.H. Kuang, J.M. Ma, X.D. Sheng, Z.P. Ye, DAMA at Gran Sasso: results and perspectives, to appear on the Proc. of ICHEP06, Mosca, Russia, 2006.

18. R. Bernabei, P. Belli, F. Montecchia, F. Nozzoli, F. Cappella, A. Incicchitti, D. Prosperi, R. Cerulli, C.J. Dai, H.L. He, H.H. Kuang, J.M. Ma, X.D. Sheng, Z.P. Ye, Investigations on Dark Matter and on some rare processes by DAMA: past, present and future, to appear on the Proc. of IDM2006 Workshop, Rhodes, Greece, 2006.

19. R. Bernabei, P. Belli, F. Montecchia, F. Nozzoli, F. Cappella, A. Incicchitti, D. Prosperi, R. Cerulli, C.J. Dai, V. Yu. Denisov, V.I. Tretyak, DAMA/LXe at LNGS: results and perspectives, to appear on the Proc. of IDM2006 Workshop, Rhodes, Greece, 2006.

20. R. Bernabei, P. Belli, F. Montecchia, F. Nozzoli, F. Cappella, A. Incicchitti, D. Prosperi, R. Cerulli, C.J. Dai, H.L. He, H.H. Kuang, J.M. Ma, X.D. Sheng, Z.P. Ye, DAMA investigations on Dark Matter at Gran Sasso: results and perspectives, to appear on the Proc. of DSU06, Madrid, Spain, 2006.

21. P. Belli, R. Cerulli, F.A. Danevich, B.V. Grinyov, A. Incicchitti, V.V. Kobychev, M. Laubenstein, S.S. Nagorny, A.V. Tolmachev, V.I. Tretyak, R.P. Yavetskiy, Intrinsic radioactivity of $Li_6Eu(BO_3)_3$ crystal and α decays of Eu, pre-print ROM2F/2006/27, to appear on Nucl. Instr. & Meth. A.

References

[1] R. Bernabei et al., Il Nuovo Cim. A 112 (1999) 545.

[2] R. Bernabei et al., Eur. Phys. J. C18 (2000) 283.

[3] R. Bernabei el al., La Rivista del Nuovo Cimento 26 n.1 (2003) 1-73

[4] R. Bernabei et al., Int. J. Mod. Phys. D 13 (2004) 2127.

[5] R. Bernabei et al., Phys. Lett. B 424 (1998) 195;

[6] R. Bernabei et al., Phys. Lett. B 450 (1999) 448.

[7] P. Belli et al., Phys. Rev. D 61 (2000) 023512.

[8] R. Bernabei et al., Eur. Phys. J. C 18 (2000) 283.

[9] R. Bernabei et al., Phys. Lett. B 509 (2001) 197.

[10] R. Bernabei et al., Eur. Phys. J. C 23 (2002) 61.

[11] P. Belli et al., Phys. Rev. D 66 (2002) 043503.

[12] R. Bernabei et al., Int. J. Mod. Phys. A 21 (2006) 1445.

[13] K.A. Drukier et al., Phys. Rev. D 33 (1986) 3495.

[14] K. Freese et al., Phys. Rev. D 37 (1988) 3388.

[15] R. Bernabei et al., Phys. Lett. B389 (1996) 757.

[16] R. Bernabei et al., Il Nuovo Cimento A112 (1999) 1541.

[17] R. Bernabei et al., Phys. Rev. Lett. 83 (1999) 4918.

[18] F. Cappella et al., Eur. Phys. J.-direct C14 (2002) 1.

[19] R. Bernabei et al., Phys. Lett. B515 (2001) 6.

[20] R. Bernabei et al., Phys. Lett. B408 (1997) 439.

[21] P. Belli et al., Phys. Rev. C60 (1999) 065501.

[22] P. Belli et al., Phys. Lett. B460 (1999) 236.

[23] A. Bottino et al., Phys. Rev. D69 (2004) 037302, Phys. Rev. D68 (2003) 043506.

[24] R. Foot, Phys. Rev. D 69 (2004) 036001.

[25] S. Mitra, Phys. Rev. D 71 (2005) 121302.

[26] L. Di Lella and K. Zioutas, Astropart. Phys. 19 (2003) 145.

[27] J.F. Navarro, C.S. Frenk, S.D.M. White, Ap. J. 462 (1996) 563.

[28] J. Diemand, B. Moore, J. Stadel, Nature 433 (2005) 389.

[29] R.A. Ibata, G. Gilmore, M.J. Irwin, Nature 370 (1994) 194.

[30] M. Bellazzini et al., Mon. Not. R. Astronom. Soc. 348 (2004) 12.

[31] D.R. Law, K.V. Johnston and S.R. Majewski, Ap. J. 619 (2005) 807; http://www.astro.virginia.edu/∼srm4n/Sgr.

[32] K. Freese et. al., Phys. Rev. D 71 (2005) 043516; New Astr. Rev. 49 (2005) 193;

[33] M. Chiba, Y. Yoshii, Astron. J. 115 (1998) 168.

[34] R. Bernabei et al., in the volume Frontier Objects in Astrophysics and Particle Physics, Vol. 90 (2005) 581.

[35] G. Prezeau et al., *Phys. Rev. Lett.* **91** (2003) 231301 .

[36] F.S. Ling, P. Sikivie, S. Wick, *Phys. Rev.* **D 70** (2004) 123503 .

[37] D. Stiff, L.M. Widrow and J. Frieman, Phys. Rev. D 64 (2001) 083516.

[38] J.D. Lewin and P. F. Smith, Astropart. Phys. 6 (1996) 87.

[39] P. Belli et al., Il Nuovo Cim. 103A (1990) 767

[40] P. Belli et al., Il Nuovo Cim. C 19 (1996) 537

[41] P. Belli et al., Astrop. Phys. 5 (1996) 217

[42] P. Belli et al., Phys. Lett. B 387 (1996) 222 and Phys. Lett. B 389 (1996) 783 (erratum)

[43] R. Bernabei et al., New J. Phys. 2 (2000) 15.1

[44] R. Bernabei et al., Eur. Phys. J.-direct C11 (2001) 1.

[45] R. Bernabei et al., Phys. Lett. B 436 (1998) 379.

[46] R. Bernabei et al., in the volume "Beyond the Desert 2003", Springer (2003) 365

[47] R. Bernabei et al., Nucl. Instr. & Meth. A482 (2002) 728

[48] R. Bernabei et al., Phys. Lett. B 527 (2002) 182

[49] R. Bernabei et al., Phys. Lett. B 546 (2002) 23

[50] F. Cappella, PhD Thesis, Universit`a di Roma "Tor Vergata", 2005.

[51] P. Belli et al., Phys. Rev. D 61 (2000) 117301

[52] P. Belli et al., Phys. Lett. B 465 (1999) 315

[53] R. Bernabei et al., Phys. Lett. B 493 (2000) 12

[54] R. Bernabei et al., in the volume "Cosmology and particle Physics", AIP ed. (2001) 189.

[55] R. Bernabei et al., Il Nuovo Cimento A110 (1997) 189.

[56] R. Bernabei et al., Astrop. Phys. 7 (1997) 73.

[57] P. Belli et al., Nucl. Phys. B563 (1999) 97.

[58] P. Belli et al., Astrop. Phys. 10 (1999) 115.

[59] R. Bernabei et al., Nucl. Phys. A705 (2002) 29.

[60] P. Belli et al., Nucl. Instr. & Meth. A498 (2003) 352.

[61] R. Cerulli et al., Nucl. Instr. & Meth. A525 (2004) 535.

[62] R. Bernabei *et al.*, Nucl. Instr. and Meth. A 555 (2005) 270.

[63] S. Weinberg, Phys. Rev. B 135 (1964) 1049.

[64] L.B. Okun, Sov. Phys. Usp. 32 (1989) 543;
L.B. Okun, Comments Nucl. Part. Phys. 19 (1989) 99;
Particle Data Group, K. Hikasa *et al.*, Phys. Rev. D 45 (1992) VI.10.

[65] F.J. Yndurain, Phys. Lett. B 256 (1991) 15;
N. Arkani-Hamed *et al.*, Phys. Lett. B 429 (1998) 263.

[66] S.L. Dubovsky *et al.*, Phys. Rev. D 62 (2000) 105011;
S.L. Dubovsky *et al.*, JHEP 08 (2000) 041;
V.A. Rubakov, Phys. Uspekhi 44 (2001) 871.

[67] G. Feinberg, M. Goldhaber, Proc. Nat. Acad. Sci. U.S.A. 45 (1959) 1301.

[68] R. Bernabei et al., Eur. Phys. J. A 27 s01 (2006) 35

[69] *Table of Isotopes*, ed. by R.B. Firestone, V.S. Shirley *et al.*, 8-th ed., John Wiley & Sons, N.Y., 1996 and 1998 CD update.

[70] W.R. Nelson *et al.*, SLAC-Report-265, Stanford, 1985.

[71] A.S. Barabash et al., Phys. Lett. B 345 (1995) 408.

[72] A.S. Barabash et al., Phys. At. Nucl. 62 (1999) 2039.

[73] L. De Braeckeleer et al., Phys. Rev. Lett. 86 (2001) 3510.

[74] D. Blum et al., Phys. Lett. B 275 (1992) 506.

GENIUS Test Facility

H.V. Klapdor-Kleingrothaus[a] and I.V. Krivosheina[b]

[a] Max-Planck Institut für Kernphysik, Heidelberg, Germany
[b] Institute of Radiophysical Research, Nishnij Novgorod, Russia
Spokesman of the Collaboration; E-mail: H.Klapdor@mpi-hd.mpg.de
Home-page: http://www.mpi-hd.mpg.de.non_acc/

Abstract

After operation of GENIUS-TF over three years with finally six naked Ge detectors (15 kg) in liquid nitrogen in Gran Sasso we realize the following problems: 1. Background from ^{222}Rn diffusing into the setup, on a level far beyond the expectation. 2. Limited long-term stability of naked detectors in liquid nitrogen. None of the six detectors is running after three years with the nominal leakage current. Three of the six detectors do not work any more at all. These problems could become relevant in realization of a full size GENIUS-like experiment.

1 Introduction

Some years ago, the status of cold dark matter search, of investigation of neutrinoless double beta decay and of low-energy solar neutrinos all required new techniques of *drastic* reduction of background in the experiments. For this purpose we proposed the GENIUS (GErmanium in liquid NItrogen Underground Setup) project in 1997 [1, 2, 3, 4, 5, 6]. The idea of GENIUS (and GENIUS-TF) is to operate 'naked' Ge detectors in liquid nitrogen (as applied routinely already for more than 20 years by the CANBERRA Company for short term technical functions tests [8], and later 'rediscovered' [22]), and thus, by removing all materials from the immediate vicinity of the Ge crystals, to reduce the background considerably with respect to conventionally operated detectors. The liquid nitrogen acts both as a cooling medium and as a shield against external radioactivity.

After the success of the HEIDELBERG-MOSCOW experiment in $0\nu\beta\beta$ decay [17, 18, 19, 20] GENIUS is no more needed for $\beta\beta$ decay experiments with ^{76}Ge, but may still be required for dark matter and solar neutrino experiments using Ge as target [15]. Therefore, we continued the research on the GENIUS Test Facility. *Monte Carlo simulations* for the GENIUS project, (and for GENIUS-TF) and investigation of the *new physics potential* of the project have been performed in great detail, and have been published elsewhere [1, 2, 6, 7, 10, 14]. We were **the first** to show (in our HEIDELBERG low-level facility already **in 1997**) that such device can be used for *spectroscopy* [1, 3, 5] at least over *short* measuring times.

The small scale version of GENIUS, the GENIUS-Test-Facility had as main goal to test the long-term stability of the detectors under liquid nitrogen conditions, and also other operational parameters. A detailed description of the GENIUS-TF project is given in [10, 13].

The GENIUS-Test-Facility has been approved by the Gran Sasso Scientific Committee in March 2001.

GENIUS-TF is up to now the only existing test facility for a project operating naked Ge detectors in liquid nitrogen such as GENIUS [2] and its copies (Cameo, Gerda) is the GENIUS-Test Facility (GENIUS-TF) operating over three years in Gran Sasso, until May 2006.

The first four naked detectors (in total 10 kg) were installed on May 5, 2003 (GENIUS-TF-I). This has been reported in Cern Courier [2] and in [13].

2 The GENIUS-TF-II and III Setups

In October 2004 we have installed a new setup GENIUS-TF-II (see Figs. 1,2,3), containing now **six naked** Ge detectors (in total 15 kg), and, as technical improvement **a second copper vessel**, for further shielding of the Radon. That ^{222}Ra diffusing into the setup has been a problem for GENIUS-TF-I, has been described in detail in [9]. The inner shielding by bricks of (5-10) cm polycristalline Germanium (∼300 kg) was used also in this setup forming the inner highly efficient shield of the Ge detectors (see Fig. 3).

Figure 1: Left - View from the top on the GENIUS-TF-II setup during installation in October 2004. Right - **The six contacted naked Ge detectors.**

The thin wall (1 mm) inner copper box containing the liquid nitrogen is made of high-purity electrolytic copper and is thermally shielded by 20 cm of special low-level styropor, the outer copper box (also made of electrolytic copper) is followed by a shield of 10 cm of electrolytic copper (15 tons) and 20 cm of low-level (Boliden) lead (>35 tons).

The high-purity liquid nitrogen used, is produced by the BOREXINO nitrogen plant, which has been extended for increase of the production capacity to be able to provide enough nitrogen also for GENIUS-TF (see [9]).

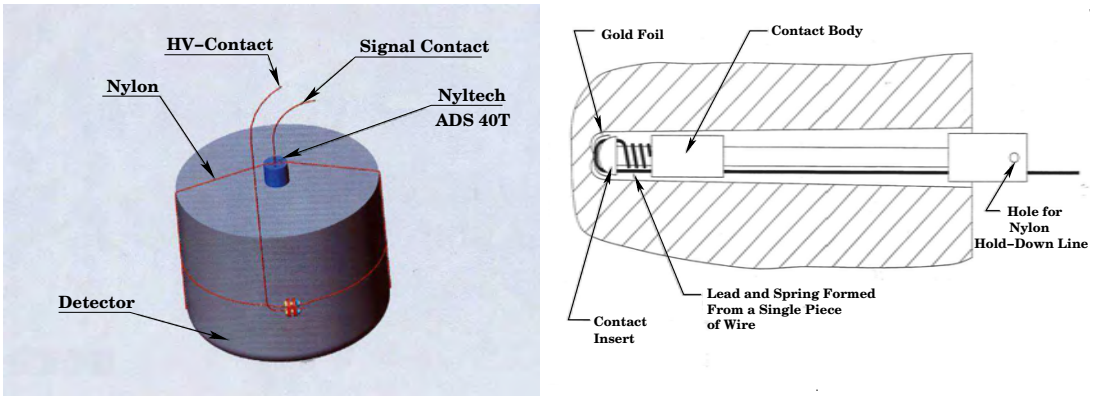

Figure 2: Left: Schematic view of a naked Ge detector for the GENIUS-TF experiment and its holder construction. Right: The construction of the signal contact of a naked Ge detector for the GENIUS-TF experiment (cortesy Ortec company).

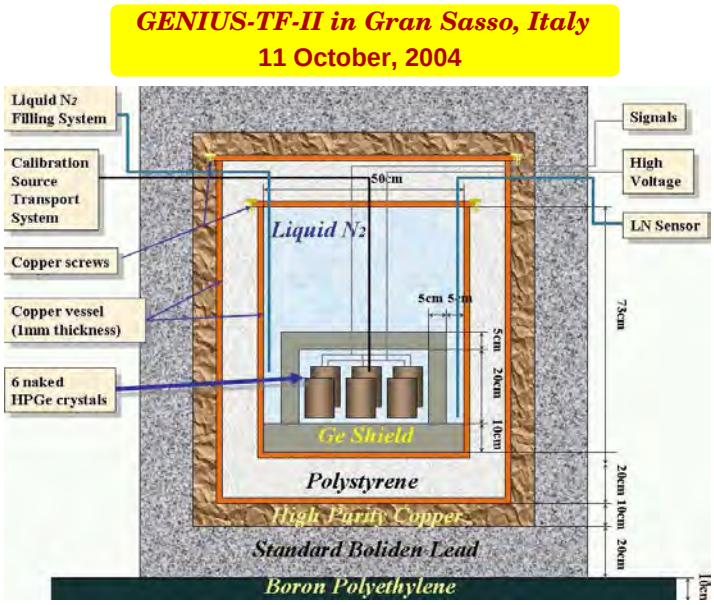

Figure 3: Schematical view of the TF-II setup.

GENIUS-TF-III started operation in beginning of March 2005 after the inner shield of polycrystalline Ge bricks had to be removed according to contract with Kurchatov institute.

Table 1: The high voltages applied to the detectors after installation in GENIUS-TF I, II and III as function of time, and the nominal voltages.

Det-s	D1	D2	D3	D4	D5	D6
GENIUS-TF-I, from 10.12.2003, till 25.09.2004						
10.12.03	2404	2603	2879	2301	n. inst.	n. inst.
06.04.04	2600	2220	2879	2301	-	-
04.05.04	2600	2220	3200	2500		
GENIUS-TF-II, from 18.11.2004, till 28.02.2005						
08.10.04	250	1296	261	954	1253	502
18.11.04	364	2200	347	2298	3501	1015
20.01.05	"	"	"	"	"	1000
GENIUS-TF-III, from 15.03.2005						
15.03.05	80	1802	20	2153	3501	980
03.05.05	0	1700	0	1500	3501	980
09.03.06	-	1700	-	-	3500	911
19.05.06	-	1600	-	-	2100	850
Nom.	**3000**	**2600**	**3200**	**2500**	**3500**	**2000**

3 Operational Parameters

Background from ^{222}Rn: The unexpected (according to our Monte Carlo simulations [10]) high background from ^{222}Rn in GENIUS-TF-I (see [9]) has been reduced in GENIUS-TF-II by about a factor 2. This ^{222}Rn background is compatible with the goal of GENIUS-TF to search for dark matter [23], but would be a *serious problem* for any full GENIUS-like experiments, because the ^{222}Rn leads to the 'famous' background from ^{214}Bi lines near the Q-value for double beta decay of ^{76}Ge [17, 21].

Long-Term Stability: The most dramatic result is obtained for the long-term stability of the detector operation in liquid nitrogen. It is shown in Table 1. As a result of increasing leakage currents, finally from initially six detectors at present only three are still working and *not one of them* with the nominal high voltage (see Table 1). The reasons for the deterioration of the surface purity with time which could lead to the increasing leakage currents need further investigation. There might, however, be also other reasons. However, for some detector experts a surface purity problem does not come very surprising [24, 25, 26]. From their experience, partly in detector producing companies, they expect

this for a naked detector, having no shield of its surface against an open surrounding (the liquid nitrogen). In fact it would not be surprising that the high voltage of several thousand volts lying at the detector surface would attract ions from the surrounding liquid nitrogen. It is further well known that recently crushed germanium pieces have a highly active surface and are a very active getter. They have been used as such in deionized water to further improve the purity of the water, and will be an active getter for impurities also in liquid nitrogen [28, 29]. Perhaps this suspicion might be checked by mass spectroscopic investigation of the detector surface material. The energy resolution on long terms also decreases systematically [27].

4 Conclusions

GENIUS-TF is the *only setup with naked Ge detectors worldwide running underground and over a longer time period*. It has lead to important insight into the conditions of technical operation of naked Ge detectors in liquid nitrogen. The relatively large background from ^{222}Ra diffusion is a problem unsolved up to now. The main problem realized, is, however, the increase of leakage current after long running of the detectors, which, among others, could be caused by increasing surface impurity of the crystals. This lead to serious restrictions of the high voltages applicable and finally to destruction of the detectors. The information GENIUS-TF delivered after almost three years of operation on the possibility of long-term operation of such experiments, has to be seriously taken into consideration for planning of experiments on larger scale in general.

5 Acknowledgement:

The authors would like to thank their colleagues from MPI Heidelberg: Herrn H. Strecker, T. Apfel, M. Reissfelder, M. Saueressig for their help during installation of GENIUS-TF-II. The authors would like to thank the technical staff of the Max-Planck Institut für Kernphysik and of the Gran Sasso Underground Laboratory. We acknowledge the invaluable support from BMBF and DFG, and LNGS of this project.

References

[1] H.V. Klapdor-Kleingrothaus, Int. J. Mod. Phys. A13 (1998) 3953.

[2] H.V. Klapdor-Kleingrothaus, J. Hellmig and M. Hirsch, *GENIUS-Proposal*, 20 Nov. 1997.

[3] J. Hellmig and H.V. Klapdor-Kleingrothaus, Z. Phys. A 359 (1997) 351-359, and nucl-ex/9801004.

[4] H.V. Klapdor-Kleingrothaus, M. Hirsch, Z. Phys. A 359 (1997) 361-372.

[5] H.V. Klapdor-Kleingrothaus, J. Hellmig and M. Hirsch, J. Phys. G24 (1998) 483-516.

[6] H.V. Klapdor-Kleingrothaus, CERN Courier, Nov. 1997, 16-18.

[7] H.V. Klapdor-Kleingrothaus et al. **MPI-Report MPI-H-V26-1999**, and Preprint: hep-ph/9910205, and in Proceedings of the 2nd Int. Conf. on Particle Physics Beyond the Standard Model BEYOND'99, Castle Ringberg, Germany, 6-12 June 1999, edited by H.V. Klapdor-Kleingrothaus and I.V. Krivosheina, *IOP Bristol* (2000) 915 - 1014.

[8] J. Verplancke, *CANBERRA Company*, priv. commun. 5.03.2004.

[9] H.V. Klapdor-Kleingrothaus et al., Nucl. Instr. Meth. A 530 (2004) 410-418.

[10] H.V. Klapdor-Kleingrothaus et al., Nucl. Instrum. Meth. A 481 (2002) 149-159.

[11] H.V. Klapdor-Kleingrothaus et al., to be publ.

[12] H.V. Klapdor-Kleingrothaus, CERN Courier 43 Nr.6 (2003) 9.

[13] H.V. Klapdor-Kleingrothaus et al., Nucl. Instr. Meth. A 511 (2003) 341;
H.V. Klapdor-Kleingrothaus, CERN Courier 43 Nr.6 (2003) 9;
H.V. Klapdor-Kleingrothaus et al., Proc. of the 3nd Intern. Conf. on Particle Physics Beyond the Standard Model, BEYOND02, Castle Ringberg, Germany, 2002, IOP 2003, ed. H.V. Klapdor-Kleingrothaus, 499.

[14] H.V. Klapdor-Kleingrothaus, "60 Years of Double Beta Decay - From Nuclear Physics to Beyond the Standard Model", WS (2001) 1281 p.

[15] H.V. Klapdor-Kleingrothaus, in Proc. of 2th Int. Workshop on Low Energy Solar Neutrino Detection, Tokyo, Japan, 4-5 Dec. 2000 (World Scientific, Singapore 2001) p.116.

[16] H.V. Klapdor-Kleingrothaus, et al., Phys. Lett. B 578 (2004) 54-62.

[17] H.V. Klapdor-Kleingrothaus, I.V. Krivosheina, A. Dietz et al., Phys. Lett. B 586 (2004) 198-212.

[18] H.V. Klapdor-Kleingrothaus, I.V. Krivosheina, A. Dietz et al., Nucl. Instrum. Meth. A 522 (2004) 371-406.

[19] H.V. Klapdor-Kleingrothaus et al. hep-ph/0201231, Mod. Phys. Lett. A 16 (2001) 2409.

[20] H.V. Klapdor-Kleingrothaus, I.V. Krivosheina, in Proc. of 2nd Scandinav. Neutrino Workshop, SNOW2006, May 2-6, 2006, Stockholm, Sweden, Physica Scripta T 127 (2006) 52-53.

[21] K.Ya. Gromov et al., J.Part. Nucl. Lett. 3 (2006) 30-41.

[22] G. Heusser, Ann. Rev. Nucl. Part. Sci. 45 (1995) 543-590.

[23] C. Tomei, A. Dietz, I. Krivosheina, H.V. Klapdor-Kleingrothaus, Nucl. Instrum. Meth. A 508 (2003) 343-352.

[24] G.F. Knoll, "*Radiation Detection and Measurement*", second ed. 1989, John Wiley & Sons;

[25] E. Flyckt (*Philips Photonics Comp.*, Brave, France) private comm. May 2006.

[26] A.B. McDonald (SNO collaboration), Queen Univ., Canada, private comm. May 2006.

[27] H.V. Klapdor-Kleingrothaus, I.V. Krivosheina et al., Gran Sasso Ann. Report 2005, p.125.

[28] T. Raudorf, ORTEC Company, private communications 07.08.2006.

[29] W.L. Hansen et al., IEEE Trans. on Nucl. Sci NS-27, No. 1, (1980); W.H. Barttain, P.J. Boddy, J. Electrochemical Soc. 109 (2062) 574; D. Frankl, El;ectrical Properties of Semiconductor Surfaces, Pergamon Press (1967).

List of Publications (2006)

1. **Status of GENIUS-TF-I and TF-II – The Long-Term Stability of Naked Detectors in Liquid Nitrogen**,
   H.V. Klapdor-Kleingrothaus and I.V. Krivosheina,
   Nuclear Instr. and Methods in Phys. Res. A 566 (2006) 472-476.

2. **Lessons After 3 years of running GENIUS-TF in Gran Sasso**,
   I.V. Krivosheina and H.V. Klapdor-Kleingrothaus,
   Phys. Scr. T 127 (2006) 52-53.

3. **Status of GENIUS-TF-II and - III. The Long-Term Stability. GENIUS-like Projects - To be or Not to be ?!**,
   H.V. Klapdor-Kleingrothaus, I.V. Krivosheina, V. Mironov, H. Strecker,
   INFN, Laboratori Nazionali del Gran Sasso, Annual Report (2005) 63-78 LNGS/EXP (2006).

List of Invited of Talks at Conferences, 2006

1. **Lessons After 3 years of running GENIUS-TF in Gran Sasso**,
   I.V. Krivosheina and H.V. Klapdor-Kleingrothaus,
   '2nd Scandinavian NeutrinO Workshop, May 2-6, 2006, AlbaNova University, Stockholm, Sweden,
   Phys. Scr. T 127 (2006) 52-53.

2. **Status of GENIUS-Test-Facility for Search of Dark Matter with Naked Ge Detectors in Liquid Nitrogen**,
   I.V. Krivosheina and H.V. Klapdor-Kleingrothaus,
   '6th International Workshop on the Identification of Dark Matter', September 11-16th, 2006
   In Proc. of Idm06, World Scientific (2007) eds. N. Spooner and J. Vergados.

HEIDELBERG-MOSCOW. A New Experimental Limit for the Stability of the Electron

H.V. Klapdor-Kleingrothaus[a], I.V. Krivosheina[b] and I.V. Titkova [c]

[a] Max-Planck Institut für Kernphysik, Heidelberg, Germany
[b] Institute of Radiophysical Research, Nishnij Novgorod, Russia
[c] JINR, Dubna, Russia
a) Spokesman of the Collaboration; E-mail: H.Klapdor@mpi-hd.mpg.de
Home-page: http://www.mpi-hd.mpg.de.non_acc/

Abstract

A lower limit of $>1.22 \times 10^{26}$ years (68% c.l.) has been determined for the mean life time of electron decay via the branch $e^- \to \gamma + \nu_e$. The limit was deduced from the spectra measured in the period 1995-2003 with the full set-up of 5 enriched ^{76}Ge detectors of the HEIDELBERG-MOSCOW $\beta\beta$ experiment in the Gran-Sasso underground laboratory. One of the detectors, and the setup 1 consisting of four detectors show an indication of a signal on a 1.4σ C.L. The best limit given by a single detector is 1.93×10^{26} y. The result is the by far sharpest limit obtained with Ge detectors. When comparing it with other limits, e.g. that from BOREXINO [10] it may be essential to note that the present limit has been deduced from the raw data without any treatment of the background. Combined with the best laboratory limit on the photon mass it gives the following restriction for *charge nonconservation*: $\epsilon^2_{e\nu\gamma} < 0.86 \times 10^{-98}$ (68% c.l.) or $< 1.14 \times 10^{-97}$ (90% c.l.).

1 Introduction

The standard model of elementary particle physics is in excellent agreement with all experimental results obtained with accelerators. Looking for physics beyond the standard model the search for rare events in testing fundamental laws of physics have been shown to be rather promising (see, e.g. [1, 2, 3]). One of the possible tests is that of charge conservation. In the context of gauge field theories, the invariance of the Lagrangian under a given gauge transformation corresponds to the conservation of some specific type of charge. In some grand unified theories, for example, terms appear in the Lagrangian which break the global gauge invariance associated with baryonic charge leading to proton decay at some level. In the electroweak sector the local gauge invariance of the Lagrangian corresponding to the equations of quantum electrodynamics dictates strict electric charge conservation and a massless photon. According to this class of theories we do not expect electrons to decay, because there is no lighter charged lepton, and the decay into photons

and/or neutrinos requires the violation of charge conservation. No conservation of the electric charge will only be possible if the Lagrangian of QED contains terms which destroy global as well as local gauge invariance.

There are two possible ways of observing the electron decay in Ge semiconductor detectors: the search for the 255.5 keV γ -rays coming from the decay $e^- \rightarrow \nu_e + \gamma$, and looking for the decay $e^- \rightarrow \nu_e + \nu_e + \bar{\nu}_e$. The second decay mode creates K-shell X-rays which are, even with a very low-background large detector, difficult to measure. Thus we searched for the decay mode $e^- \rightarrow \nu_e + \gamma$ using the data collected in the period 1995-2003 (56.66 kg yr) by the enriched germanium detectors of the Heidelberg-Moscow $\beta\beta$ experiment [1, 2, 3]. Earlier searches for electron decay have been performed with NaI detectors [4, 5, 6], Ge detectors [17, 7, 8, 9], liquid Xe [23, 24] and $C_{16}H_{18}$ [10], yielding lower half-life limits in the range $10^{23} \div 10^{26}$ years (see Table 1).

Table 1: The present limits for the mean life time τ (till 2006) for the electron decay for the decay mode $e^- \rightarrow \nu_e + \gamma$. Presented are all experiments from 1959 which measured this mode. The energy resolution is given for the case without and with Doppler-broadening in keV. Indicated is also the structure of the analysed data - raw data or after background subtraction.

Type of the Detector	Mass, kg	Resolution keV	Backgr. (keV kg y)$^{-1}$	Raw data	Limits τ (yr) (c.l.) mode: $e^- \rightarrow \nu_e + \gamma$	Ref., Year Ref.,
NaI	5	-	-	-	$>1.0\times10^{19}$ (68%)	[4] , 1959
NaI	1.4	44(-)	$\sim$21020	No	$>4.0\times10^{22}$ (68%)	[5] , 1965
NaI	6	43(-)	$\sim3\cdot10^5$	Yes	$>3.5\times10^{23}$ (68%)	[6] , 1979
Ge(Li)	0.69	$\sim$1.5	1500	Yes	$>3\times10^{23}$ (68%)	[17] , 1983
HPGe	0.71	1.9(5.13)	240	Yes	$>1.5\times10^{25}$(68%)	[7], 1986
HPGe	3.1	2.5(7.6)	25.8	Yes	$>2.4\times10^{25}$ (68%)	[8] , 1993
HPGe	2.2	1.8(5.3)	10-80	Yes	$>3.7\times10^{25}$ (68%)	[9] , 1995
LXe (DAMA)	6.5	-	-	Yes	$>1.0\times10^{25}$ (90%)	[23] , 1996
LXe (DAMA)	6.5	78(80)	0.04	Yes	$>3.4\times10^{26}$ (68%)	[24] , 2000
CTF($C_{16}H_{18}$) (Borexino)	4170	72(-)	0.06	No	$>4.6\times10^{26}$ (90%)	[10] , 2002
HPGeII	10.96	2.3(7.7)	25	Yes	$>1.93\times10^{26}$ (68%)	this work 2006

The sharpest limit is given according to Table 1 by BOREXINO [10]. However, in deduction of the life time limit from the Borexino data some major uncertainties may have entered into the analysis, since 1. The background whose origin seems not to be fully known has been parameterized by six parameters - and it has to be assumed to behave linearly down to low energies 2. Strong and perhaps not unique cuts have been applied to reduce the contamination of the spectrum in the range of interest by betas and

gammas from ^{40}K and from ^{14}C 3. It is not clear that threshold effects on the spectrum in the range of interest are really excluded 4. There do not exist direct measurements of the dependence between light yield of the electrons and their energy for the scintillator used in Borexino 5. The energy resolution in the Borexino experiment is by a factor of 30 worse than that of the present Ge experiment. These points may make it useful to have an independent experiment, as presented in this paper, not suffering from all these potential drawbacks.

2 Experimental setup

The search for the rare electron decay requires a detector with ultralow background, not to loose the expected weak signal of the expected $\sim$ 255.5 keV γ -line of the decay in the background radiation. The enriched germanium detectors of the HEIDELBERG-MOSCOW $\beta\beta$ experiment [11, 13, 1, 2] which has been used for search for neutrinoless double-beta decay give such possibility as byproduct.

The experiment operated in the Gran Sasso Underground Laboratory five p-type high-purity enriched ^{76}Ge detectors (Fig. 1) with total active mass of 10.96 kg, corresponding to 125.5 mol of ^{76}Ge in the period August 1990 - November 2003. The experiment and its shielding have been described in detail in [12, 13, 1, 2, 3, 14], to which we refer for experimental details.

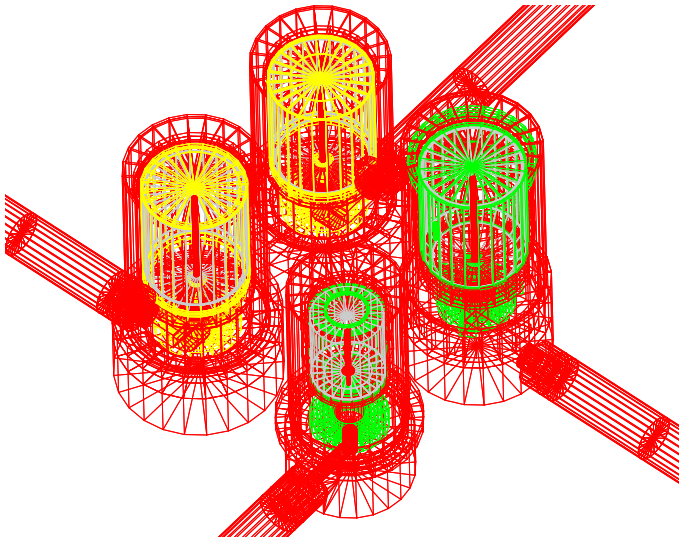

Figure 1: Geometry of the setup 1 of the HEIDELBERG-MOSCOW experiment, containing four of five enriched detectors (detectors 1,2,3,5). The germanium detectors (grey) are mounted in copper cryostats (red). The detector holder system consists of teflon (green) and vespel (yellow).

For the analysis with respect to electron decay we use the data taken in the period

November 1995 till May 2003 (see Table 2).

Table 2: Main parameters of the ^{76}Ge detectors in the HEIDELBERG-MOSCOW experiment (November 1995 till May 2003).

	ANG1	ANG2	ANG3	ANG4	ANG5
Active mass, kg	0.920	2.657	2.324	2.295	2.666
Measurement times, days	2090.61	1894.11	2079.46	1384.69	2076.34
^{76}Ge content, %	85.9	86.6	88.3	86.3	85.6

3 Data Analysis and Results

The idea of the present work is to search for γ rays with $\sim 255.5\,\mathrm{keV}$ energy which could accompany the possible decay of any electron in germanium and in its surroundings, by analyzing the spectra collected during the measurement time with these detectors (see Table 2). The exact value of the total energy deposited in the detector depends on the place where the electron decay occurs. If it happens outside the sensitive volume of the detector the deposited energy is simply equal to the energy released by the photon: $E_t = \frac{m_e c^2 - E_b}{2}$, where $m_e c^2\,\mathrm{keV}$ is the electron mass and E_b is the binding energy of the decaying electron in the corresponding atomic shell. If the electron decay occurs in the sensitive volume of the detector, the energy deposited in the detector is a sum of the photon energy E_γ and of the energy released by the X rays or Auger electrons following the atomic deexcitation (with total energy of E_b): $E_t = \frac{m_e c^2 - E_b}{2} + E_b = \frac{m_e c^2 + E_b}{2}$. Data for binding energies are taken from [15]. To obtain the lower limit for the mean life time τ of the electron decay we write

$$\tau \geq \frac{t}{\lambda} \cdot (P_{Cu} N_{Cu} + P_{Ge} N_{Ge}), \tag{1}$$

where $N_{Cu,Ge}$ are the number of electrons in the copper cryostat and germanium detector, respectively, $P_{Cu,Ge}$ are the detection efficiencies for the $255.5\,\mathrm{keV}$ γ -ray and t is the measuring time. The efficiencies were calculated with the aid of the GEANT4 program [16]. For ANG2 and ANG5 $P_{Cu,Ge}$ were calculated and used for the mean life time determination, for ANG1, ANG3, ANG4 and the full setup (all five detectors) only P_{Ge} was used for the half-life limit calculations (see Table 3). The quantity λ is the maximum number of electron decay events that can be excluded at the peak position.

To obtain the value λ one has to take into account the Doppler broadening (first mentioned by [17]), resulting from the average kinetic energy of the electrons in their orbital motion [7, 8, 9, 24], or - in the language of atomic and solid state physics - being due to the Compton profile of the bound electrons, i.e. their linear moments [26]. This

Table 3: Detection efficiencies for germanium and copper for both setups.

	Detector	P_{Ge}, %	P_{Cu} %
Setup 1	ANG1	30.824	-
	ANG2	63.548	4.620
	ANG3	61.514	-
	ANG5	64.439	6.940
	Full setup1	55.471	-
Setup 2	ANG4	60.862	-
Full setup: setup 1 + setup 2		58. 166	-

effect is not negligible, for instance, for Ge K-shell electrons a Gaussian line centered at 261.05 keV with width (full width at half maximum (FWHM)) equalling 91.37 keV will be expected, for copper the values are 251.01 keV and 79.01 keV, respectively. On the other hand for Ge M5-shell electrons a Gaussian line centered at 255.51 keV with FWHM 4.59 keV is expected. The lines expected from different atomic shells for germanium and copper atoms are presented in Fig. 2.

The Doppler broadening is calculated here (following [7, 8, 9, 24]) under the assumption that the electrons have a temperature corresponding to the expectation value of the kinetic energy in a given energy level, and that the virial theorem
$\langle E_{kin} \rangle = -\frac{1}{2} \langle E_{pot} \rangle$, is fulfilled. The Doppler line shape is then given by,

$$I(E) = \frac{1}{\sqrt{2\pi}\sigma} \; exp\left[-\frac{(E-E_t)^2}{2\sigma^2}\right], \tag{2}$$

with $\sigma = E_t\sqrt{\frac{kT}{m_e c^2}}$, where k is Boltzmann's constant, T is the absolute electron temperature. This can be expressed in terms of the absolute binding energy of the electron, $\sigma = 4.47 \cdot 10^{-2} E_t \sqrt{E_b(keV)}$. The full line shape can be expressed as

$$I(E) = \sum_{Cu,i} \frac{n_i}{\sqrt{2\pi}\sigma_i} exp\left[-\frac{(E-E_{t,i})^2}{2\sigma^2}\right] \cdot N_{at}(Cu) + \sum_{Ge,i} \frac{n_i}{\sqrt{2\pi}\sigma_i} exp\left[-\frac{(E-E_{t,i})^2}{2\sigma^2}\right] \cdot N_{at}(Ge) \tag{3}$$

with $\sigma_i = 4.47 \cdot 10^{-2} E_{t,i} \sqrt{E_{b,i}(keV)}$, where n_i is the fraction of electrons, the index i runs over the used atomic shells. The number of atoms (N_{at}) for germanium and copper are presented in Table 4.

We have done two types of analysis: at first we took into account only M-shell electrons for the copper and germanium (ME case), in the second analysis we used all shell electrons (AE case). The overall FWHM's for all detectors arising from Doppler broadening are presented in Table 4 for the ME and AE cases. The expected lines for one detector are shown in Fig. 3. The situation is very similar for the other detectors. The effect of the *intrinsic* resolution of the detectors is negligible within a few percent, and has been neglected.

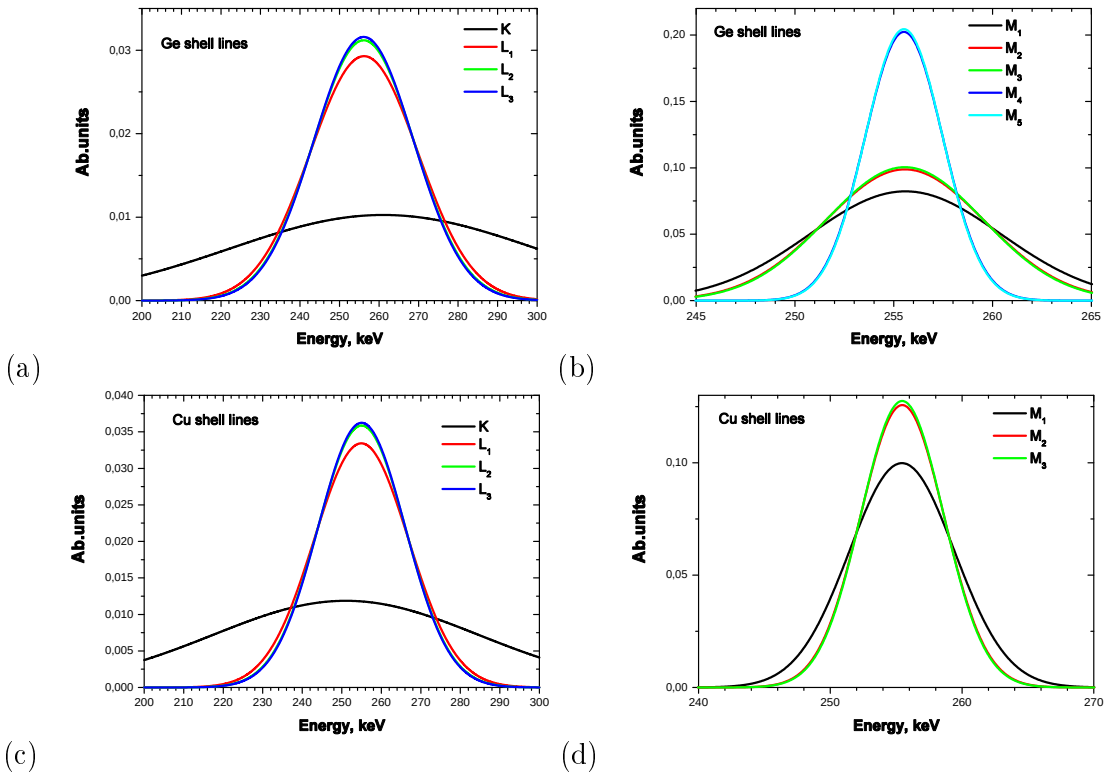

Figure 2: Lines expected from decay of electrons in different atomic shells for germanium and copper atoms.

Table 4: Numbers of atoms and Doppler-broadened FWHM for all detectors.

		Number of atoms:		**FWHM, keV:**	
	Detectors	Ge	Cu	ME case	AE case
Setup 1	ANG1	$0.730 \cdot 10^{25}$	$4.562 \cdot 10^{25}$	7.83	9.67
	ANG2	$2.231 \cdot 10^{25}$	$8.966 \cdot 10^{25}$	7.70	9.47
	ANG3	$1.844 \cdot 10^{25}$	$7.523 \cdot 10^{25}$	7.67	9.57
	ANG5	$2.116 \cdot 10^{25}$	$7.252 \cdot 10^{25}$	7.63	9.37
	Full setup1	$6.921 \cdot 10^{25}$	$2.830 \cdot 10^{26}$	7.7	9.5
Setup 2	ANG4	$1.821 \cdot 10^{25}$	$8.371 \cdot 10^{25}$	7.73	9.5
Full setup: (setup 1 + setup 2):		$8.742 \cdot 10^{25}$	$3.667 \cdot 10^{26}$	7.70	9.47

The measured spectra (after calibration) for all detectors separately, for setup1 and for the full setup are presented in Figs. 4,5. The calibration was done by using known

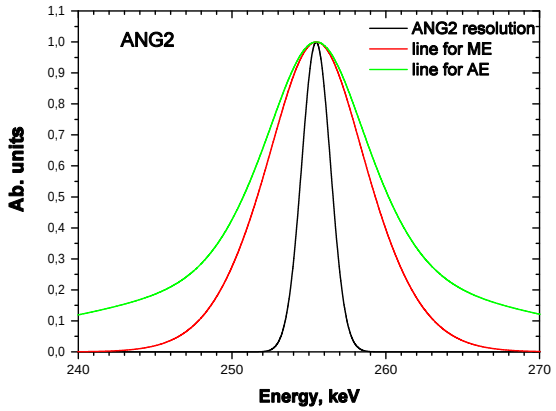

Figure 3: The expected line shape at 255.5 keV when only M-shell/all shell electrons are taken into account. The black curve shows for comparison the detector resolution without Doppler broadening.

background lines in that energy range from $^{212,214}Pb$. The typical energy resolution is about 2.1 keV.

3.1 Determination of limits for electron decay events

3.1.1 One sigma approach

The maximum number of electron decay events has been determined in three ways. First, it has been evaluated by using the so-called 'one sigma approach' in which the excluded number of events due to the effect searched for is estimated simply as the square root of the number of background counts in a suitably chosen energy window ΔE (see, for example [18]). This method, inspite of its simplicity, gives the right scale of the sensitivity of the experiment. For example, for ANG2 3045 and 3684 counts are present in the spectrum of Fig. 4 within the maximal sensitivity intervals 250.161-260.957 keV (for the ME case) and 248.768-262.002 keV (for the AE case) which contain 90% of the expected peak; thus, the square root estimated gives λ<61.31/67.44 events (ME/AE cases). Using these values, the number of electrons in the germanium ($4.909{\cdot}10^{26}/7.1408{\cdot}10^{26}$ for ME/AE cases) and in the copper ($1.704{\cdot}10^{27}/2.600{\cdot}10^{27}$), the measuring time and the calculated efficiencies, we obtain the mean lifetime limit $\tau > 3.306{\cdot}10^{25}/4.416{\cdot}10^{25}$yr (ME/AE cases). In the same way, the mean lifetime limits for all detectors, for setup1 and for the full setup were obtained (see Table 5).

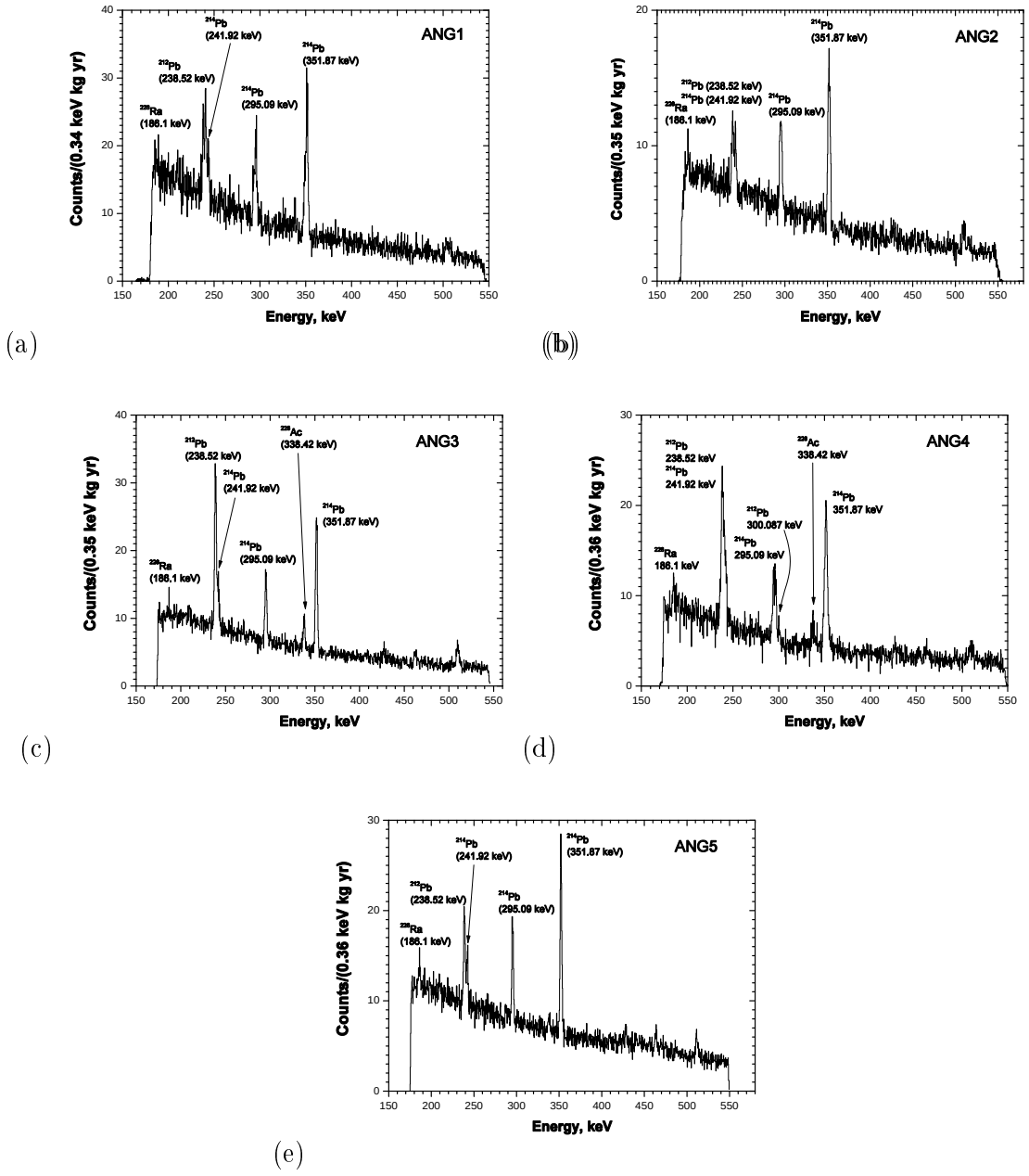

Figure 4: Measured spectra for all five detectors of the HEIDELBERG-MOSCOW experiment in the energy range of interest for the process $e^- \to \nu_e + \gamma$.

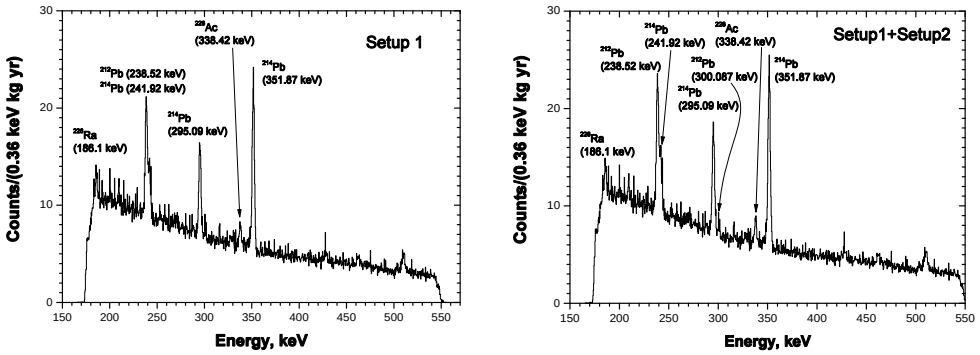

Figure 5: Measured spectra for the full setup of the HEIDELBERG-MOSCOW experiment, and setup1 separately, in the energy range of interest for the process $e^- \to \nu_e + \gamma$.

Table 5: Calculated values of the maximum number of electron decay events that can be excluded at the peak position (λ) and respective limits of the lifetimes in the frame of the 'one sigma approach' (90% of expected peak).

		λ, counts		Lifetime limit, yr	
	Detectors	ME case	AE case	ME case	AE case
Setup 1	ANG1	49.229	55.255	$5.760 \cdot 10^{24}$	$7.464 \cdot 10^{24}$
	ANG2	61.313	67.440	$3.306 \cdot 10^{25}$	$4.416 \cdot 10^{25}$
	ANG3	63.945	71.552	$2.224 \cdot 10^{25}$	$2.890 \cdot 10^{25}$
	ANG5	73.148	80.359	$3.076 \cdot 10^{25}$	$4.121 \cdot 10^{25}$
	Full setup1	125.485	140.330	$4.064 \cdot 10^{25}$	$5.286 \cdot 10^{25}$
Setup 2	ANG4	46.081	51.568	$2.008 \cdot 10^{25}$	$2.611 \cdot 10^{25}$
Full setup: (setup 1 + setup 2):		133.551	149.443	$4.179 \cdot 10^{25}$	$5.530 \cdot 10^{25}$

3.1.2 Analysis by Maximum Likelihood Method and the Least Squares Method

Second we used the approximate analytical maximum likelihood technique [18, 19] to fit the experimental spectrum in the neighborhood of the peak searched for. We fitted the energy range 210-310 keV, assuming a linear background and 3 lines (and 4 lines for ANG4 and the full setup) from $^{212,214}Pb$ (see Figs. 4,5), and the Doppler-broadened expected line. The numbers of electron decay events, calculated according to the maximum likelihood analysis, due to an effect, which can be excluded at 68% (90%) C.L. [19, 20] and the mean life-time limits for the ME/AE cases are presented in Table 6.

Table 6: Calculated values of the maximum number of electron decay events that can be excluded at the peak position (λ) and respective limits of the mean lifetimes τ in the frame of the analytical maximum likelihood technique.

		λ (68%/90% C.L.), counts	
	Detectors	ME case	AE case
Setup 1	ANG1	13.777/18.943	16.441/21.104
	ANG2	32.204/48.610	60.627/81.109
	ANG3	20.889/30.695	47.836/55.551
	ANG5	12.518/20.793	17.620/28.728
	Full setup1	80.754/104.842	132.532/187.610
Setup 2	ANG4	6.841/16.248	17.826/38.365
Full setup: (setup 1 + setup 2):		41.169/60.153	69.129/105.817

		Lifetime limit (68%/90% C.L.), yr	
	Detectors	ME case	AE case
Setup 1	ANG1	$2.058{\cdot}10^{25}/1.497{\cdot}10^{25}$	$2.513{\cdot}10^{25}/1.954{\cdot}10^{25}$
	ANG2	$6.295{\cdot}10^{25}/4.170{\cdot}10^{25}$	$4.912{\cdot}10^{25}/3.671{\cdot}10^{25}$
	ANG3	$6.807{\cdot}10^{25}/4.632{\cdot}10^{25}$	$4.326{\cdot}10^{25}/3.723{\cdot}10^{25}$
	ANG5	$1.797{\cdot}10^{26}/1.082{\cdot}10^{26}$	$1.880{\cdot}10^{26}/1.153{\cdot}10^{26}$
	Full setup1	$6.315{\cdot}10^{25}/4.864{\cdot}10^{25}$	$5.597{\cdot}10^{25}/3.954{\cdot}10^{25}$
Setup 2	ANG4	$1.352{\cdot}10^{26}/5.698{\cdot}10^{25}$	$7.554{\cdot}10^{25}/3.510{\cdot}10^{25}$
(setup 1 + setup 2):		$1.380{\cdot}10^{26}/0.944{\cdot}10^{26}$	$1.195{\cdot}10^{26}/0.781{\cdot}10^{26}$

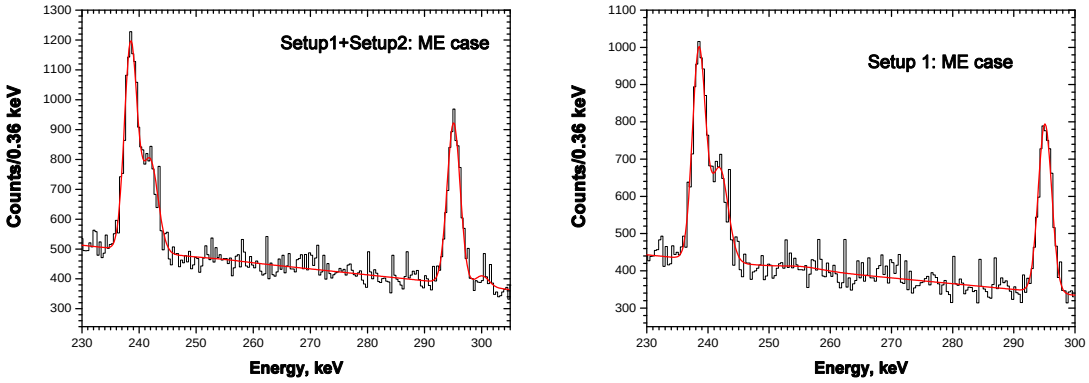

Figure 6: Full spectrum with the least-squares fitting curve for the ME case for setups 1 and 1+2 of the HEIDELBERG-MOSCOW experiment, in the range around the expected signal from e^- decay.

Table 7: Results calculated in the frame of the standard least squares procedure.

Detectors	$\frac{\chi^2}{NDF}$ ME/AE case	Peak area ME/AE case, counts	λ (68%/90% C.L.), counts ME case	AE case
ANG1	1.422/1.423	-38.187±51.077/ -83.759±90.216	13.216/22.850	12.350/22.824
ANG2	0.991/0.992	89.444±63.058/ 146.341±110.710	38.354/51.138	64.772/86.362
ANG3	1.275/1.243	-38.301±67.374/ -57.914±118.130	13.216/22.850	21.295/37.497
ANG5	1.393/1.391	-33.273±75.947/ -111.978±132.749	14.343/24.867	19.764/35.699
Setup1	2.092/2.095	185.881±144.264/ 293.838±273.878	83.392/111.531	138.429/189.972
ANG4	1.339/1.368	-76.249±47.401/ -114.450±83.968	4.789/9.065	10.386/20.771
Setups 1 + 2	2.143/2.144	45.587±153.863/ 26.670±292.608	46.501/74.146	72.604/88.052

Detectors	Lifetime limit (68%/90% C.L.), yr ME case	AE case
ANG1	$2.146 \cdot 10^{25}/1.241 \cdot 10^{25}$	$3.340 \cdot 10^{25}/1.807 \cdot 10^{25}$
ANG2	$5.285 \cdot 10^{25}/3.964 \cdot 10^{25}$	$4.598 \cdot 10^{25}/3.448 \cdot 10^{25}$
ANG3	$1.076 \cdot 10^{26}/0.622 \cdot 10^{26}$	$9.712 \cdot 10^{25}/5.516 \cdot 10^{25}$
ANG5	$1.569 \cdot 10^{26}/0.905 \cdot 10^{26}$	$1.676 \cdot 10^{26}/9.277 \cdot 10^{25}$
Setup1	$6.115 \cdot 10^{25}/4.572 \cdot 10^{25}$	$5.358 \cdot 10^{25}/3.905 \cdot 10^{25}$
ANG4	$1.933 \cdot 10^{26}/1.021 \cdot 10^{26}$	$1.297 \cdot 10^{26}/6.483 \cdot 10^{25}$
Setups 1+2	$1.222 \cdot 10^{26}/0.766 \cdot 10^{26}$	$1.138 \cdot 10^{26}/0.939 \cdot 10^{26}$

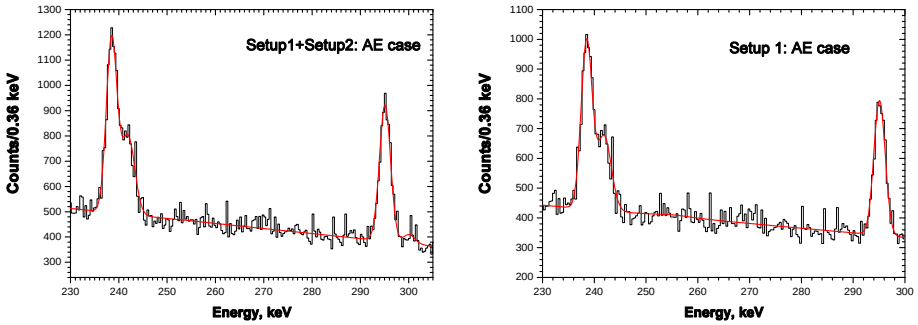

Figure 7: Full spectrum with the least-squares fitting curve for the AE case, setups 1 and 1+2 of the HEIDELBERG-MOSCOW experiment, in the range around the expected signal from e^- decay.

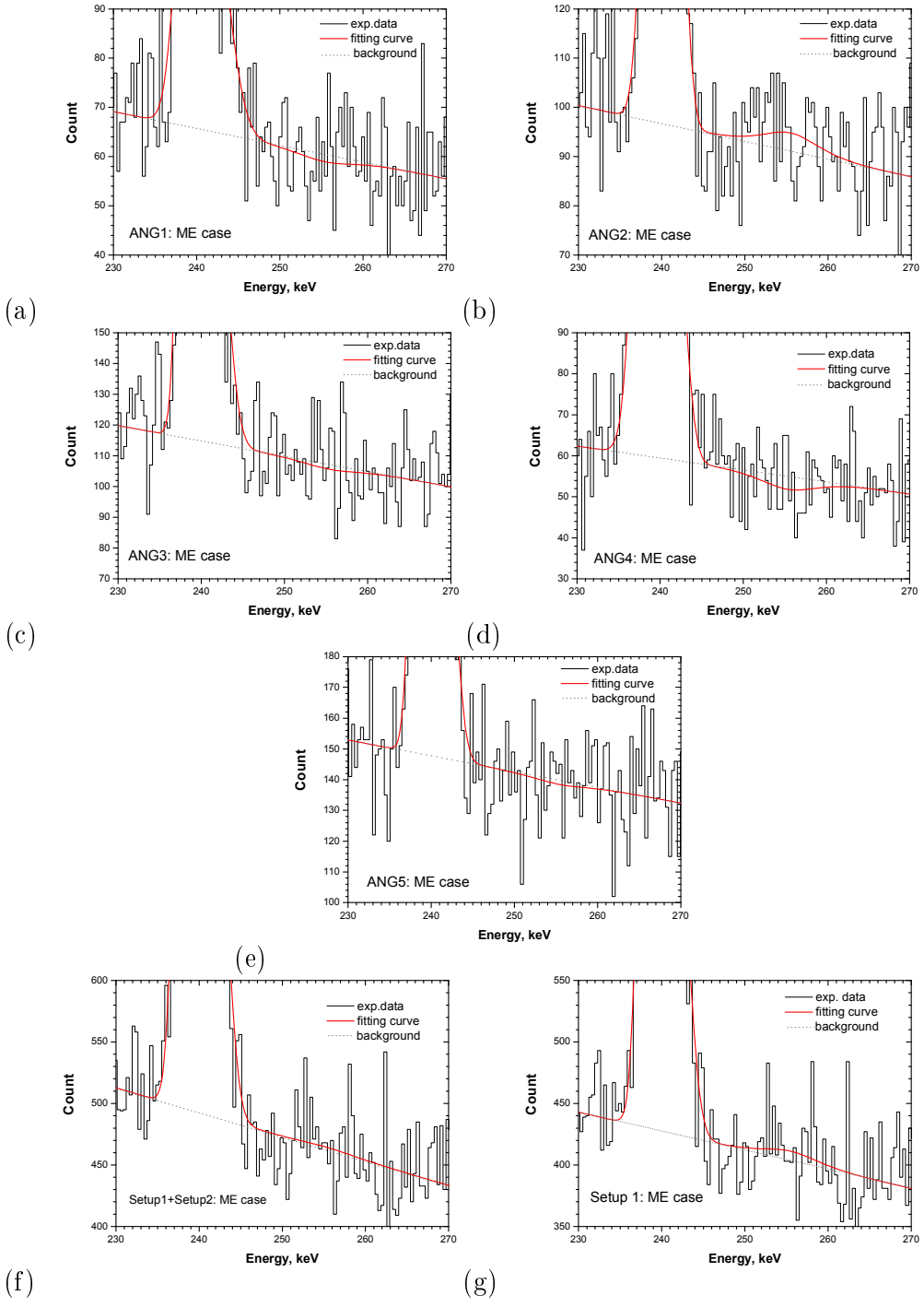

Figure 8: Spectrum in the energy region of interest for e^- decay (counts/bin) over the full measuring time (see Table 2) with the least squares fitting curve for the ME case, for all five detectors, and setups 1 and 1+2 of the HEIDELBERG-MOSCOW experiment (zoom of Fig. 6, which shows the full fitted range only for Figs. 8 f,g).

Finally, the λ value was determined by using the standard least squares procedure. Some of fitting curves are shown in Figs. 6,8,7. As for the maximum likelihood fit, the Gaussian centroids are fixed at the values E_1=238.52 keV, E_2=241.92 keV, E_3=295.09 keV and E_4=300.087 keV [15]. From the fit, ANG1, ANG3, ANG4 and ANG5 give no evidence of an effect (line) near 255 keV. (In ANG2 and setup1 there is a small peak in the energy region of the electron decay.) The peak areas (counts), number of the events due to the effect which can be excluded at 68% (90%) C.L. [19], and the mean life-time limit for the ME-AE cases are presented in Table 7.

The mean life time limit for the electron decay mode $e^- \to \gamma + \nu_e$ after 6.038 years of effective measuring time of the full HEIDELBERG-MOSCOW setup is
$T_{1/2} > 1.222 \cdot 10^{26}/7.662 \cdot 10^{25}$ yr (68%/90% C.L.) if we are taking into account only M-shell electrons for germanium, and $T_{1/2} > 1.138 \cdot 10^{26}/9.385 \cdot 10^{25}$ yr (68%/90% C.L.) for the case, when all electrons are taken into account. The best limit obtained from a single detector is 1.93×10^{26} y. We see a small peak in the energy region near 255.5 keV, at a $1.42\sigma/1.29\sigma$ (for ANG2/Setup1), corresponding to a mean life time of $(4.51 \pm 3.18) \times 10^{25}$ y.

4 Conclusions

From the analysis of the data of the HEIDELBERG-MOSCOW $\beta\beta$ experiment we derive one of the sharpest limits for the stability of the electron for the process $e^- \to \gamma + \nu_e$.

Setups 1+2 together yield a lower mean life time limit of 1.2×10^{26} y. The best limit from a single detector comes from detector 4 with 1.93×10^{26} years. This is the by far best limit - more than one order of magnitude stronger - than those obtained in previous Ge experiments (see Table 1), and it is one of the best limits in general.

If comparing this limit with the presently sharpest claimed limit given by Borexino [10], of 4.6×10^{26} years, it may be essential to note that the present limit has been deduced from the data without any uncertainties resulting from any treatment of the background (see section 1).

As discussed e.g. in [24] there is currently no self-consistent and noncontradictory theory describing possible violations of the charge conservation and allowing to suitably parameterize information from the experimental lifetime limits. If one introduces however, following [21], a charge nonconservation parameter by assuming that the weak interaction Lagrangian includes a small charge nonconservation part having the usual form, but with a neutrino replacing the electron in the lepton current; then

$$L_{CNC} = \frac{1}{2} e \epsilon_{e\nu\gamma} \bar{\Psi}_e \gamma_\mu (1 - \gamma_5) \Psi_\nu A^\mu + h.c., \tag{4}$$

where the parameter $\epsilon_{e\nu\gamma}$ gives a measure of the charge nonconservation. The transition probability for the electron decay $e^- \to \gamma + \nu_e$ can be written, according to [22], as:

$$\lambda^{CNC}_{e\nu\gamma} = \epsilon^2_{e\nu\gamma} \frac{\alpha}{32\pi} \frac{m_e c^2}{\hbar} \left[1 + \left(\frac{m_e}{m_\gamma} \right)^2 \right] \approx \epsilon^2_{e\nu\gamma} \frac{\alpha}{32\pi} \frac{m_e c^2}{\hbar} \left(\frac{m_e}{m_\gamma} \right)^2, \tag{5}$$

where α is the fine structure constant. According to [24] $\epsilon^2_{e\nu\gamma}\left(\frac{m_e}{m_\gamma}\right)^2 = \frac{5.6\cdot 10^{-25}}{\tau}$ and thus the experimental limit for the full setup 1+2 leads to the bound $\epsilon^2_{e\nu\gamma}\left(\frac{m_e}{m_\gamma}\right)^2 = 4.59\cdot 10^{-51}/0.73\cdot 10^{-50}$ (68%/90% C.L.) for the ME case and $\epsilon^2_{e\nu\gamma}\left(\frac{m_e}{m_\gamma}\right)^2 = 4.92\cdot 10^{-51}/0.60\cdot 10^{-50}$ (68%/90% C.L.) for the AE case. If we combine the latter expression with the best laboratory limit on the photon mass $m_\gamma < 7\cdot 10^{-19}$ eV [25], we obtain the following restrictions for charge nonconservation: for the ME case $\epsilon^2_{e\nu\gamma} < 0.86\cdot 10^{-98}/1.14\cdot 10^{-98}$ and for the AE case $\epsilon^2_{e\nu\gamma} < 0.92\cdot 10^{-98}/1.13\cdot 10^{-98}$ at 68%/90% C.L.

5 Acknowledgement:

The authors acknowledge the support from BMBF and DFG (RFBR 06-02-04009) and RFFI (RFBR 06-02-04003) of this project. I.V. Titkova thanks personally Dr. A.V. Derbin for useful and friendly discussions.

References

[1] H.V. Klapdor-Kleingrothaus, I.V. Krivosheina, A. Dietz et al., *Phys. Lett.* **B 586** (2004) 198-212.

[2] H.V. Klapdor-Kleingrothaus, A. Dietz, I.V. Krivosheina et al., *Nuclear Instr. and Methods* **A 522** (2004) 371-406.

[3] H.V. Klapdor-Kleingrothaus, in Proc. of 2nd Scandinav. Neutrino Workshop, SNOW2006, May 2-6, 2006, Stockholm, Sweden, Physica Scripta T 127 (2006) 40-42.

[4] G. Feinberg, M. Goldhaber, Proc. Nat. Acad. Sci. USA, 45 (1995) 1301.

[5] M.K. Moe and F. Reines, Phys. Rev 140 (1965) 992.

[6] E.L. Kovalchuk et al., JETP Lett. 29 (1979) 145.

[7] F.T.Avignone III et al., Phys. Rev. D 34 (1986) 97-100.

[8] HEIDELBERG-MOSCOW Collaboration, Phys. Lett. B (1993) 278-282.

[9] Y. Aharonov et al., Phys. Rev. D 52 (1995) 3785; Phys. Lett. B 353 (1995) 168.

[10] H.O. Back et al., Phys. Lett. B 525 (2002) 29-40.

[11] H.V. Klapdor, Proposal, Internal Report, MPI-1987-V17, September 1987.

[12] H.V. Klapdor-Kleingrothaus et. al, Eur. Phys. J. A 12 (2001) 147.

[13] M. Gunther et al, HEIDELBERG-MOSCOW Collaboration, Phys. Rev. D 55 (1997) 54.

[14] Ch. Dörr, H.V. Klapdor-Kleingrothaus, Nucl. Instr. Meth. A513 (2003) 596-621.

[15] D.R. Lide, 'Handbook of chemistry and physics', 85-th edition 2004-2005, CRC PRESS.

[16] GEANT4 Collaboration, http://geant4.web.cern.ch/geant4.

[17] E. Bellotti et. al, Phys. Lett. B 124 (1983) 435-438.

[18] P.R. Bevington, D.K. Robinson, 'Data Reduction and Error Analysis for the Physical Sciences', Third Edition, McGraw Hill, 2003.

[19] 'Review of particle physics', by Particle Data Group, Phys. Lett B 592 (2004).

[20] G.J. Feldman, R.D. Cousins, Phys. Rev.D 57 (1998) 3873.

[21] J.N. Bahcall, Rev. Mod. Phys. 50 (1978) 881; 'Neutrino Astrophysics', (Cambridge University Press, Cambridge, England, 1993), p.360.

[22] M. Suzuki, Phys. Rev.D 38 (1988) 1544.

[23] P. Belli, et al., Astroph. Phys. 5 (1995) 217.

[24] P. Belli, R.Bernabei, C.J.Dai et al, Phys. Rev. D 61 (2000) 117301.

[25] J. Luo et al., Phys. Rev. Lett. 90 (2003) 081801, Phys. Rev. Lett. 91 (2003) 149102; PDG, Phys. Lett. B 592 (2004) 1.

[26] W.A. Reed, P. Eisenberger, Phys. Rev. B 6 (1972) 4596.

List of Publications (2006)

1. **A New Experimental Limit for the Stability of the Electron,**
   H.V. Klapdor-Kleingrothaus, I.V. Krivosheina, I.V. Titkova,
   Phys. Lett. B 644 (2006) 109-118.

HEIDELBERG - MOSCOW. The Evidence for Lepton Number Violation: The Identification of $0\nu\beta\beta$ Events from the Full Spectra - Lessons After the Evidence - The Next Step

H.V. Klapdor-Kleingrothaus[a] and I.V. Krivosheina[b]

[a] Max-Planck Institut f̈urKernphysik, Heidelberg, Germany
[b] Institute of Radiophysical Research, Nishnij Novgorod, Russia
[a] Spokesman of the Collaboration; E-mail: H.Klapdor@mpi-hd.mpg.de
Home-page: http://www.mpi-hd.mpg.de.non_acc/

Abstract

The final result of the HEIDELBERG-MOSCOW experiment, which searched with 11 kg of enriched ^{76}Ge for double beta decay in the Gran Sasso underground laboratory, is presented for the main set of data taken in the period Nov. 1995 - May 2003 [3, 4, 5]. In this period the time structures of all events have been registered. Two different methods of pulse shape analysis [4, 5, 7, 8, 9, 14, 3] lead to selection of potential $0\nu\beta\beta$ events at $Q_{\beta\beta}$ with almost no γ-background in a wide range around $Q_{\beta\beta}$. The background achieved in the energy region around $Q_{\beta\beta}$ is 0.006 events $kg^{-1}yr^{-1}keV^{-1}$. A line at $Q_{\beta\beta}$ is observed on a confidence level of more than 6σ. It is not necessary that we identify this line with neutrinoless double beta decay, but this does seem the most reasonable explanation at present.

1 Introduction

Nuclear double beta decay provides an extraordinarily broad potential to search for beyond standard model physics [1, 2, 23]. Its occurrence has enormeous consequences: it means that total lepton number is not conserved, and second that the neutrino is a Majorana particle. Furthermore it can provide, *under some assumptions*, an absolute scale of the neutrino mass, and yields sharp restrictions for SUSY models, leptoquarks, compositeness, left-right symmetric models, test of special relativity and equivalence principle in the neutrino sector and others [1, 2]. Among the many existing efforts in search for this process, since 13 years now the HEIDELBERG-MOSCOW experiment [12] which operated 11 kg of enriched ^{76}Ge in the period Nov. 1990 - May 2003 in the Gran Sasso underground laboratory is the by far most sensitive double beta experiment, and probably will remain this at least for the next decade.

The *first* and up to now only evidence for $0\nu\beta\beta$ decay has been reported from this experiment [6, 4, 5, 10, 2, 11, 28]. From the analysis of the full spectrum *without any background subtraction* a line was observed at $Q_{\beta\beta}$ on a 4.2σ c.l. [1]. In the period Nov. 1995 - May 2003 which delivered *the main set of data*, the time structures of all events have been registered. In this contribution we concentrate on an analysis of *these* data, and try to select $0\nu\beta\beta$ event candidates from the surrounding γ -background by two different and completely independent methods of pulse shape analysis. For a proof of observation of neutrinoless double beta decay a method is required, which fulfills the following criteria: (1) - select $0\nu\beta\beta$ events at $Q_{\beta\beta}$; (2) - reduce strongly surrounding γ events.

In this Contribution we show that both of our pulse shape analysis methods, neuronal net method [14, 4, 5, 6] and method based on calculated pulse-shape libraries [15, 3], fulfill these criteria, and lead to consistent results. We show that we have now *two projections of events with almost no background*, which both prove the existence of a line at $Q_{\beta\beta}$. The signal seen in *each* of the pulse shape analyzed spectra has a confidence level of $\sim 6\sigma$. It is not necessary that we identify this line with neutrinoless double beta decay, but this does seem the most reasonable explanation at present.

2 The Identification of $0\nu\beta\beta$ Events

2.1 The Applied Pulse Shape Analysis (PSA) Methods

2.1.1 The Neuronal Net Method

A general description of the neuronal method used in this analysis is given in [14]. It was applied in a first step already in [4, 5]. This neuronal method (which we call N or 'total' neuronal net here), was trained with one γ -double escape line (DE), and a second one (called R) trained with *two* γ lines. For the following discussion we have to explain some notations. The 'total' projection N by the neuronal method can be subdivided into events seen *only* by method N (called NN here), events seen by methods N *and* R (called NR), seen by methods N,R and the method (called H) developed in [13], (called HNR). So the total projection by N can be written as sum of subprojections N=HNR+NN+NR+HN+HR. In Fig. 31 of [5] we show the projection obtained by HNR+NN (which we call 'global' neuronal net here) which contains *most* of the N-events. We will show below that the selectivity of events around $Q_{\beta\beta}$ increases drastically, if we use only the subclass NN of the projection.

2.1.2 Zero Range Library

Since our Monte Carlo calculations (see [7, 8, 9]) show, that most $\beta\beta$ -events have a small size, a library of pulses has been built up for pulses, in which all energy of the event is assumed to be deposited in one point in the detector (zero range approximation), for the four enriched ^{76}Ge detectors of the HEIDELBERG-MOSCOW experiment [7, 8, 9, 15, 16], which measured the time structure of events in the period Nov. 1995 - May 2003 with 250 MHz flash ADCs, throughout the detector volume. This is found to be a good approximation for $\sim 80\%$ of the $\beta\beta$ events (see [15, 16]). This is shown by calculations,

[1] An independent analysis of the data taken *until 2000*, which confirmed our earlier result published in [6], has been performed in [29]. Another analysis of part of the data (which was performed by the Kurchatov part of the collaboration - which left the collaboration in 2001) has been shown to be *wrong* in [4], page 201, and [5], p.382, 385. Some earlier criticism has been *ruled out* already in [10, 30], i.e. it was already history before the higher statistics data were presented in [4, 5]

starting from Monte Carlo simulated time history and spatial distribution of $0\nu\beta\beta$ events as function of location in the detector (including the dependence on the spectral angular correlation of the emitted electrons) [7, 15] (see Fig.1).

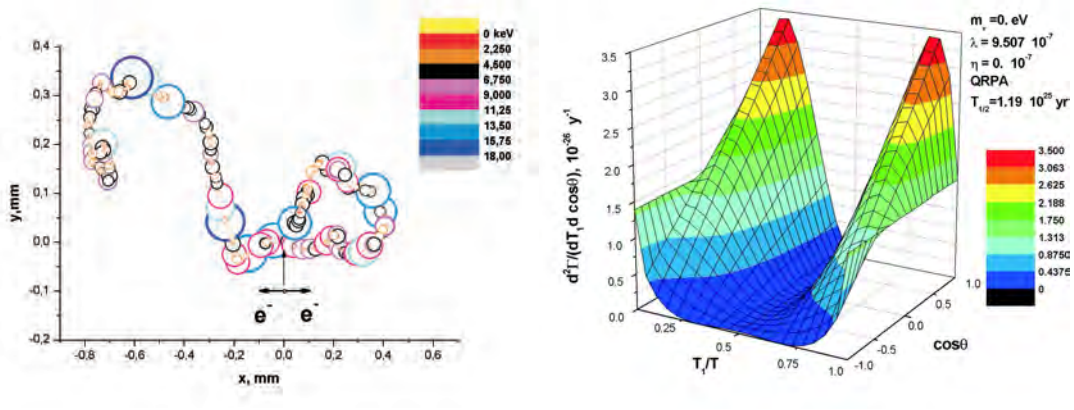

Figure 1: Typical calculated event for $0\nu\beta\beta$ decay without photon emission (bremstrahlung). Right: Calculated spectral angular correlation for the $\langle\lambda\rangle^2$ - term for $0\nu\beta\beta$ decay of ^{76}Ge (see [7]).

The pulses *measured* in the HEIDELBERG-MOSCOW experiment will later in this paper be compared to pulses of this library. The method of calculation follows the standard procedure and has been described in [15]. The library of pulses was calculated as function of location (R,Z) of the event in the detectors. It was optimized and checked by measurements with collimated γ -sources. For this purpose γ -source measurements have been performed with a collimator in the period July to September 2004 in Gran Sasso, in which shapes of pulses were measured as function of radius and height of the enriched detectors (see [15]). The calculated library was iteratively optimized in order to reach simultaneously the best possible localization of events along the detector volume for a given placement of the collimator in the source measurements, as well as to reach the best suppression of the 1620 keV line which is mainly consisting of higher multiplicity (larger size) events, with respect to the double escape γ -line of the 2614 keV transition, which is known (see, e.g. [7, 8, 9]) to consist of sharply localized events at 1592 keV (for details seen [15, 16]). The radial position resolution obtainable by analysis with the calculated libraries can be seen in [15].

2.2 Analysis of the Double Beta Decay Data of the HEIDELBERG-MOSCOW Experiment with Neuronal Net and Calculated Libraries

The nature of invention of suitable PSA methods is not simple. We will see, that the experimental data exhibit a greater swing of potential than indicated by theory [7, 8, 15]. This will be exploited here. We discuss now the pulse shape analysis (PSA) of the spectra measured in the period Nov. 1995 - May 2003 (see [4, 5]) by the two PSA methods.

The application of the neuronal net as described in section 2.2 ('first order neuronal net') reduced normal γ -lines (full energy peaks), see, e.g. Fig. 30, 31 of [5], which show

the selection by HNR+NN, (see section 2.2). However it is obvious, that this suppression is not sufficient to clearly separate a signal at $Q_{\beta\beta}$ from the surrounding background γ -lines, in particular at low statistics. We thus have to find a way to suppress the γ -lines *stronger*. We observe that this can be achieved by accepting from the events selected in the first order approach, only a *subclass* of events, namely when accepting only the subclass NN. In the library method, accepting only measured pulses which are fitted by a library event with a χ^2 smaller then required for optimal selection of 1592 keV single site events (see [15]) allows this ($\chi^2 <$ 0.4, 0.4, 0.7, 0.35 for detectors 2,3,4,5, respectively)[2]. In contrast to the 'first order' PSA-cuts in [5] *we now obtain by both methods an almost complete suppression of* γ *-lines* (see also [5, 3, 28]).

Fig. 2 shows the results of the cuts in the full detector volumes *and* those obtained when cutting 1 or 2 mm from the detector borders. This is the typical length which could be passed by electrons emitted on the surface (e.g. conversion electrons). By such cut we should loose on the other hand almost no $\beta\beta$ -events, since for most $0\nu\beta\beta$ events produced in this border zone, not the full energy will be deposited in the detector and thus they will not show up in the line at $Q_{\beta\beta}$. According to Monte Carlo calculations about 4% of all $0\nu\beta\beta$ events produced homogeneously in the detector, are lost in this way in the border range (see [8]). The surrounding γ -lines are now practically completely erased (compare to Fig.3 right). This includes the structure at $\sim$ 2030 keV. Only a tiny part is still seen of the 2053 keV ^{214}Bi line. The indication of a structure seen at $\sim$ 2024 keV in the full spectrum (Figs. 17,18 in [5]) which is still visible in Fig. 2 without border cut, seems to be a surface impurity vanishing with the 2 mm cut completely. What is remaining for the cut with the pulse library is a signal at 2038.4 $\pm$ 0.3(stat) $\pm$ 1.2(syst) keV. The estimated systematic error comprises ballistic deficit, energy non-linearity, etc. It is important to be noted, that the result is not dependent on details of the applied library – it is obtained for the library in which the impurity distribution in the detectors is approximated by a constant distribution [15] and also when the library is calculated using the realistic variation [17] of the impurities along the direction of the detector axis, given by the manufacturers (see Table 2 in [15]), and further, if we change the detector parameters within limits, still allowing to reproduce the location of the events measured with the collimated source. The χ^2 values of the cuts change slightly, but the selected events remain the same.

From the cut with the neuronal net (NN - see section 2.2) we obtain (Fig. 2 right) a signal at 2036.7 $\pm$ 0.2(stat) $\pm$ 1.2(syst) keV. The fits in Fig. 2 are made, conservatively assuming only one line in the energy window 2000-2100 keV, and treating all other structures as constant background. If we allow lines at the positions of the known ^{214}Bi lines, the confidence levels in Fig. 2 become somewhat larger (see Fig. 3). We obtained similar confidence levels for the signal when we analyzed a slightly smaller energy window, 2000-2060 keV (see [3]).

[2] We define chisquared here as a sum of squared deviations between the time structures of measured pulse and library pulse: $\chi^2 = \sum_{n=t05-f}^{t05-l} \frac{(i^n_{exp} - i^n_{lib})^2}{w5} \cdot 10^3$. Here i^n_{exp} and i^n_{lib} are the (normalized) experimental and library currents for the (time) channel n (one time step is 4 ns per channel of the flash-ADC sampling frequency of 250 MHz). $w5$ is the width at the 5% level of the amplitude (see Fig. 2). χ^2_{min} gives the degree of agreement of a measured pulse with the library pulse 'closest' in shape (time structure) to the measured pulse. For a detailed description see [15].

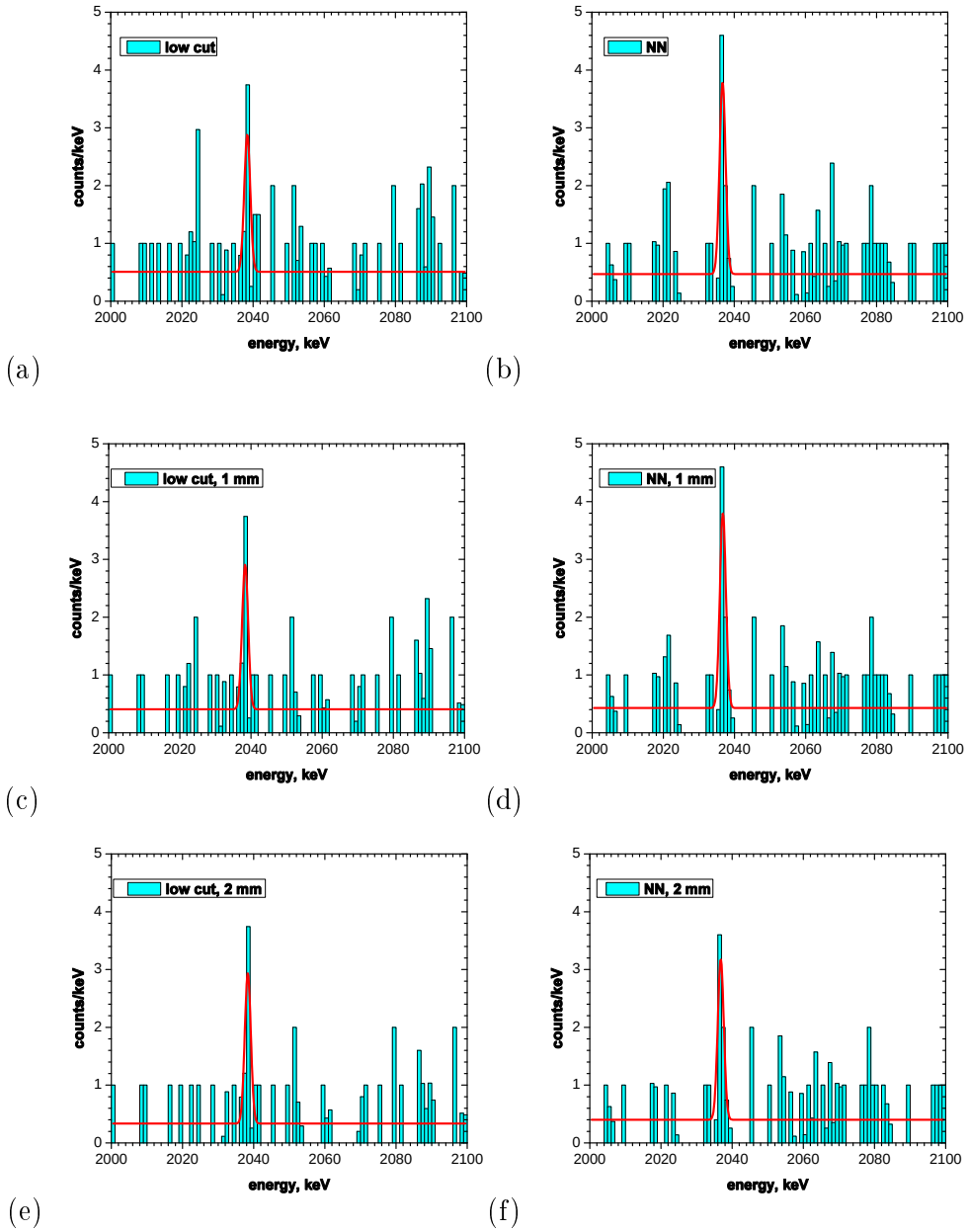

Figure 2: Left column: The pulse shape selected spectrum after applying the zero range library with 'small' cuts (left: (a),(c),(e)) measured with detectors 2,3,4,5 from 1995 to 2003 in the energy range of (2000-2100) keV. Shown are the events in the full detector (a) and cutting boundary areas of 1(2) mm -(c) and (e). Signals are found near $Q_{\beta\beta}$: 5.05±1.23, 5.33±1.08, and 5.54±0.96 events (a,c,e, respectively), corresponding to 4.1, 4.9 and 5.8σ levels. Right column: The pulse shape selected spectra (subsection NN by neuronal net, see also Fig. 33 from [5]) measured with detectors 2,3,4,5 from 1995 to 2003 in the energy range of (2000-2100) keV. Shown are the events in the full detector (b) and cutting boundary areas of 1(2) mm - (d) and (f). Signals near $Q_{\beta\beta}$ are found: 7.05±1.11, 7.18±1.03, and 5.91±0.97 events (b,d,f, respectively), corresponding to 6.4, 7.0 and 6.1σ confidence levels. The non-integral numbers of counts in the spectra in Figs. 2,3 are simply a binning effect (see [4]).

The spectra shown in Fig. 2 should be compared to the full spectra measured, shown in Fig. 3 (right) (see Figs. 4, 19 in [4, 5]). It is clear, that after applying the (NN) method (and similarly the library method) all γ -lines are drastically reduced and only a line at $Q_{\beta\beta}$ survives.

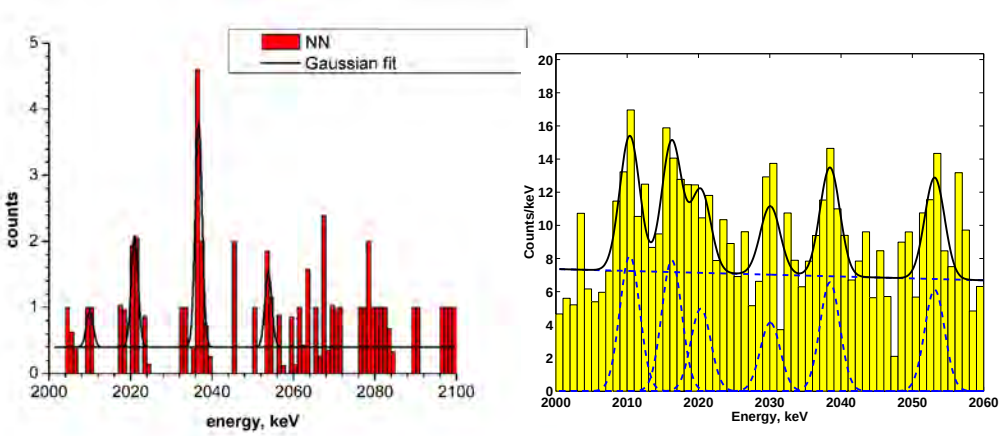

Figure 3: Left: The pulse shape selected spectrum (selection by the neuronal net-(NN) method, see also Fig. 33 from [5] and text below) measured with detectors 2,3,4,5 from Nov. 1995 to May 2003 in the energy range of (2000-2100) keV. The fit assumes a constant background and three lines at the position of known Bi lines and a signal at $Q_{\beta\beta}$. The signal at $Q_{\beta\beta}$ has consists of 7.27 ± 1.05 events (6.9σ). Right: The full spectrum measured in the same period (from [5]), in the energy range 2000-2060 keV.

If we sum the complementary spectra shown in Fig. 2, a line at $2037.4 \pm 0.5(\text{stat}) \pm 1.2(\text{syst})$ keV is seen at a 5.4, 6.4, 6.7σ level (0, 1, 2 mm border cut) (see [28, 3]). That the c.l. is smaller than would be expected from the summed information from the two different PSA approaches, has its reason in the larger width of the line resulting from the slight difference in energy in the lines from both methods, which again is coming from the ballistic deficit (see below).

Let us now look into the individual events and discuss them. First we note, that the events found by the zero range library and by the neuronal net subset (NN) are found to be complementary (see Table 1).

How can we understand these findings? Interestingly, parts of the full line at $Q_{\beta\beta}$ in Fig. 3 (right) can be *projected out of the full data, practically without background,* by the subset NN (defined in section 2.2) of the neuronal net given in [4, 5] and also by the low-χ^2 cut of the pulse shape analysis (PSA) described in [15]. All events projected out by these two procedures are selected also by the less restrictive full ('total', (see section 2.2)) neuronal net of [4, 5, 14] (see Table 1). So, the present result is fully consistent with those presented earlier [4, 5]. They contain no multiple site events (except for one event). In total, by the two projections, which show each a line near $Q_{\beta\beta}$ with almost no background, we find 9+8=17 events in the energy range 2036-2043 keV according to Table 1. From these, $\sim$11 events from the fits in Figs. 2, 3 remain in the line. This means we can identify the major part of the 19.6 ± 5.4 events determined from the fit of the line in the full spectrum (Fig. 19 and Table 7 in [5]), as $0\nu\beta\beta$ *candidate events.*

That the two projections select different events, we may understand in the following

way: the projections may select events in different parts of the volume of the detector. Table 1 shows that the neuronal net (NN) mainly selects events in the outer part of the detector, while the zero range library mainly selects in the inner parts. This would easily explain the slightly different energies of the lines observed by both methods - by the ballistic deficit (see below). The reason may lie in tiny deviations of the calculated electric fields from the real ones for the outer part of detector for the library method, and in limitations of the training process with the 1592 keV line for the neuronal method.

Table 1: Events selected by different methods in the energy region 2035-2043 keV for detectors 2,3,4,5 [4, 5]. 0 - global neuronal net selection NN+HNR; 1- Events selected by subclass of neuronal net method (NN); 2 - selected by low-χ^2 (see text) library cuts.

								Index:		
Det.	run	event	type	Date	Energy	χ^2	R[cm]	0	1	2
5	3357	2948	HNR	24.09.02	2034.39	0.33	3.45	+		+
3	3383	180	HNR	18.10.02	2035.14	0.77	1.84	+		
3	1627	172	HNR	15.05.99	2036.0	0.49	2.51	+		
3	749	295	NN	08.07.97	2036.04	1.68	2.7	+	+	
5	1067	421	NN	20.02.98	2036.31	0.98	2.65	+	+	
4	2613	47	NN	23.07.01	2036.37	1.72	1.99	+	+	
4	1762	97	HNR	28.08.99	2036.43	3.38	2.75	+		
3	3463	27	NN	07.01.03	2036.49	6.84	2.7	+	+	
5	2390	199	NN	27.01.01	2036.57	0.81	3.82	+	+	
2	2094	42	NR	20.05.00	2036.91	0.3	1.31			+
3	3385	354	HNR	21.10.02	2037.22	0.8	1.35	+		
5	1787	359	HNR	17.09.99	2037.22	0.31	1.91	+		+
5	2744	430	NN	21.11.01	2037.35	1.18	3.63	+	+	
3	108	112	NN	23.03.96	2037.58	0.81	2.45	+	+	
4	1271	251	HNR	01.08.98	2038.0	1.96	3.52	+		
3	2216	526	MSE	10.09.00	2038.3	0.38	1.1			+
4	1465	46	HNR	03.01.99	2038.33	5.9	2.75	+		
3	49	226	HNR	28.12.95	2038.53	0.26	2.27	+		+
4	1592	144	HNR	18.04.99	2038.57	0.53	1.99	+		+
2	735	131	HNR	28.06.97	2038.91	2.31	3	+		
4	2133	138	NR	24.06.00	2038.92	0.56	1.64			+
5	670	486	NN	09.05.97	2038.92	0.7	1.17	+	+	
3	3501	142	HNR	07.02.03	2038.97	0.74	2.7	+		
5	1036	73	HNR	26.01.98	2039.92	5.88	0.92	+		
3	1513	342	HNR	13.02.99	2039.93	0.55	2.27	+		
5	1650	206	HNR	03.06.99	2040.82	0.25	3.69	+		+
4	3449	74	HNR	22.12.02	2041.0	0.64	3.69	+		+
4	1378	490	HNR	27.10.98	2041.53	0.55	2.05	+		+
4	1125	296	HNR	05.04.98	2042.56	0.7	2.23	+		
4	3476	259	HNR	18.01.03	2042.75	0.78	1.35	+		
4	1833	74	HNR	22.10.99	2042.97	1.76	3.69	+		

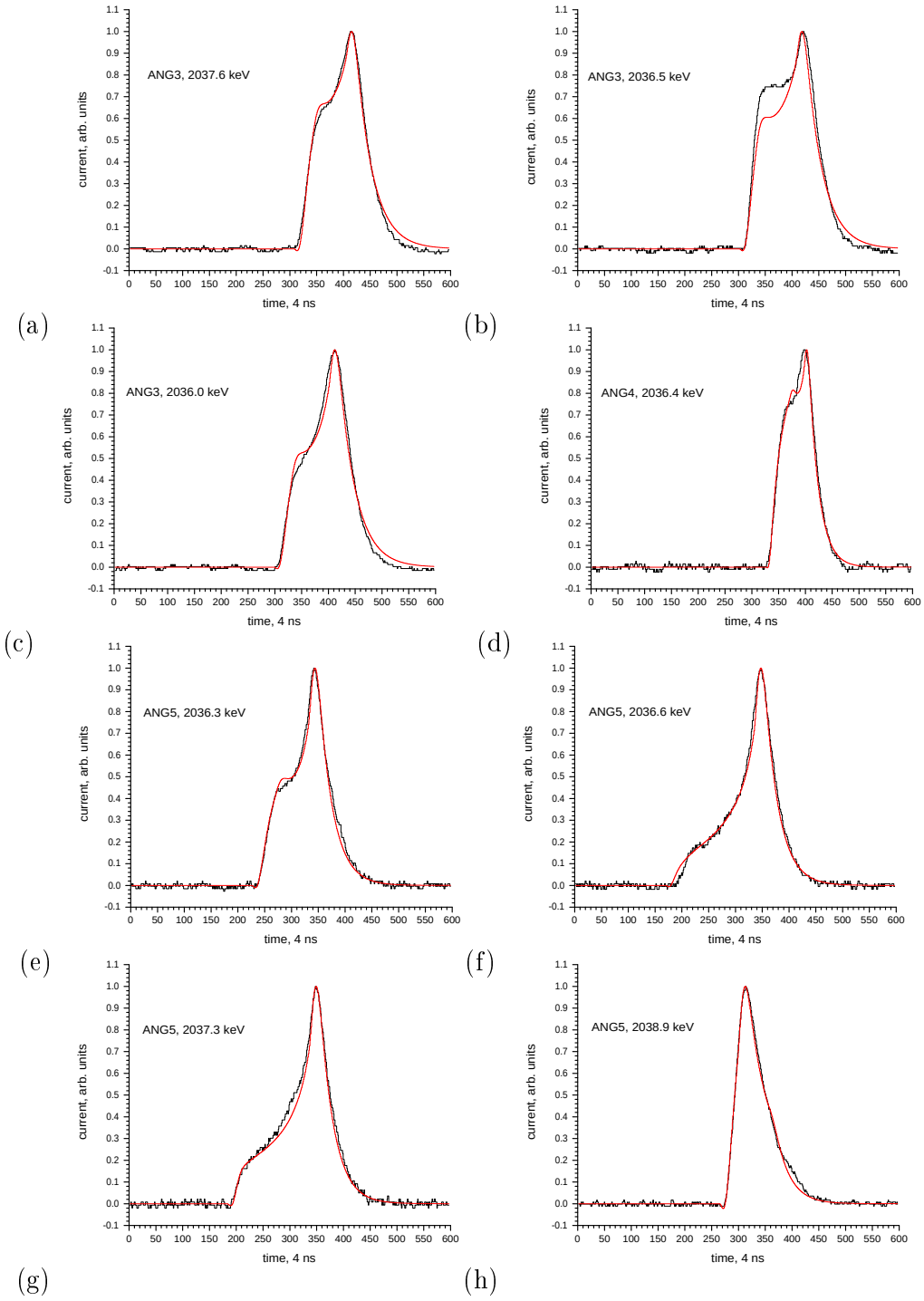

Figure 4: Time structure of those events (black) measured in the HEIDELBERG-MOSCOW experiment in the energy region 2036-2042 keV by the four enriched ^{76}Ge detectors (ANG2, ANG3, ANG4, ANG5), during the period Nov. 1995 - May 2003 selected by the neuronal net (NN selection, see text) as single-site events (see Table 1, and Fig. 9 in [4]). The red lines show fits of the events by the zero range pulse shape approximation library, as described in this paper. The χ^2 for the fit by the zero range library and the radii determined from the latter are: Det.3: (a)- 0.81(2.45 cm), (b)- 6.84(2.7 cm) and (c)- 1.68((2.7 cm); Det.4: (d)- 1.72(1.99 cm); Det.5: (e)- 0.98(2.65 cm), (f)- 0.81(3.82 cm), (g)- 1.18(3.63 cm), (h)- 0.7(1.17 cm) (see also Table 1).

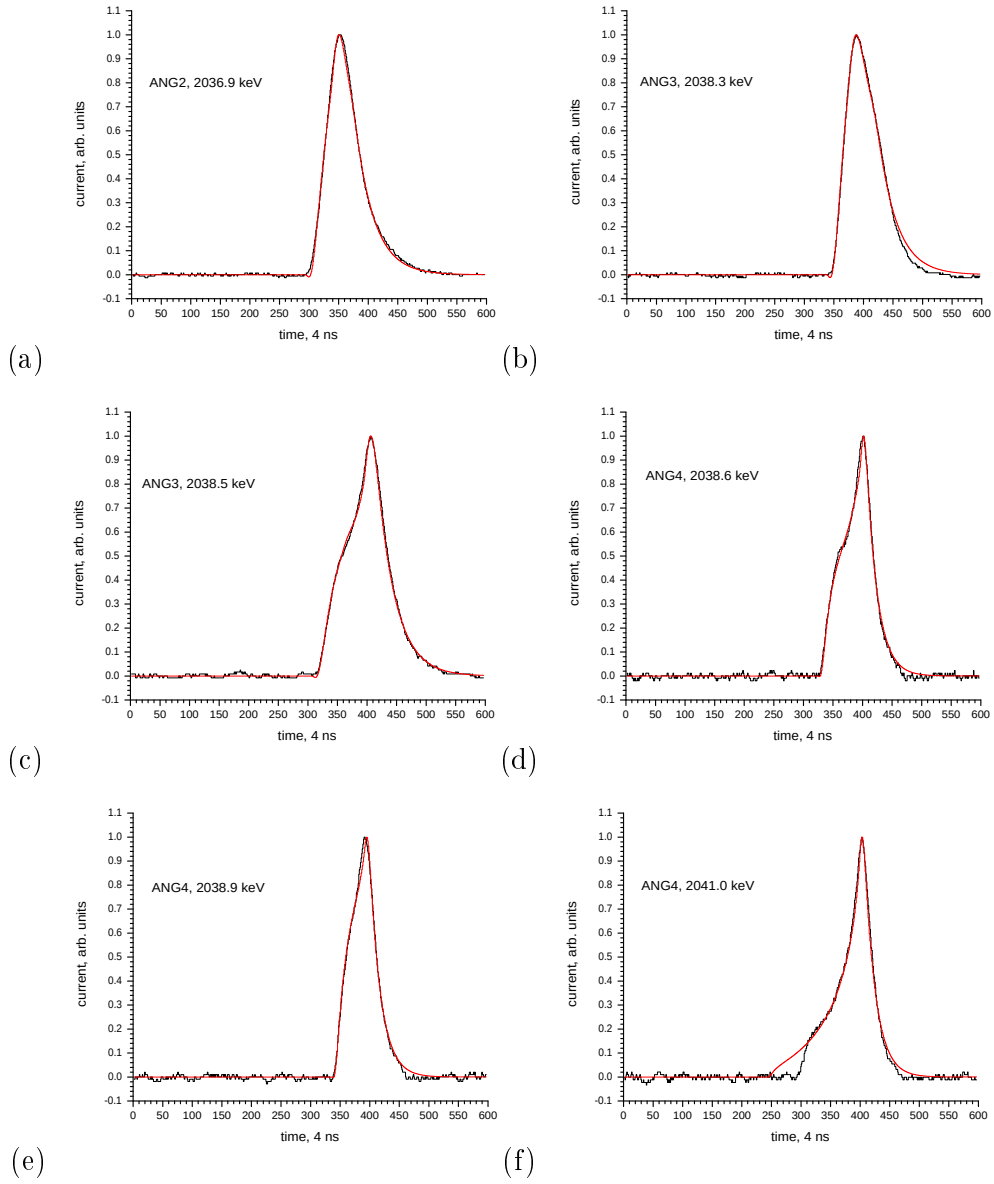

Figure 5: Time structure of those events (black) measured in the HEIDELBERG-MOSCOW experiment in the energy region 2036-2042 keV by the four enriched ^{76}Ge detectors (ANG2, ANG3, ANG4, ANG5), which were identified, by the low-cut PSA method (section 3) as single site events (see Table 1). The red lines show fits of the events by the zero range pulse shape approximation library, as described in this paper and in [15]. The χ^2 for the fit by the zero range library, and the radii determined from the latter are: Det.2: (a) - 0.3(1.31 cm); Det.3: (b) - 0.38((1.1 cm) and (c) - 0.26(2.27 cm); Det.4: (d) - 0.53(1.99 cm), (e) - 0.56(1.64 cm), (f) - 0.64(3.69 cm), and (g) - 0.55(2.05 cm); Det.5: (h) - 0.31(1.91 cm) and (i) - 0.25(3.69 cm), (see also Table 1).

It is important to note, that if we relax a bit the sharp cut conditions, then all selected events are seen by each of these methods. The softer cuts then are, however, not any more able to sufficiently strongly suppress the gamma background events, which then are also partly accepted by the cuts (see Fig. 31 in [5], which shows the neuronal net cut including in addition to NN events also HNR events, also see Table 1).

We should keep in mind that the selection methods have to look for differences between gamma events and double beta events - which could be extremely small. In that sense such effect of slight inhomogeneities of the methods over the detector volume, when strongly sharpening the cuts, may also not be surprising. It may be a question, whether the precision of the simulations of the electric field in the detectors can be pushed to such level at all, that such inhomogeneities fully disappear.

Concluding, by the two projection procedures, the major part of the line near $Q_{\beta\beta}$ in the full spectrum is selected as single site events, while at the same time the surrounding γ -lines are drastically reduced. Figs. 4,5 show these events, and fits by the zero range approximation of section 2.1. The radii at which the events are observed in the detector (determined by the zero range approximation) are given in Table 1. The observed distribution as function of R is found within the statistics to be consistent with that expected for a homogeneous source distribution. It is not necessary that we identify the observed line with neutrinoless double beta decay, but this does seem the most reasonable explanation at present.

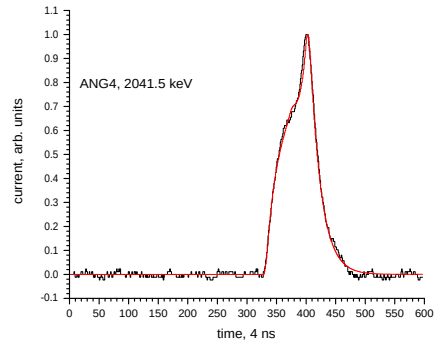

(g)

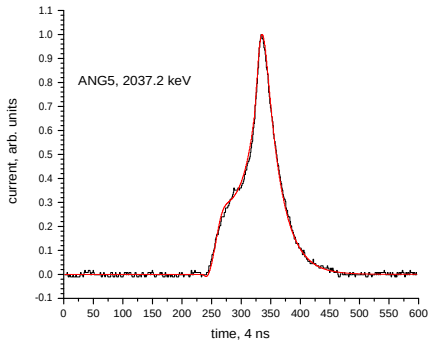

(h)

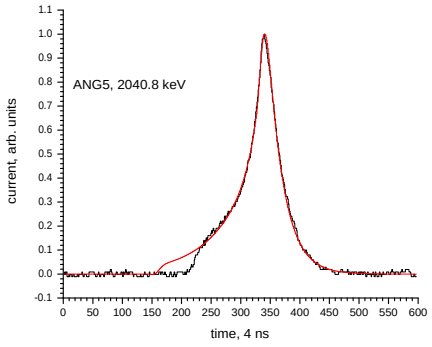

(i)

Fig. 5 continued.

The energy of the line observed, with 2037.4 $\pm$ 0.5(stat) $\pm$ 1.2(syst) keV seems to be slightly below the 'best' value reported for $Q_{\beta\beta}$ [36] of 2039.006$\pm$0.050 keV. Other

measurements report $Q_{\beta\beta}$ =2040.71±0.52 keV [33], 2038.56±0.32 keV [34] and 2038.668±2.142 keV [35].

Part of this difference, and the difference in energy of the (NN) and low-cut lines in Fig. 2, seems to be due to the effect of the ballistic deficit (see [18, 19]). Since in axial Ge detectors different radial location of events corresponds to large variation in the charge collection times, and the latter may come close to the differentiation time of the electronic circuit, this leads if uncorrected, to a dependence of the measured energy from the radial location of the individual event and to a broadening of the observed line. We have investigated this effect. We find [3] that for energies around $Q_{\beta\beta}$, a difference in energy between the relatively slow pulses that start from the peripheral parts of the crystal, with respect to the fastest pulses with initial radii of around 1.5 cm, of about 0.8-1.8 keV can be expected for the four enriched detectors used here.

3 Lessons after the Evidence - The Next Step

3.1 Status of search for $0\nu\beta\beta$

What is the main result from the HEIDELBERG-MOSCOW experiment (see [6, 4, 7, 15, 3, 28]).
- There is now a $>6\sigma$ signal for $0\nu\beta\beta$ decay.
- The neutrino is a Majorana particle.
- *Total* lepton number is violated (neutrino oscillations prove only violation of *family* lepton number).
- The neutrinos are (if we assume vanishing contributions of right-handed weak currents and of other contributions to the $0\nu\beta\beta$ amplitude, see below) degenerate in mass or (if the LSND result will be confirmed) allow existence of a *sterile* neutrino [4, 20]).
- The $0\nu\beta\beta$ process yields very strong limits for other fields of Beyond SM physics often well competitive to high energy accelerators (see [1, 10, 2]).

To put the experiment into historical perspective, the first (non-geochemical) discovery of $2\nu\beta\beta$ decay, in 1987 with a half-life of 1.1×10^{20} y for ^{82}Se, relied on a 2.2σ signal (35 events) [32].

Now we see this decay process, for ^{76}Ge, in the HEIDELBERG-MOSCOW experiment with **160 000 events** ($T^{2\nu}_{1/2} = 1.74\times10^{21}$ y) [21], i.e. the experimental sensitivity has been increased by a factor of **50 000 !!** This is what *allowed us* to see the $0\nu\beta\beta$ signal, with a half-life of $\mathbf{1.19\times10^{25}}$ **y** on a $>\mathbf{6}\sigma$ c.l. [4, 3, 28] (without methods to reduce the γ - background, on a 4.2σ level). The experiment is the by far most sensitive $0\nu\beta\beta$ experiment since 13 years and its sensitivity will be unfortunately not reached by other experiments in near future (see below).

It has the largest source strength ever in operation (11.0 kg), the lowest background in such type of experiment (0.17 counts kg y keV *without* pulse shape analysis), the highest efficiency for detection of $\beta\beta$ events ($\sim$95%), the highest energy resolution ($\sim$3.3 keV), the highest duty cycle and the highest collected statistics (71.7 kg y, i.e by a factor of 8.2 more than one of the other ^{76}Ge experiments (IGEX) which finished operation in 1999 (see e.g. [31])). Further, the background of the experiment is very well understood from extensive Monte Carlo simulations [21] and from independent analysis by [29].

Of decisive importance for the reduction of the γ -background in the range of the $Q_{\beta\beta}$ value of the $0\nu\beta\beta$ process was, to develop methods of pulse shape analysis which were able to separate $0\nu\beta\beta$ from γ background events (see section 2).

3.2 Lessons for present and future

3.2.1 To 'confirmation' of the ^{76}Ge experiment

The actual experimental status is in 2006 similar as it was in 2001. There is an observed signal and various experiments trying to check this result (some of them meanwhile stopped operation). What is required: - *Very good energy resolution.* Not fulfilled by NEMO III [43] and EXO which have 400 and 100 keV, respectively, to be compared to 3.3 keV in the HEIDELBERG-MOSCOW experiment [4, 10, 28]. - *Large efficiency.* Nemo III has only 14%, i.e. a 10 kg experiment is effectively only a 1.4 kg experiment. - *The measured spectrum should be shown and analysed over the full energy range* to show that the background is fully understood. - the $2\nu\beta\beta$ spectrum should be measured as well as a help for normalization of the $0\nu\beta\beta$ matrix element. This is at present not possible with sufficient precision for CUORICINO/CUORE.

Problems:

The main problem is that present and future 'confirmation' experiments partly because of the reasons mentioned are usually not sensitive enough: A good example is the NEMO III experiment. The half-life limits reached (at a 1.5σ level) of $T^{0\nu}_{1/2}$ =1.0×10^{23} and 4.6×10^{23} years for ^{100}Mo and ^{82}Se (see [43]) after 389 days of effective measurement are a factor of $\sim$ 20 away from the half-lives required to check the HEIDELBERG-MOSCOW ^{76}Ge result on a 1.5σ level. Since the half-life is connected with the measuring time by $T^{0\nu}_{1/2} = \sqrt{\frac{t\cdot M}{\delta E\cdot B}}$, this means that NEMO III would have to measure *more than 400 years, to see the signal on a 1.5σ level*, and correspondingly longer, to see it on a higher c.l. [10]. The future project SuperNEMO, with a by a factor large source strength, would still require 40 years for the same purpose (!!).

CUORICINO - which has the general problem, that it *cannot* distinguish between β and γ-events, and because of its high background cannot see the $2\nu\beta\beta$ spectrum of ^{130}Te, could see the HEIDELBERG-MOSCOW ^{76}Ge signal, assuming an uncertainty in the knowledge of the nuclear matrix element [22] of a factor of only 2, within 1 and 30 years - on a 1.5σ c.l. [10]. It can thus *never disprove* the HEIDELBERG-MOSCOW ^{76}Ge result (see also [40]).

The large version CUORE with a by a factor of 16 larger mass, also would need many years for a statement on a 6σ level.

EXO - the main problem is that *no tracks* are visible in a liquid ^{136}Xe experiment [41]. This kills the main idea of the experiment to separate $\beta\beta$ from γ events, and just reduces it to complicated calorimeter. Since the other main idea - laser identification of the daughter nucleus, is not (yet) working, the present rather modest aim is to reach a background level as reached in the HEIDELBERG-MOSCOW ^{76}Ge experiment, instead of the factor of 1000 less, projected earlier [42].

GERDA/MAJORANA - (the first of them being essentially a copy of the GENIUS project proposed in 1997 [37], planning to operate naked ^{76}Ge crystals in liquid nitrogen).

From our earlier Monte Carlo calculations we expected to get a large potential of GENIUS for $\beta\beta$ research. The only long-term experience with naked detectors in liquid nitrogen has been collected since then with our GENIUS-Test-Facility [38, 39]. The main problem found [28, 39] is that over longer operation time the leakage current of the detectors raised which led to *serious restrictions of the high voltages applicable* and finally to *destruction of the detectors*. MAJORANA, if performed with conventional detector mounting in Cu cups, will have serious difficulties - as already visible by the IGEX experiment stopped in 1999 [31] - to improve the background beyond the level reached by the HEIDELBERG-MOSCOW -experiment. If MAJORANA will also take up the GENIUS idea, the remarks given for GERDA should be considered.

COBRA - using or planning to use CdTe pixelized semiconductor detectors which may have in principle the potential of looking for $\beta^+\beta^+$ and β^+EC decay, still *is almost 10 orders of magnitude* away (see [44]) from the required sensitivity, to become useful for double beta decay research (see [7, 25]), e.g. for the points discussed in section 3.3. The increase in sensitivity of about one order of magnitude in the last four years shows that rather long time scales may be expected for this technique to come to fruitful applicability for $\beta\beta$ decay.

3.2.2 A problem of present and future experiments concerning the neutrino mass and right-handed weak currents

Concerning expected information on the ν mass, there is another problem in present and future experimental approaches. Even if one of the above or other $\beta^-\beta^-$ experiments would be able to confirm the HEIDELBERG-MOSCOW ^{76}Ge result, no *new* information would be obtained.

It is known for 20 years - but surprisingly often overlooked - that a $\beta^-\beta^-$ experiment can give information on the effective neutrino mass *only* under some *assumption* on the contribution of right-handed weak currents (parameters η, λ) or of others like SUSY etc. to the $\beta\beta$ -amplitude (see e.g. [1]). The half-life for the neutrinoless decay mode is given, if we neglect for simplicity contributions from SUSY, leptoquarks, etc. (for Refs. see [1]) by [26, 24]

$$[T^{0\nu}_{1/2}(0^+_i \to 0^+_f)]^{-1} =$$
$$= C_{mm}\frac{\langle m\rangle^2}{m_e^2} + C_{\eta\eta}\langle\eta\rangle^2 + C_{\lambda\lambda}\langle\lambda\rangle^2 + C_{m\eta}\langle\eta\rangle\frac{\langle m\rangle}{m_e} + C_{m\lambda}\langle\lambda\rangle\frac{\langle m_\nu\rangle}{m_e} + C_{\eta\lambda}\langle\eta\rangle\langle\lambda\rangle,$$
$$\langle m\rangle = |m^{(1)}_{ee}| + e^{i\phi_2}|m^{(2)}_{ee}| + e^{i\phi_3}|m^{(3)}_{ee}|\,,$$

where $m^{(i)}_{ee} \equiv |m^{(i)}_{ee}|\exp(i\phi_i)$ $(i = 1, 2, 3)$ are the contributions to the effective mass $\langle m\rangle$ from individual mass eigenstates, with ϕ_i denoting relative Majorana phases connected with CP violation, and $C_{mm}, C_{\eta\eta}, ...$ denote nuclear matrix elements squared. Ignoring contributions from right-handed weak currents on the right-hand side of the above equation, only the first term remains.

Thus, *in general* one obtains *only an upper limit on* $\langle m\rangle$. So if neutrino masses are deduced from $0\nu\beta\beta$ experiments, this is always done under the *assumption* of vanishing η, λ etc. In that sense it is highly premature to compare as often done such number with numbers deduced e.g. from cosmological experiments, such as WMAP or other experiments, or to use it as a landmark for future tritium experiments.

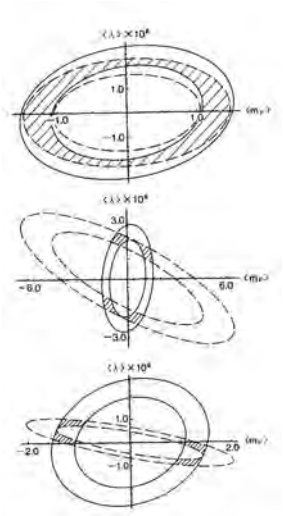

Figure 6: Allowed region of parameter space if $0\nu\beta\beta$ decay would be observed in two $0\nu\beta\beta$ decay experiments. Shown is only the $\langle\lambda\rangle - \langle m_\nu\rangle$ plane for simplicity. Upper part: For the plot schematically a $0\nu\beta\beta$ decay half life of $(1.5\pm0.50 \times 10^{24}$ y has been assumed for ^{76}Ge (full lines) and ^{136}Xe (dashed lines). The dashed area is consistent with both experiments (for discussions see [25]). Middle part: As upper part, but for one $0\nu\beta^-\beta^-$ decay experiment (^{76}Ge) and one experiment measuring the neutrinoless mixed mode β^+EC$^-$ decay of ^{124}Xe. For ^{124}Xe a $0\nu\beta\beta$ decay half life of $T_{1/2}^{0\nu\beta\beta}$=$(1.5\pm0.50 \times 10^{25}$ y has been assumed. Bottom part: As in middle part, but for a $0\nu\beta^+$EC decay half life of $T_{1/2}^{0\nu\beta\beta}$=$(1.5\pm0.50 \times 10^{26}$ y) for ^{124}Xe (see [25]).

It is unfortunate that even an additional high-sensitive $\beta^-\beta^-$ experiment (e.g. ^{136}Xe) *together* with the ^{76}Ge result can give *no* information to decide the individual contribution of $\langle m\rangle$, $\langle\eta\rangle$, $\langle\lambda\rangle$ to the $0\nu\beta\beta$ decay rate. This has been shown already in 1994 [7, 25] (see Fig. 6).

3.2.3 A proposed way out

In the same paper [25] it has been shown that the only realistic way to get this information on the individual contributions of m, η, λ is to combine the $\beta^-\beta^-$ result from ^{76}Ge, with a very high-sensitivity mixed mode β^+EC decay experiment (e.g. of ^{124}Xe) on a half-life level of 10^{27}years (see [7] and Fig. 6). The essential point is that the $0\nu\beta^+$EC decay is relatively more sensitive to the $\langle\lambda\rangle$ mechanism, than to the mass mechanism. The reasons for this are described in [25]. While in Fig. 3 the *principle* behaviour is shown, recent calculations, with the *measured* $0\nu\beta\beta$ half-life of ^{76}Ge, and with ^{124}Xe and some other $\beta\beta$ sources confirm this general behavior [27].

Another theoretical possibility is to look for the $0\nu\beta\beta$ half-life for the $0^+ \rightarrow 2^+$ transition, e.g. in ^{76}Ge, for which the mass mechanism vanishes in first order and the transition is driven mainly by the λ and η mechanism. Since the half-life to be expected [25, 26] for these modes would lie, however, with $\sim 10^{30}$ and $\sim 5 \times 10^{32}$ years almost in the range of that of proton decay, such experiment may be only of academic interest.

So it might be wise to combine future efforts to confirm the ^{76}Ge result with a possibility to pin down the various contributions to the $0\nu\beta\beta$ decay amplitude.

4 Summary and Outlook

We reached with the HEIDELBERG-MOSCOW ^{76}Ge experiment [12, 4, 3, 28], what we wanted to learn from our large GENIUS project, proposed in 1997 [37] - at a time where a signal was not yet seen - namely observation of $0\nu\beta\beta$ decay. There is now a $>6\sigma$ signal for $0\nu\beta\beta$ decay. The neutrino is a Majorana particle. Total lepton number is violated. Presently running and planned experiments are usually not sensitive enough to check the ^{76}Ge result on a reasonable time scale. They further cannot give *any* information on the absolute (effective) neutrino mass and on the contribution of other processes to the total $0\nu\beta\beta$ amplitude. A way out of this dilemma is outlined [28].

Starting from an intensity of the line in the pulse shape selected spectrum (sum of NN and low-cut spectra, see Fig. 2), of 11 ± 1.8 (stat) events (average of intensity in the sum spectra for 0, 1, 2 mm cuts, see [3]), leads to a half-life for $0\nu\beta\beta$ decay of $T^{0\nu}_{1/2} = \left(2.23\ ^{+0.44}_{-0.31}(stat)\right) \times 10^{25}$ y. This agrees with the central value of the half-life determined from the full spectrum (see [4, 5]) within a 1.7σ error of the latter. From the half-life one can derive some information on the effective neutrino mass $\langle m \rangle$ and the right-handed weak current parameters $\langle \eta \rangle$, $\langle \lambda \rangle$. In general we *cannot* determine the individual contributions of $\langle m \rangle, \langle \eta \rangle, \langle \lambda \rangle$ from a single $\beta\beta$ experiment, but only *upper limits* (see eq. (1) of [4]). Only under the *assumption*, that only one of the terms contributes to the decay process, and ignoring potential other processes connected with SUSY theories, leptoquarks, compositeness, etc. (see [1]), we can fix $\langle m \rangle = \left(0.32\ ^{+0.03}_{-0.03}\right)$ eV, *or* $\langle \eta \rangle = \left(3.05\ ^{+0.26}_{-0.25}\right) \times 10^{-9}$, *or* $\langle \lambda \rangle = \left(6.92\ ^{+0.58}_{-0.56}\right) \times 10^{-7}$. *Thus we can fix the effective neutrino mass only, when we assume* $\langle \eta \rangle, \langle \lambda \rangle = 0$. In that sense it is highly premature to compare, as often done, such number with numbers deduced from e.g. WMAP or other cosmological experiments, or to use it as a landmark for future tritium experiments - other than as an upper limit. This fact also strongly relativates the popular efforts to calculate the nuclear matrix elements entering into eq. (1) in [4]. They are not very relevant at the moment for the extraction of *fundamental* physics. We use in derivation of the limits given above the nuclear matrix elements of [22, 24]. Since the corresponding matrix element for $2\nu\beta\beta$ decay underestimates this decay by $\sim$30% (see [4, 5, 21]) these calculations may also underestimate the $0\nu\beta\beta$ matrix element, and consequently the upper limit for the effective neutrino mass could be lower, down to $\sim$0.22 eV.

It might be finally asked what else could be done in principle to prove observation of double beta decay - after having proved that there is a line at $Q_{\beta\beta}$ - after having shown that this line is not a double escape peak (which should consist of single site events) of an unknown gamma line (see [4, 5]) - after having shown that -with two completely independent methods - only these events are selected at $Q_{\beta\beta}$, while at the same time gamma events around $Q_{\beta\beta}$ are suppressed almost completely.

The answer to this question in our opinion is: "Unfortunately practically nothing else could be done." An idea could be to look for angular correlations of the emitted electrons for the double beta candidate events. However: first, no future experiment, if it would be sensitive enough to see double beta decay, could do that (see [7, 8]). Second, even if some future experiment could measure these angular correlations, probably no clear conclusion could be made (see the discussion of the expected angular correlation, for different combi-

nations of $\langle m \rangle, \langle \eta \rangle, \langle \lambda \rangle$ in [7, 8, 28]). It might be added that the perhaps most promising of the projected experiments (CUORE) has even unfortunately no chance to perform a pulse shape analysis as it has been performed for the HEIDELBERG-MOSCOW experiment, since the signal produced in the bolometer cannot differentiate between a $\beta\beta$ and γ -event.

Concluding, the search for double beta decay may have reached some point, after which further progress will require huge efforts and different types of experiments than considered at present (see [7, 8, 28]).

Acknowledgements

The authors would like to thank the Deutsche Forschungsgemeinschaft (DFG) for the important support of their work (436 RUS 113/670/0-2), further the BMBF and the LNGS for the invaluable support.

The authors would like to thank all colleagues, who have contributed to the experiment over the last 15 years. In particular we thank Prof. V. Bednyakov for his continuous interest and encouragement. Our thanks extend also to the technical staff of the Max-Planck Institut für Kernphysik and of the Gran Sasso Underground Laboratory. We are grateful to the former State Committee of Atomic Energy of the USSR for providing the enriched material used in this experiment.

References

[1] H.V. Klapdor-Kleingrothaus, "60 Years of Double Beta Decay - From Nuclear Physics to Beyond the Standard Model", World Scientific, Singapore (2001) 1281 pages.
[2] H.V. Klapdor-Kleingrothaus, Int. Journ. of Mod. Phys. D 13 (2004) 2107-2126
[3] H.V. Klapdor-Kleingrothaus, I.V. Krivosheina, Mod. Phys. Lett. A 21 (2006) 1547-1566.
[4] H.V. Klapdor-Kleingrothaus, I.V. Krivosheina et al., Phys. Lett. B586 (2004) 198.
[5] H.V. Klapdor-Kleingrothaus, A. Dietz, I.V. Krivosheina et al., Nuclear Instr. and Methods A 522 (2004) 371-406.
[6] H.V. Klapdor-Kleingrothaus et al. Mod. Phys. Lett. A 16 (2001) 2409-2420, hep-ph/0201231, and Found. Phys. 31 (2002) 1181-1123 (Corrigenda: 33 (2003) 678-684).
[7] H.V. Klapdor-Kleingrothaus et al., Phys. Lett. B 632 (2006) 623-631.
[8] H.V. Klapdor-Kleingrothaus et al., Phys. Rev. D 73 (2006) 013010.
[9] H.V. Klapdor-Kleingrothaus et al., Intern. J. of Modern Phys. A 21 (2006) 1159-1188.
[10] H.V. Klapdor-Kleingrothaus, In Proc. of Intern. Conf. "Neutrinos and Implications for Physics Beyond the Standard Model", Stony Brook, USA, 11-13 October, 2002, ed. R. Shrock, World Scientific, 2003, 367-382, hep-ph/0303217; in Proc. of Intern. Conf. "Beyond the Desert 2003", BEYOND03, Tegernsee, Germany, 9-14 June, 2003, Springer, Heidelberg 2004, ed. H.V. Klapdor-Kleingrothaus, pp. 307-364; in Proc. of Intern. Conf. "Neutrino Telescopes", February 2005, Venice, Italy, ed. M. Baldo-Ceolin., p. 215, hep-ph/0512263.
[11] H.V. Klapdor-Kleingrothaus, Nucl. Phys. B (Proc. Suppl.) 143 (2005) 229-232, Proc. of International Conf. "Neutrino 2004", 14-19 June, 2004, Paris, France, and Nucl. Phys. B (Proc. Suppl.) 145 (2005) 219, Proc. of International Worksh. "Neutrino Oscillation - NOW 2004", 11-17 September, 2004, Bari, Italy, eds. by G. Fogli et al.
[12] H.V. Klapdor, Proposal, Internal Report, MPI-1987-V17, September 1987.
[13] J. Hellmig, H.V. Klapdor-Kleingrothaus, Nucl. Instrum. Meth. A 455 (2000) 638-644; and J. Hellmig, F. Petry, H.V. Klapdor-Kleingrothaus, Patent DE19721323A.
[14] B. Majorovits, H.V. Klapdor-Kleingrothaus. Eur. Phys. J. A6 (1999) 463 and B. Majorovits, Dissertation December 2000, MPI-Heidelberg.
[15] H.V. Klapdor-Kleingrothaus, I.V. Krivosheina, et al., Phys. Lett. B 636 (2006) 235-247.
[16] H.V.Klapdor-Kleingrothaus, I.V.Krivosheina, I.V.Titkova, Mod.Phys.Lett. A21(2006)1257.
[17] ORTEC company, T.W. Raudorf, private communication, 2006.
[18] G.F. Knoll, "Radiation Detection and Measurement", second ed. 1989, John Wiley & Sons.

[19] F.S. Goulding and D.A. Landis, IEEE Trans.Nucl. Sci. 35 (1998) 119; B.W. Loo et al., IEEE Trans. Nucl. Sci. 35 (1998) 114; S.M. Hinshaw, D.A. Landis, IEEE Trans. Nucl. Sci. 37 (1990) 374; A. Georgiev and W. Gast, IEEE Trans. on Nucl. Science 40 (1993) 770.
[20] H.V. Klapdor-Kleingrothaus, H. P"as, A.Yu. Smirnov, Phys. Rev. D 63 (2001) 073005.
[21] Ch. D"orr, H.V. Klapdor-Kleingrothaus, Nucl. Instr. Meth. A 513 (2003) 596-621.
[22] A. Staudt, K. Muto, H.V. Klapdor-Kleingrothaus, Eur. Lett. 13 (1990) 31.
[23] K. Grotz, H.V. Klapdor, "Die Schwache Wechselwirkung in Kern-, Teilchen- und Astrophysik", B.G. Teubner, Stuttgart (1989), "The Weak Interaction in Nuclear, Particle and Astrophysics", IOP Bristol (1990), Moscow, MIR (1992) and Shandong Science and Technology Press, Jinan, (1998).
[24] K. Muto, E. Bender, H.V. Klapdor, Z. Phys. A - Atomic Nuclei 334 (1989) 187 and 177.
[25] M. Hirsch, K. Muto, T. Oda, H.V. Klapdor-Kleingrothaus, *Z. Phys. A*, **347** (1994) 151.
[26] T. Tomoda, *Nucl. Phys. A*, **484** (1998) 635.
[27] H.V. Klapdor-Kleingrothaus et al., in preparation
[28] H.V. Klapdor-Kleingrothaus, in Proc. Int. Conf. SNOW2006. May 2006, Stockholm, Sweden, Phys. Scripta T127 (2006) 40-42.
[29] K.Ya. Gromov et al., J. Part. Nucl. Lett. 3 (2006) 30.
[30] H.V. Klapdor-Kleingrothaus et al., Phys. Lett. B 578 (2004) 54-62 and Nucl. Instr. Meth. A 511 (2003) 335; H.V. Klapdor-Kleingrothaus hep-ph/0205228.
[31] H.V. Klapdor-Kleingrothaus et al., PRD 70 (2004) 078301.
[32] M. Moe et al., Phys. Rev. Letters 59 (1987) 989.
[33] R.J. Ellis et al., Nucl. Phys. A 435 (1985) 34-42.
[34] J.G. Hykawy et al., Phys. Rev. Lett. 67 (1991) 1708.
[35] G. Audi, A.H. Wapstra, Nucl. Phys. A 595 (1995) 409-480.
[36] G. Douysset et al., Phys. Rev. Lett. 86 (2001) 4259; I. Bergström et al., in Proc. of Intern. Conf. on Particle Physics Beyond the Standard Model, BEYOND'02, Oulu, Finland June 2002, IOP, 2003, ed. H.V. Klapdor-Kleingrothaus; in BEYOND 2003, Castle Ringberg, Germany, 10-14 June, 2003, Springer, Heidelberg, 2003, ed. H.V. Klapdor-Kleingrothaus.
[37] H.V. Klapdor-Kleingrothaus, J. Hellmig and M. Hirsch, *GENIUS-Proposal*, 20 Nov. 1997; J. Hellmig and H.V. Klapdor-Kleingrothaus, *Z. Phys. A*, **359** (1997) 351-359 and nucl-ex/9801004; H.V. Klapdor-Kleingrothaus, M. Hirsch, *Z. Phys. A*, **359** (1997) 361-372; H.V. Klapdor-Kleingrothaus, J. Hellmig, M. Hirsch, J. Phys. G 24 (1998) 483-516.
[38] H.V. Klapdor-Kleingrothaus et al., *Nucl. Instr. Meth. A*, **511** (2003) 341; H.V. Klapdor-Kleingrothaus, CERN Courier **43 Nr.6** (2003) 9;
H.V. Klapdor-Kleingrothaus et al., Proc. of the 3nd Intern. Conf. on Particle Physics Beyond the Standard Model, BEYOND02, Castle Ringberg, Germany, 2002, IOP 2003, ed. H.V. Klapdor-Kleingrothaus, 499.
[39] H.V. Klapdor-Kleingrothaus et al., *Nucl. Instr. Meth. A*, **530** (2004) 410-418; and H.V. Klapdor-Kleingrothaus, I.V. Krivosheina, *Nucl. Instr. Meth. A*, **566** (2006) 472-476.
[40] For CUORICINO and CUORO Collab. C. Brofferio, in Proc. of Int. Conf. "Neutrino Telescopes", Febr. 2005, Venice, Italy, ed. M. Baldo-Ceolin, p. 239; and in Proc. Int. Conf. "NEUTRINO", June 2006, Santa Fe, USA.
[41] J. Vuilleumier for the EXO coll., Proc. idm2004, Edinburg, Scotland 2004, World Scientific, Singapore (2005) 635.
[42] A. Piepke, Talk at Heidelberg, ν Workshop, 2005.
[43] NEMO Collabor., *Phys. Rev. Lett.*, **95** (2005) 182302.
[44] H. Kiel et al., Nucl. Phys. A 723 (2003) 499-514.

List of Publications (2006)

1. **The evidence for the observation of $0\nu\beta\beta$ beta beta decay: The identification of $0\nu\beta\beta$ beta beta events from the full spectra,**
   H.V. Klapdor-Kleingrothaus, I.V. Krivosheina,
   Mod. Phys. Lett. A 21 (2006) 1547-1566

2. **Lessons after the Evidence for $0\nu\beta\beta$ Decay**,
H.V. Klapdor-Kleingrothaus, Phys. Scr. T 127 (2006) 40-42.
3. **Theoretical Investigation of pulse Shapes of Double Beta Events in a Ge-76 Detector, their Dependence on Particle Physics Parameters, and their Separability from Background Gamma Events**, H.V. Klapdor-Kleingrothaus, I.V. Krivosheina, I.V. Titkova, Mod. Phys. Letters A 21, No. 16: 1257-1278, 2006.
4. **Microscopic calculations of signals of double beta decay in a Ge-76 detector and first application to the Heidelberg-Moscow experiment**,
H.V. Klapdor-Kleingrothaus, I.V. Krivosheina, V. Mironov, I.V. Titkova, Phys. Lett. B 636: 235-247, 2006.
5. **Theoretical description of double beta decay tracks in a germanium detector and of their dependence on particle and nuclear physics**, H.V. Klapdor-Kleingrothaus, I.V. Krivosheina, I.V. Titkova,
Int. J. Mod. Phys. A 21: 1159-1188, 2006.
6. **Theoretical investigation of the dependence of double beta decay tracks in a Ge detector on particle and nuclear physics parameters and separation from gamma ray events**, H.V. Klapdor-Kleingrothaus, I.V. Krivosheina, I.V. Titkova, Phys. Rev. D 73: 013010, 2006
7. **Particle and nuclear physics parameters: How do they affect the tracks of double beta events in a germanium detectors, and their separation from gamma events**, H.V. Klapdor-Kleingrothaus, I.V. Krivosheina, I.V. Titkova,
Phys. Lett. B 632: 623-631, 2006.
8. **First Monte Carlo Simulation of Double Beta Decay Tracks in a Ge Detector and their Dependence on Particle and Nuclear Physics Parameters**, H.V. Klapdor-Kleingrothaus, I.V. Krivosheina, I.V. Titkova, INFN, Laboratori Nazionali del Gran Sasso, Annual Report (2005) 79-96, LNGS/EXP (2006).

List of Invited Talks at Conferences, 2006

1. **Lessons after the Evidence for $0\nu\beta\beta$ Decay**,
H.V. Klapdor-Kleingrothaus, '2nd Scandinavian NeutrinO Workshop, May 2-6, 2006, AlbaNova University, Stockholm, Sweden, Phys. Scr. T 127 (2006) 40-42.
2. **A New View on the Future of Nuclear Double Beta Decay and Consequences for Beyond Standard Model Physics**, H.V. Klapdor-Kleingrothaus,
'6th International Workshop on the Identification of Dark Matter', September 11-16th, 2006 In Proc. of Idm06, World Scientific (2007) eds. N. Spooner et al.
3. **Status and Role of Double Beta Decay in Particle Physics and New View into the Future of the Field**, H.V. Klapdor-Kleingrothaus,
'Challenges in Particle Phenomenology', 3rd Vienna Central European Seminar on Particle Physics and Quantum Field Theory, December 1-3, 2006.

The ICARUS T600 Experiment at GranSasso Laboratory

A. Ankowski[1], M. Antonello[2], P. Aprili[3], F. Arneodo[3], B. Baibussinov[4], M. Baldo Ceolin[4], G. Battistoni[5], P. Benetti[6], A. Borio[6], E. Calligarich[6], M. Cambiaghi[6], F. Carbonara[7], F. Cavanna[2], S. Centro[4], A. Cesena[5], K. Cieslik[8], A. G. Cocco[7], A. Dabrowska[8], R. Dolfini[6], C. Farnese[4], A. Fava[4], A. Ferrari[5], G. Fiorillo[7], S. Galli[2], D. Gibin[2], A. Gigli Berzolari[6], A. Giuliano[9], K. Graczyk[1], S. Gninenko[10], A. Guglielmi[4], C. Juszczak[1], J. Holeczek[11], D. Kielczewska[12], M. Kirsanov[10], J. Kisiel[11], T. Kozlowski[13], N. Krasnikov[10], M. Lantz[5], G. Mannocchi[9], M. Markiewicz[8], V. Matveev[10], F. Mauri[6], A. Menegolli[6], G. Meng[4], C. Montanari[6], S. Muraro[5], J. Nowak[1], O. Palamara[3], L. Periale[9], G. PianoMortari[2], A. Piazzoli[6], P. Picchi[9], F. Pietropaolo[4], W. Polchlopek[14], M. Posiadala[12], M. Prata[6], P. Przewlocki[13], A. Rappoldi[6], G. L. Raselli[6], E. Rondio[13], M. Rossella[6], C. Rubbia[3], P. Sala[5], L. Satta[9], D. Scannicchio[6], E. Segreto[3], F. Sergiampietri[15], J. Sobczyc[1], D. Stefan[8], J. Stepaniak[13], R. Sulej[16], M. Szarska[8], M. Terrani[5], G. Trinchero[9], F. Varanini[4], S. Ventura[4], C. Vignoli[6], T. Wachala[8], A. Zalewska[8], K. Zaremba[16]

[1] *Wroclaw University of Technology, Wroclaw, Poland*
[2] *Dipartimento di Fisica e INFN, Universit`a di L'Aquila, Italy*
[3] *Laboratori Nazionali del Gran Sasso dell'INFN, Assergi (AQ), Italy*
[4] *Dipartimento di Fisica e INFN, Universit`a di Padova, Italy*
[5] *Dipartimento di Fisica e INFN, Universit`a di Milano, Italy*
[6] *Dipartimento di Fisica Nucleare Teorica e INFN Universit`a di Pavia, Italy*
[7] *Dipartimento di Scienze Fisiche, INFN e Universit`a Federico II di Napoli, Italy*
[8] *H. Niewodniczansky Institute of Nuclear Physics, Krakow, Poland*
[9] *Laboratori Nazionali di Frascati dell'INFN, Frascati, Italy*
[10] *INR RAS, prospekt 60-letiya Oktyabrya 7A, Moscow, Russia*
[11] *University of Silesia, Katowice, Poland*
[12] *Warsaw University, Warszawa, Poland*
[13] *A.Sołtan Institute for Nuclear Studies, Warszawa, Poland*
[14] *AGH University of Science and Technology, Kracow, Poland*
[15] *Dipartimento di Fisica, Universit`a di Pisa, Italy*
[16] *University of Technology, PI. Politechniki 1, warsaw, Poland*

Abstract

The ICARUS T600 detector is the largest liquid Argon TPC ever built, with a size of about 600 tons of fully imaging mass. The design and assembly of the detector relied on industrial support and represents the application of concepts matured in laboratory tests to the kton-scale.

The detector was developed to act as an observatory for astroparticle and neutrino physics at the Gran Sasso Underground Laboratory and a second generation nucleon decay experiment.

The ICARUS T600 was commissioned in 2001 for a technical run performed at surface in the Pavia INFN site. During this period all the detector features were extensively tested with an exposure to cosmic–rays. During 2004 the detector was moved from Pavia to the LNGS underground site. In 2005 and 2006 remounting of the detector and of the cryogenic system has been undertaken. This delicate phase is still under way and the installation in the underground site at LNGS (HAll B) is proceeding smoothly. The final commissioning is expected within 2007.

In this report some results from analysis and studies based on the experimental data collected during the technical run are summarized.

1 Introduction

The technology of the Liquid Argon Time Projection Chamber (LAr TPC), first proposed by C. Rubbia in 1977 [1], was conceived as a tool for a completely uniform imaging with high accuracy of massive volumes. The operational principle of the LAr TPC is based on the fact that in highly purified LAr ionization tracks can be transported practically undistorted by a uniform electric field over macroscopic distances. Imaging is provided by a suitable set of electrodes (wires) placed at the end of the drift path continuously sensing and recording the signals induced by the drifting electrons.

Non–destructive read–out of ionization electrons by charge induction allows to detect the signal of electrons crossing subsequent wire planes with different orientation. This provides several projective views of the same event, hence allowing space point reconstruction and precise calorimetric measurement.

The LAr TPC was developed in the context of the ICARUS programme and currently finds its application in studies concerning some of the major issues of particle and astroparticle physics:

- the study of neutrino oscillations with the CNGS beam;
- the detection of neutrinos following a Supernova explosion;
- the study of solar and atmospheric neutrino interactions;
- the study of nucleon decay for some channels predicted by GUTs;

After the original proposal, the feasibility of the technology has been first demonstrated by an extensive R&D programme, which included ten years of studies on small LAr volumes and five years of studies with several prototypes of increasing mass[2, 3, 4, 5, 6, 7, 8, 9, 10, 11, 12, 13, 14, 15, 16].

The second step was represented by the construction of the T600 module[17]: a detector employing about 600 tons of liquid Argon to be operated at LNGS. This step–wise strategy allowed to progressively develop the necessary know–how to build a multi–kton liquid Argon detector.

The realization of the T600 detector (from design to construction) lasted about four years and culminated with the full test of the experimental set–up, carried out at surface during 2001. This test demonstrated the maturity of the project. All technical aspects of the system, namely cryogenics, LAr purification, read–out chambers, detection of LAr scintillation light, electronics and DAQ had been tested and performed as expected. Statistically significant samples of cosmic–ray events (long muon tracks, spectacular high–multiplicity muon bundles, electromagnetic and hadronic showers, low energy events) were recorded. The subsequent analysis of these events, carried out in 2002-03, has allowed the development and fine tuning of the off–line tools for the event reconstruction and the extraction of physical quantities. It has also demonstrated the performance of the detector in a quantitative way, issuing in a number of papers published in 2003-04:

- Analysis of the liquid Argon purity in the T600 detector [18];
- Observation of very long ionizing tracks [19];
- Measurement of the muon decay spectrum [20];
- Study of ionization quenching in liquid Argon [21];

A detailed description of the T600 detector and of its technical performance as obtained from the acceptance tests has been reported in a dedicated milestone paper [22] published in 2004.
In 2005, a paper dedicated to the characterization tests at cryogenic temperature of the photomultipliers adopted in ICARUS for the detection of the LAr scintillation light has been published [23].

In 2006 other results, based on the T600 data from the test run, have been finalized from dedicated studies on (1) optimization of methods for particle identification and on (2) LAr scintillation light signal reconstruction and application for deposited energy reconstruction:

- Measurement of through-going particle momentum by means of multiple scattering with the ICARUS T600 TPC [24].
- Analysis of liquid Argon scintillation light signals with the ICARUS T600 Detector [26].

In parallel with data analysis from the T600 test run, another important data set from a 50 liters ICARUS-like chamber located between the CHORUS and NOMAD experiments at the CERN West Area Neutrino Facility (WANF) has been exploited for the study of the LAr-TPC capability to identify and reconstruct low multiplicity neutrino interactions. The results from this work have been also published in 2006:

- Performance of a liquid argon time projection chamber exposed to the CERN West Area Neutrino Facility neutrino beam [25].

2 Performance of a 50 liters TPC exposed to the CERN WANF neutrino beam

Extracted from [25] "Performance of a liquid argon time projection chamber exposed to the CERN West Area Neutrino Facility neutrino beam", ICARUS Collaboration, Physical Review D (2006) (Vol. 74, No. 11)

In 1997, the ICARUS collaboration together with a group from INFN and Milano University proposed to expose a 50 liter LAr TPC to the multi-GeV wide band neutrino beam of the CERN West Area Neutrino Facility (WANF), during the NOMAD and CHORUS data taking. The test was part of an R&D program for a medium baseline ν_τ appearance experiment. The idea was to collect a substantial sample of quasi-elastic interactions (ν_μ + n $\rightarrow$ p + μ^-) to study the following physics items:

- Measurement of the acoplanarity and missing transverse momentum in events with the μ-p topology in the final state, in order to assess Fermi motion and proton re-scattering inside the nucleus.
- Appearance of nuclear fragments (short tracks and *blobs* around the primary interaction vertex) in quasi-elastic events.

The data collected in 1997 offer the unique opportunity to study nuclear effects in the Argon nucleus and to assess the identification and reconstruction capability of a LAr TPC for low-multiplicity neutrino events. The present work shows, for the first time, a comprehensive set of results from the 1997 test.

The LAr TPC was placed on a platform 4.5 meters above ground, right in between the CHORUS and NOMAD detectors (Fig. 1). The modest size of the LAr TPC fiducial volume ($\sim$50 liters), coupled with the high energy of the WANF ν beam, made necessary a muon spectrometer downstream the TPC. A coincidence with the NOMAD DAQ was set up to use the detectors located into the NOMAD magnetic dipole as a magnetic spectrometer. The experimental setup was completed with additional counters for the trigger and veto systems.

The LAr TPC (Fig.2) has an active volume of $32\times32\times46.8$ cm^3, enclosed in a stainless steel vessel in the shape of a bowed-bottom cylinder 90 cm high and with a radius of 35 cm. The active volume corresponds to 67 kg of Liquid Argon ($T = 87$K at 1 atm, $\rho = 1.395$ g/cm^3). Ionization electrons produced by the passage of charged particles drift vertically toward the anode by means of a constant electric field of 214 V/cm. The readout area (anode) is made up of two orthogonal wire planes mounted at a distance of 4 mm. The distance between the wires is 2.54 mm and each plane is made up of 128 wires.

The chamber has been exposed to the ν beam produced at the CERN West Area Neutrino Facility (WANF). The mean energy of the ν_μ reaching the NOMAD detector is 24.3 GeV, while contaminations from other flavors are below 7% for $\bar{\nu}_\mu$ and $\sim$ 1% for ν_e. Being the TPC centered on the beam axis and covering a small surface, an harder neutrino flux is expected (with a mean energy of about 30 GeV). The trigger is provided by a set of scintillators located between the chamber and the NOMAD apparatus (Fig. 1).

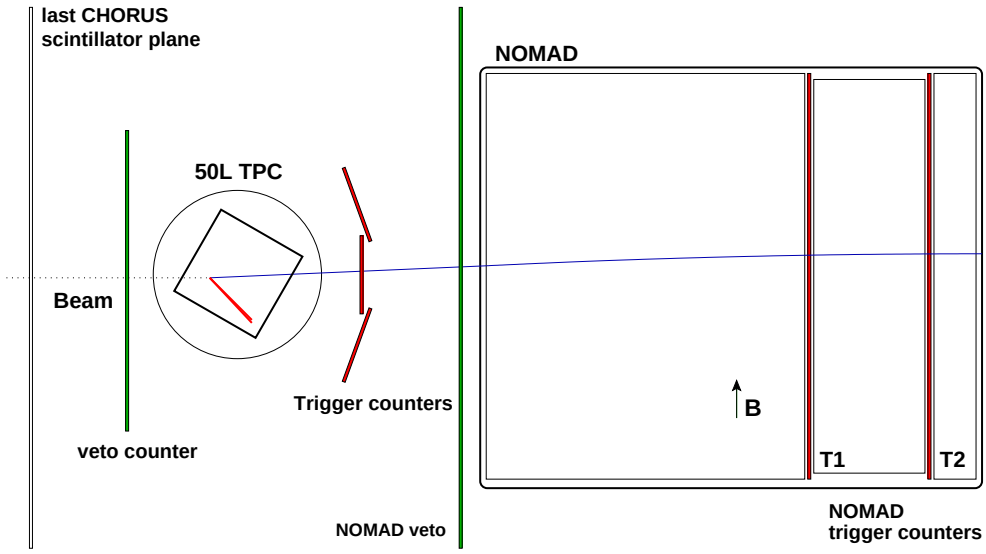

Figure 1: *A sketch of the experimental setup (top view). Relative sizes are not to scale.*

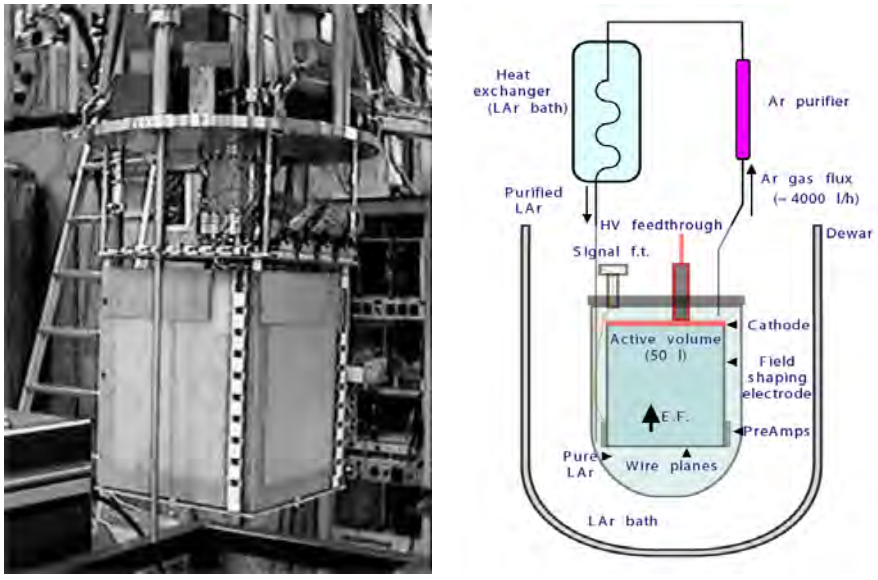

Figure 2: *The 50 liters Liquid Argon Time Projection Chamber.*

2.1 *Event reconstruction and particle identification*

Interactions happening in the TPC fiducial volume were fully registered in two 2D images with a common coordinate (time), with full calorimetric information associated to each point. Each 2D-image represents the signal amplitude digitized by the ADC (in a linear gray scale) versus the time sample (drift coordinate) and the wire number. Fig. 3 and Fig. 4 (top part) show the raw images of two ν_μ CC events in the collection (left panel) and induction plane (right panel). These raw images represent the time evolution (in vertical axis) of the signal induced in the wires (in horizontal axis). The purpose of the reconstruction procedure is to extract the physical information provided by the wire output signals, i.e. the energy deposited by the different particles and the point where such a deposition has occurred, to build a complete 3D and calorimetric picture of the event.

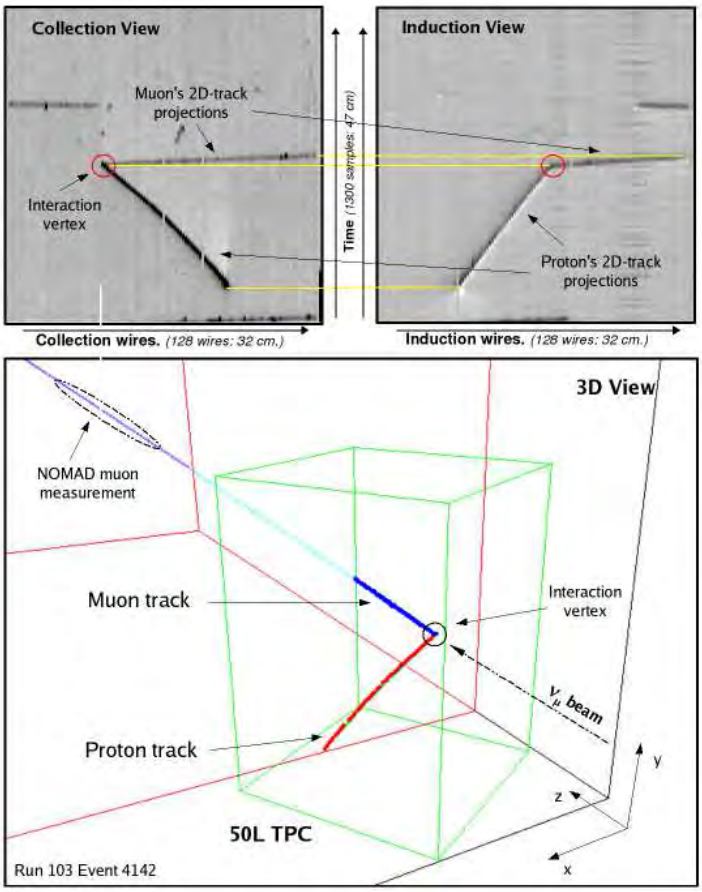

Figure 3: *Example of the 3D reconstruction of a low-multiplicity ν_μ CC event. The raw image from collection and induction wire planes (on top): Hits and 2D track projections have been identified. Three dimensional view of the reconstructed event (bottom picture) embedded in a 3D recreation of the experimental setup.*

In Fig. 3, we show an example of the full reconstruction procedure for a low-multiplicity

ν_μ CC event. This algorithm allows the reconstruction of more complicated event topologies (see Fig. 4). This is the first time that interactions of multi-GeV accelerator neutrinos occurring in a LAr TPC are fully reconstructed in 3D.

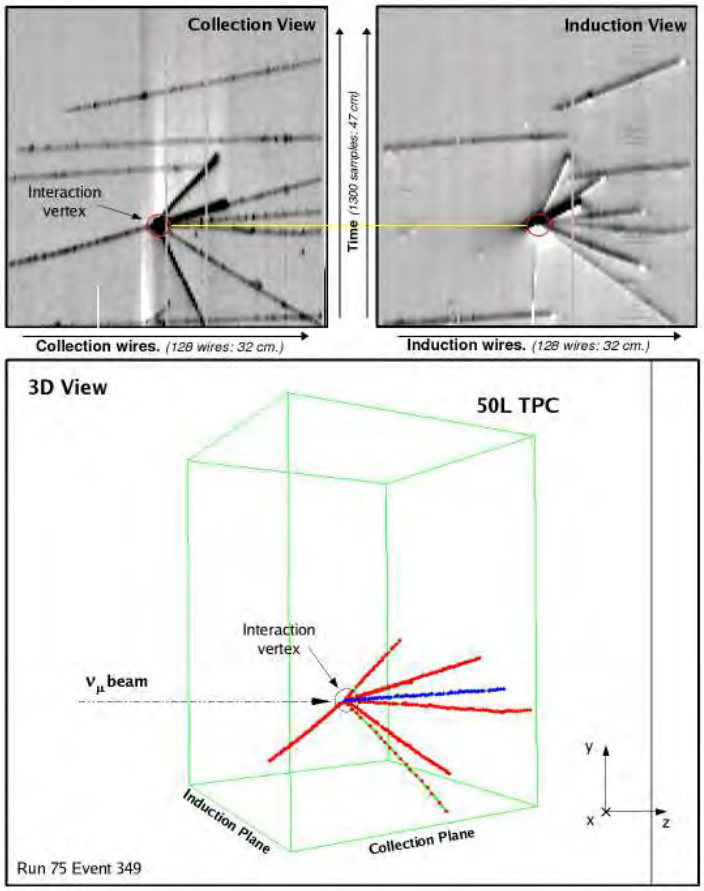

Figure 4: *(Top) The raw images of a high multiplicity event (ν_μ CC DIS) in the collection (left panel) and induction plane (right panel). Below, the 3D reconstruction of a high multiplicity event (ν_μ CC DIS) with eight primary particles. Two of them stop in LAr and are recognized as protons.*

Proton identification and momentum measurement were performed using only information provided by the TPC. The discrimination between protons and charged pions is performed exploiting their different energy loss behavior as a function of the range, see Fig. 5 . For the case of candidates stopping in the fiducial volume of the chamber, as the ones of the "golden sample", p/$\pi^{\pm}$ separation is unique. Monte-Carlo studies reveal that almost 100% of protons are identified as such on the basis of their dQ/dx shape on the vicinity of the stopping point; in addition, the fraction of pions and kaons misidentified as protons is negligible. Once a contained proton is identified, its kinetic energy is calculated from range, which only depends on the spatial reconstruction of the tracks. In this case, the momentum uncertainty is dominated by the finite pitch of the wires (2.54 mm) and

the performance of the reconstruction tools. These have been tested using a Monte-Carlo simulation of the detector. The resolution on the kinetic energy (T_p) varies from 3.3% for protons with $T_p = 50$ MeV up to 1% for T_p larger than 200 MeV.

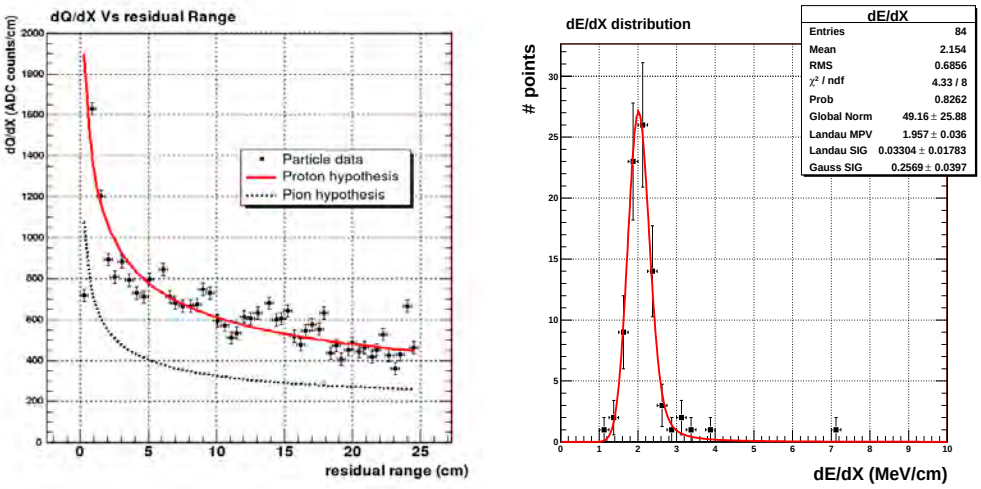

Figure 5: *(left) dQ/dx as a function of the residual range for the reconstructed proton in the event shown in Fig. 3: continuous (dashed) line represents the expected behavior of protons (pions) in the detector. (right) dE/dx distribution for the muon reconstructed in Fig. 3: data is fitted to a convoluted Landau-Gaussian distribution.*

The kinematic reconstruction of the outgoing muons exploits the tracking capability of NOMAD. The reconstructed particle is traced back to the TPC accounting for the magnetic field and the presence of the forward NOMAD calorimeter.

2.2 *Analysis of quasi elastic ν_μ interaction*

The data set recorded with the 50L chamber amounts to 1.2×10^{19} protons on target. The trigger efficiency was monitored during data taking and its integrated value is 97%. Over the whole data taking period around 70000 triggers were collected in the TPC from which 20000 have at least a reconstructed muon possibly transversing the fiducial volume. From all these a priory ν_μ CC candidates, a visual scanning reveals that around half of them show a vertex in the fiducial volume. Therefore, we have a collection of around 10000 ν_μ CC events from which we have selected a set of 86 events called the "golden sample". This set consists of events with an identified proton of kinetic energy larger than 40 MeV fully contained in the TPC and one muon whose direction extrapolated from NOMAD matches the outgoing track in the TPC. The selection efficiency for QE interactions and their intrinsic background have been evaluated using a Monte-Carlo sample generated using the FLUKA package, which offers a full description of nuclear effects in neutrino interactions. The expected number of "golden events" is obtained taking the MC evaluated 16% (golden fraction) of the total QE, and adding the corresponding 20% due to

background contribution, which finally gives $80 \pm 9(stat) \pm 13(sys)$ "golden events" to be compared with the observed 86 events.

In spite of the limited statistics (86 events), the "golden sample" provides information on the basic mechanisms that modify the kinematics of neutrino-nucleus interactions with respect to the corresponding neutrino-nucleon process.

The proton kinetic energy is bounded by the $T_p > 40$ MeV cut and the requirement of full containment in the fiducial volume. This distribution is shown in Fig. 6 together with the transverse momentum of the proton for the "golden sample" with comparison with MC simulation. They demonstrate that Monte-Carlo reproduces the kinematic selection performed during the scanning and analysis of the "golden channel". They also show that our selected sample contains a non-negligible contamination from non-QE events. As already indicated, we estimate this contamination to be 20 %.

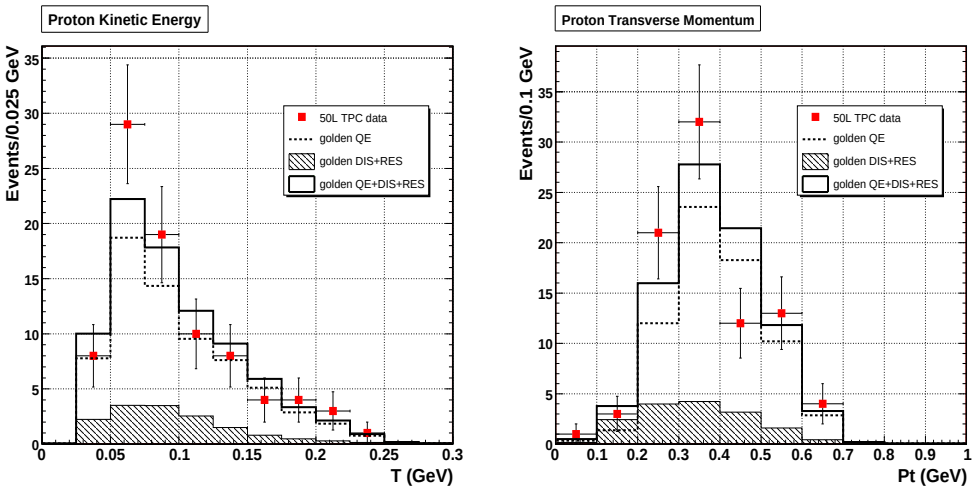

Figure 6: *Distribution of the proton kinetic energy for the "golden sample" (squared marks). Dotted histogram represents the expectation from simulated Monte-Carlo QE events, while the hatched one represents the simulated background from non-QE events. Both contributions are summed in the filled histogram and normalized to the golden sample data.*

These results clearly demonstrate the effectiveness of LAr imaging in the characterization of low-multiplicity multi-GeV neutrino interactions.

3 Analysis of Liquid Argon Scintillation Light Signals with the ICARUS T600 Detector

Extracted from [26] "Analysis of Liquid Argon Scintillation Light Signals with the ICARUS T600 Detector", ICARUS Collaboration, ICARUS-TM/06-03 (to be published on NIM A)

Ionization in liquid Argon (LAr) is accompanied by scintillation light emission. Charged particles interacting in LAr create ionized and excited Ar molecular states which produce

prompt scintillation radiation through recombination and de–excitation processes. Therefore, free electron separation and light emission are the two features that characterize the use of LAr as active medium. The two processes are complementary and their relative weight depends on the actual strength of the electric field applied to the active LAr volume. The free electron yield (from ionization) rises with the field value while the photon yield (from scintillation) decreases. At low fields the photon yield for a minimum ionizing particle (*mip*) is very high (e.g. comparable to NaI(Tl) crystal), for more densely ionizing particles is even higher. This light emission is characterized by a narrow–band intrinsic spectrum in the deep ultra-violet region (Vacuum-UV, VUV) and by a very fast response (e.g. comparable to plastic scintillator). Detection of scintillation light can provide, at one hand, an effective method for an absolute time measurement of the event (T_0 signal) as well as for an internal trigger signal formation, at the other hand, the light pulse amplitude and shape can provide additional information suitable for total energy deposition reconstruction and for particle identification.

With the ICARUS technology the spatial reconstruction of ionizing tracks inside the LAr volume is performed by the simultaneous exploitation of the charge and of the light release following the energy loss processes of charged particles which cross the detector, Fig.7:

1. free electrons from ionization induce detectable signals on the wires of the Time Projection Chambers (TPC) during their drift motion towards and across the wire planes (wire coordinates);

2. VUV photons from scintillation provide a prompt signal on the photo-multipliers (PMTs) directly immersed in LAr, that allows the measurement of the absolute drift time (T_0 signal) and, hence, of the distance traveled by the drifting electrons (drift coordinate).

Detection of the scintillation light is obtained by coating the PMT surface with a proper fluorescent compound acting as wavelength shifter from the VUV–light region to the PMT sensitive spectrum.

The realization of the ICARUS T600 module, a detector of about 600 t of LAr ($\sim$ 470 t active), has been completed in 2000 and a full test of the experimental set–up has been carried out at surface during 2001. A detailed description of the T600 detector, including the imaging detector (LAr-TPC) and the light detection system, and of its technical performance as obtained from the acceptance tests are given in Ref.[22].

In the present summary we report on the light data: light signals have been recorded in coincidence with ionizing events of various topologies, the waveform features have been here reconstructed and analyzed. The results have been compared with dedicated MonteCarlo (MC) simulations of the light emission, propagation and collection processes embedded in the standard MC code for the ICARUS detector simulation. The results obtained, in comparison with MonteCarlo simulations, demonstrate that the main features of the scintillation light emission, beyond the acquisition of the T_0 signal, are well understood and that the light detection system coupled to the ICARUS imaging technology performs according to expectations, see Fig.7.

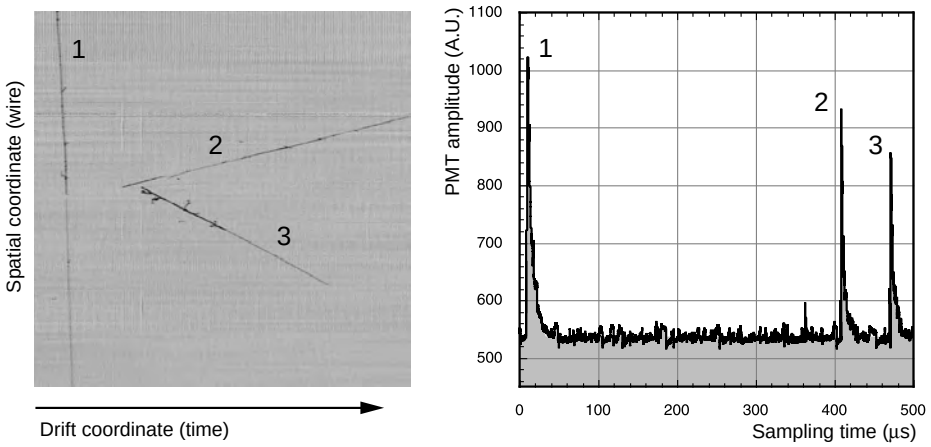

Figure 7: *Cosmic muon event: 2D image from the LAr-TPC reconstruction and the corresponding PMT waveform recorded by one of the equipped PMT.*

3.1 *Analysis of LAr scintillation light signals*

The data sample for this analysis consists of a selection of digitized waveforms recorded by the active PMT's strictly in coincidence with the passage of atmospheric muons identified by an external trigger system. A total statistics of 224 tracks have been accumulated for the present analysis, of which the selected events amounts to **200 μ-tracks**. Scintillation light emitted along the ionization track is detected by the PMT's equipped with the complete read-out electronics. In this case for each PMT a waveforms is recorded: a sample of **347 PMT waveforms** is made available for the light analysis (after appropriate selection cuts).

The comparison between the integral of the recorded waveform signal and corresponding MC number of detected photo-electrons showed a relation of strict proportionality. The linear correlation coefficient between two variables turns out to be very close to unity. This shows that the integral of the waveform carries a relevant physical information useful for the extraction of a reliable estimate for the *light calibration factor* to translate physical quantities into experimentally measurable quantities (and viceversa). The determination

Table 1: *Specific energy loss and deposited energy from light signal analysis: numerical results and expectation values.*

Run	$\langle \ell \rangle$ [m]	$\langle \frac{dE}{dx} \rangle$ [MeV cm^2 g^{-1}]	E$[\langle \frac{dE}{dx} \rangle]$ [MeV cm^2 g^{-1}]	$\langle \Delta E \rangle$ [GeV]	E$[\langle \Delta E \rangle]$ [GeV]
long-μ	19.1	2.18	2.186	5.8	5.80
650	4.4	1.82	1.888	1.1	1.15

of this calibration factor [26] was used to attempt to a first calorimetric reconstruction of the energy deposited in LAr by through-going muons from the recorded scintillation light

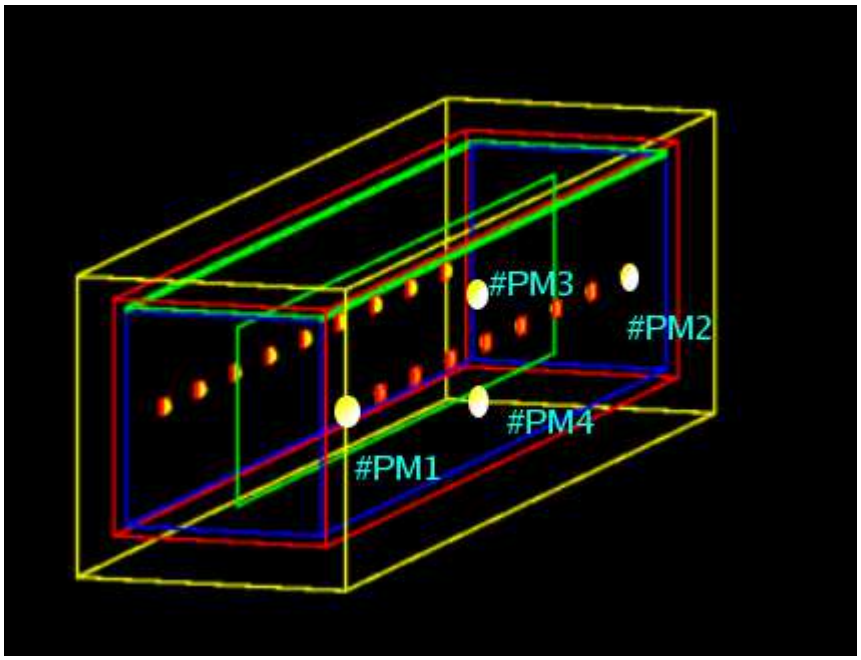

Figure 8: *Sketch of the PMT array in the T300 half-module. #PMT1-4 are instrumented with the complete read-out chain.*

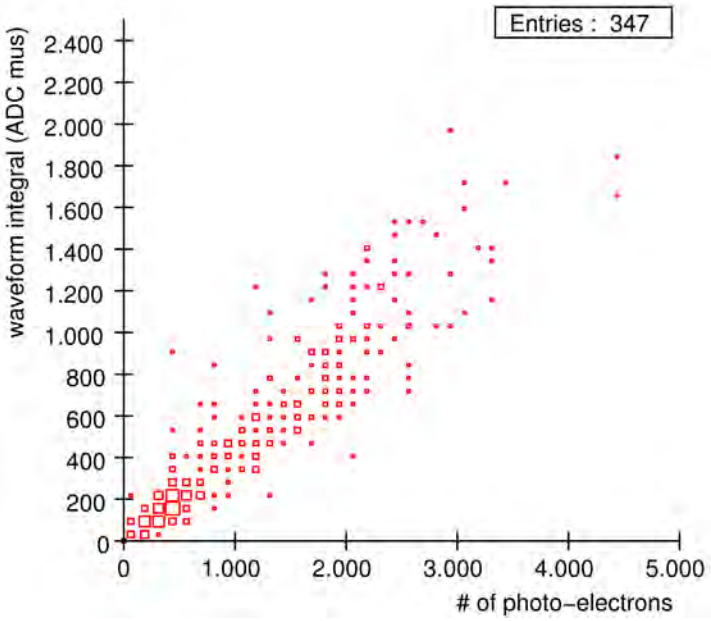

Figure 9: *Real data and MC simulation: $\mathcal{I}_O$ vs N_{MC}^{phel} (full statistics). The strong linear relationship is evident from this plot ($correlation\ coefficient\ r = 0.92$, see text).*

signals.
Given a muon track, up to $k = 4$ PMT signals can be associated to it. Through the calibration factor, the PMT signals can be converted into physical quantities (N_k^{phel}). These correspond to the total amount of photo-electrons at the k-th PMT induced by the muon track and an independent measurement of $\langle dE/dx \rangle_k$ along the muon track can be obtained from each PMT. The mean value from these measurements represents the best estimate of the specific energy loss averaged along the muon track of length ℓ_μ.
In Tab.1 the specific energy loss and total deposited energy (mean values) determined with a subset of experimental muon data are reported. These results well agree on average with expectations.

The calorimetric measurements from scintillation light could subsequently be used to improve the energy resolution when combined with the ionization charge information.

4 Conclusions

We have presented a brief description of the ICARUS T600 detector, a large–mass Liquid Argon TPC meant as the basic unit for a multi-kton astroparticle observatory and neutrino detector to be installed in the underground Gran Sasso Laboratory.

An extended technical run with the T600 detector has been performed at surface in the Pavia INFN site during 2001. The design, the description of the basic components, assembly, start–up and test-run procedures of the detector have been recently published, as well as the demonstration of the off–line event reconstruction capabilities. The detector space and energy resolution, particle identification and full events reconstruction have been also the subjects of several analyses published during the last two years. Additional results from more recent studies are here briefly reported and will be soon matter of dedicated publications.

The main conclusion from the test is that the measurements and the experimental results demonstrate that it is feasible to master all technical issues related to the construction and operation of a large size LAr TPC, within and sometimes beyond the design specifications.

The T600 detector has been transported from Pavia to the INFN Gran Sasso Underground Laboratory in 2004. The installation of the ancillary infrastructures in the LNGS Hall B represented the main hardware activity in 2005-06 and is presently still under way. The re-assembly of the detector components will be the main goal of the activity during 2007.

References

[1] C. Rubbia, *The Liquid-Argon Time Projection Chamber: A New Concept For Neutrino Detector*, CERN–EP/77–08, (1977).

[2] P. Benetti *et al.* [ICARUS Collaboration], *A 3 Ton Liquid Argon Time Projection Chamber*, Nucl. Instrum. Meth. A **332**, (1993) 395.

[3] P. Cennini *et al.* [ICARUS Collaboration], *Performance Of A 3 Ton Liquid Argon Time Projection Chamber*, Nucl. Instrum. Meth. A **345**, (1994) 230.

[4] F. Arneodo *et al.* [ICARUS Collaboration], *The ICARUS 50 l LAr TPC in the CERN neutrino beam*, arXiv:hep-ex/9812006.

[5] F. Arneodo *et al.* [ICARUS Collaboration], *First Observation Of 140-Cm Drift Ionizing Tracks In The Icarus Liquid-Argon Tpc*, Nucl. Instrum. Meth. A **449**, (2000) 36.

[6] F. Arneodo *et al.* [ICARUS Collaboration], *Determination Of Through-Going Tracks' Direction By Means Of Delta-Rays In The Icarus Liquid Argon Time Projection Chamber*, Nucl. Instrum. Meth. A **449**, (2000) 42.

[7] P. Cennini *et al.* [ICARUS Collaboration], *Detection Of Scintillation Light In Coincidence With Ionizing Tracks In A Liquid Argon Time Projection Chamber*, Nucl. Instrum. Meth. A **432**, (1999) 240.

[8] F. Arneodo *et al.* [ICARUS Collaboration], *Performance Evaluation Of A Hit Finding Algorithm For The Icarus Detector*, Nucl. Instrum. Meth. A **412**, (1998) 440.

[9] P. Cennini *et al.* [ICARUS Collaboration], *A Neural Network Approach For The Tpc Signal Processing*, Nucl. Instrum. Meth. A **356**, (1995) 507.

[10] P. Cennini *et al.* [ICARUS Collaboration], *Improving The Performance Of The Liquid Argon Tpc By Doping With Tetramethyl Germanium*, Nucl. Instrum. Meth. A **355**, (1995) 660.

[11] P. Benetti *et al.* [ICARUS Collaboration], *A 3D Image Chamber For The Lar Tpc On Multilayer Printed Circuit Board*, Nucl. Instrum. Meth. A **346**, (1994) 550.

[12] P. Benetti *et al.* [ICARUS Collaboration], *Argon Purification In The Liquid Phase*, Nucl. Instrum. Meth. A **333**, (1993) 567.

[13] A. Bettini *et al.* [ICARUS Collaboration], *A Study Of The Factors Affecting The Electron Lifetime In Ultrapure Liquid Argon*, Nucl. Instrum. Meth. A **305**, (1991) 177.

[14] S. Bonetti *et al.* [ICARUS Collaboration], *A Study Of The Electron Image Due To Ionizing Events In A Two-Dimensional Liquid Argon Tpc With A 24-Cm Drift Gap*, Nucl. Instrum. Meth. A **286**, (1990) 135.

[15] F. Arneodo *et al.* [ICARUS Collaboration], *Performance Of The 10 m^3 Icarus Liquid Argon Prototype*, Nucl. Instrum. Meth. A **498**, (2003) 293.

[16] F. Arneodo *et al.* [ICARUS Collaboration], *Detection Of Cerenkov Light Emission In Liquid Argon*, Nucl. Instrum. Meth. A **516** (2004), 348.

[17] ICARUS Collaboration, *A First 600 Ton ICARUS Detector Installed At The Gran Sasso Laboratory*, Addendum to Proposal by the ICARUS Collaboration, LNGS–95/10, (1995).

[18] S. Amoruso *et al.* [ICARUS Collaboration], *Analysis Of The Liquid Argon Purity In The ICARUS T600 TPC*, Nucl. Inst. Meth., A **516**, (2004) 68.

[19] F. Arneodo *et al.* [ICARUS Collaboration], *Observation Of Long Ionizing Tracks With The ICARUS T600 First Half–Module*, Nucl. Inst. Meth., A **508**, (2003) 287.

[20] S. Amoruso *et al.* [ICARUS Collaboration], *Measurement Of The Muon Decay Spectrum With The ICARUS T600 Liquid Argon TPC*, Eur. Phys. J., C 33 (2004) 233.

[21] S. Amoruso *et al.* [ICARUS Collaboration], *Study Of The Electron Recombination In Liquid Argon With The ICARUS TPC*, Nucl. Inst. Meth., A 523 (2004) 275.

[22] S. Amerio *et al.* [ICARUS Collaboration], *Design, construction and tests of the ICARUS T600 detector*, Nucl. Inst. Meth., A 527 (2004) 329.

[23] A. Ankowski *et al.*, [ICARUS Collaboration], *Characterization of ETL 9357 FLA Photomultiplier Tubes for cryogenic temperature applications*, Nucl. Inst. and Meth. A 556 (2005) 146.

[24] A. Ankowski *et al.*, [ICARUS Collaboration], *Measurement of through-going particle momentum by means of multiple scattering with the ICARUS T600 TPC*, Eur. Phys. J. C 48 (2006), 667.

[25] F. Arneodo *et al.*, [ICARUS-Milano Collaboration], *Performance of a liquid argon time projection chamber exposed to the CERN West Area Neutrino Facility neutrino beam*, Physical Review D (2006) (Vol. 74, No. 11).

[26] M. Antonello *et al.*, *Analysis of Liquid Argon Scintillation Light Signals with the ICARUS T600 Detector*, ICARUS-TM/06-03 (to be published on NIM A).

[27] F.Arneodo *et al.*, [ICARUS Collaboration], *The ICARUS Experiment: a Second Generation Proton Decay and Neutrino Observatory at The Gran Sasso Laboratory*, LNGS-P28, 2001, LNGS-EXP13/89 add. 1/01.

LUNA. Laboratory for Underground Nuclear Astrophysics

D.Bemmerer[1,*], R.Bonetti[2], C.Broggini[1†], F.Confortola[3], P.Corvisiero[3], H.Costantini[3], A.Formicola[4], E.Elekes[5], Z.F¨ul̈op[5], G.Gervino[6], A.Guglielmetti[2], C.Gustavino[4], G.Gyürky[5], G.Imbriani[7], M.Junker[4], A.Lemut[3], B.Limata[8], V.Lozza[1], M.Marta[2*], R.Menegazzo[1], P.Prati[3], V.Roca[8], C.Rolfs[9], M.Romano[8], C.Rossi Alvarez[1], E.Somorjai[5], O.Straniero[7], F.Strieder[9], F.Terrasi[10], H.P.Trautvetter[9]

[1] INFN, Padova, Italy
[2] Università di Milano, Dipartimento di Fisica and INFN, Milano, Italy
[3] Università di Genova, Dipartimento di Fisica and INFN, Genova, Italy
[4] Laboratori Nazionali del Gran Sasso, Assergi, Italy
[5] ATOMKI, Debrecen, Hungary
[6] Politecnico di Torino, Dipartimento di Fisica and INFN, Torino, Italy
[7] Osservatorio Astronomico di Collurania, Teramo
[8] Università di Napoli, Dipartimento di Fisica and INFN, Napoli, Italy
[9] Institut für Experimentalphysik III, Ruhr-Universität Bochum, Germany
[10] Dipartimento di Scienze Ambientali, Seconda Università di Napoli, Caserta, Italy

Abstract

LUNA is measuring fusion cross sections down to the energy of the stellar nucleosynthesis. In particular, this year we completed the study of $^{3}\mathrm{He}(\alpha,\gamma)^{7}\mathrm{Be}$, the key reaction for the production of ^{7}Be and ^{8}B neutrinos in the Sun, and we started the measurement of the $^{25}\mathrm{Mg}(\mathrm{p},\gamma)^{26}\mathrm{Al}$ cross section.

*now at Forschungszentrum Dresden-Rossendorf, Dresden, Germany
†Spokesperson

Introduction

Nuclear reactions that generate energy and synthesize elements take place inside the stars in a relatively narrow energy window: the Gamow peak. In this region, far below the Coulomb energy, usually below 100 keV, the reaction cross-section σ(E) drops almost exponentially with decreasing energy E:

$$\sigma(E) = \frac{S(E)}{E}\, exp(-2\,\pi\,\eta), \tag{1}$$

where $S(E)$ is the astrophysical factor and η is the Sommerfeld parameter, given by $2\,\pi\,\eta = 31.29\,Z_1\,Z_2(\mu/E)^{1/2}$. Z_1 and Z_2 are the nuclear charges of the interacting particles in the entrance channel, μ is the reduced mass (in atomic mass units), and E is the center of mass energy (in units of keV).

The extremely low value of the cross-section inside the Gamow peak, from pico to femto-barn and even below, has always prevented its measurement in a laboratory at the Earth's surface, where the signal to background ratio is too small because of cosmic ray interactions. In order to explore this new domain of nuclear astrophysics we have installed two electrostatic accelerators underground at LNGS: a 50 kV accelerator and a 400 kV one. The qualifying features of both the accelerators are a very small beam energy spread and a very high beam current even at low energy.

Outstanding results obtained up to now are the only existing cross-section measurements within the Gamow peak of the sun: ^{3}He(^{3}He,2p)^{4}He[1] and D(p,γ)^{3}He [2]. The former plays a big role in the proton-proton chain, largely affecting the calculated solar neutrino luminosity, whereas the latter is the reaction that rules the proto-star life during the pre-main sequence phase. With these measurements LUNA has shown that, by going underground and by using the typical techniques of low background physics, it is possible to measure nuclear cross sections down to the energy of the nucleosynthesis inside stars.

In the following we report on the activity during the year 2006, when we started a new high precision measurement of the ground state capture in ^{14}N(p,γ)^{15}O, we completed the study of ^{3}He(^{4}He, γ)^{7}Be and we started the ^{25}Mg(p, γ)^{26}Al experiment.

1 The ^{14}N(p,γ)^{15}O reaction

^{14}N(p, γ)^{15}O (Q=7.297 MeV) is the slowest reaction of the CNO cycle, the one which determines the rate of the cycle. The results we obtained first with the germanium detector data [3, 4] and then with the BGO set-up down to 70 keV [5] are about a factor two lower than the existing extrapolation at very low energy [6, 7]. The astrophysical consequences of this reduction are significant: the CNO neutrino yield in the Sun is decreased by about a factor two [8, 13, 14], with respect to the current estimates, the age of the oldest Globular Clusters is increased by 0.7-1 Gyr [15, 8] and the dredge-up of carbon to the surface of AGB stars is much more efficient [16].

The main conclusion from the LUNA data has been confirmed by an independent study at higher energy [9]. However, a discrepancy amounting to 15 % of the total extrapolated S factor at energies corresponding to solar hydrogen burning remains between the R-matrix extrapolations of the different experiments [3, 9]. This discrepancy is due to

the extrapolation of the capture to the ground state in ^{15}O, a transition that is strongly affected by interference effects between several resonances and the direct capture mechanism. Removing this discrepancy by precision cross section data would make it possible to study the solar center [10] by comparing the calculated flux of CNO neutrinos with the low energy neutrino data to be provided by the BOREXINO experiment at Gran Sasso.

Therefore, a new experiment is currently underway at LUNA to provide precision cross section data for the ground state capture at energies where the R-matrix fit can be effectively constrained.

The unique low gamma-ray background for $E_\gamma \sim 7\,\mathrm{MeV}$ [11] that is evident in the Gran Sasso underground accelerator facility essentially removes laboratory background as a source of uncertainty in such an experiment. Based on the experience from the previous LUNA ^{14}N(p,γ)^{15}O experiment, stable titanium nitride targets with low levels of ^{11}B and ^{19}F contamination have been produced by reactive sputtering at Laboratori Nazionali di Legnaro, effectively reducing ion beam induced background.

Low energy studies of the radiative capture to the ground state in ^{15}O (Fig. 1) are hampered by the systematic uncertainty stemming from the (beam energy dependent) correction for the true coincidence summing effect. This effect becomes apparent when placing the detector at close distance to the target, which is necessary because of the low absolute value of the cross section to be measured. Primary and secondary gamma rays from the strong cascade transitions through the states at 6.792, 6.172 and 5.181 MeV (Fig. 1) can be detected in coincidence and have the same signature in the detector as a true ground state capture gamma ray. This true coincidence summing effect limited data taking in the previous LUNA ^{14}N(p,γ)^{15}O solid target experiment [3].

The new experiment currently underway at LUNA uses a segmented Clover germanium detector [12] to reduce the summing correction, decisively improving the systematic uncertainty for the ground state capture. In order to obtain sufficient statistics, we con-

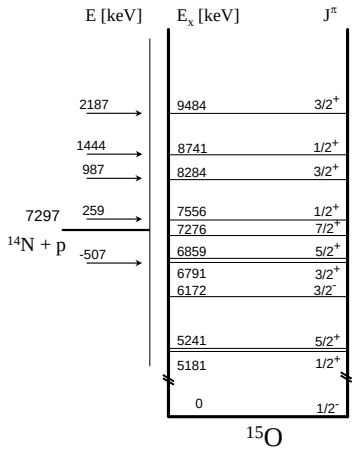

Figure 1: Level scheme of ^{15}O.

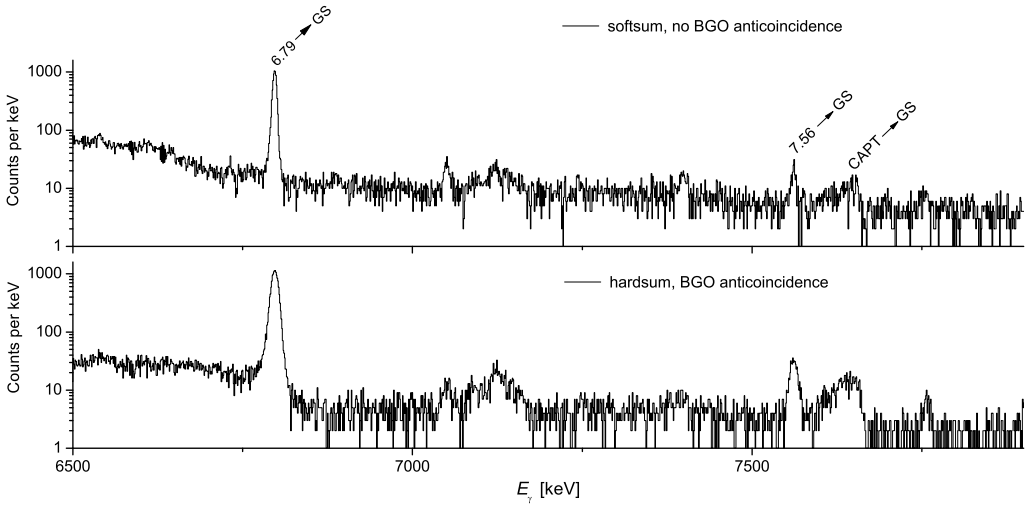

Figure 2: Gamma-ray spectra observed at LUNA with the ATOMKI Clover detector above the $E = 259$ keV resonance. The software sum of the four segments (free running, softsum) is compared with the sum of the analog signals of the same segments (veto from the Clover BGO anticompton shield, hardsum).

centrate on the beam energy region immediately above the 259 keV resonance, where precision data will effectively constrain the R-matrix fit for the ground state transition. Data taking for this experiment is in progress (Fig. 2).

2 The ^{3}He$(\alpha,\gamma)^7$Be measurement

^{3}He$(\alpha,\gamma)^7$Be (Q-value=1.586 MeV) is the key reaction for the production of ^{7}Be and ^{8}B neutrinos in the Sun. The error on $S_{3,4}$, 9.4% [6] is the main nuclear limitation to the extraction of physics from the ^{8}B and, very soon, ^{7}Be neutrino flux measurements from the Sun [10, 13]. The ^{3}He$(\alpha,\gamma)^7$Be reaction is also responsible for the production of ^{7}Li in big-bang nucleosynthesis. Its uncertainty strongly affects the prediction of the primordial ^{7}Li abundance [17].

The capture reaction is dominated, at low energies, by the non-resonant direct capture mechanism to the ground state and the 429 keV first excited state of ^{7}Be. One expects to observe two primary γ-ray transitions, DC $\rightarrow 0$ and DC $\rightarrow 429$ keV with the latter followed by a 429 keV secondary transition. An independent determination of the number of ^{7}Be nuclei produced in the reaction requires the detection of the 478 keV γ-ray due to the excited ^{7}Li populated in the EC decay of ^{7}Be (branching ratio of 10.44 ± 0.04 %, $T_{1/2} = 53.22 \pm 0.06$ days). Both methods have been used in the past to determine the absolute cross section σ(E) in the energy range $E_{c.m.} \geq 107$ keV (see [18], [19] and references

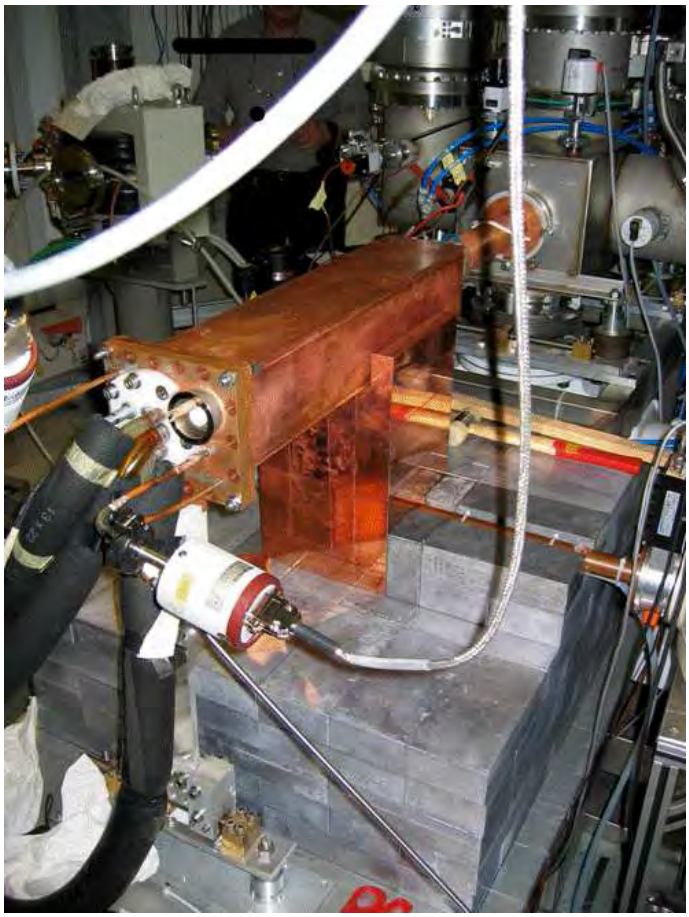

Figure 3: The set-up for the ^{3}He$(\alpha,\gamma)^7$Be study before completing the construction of the lead shield.

.

therein) but the dispersion of the evaluated $S_{3,4}$ astrophysical factors produces a significant uncertainty on the adopted $S_{3,4}$ value. Moreover, the $S_{3,4}$ extracted from the measurements of the induced ^{7}Be activity are 13% higher [6] than the values obtained from the measurements of the prompt capture γ-rays transitions.

The key features of our study of ^{3}He$(\alpha,\gamma)^7$Be are the detection in the same experiment of both the prompt capture γ-ray and of the 478 keV γ-ray from the ^{7}Be decay, the extremely low laboratory background and the high accuracy (relative error $\leq 4\,\%$) down to very low energy ($E_{c.m.} \simeq 90$ keV). The experiment is performed with the ^{4}He$^+$ beam from the 400 kV accelerator in conjunction with a windowless gas target made of oxygen free high conductivity (OFHC) copper, chosen because of its radioactive cleaness, and filled with ^{3}He at 0.7 mbar.

The beam enters the target chamber (Fig. 3) through a 7 mm diameter collimator and it is stopped on a power calorimeter placed 35 cm downstream. The prompt capture γ-ray is detected by a 150 % relative efficiency ultra-low background HpGe detector placed in

close geometry with the target. The germanium detector is surrounded by a 4 cm copper + 25 cm lead shielding and everything is closed inside an anti-radon box. At energies higher than 0.5 MeV we measured a background rate of 4.1 count/h/kg, a factor 7 only worse than the best ultra-low background germanium set-up running in Gran Sasso (in spite of the presence of the beam-pipe entering our shielding and of the calorimeter inside the target chamber).

The ^{7}Be nucleus produced by the ^{3}He$(\alpha,\gamma)^7$Be reaction inside the ^{3}He gas target are implanted into the calorimeter cap (thanks to the forward kinematics and low lateral straggling). After the irradiation, this cap (7 cm diameter) is removed and transported to the counting facility. Two detectors are used to measure the collected ^{7}Be activity. Both are placed in the low level laboratory of LNGS. The first detector is a 120 % relative efficiency HPGe detector with lead + copper shielding. The laboratory background in this detector at 478 keV is roughly 6 counts/keV/day. The second HPGe detector has similar efficiency but it is an ultra-low background detector equipped with lead shielding and radon box. The relevant laboratory background here is 0.2 counts/keV/day (more than 3 orders of magnitude lower than what can be achieved in an external laboratory).

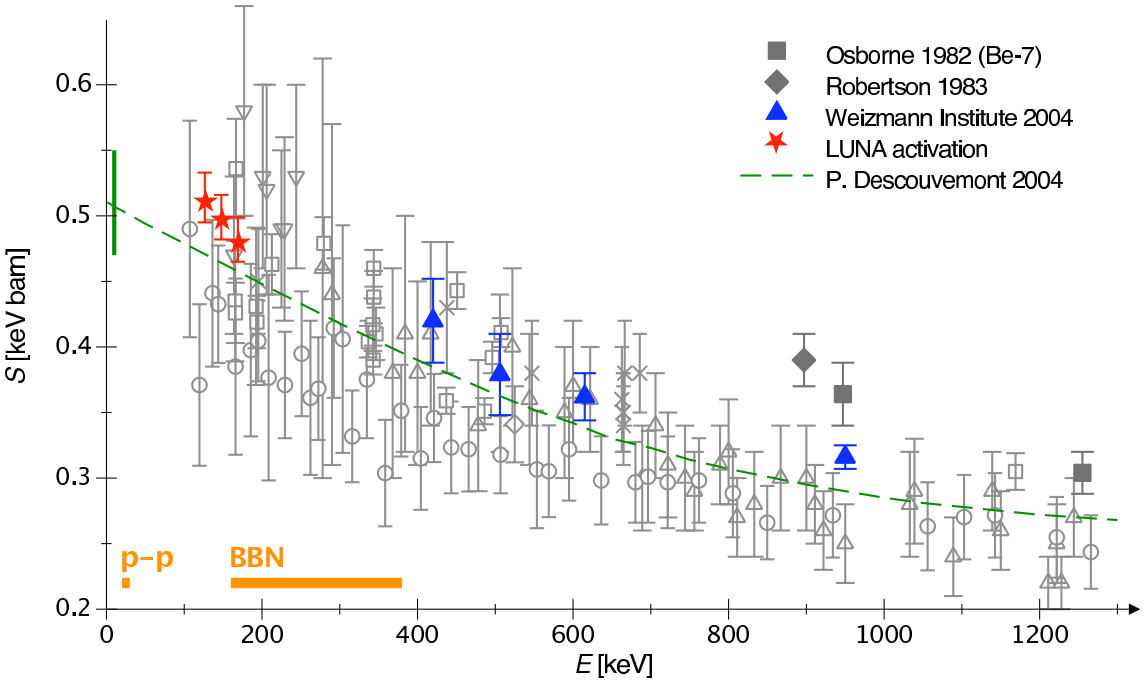

Figure 4: Astrophysical S-factor for ^{3}He$(\alpha,\gamma)^7$Be. Activation data: filled squares [22], filled diamonds [23], filled triangles [19], stars (present work). Prompt-γ data: triangles [25], inverted triangles [26], circles [27] (renormalized by a factor 1.4 [18]), squares [22], diamonds [28], crosses [18]. Dashed line: previously adopted R-matrix fit [21]. Horizontal bars: energies relevant for p–p chain and for BBN.

Data taking started in autumn 2005 and it has been completed by September 2006. We have already obtained the ^{3}He$(\alpha,\gamma)^7$Be cross section at the beam energy of 400, 350

and 300 keV from the activation data [20] alone, i.e. by counting the ^{7}Be nuclei collected on the calorimeter cap. The dominant error is the systematic one, mainly due to the uncertainties on ^{7}Be counting efficiency (1.8%), beam intensity (1.5%) and effective target thickness (1.3%). These data, Fig. 4, are the first activation results at energies directly relevant to big-bang ^{7}Li production. Their uncertainty of 4 % (systematic and statistical combined in quadrature) is comparable to or lower than previous activation studies at high energy and lower than prompt-γ studies at comparable energy. To give an estimate for the low-energy implications, rescaling the most recent R-matrix fit [21] to the present data results in $S(0) = 0.547 \pm 0.017$ keV barn, consistent with, but more precise than, Ref. [19]. All activation data combined (Refs. [22, 23, 24, 19] and the present work) give $S(0) = 0.550 \pm 0.012$ keV barn, higher than the weighted average of all previous prompt-γ studies, $S(0) = 0.507 \pm 0.016$ keV barn [6]. However, the claimed discrepancy between the results obtained with the two different methods can not be solved by activation (or prompt γ) data only, even if very precise. As a matter of fact, we are now analyzing our prompt-γ data (Fig. 5), taken simultaneously with the activation one, in order to obtain a cross section measurement with similar precision.

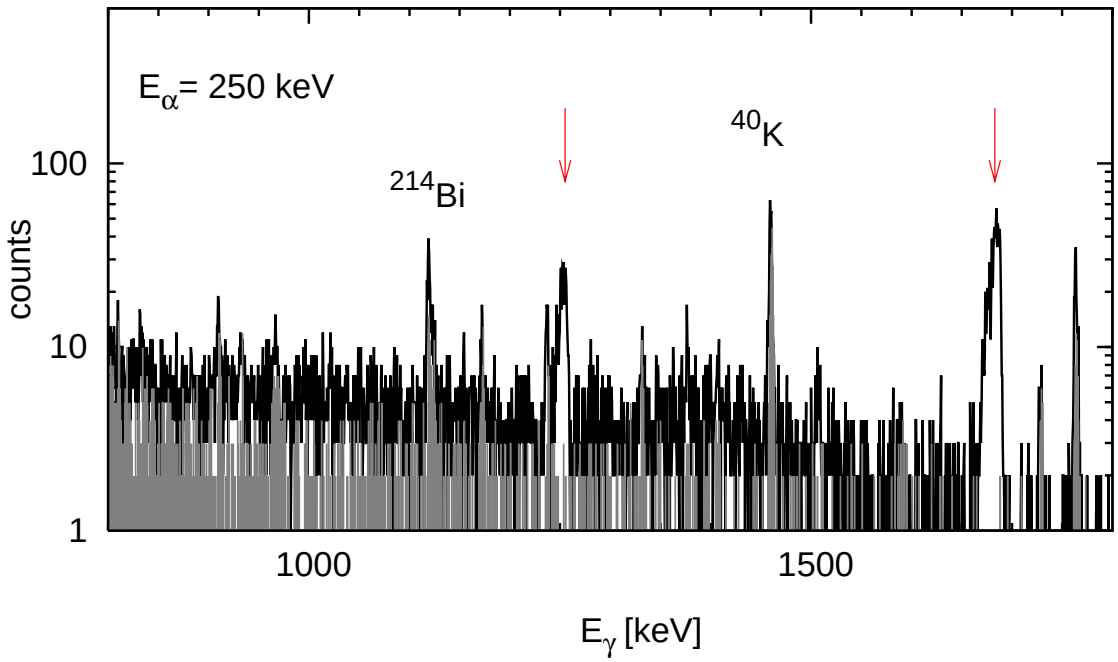

Figure 5: γ-ray spectrum at 250 keV beam energy compared with natural laboratory background (in grey) normalized to the beam measurement life time of 21.3 days. Arrows indicate the primary transition peaks to the ground state and to the first excited state.

3 The ^{25}Mg(p,γ)^{26}Al reaction

The 'non solar' phase of LUNA has already started with the now running experiment on ^{25}Mg(p, γ)^{26}Al (Q-value 6.3 MeV). This is the slowest reaction of the Mg-Al cycle. The β^+ decay of ^{26}Al$_{gs}$ [1] to the excited state of ^{26}Mg gives rise to a 1.8 MeV γ-ray, one of the most important line for γ astronomy. Two reasons make the low energy measurement of this cross section so relevant: the 1.8 MeV full sky map taken by the satellites which look at the γ sky and the anomalous meteoritic abundance of ^{26}Mg ([29] and references therein).

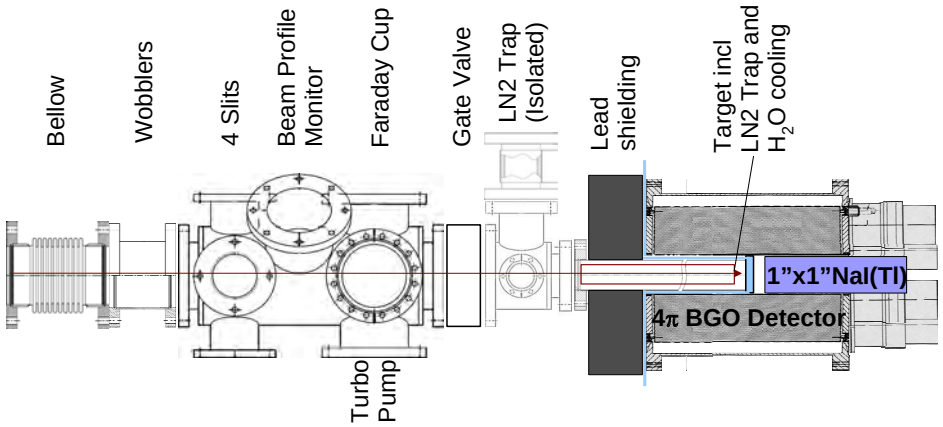

Figure 6: Drawing of the line for the BGO measurement phase.

The aim of the experiment is to directly measure the strength of the resonances at 190, 130 and 93 keV using a high efficiency detector, in particular a summing crystal based on a 4π BGO. In 2006 we obtained the permission to operate the second beam of the LUNA 400kV accelerator. The new beam line has been mounted in summer 2006 and it has been integrated in the LUNA400 control system. Transmission tests have been performed and have proven that the optical properties of the two lines are comparable. The setup (Fig. 6) for the study of ^{25}Mg(p, γ)^{26}Al is currently under construction at the

[1] About 80% of the released ^{26}Al is in the ground state ($t_{1/2} = 7 \cdot 10^5$ year), the remaining 20% goes into the 228 keV isomeric state ($t_{1/2} = 6$s).

new beam line. The water cooled target is located in the centre of the axial borehole (Φ = 60mm, L=310mm) of the BGO detector, thus maximizing efficiency and signal to background ratio. A 1"x1" NaI(Tl) detector is inserted into the BGO detector. The detector is located on a movable support to allow for an easy change of the targets.

Since the target is inside the detector, it is not possible to mount a pumping system close to the target itself. In order to avoid carbon build up on the target, which would result in a wrong determination of the reaction energy and in beam induced background, a vacuum of better than $5 \cdot 10^{-7}$ mbar must be maintained in the target area. This is achieved by constructing its final part with conflat fittings and by inserting a LN_2 cooled copper which goes close to the target and works as sorption pump. The copper tube is biased with a negative voltage, which suppresses secondary electrons produced by the beam impinging on the target. Beam optics calculations have been performed in order to verify that a sufficiently parallel beam can be achieved and transported to the target without hitting the copper tube. The beam trajectory is defined by a series of apertures located outside the detector and shielded with lead from the BGO detector. The electrical current needed to maintain the suppression voltage of the copper tube is monitored with a precession of 0,01 μA in order to assure that no beam is hitting the copper tube.

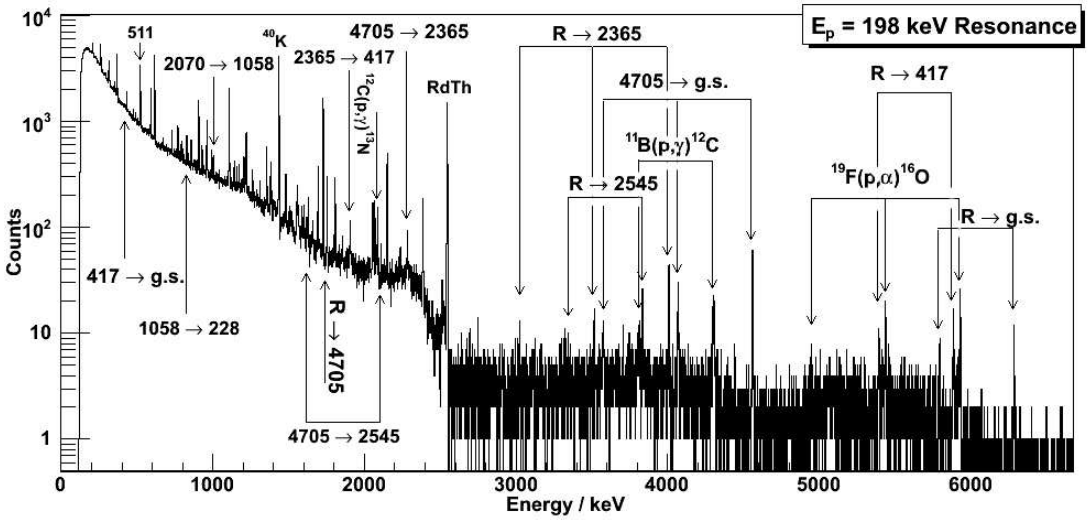

Figure 7: γ-ray spectrum for the ^{25}Mg(p, γ)^{26}Al reaction taken at 190 keV center of mass energy.

Recently, the resonance at 190 keV (together with other resonances at higher energy) has been measured with the AMS technique [30], finding a value about 5 times lower than the literature one. We decided to measure in LUNA this resonance, which has a high enough rate to be studied with a Ge detector, in order to improve the accuracy of the strength determination and to assess the structure of the γ-ray cascade. Last year we performed some testing measurement at this energy showing the possibility to improve the knowledge of this astrophysically relevant resonance (see Fig. 7). The two resonances

at 93 and 130 keV, for which no direct measurement exists and which have been indirectly measured using the ^{25}Mg$(^3He, d)^{26}$Al reaction[31], will be measured in LUNA with the 4π BGO summing crystal in 2007.

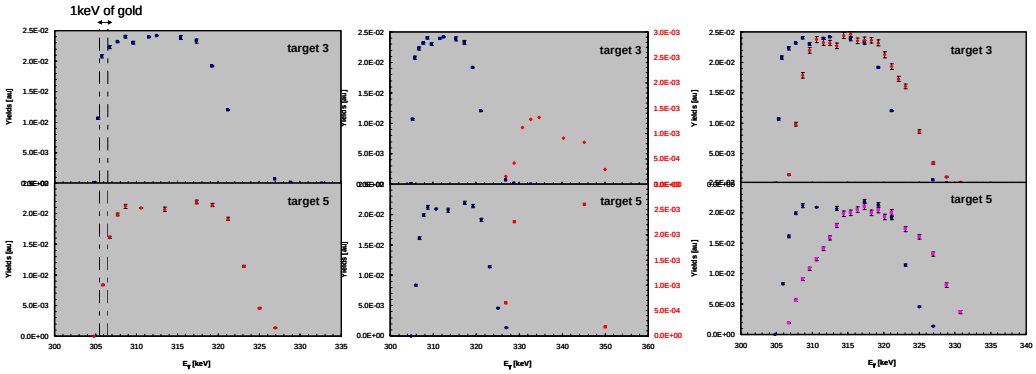

Figure 8: The figure shows the results of the target analysis. Target number 3 is just ^{25}Mg on tantalum backing, while ^{25}Mg target number 5 has a 1 keV upper layer of Au and a thick layer of Au on the Ta backing. Starting from the left, the first pannel shows the thicknesses of targets, the second the fluorine content and the last the stability after a long proton bombardment of about 1 C.

The enriched ^{25}Mg targets have been produced in Münster by evaporating magnesium oxide enriched in the mass 25 isotope (99.2%) on Ta backings. We prepared targets using tantalum backings (0.3mm) and, to reduce the magnesium oxide, we mixed it with tantalum powder. We then evaporated the ^{25}Mg by using an electron gun. We produced different kind of targets:

- evaporating just ^{25}Mg on Ta backing;
- evaporating a layer of Au before the ^{25}Mg, to try to reduce the background contribution from the F content of the backing;
- evaporating a thin layer of Au after the ^{25}Mg, to prevent the Mg oxydation.

The target thicknesses are $\simeq 65\mu/cm^2$ and $\simeq 45\mu/cm^2$, which correspond to a thickness of 30 keV and 20 keV, calculated by using the energy loss table of Ziegler [32] at 100 keV. We checked these results measuring the excitation function at the energy corresponding to the 304 keV resonance (see figure 8). After high dose bombardment we checked the excitation function of different targets observing that the fluorine contamination comes from the evaporation procedure and the Au layer on the Ta backing does not play any role (see Fig. 8). The magnesium diffuses on the surface Au layer, while the targets without Au do not show the typical step due to the oxidation (see figure 8). This lead us to conclude that the targets for the measurement will be directly evaporated on Ta backing without any Au film on surface.

References

[1] R. Bonetti et al. (LUNA Coll.), Phys. Rev. Lett. 82(1999)5205

[2] C. Casella et al. (LUNA Coll.), Nucl. Phys. A 706(2002)203

[3] A. Formicola et al. (LUNA Coll.) Phys. Lett. B 591(2004)61

[4] G. Imbriani et al. (LUNA Coll.) Eur. Phys. J A 25(2005)455A

[5] A. Lemut et al. (LUNA Coll.), Phys. Lett. B 634(2006)483

[6] E.G. Adelberger et al., Rev. Mod. Phys. 70(1998)1265

[7] C. Angulo et al. (NACRE Coll.), Nucl. Phys. A 656(1999)3

[8] S. Degl'Innocenti et al., Phys. Lett. B 590(2004)13

[9] R.C. Runkle et al., Phys. Rev. Lett. 94(2005)082503

[10] G. Fiorentini et al., astro-ph/0310753

[11] D. Bemmerer et al., Eur. Phys. J.A 24 (2005) 313

[12] Z. Elekes et al., Nucl. Inst. Meth. A 503 (2003) 580

[13] J.N. Bahcall and M. Pinsonneault, Phys. Rev Lett. 92(2004)121301

[14] J.N. Bahcall et al., astro-ph/0412440

[15] G. Imbriani et al. (LUNA Coll.), Astronomy and Astrophysics 420(2004)625

[16] F. Herwig and S.M. Austin, Astrophys. J 613(2004)L73

[17] R. Cyburt, Phys. Rev. D 70(2005)023505

[18] M.Hilgemeier *et al.*, Z. Phys. A 329(1988)243

[19] B.S. Nara Singh *et al.*, Phys. Rev. Lett. 93(2004)262503

[20] D. Bemmerer et al., Phys. Rev. Lett. 97 (2006) 122502

[21] P. Descouvement et al., Data Nucl. Data Tables 88 (2004) 203

[22] J. Osborne et al., Nucl. Phys. A 419 (1984) 115

[23] R. Robertson et al., Phys. Rev. C 27 (1983) 11

[24] H. Volk et al., Z. Phys. A 310 (1983) 91

[25] P. Parker and R. Kavanagh, Phys. Rev. 131 (1963) 2578

[26] K. Nagatani et al., Nucl. Phys. A 128 (1969) 325

[27] H. Krawinkel et al., Z. Phys. A 304 (1982) 307

[28] T. Alexander et al., Nucl. Phys. A 427 (1984) 526

[29] D. Bemmerer et al., LNGS Annual Report (2005) 115

[30] A. Arazi et al., Phys. Rev. C 74 (2006) 025802

[31] Ch. Iliadis et al., Nucl. Phys.A 512(1990)509

[32] J. F. Ziegler et al, SRIM program, version 2003-20, srim-org 2003 (www.srim.org)

4 Publications and Conferences

1. A. Lemut et al. (LUNA Coll.), "First measurement of the ^{14}N(p, γ)^{15}O down to 70 keV", Phys. Lett. B 634(2006)483
2. D. Bemmerer et al. (LUNA Coll.), "Activation measurement of the ^{3}He(α, γ)^{7}Be cross section at low energy", Phys. Rev. Lett. 97(2006)122502
3. D. Bemmerer et al. (LUNA Coll.), "Low energy measurement of the ^{14}N(p, γ)^{15}O total cross section at the LUNA underground facility", Nucl. Phys. A 779(2006)297
4. M. Marta et al. (LUNA Coll.), "Study of beam heating effect in a gas target through Rutherford scattering", NIM A 569(2006)727
5. C. Broggini, invited talk at Fusion06, Venice
6. C. Broggini, invited talk at the 11th Int. Conf. Nucl. Reac. Mechanisms, Varenna
7. C. Broggini, invited talk at NOW2006, Otranto
8. C. Broggini, meeting of the Italian Nuclear Astrophysicists, Perugia
9. F. Confortola, meeting of the Italian Nuclear Astrophysicists, Perugia
10. H. Costantini, invited talk at Nuclei in the Cosmos, Geneva
11. H. Costantini, invited talk at the Tours Symposium on Nuclear Physics VI, Tours
12. H. Costantini, invited talk at the APS Division of Nuclear Physics, Nashville
13. V. Lozza, Congresso della Soc. Italiana di Fisica, Torino
14. G. Imbriani, International School of Nuclear Physics, 28th course, Erice
15. G. Imbriani, invited talk at the ECOS Town Meeting, Paris
16. M. Marta, Congresso della Soc. Italiana di Fisica, Torino
17. R. Menegazzo, invited talk at the Neutrino Conference, Santa Fe
18. Zs. Fulop, invited talk at the 3rd ILIAS Ann. Meeting, LNGS

LVD. Large Volume Detector

N.Yu.Agafonova[9], M.Aglietta[14], E.D.Alyea[7], P.Antonioli[1], G.Badino[14], G.Bari[1], M.Basile[1], V.S.Berezinsky[9], M.Bertaina[14], R.Bertoni[14], A. Bonardi[14], G.Bruni[1], G.Bruno[14], G.Cara Romeo[1], A.Chiavassa[14], J.A.Chinellato[3], L.Cifarelli[1], F.Cindolo[1], A.Contin[1], V.L.Dadykin[9], E.A. Dobrynina[9], L.G.Dos Santos[3], R.I.Enikeev[9], W.Fulgione[14], P.Galeotti[14], M.Garbini[1], P.L.Ghia[5,14], G.Giuliani[5,14], P.Giusti[1], F.Gomez[14], F.Grianti[4], G.Iacobucci[1], E.Kemp[3], E.V.Korolkova[9], V.B.Korchaguin[9], V.V.Kuznetsov[9], M.Luvisetto[1], A.A.Machado[15], A.S.Malguin[9], H.Menghetti[1], N.Mengotti Silva[3], C.Morello[14], R.Nania[1], G.Navarra[14], K.Okei[10], L.Periale[14], R.Persiani[1], A.Pesci[1], P.Picchi[14], I.A.Pless[8], A.Porta[14], A.Romero[14], V.G.Ryasny[9], O.G.Ryazhskaya[9], O.Saavedra[14], K.Saitoh[13], G.Sartorelli[1], M.Selvi[1], N.Taborgna[5], N.Takahashi[12], V.P.Talochkin[9], G.C.Trinchero[14], S.Tsuji[11], A.Turtelli[3], P.Vallania[14], S.Vernetto[14], C.Vigorito[14], L.Votano[4], T.Wada[10], R.Weinstein[6], M.Widgoff[2], V.F.Yakushev[9], G.T.Zatsepin[9], A.Zichichi[1]

[1] *University of Bologna and INFN-Bologna, Italy*
[2] *Brown University, Providence, USA*
[3] *University of Campinas, Campinas, Brazil*
[4] *INFN-LNF, Frascati, Italy*
[5] *INFN-LNGS, Assergi, Italy*
[6] *University of Houston, Houston, USA*
[7] *Indiana University, Bloomington, USA*
[8] *Massachusetts Institute of Technology, Cambridge, USA*
[9] *Institute for Nuclear Research, Russian Academy of Sciences, Moscow, Russia*
[10] *Okayama University, Okayama, Japan*
[11] *Kawasaki Medical School, Kurashiki, Japan*
[12] *Hirosaki University, Hirosaki, Japan*
[13] *Ashikaga Institute of Technology, Ashikaga, Japan*
[14] *IFSI-INAF, Torino; University of Torino and INFN-Torino, Italy*
[15] *Centro Brasileiro de Pesquisas Fisicas, Rio de Janeiro, Brasil*

Abstract

The Large Volume Detector (LVD) in the INFN Gran Sasso National Laboratory, Italy, is a ν observatory mainly designed to study low energy neutrinos from the gravitational collapse of galactic objects.

The experiment has been monitoring the Galaxy since June 1992, under increasing larger configurations: in January 2001 it has reached its final active mass $M = 1$ kt. LVD is one of the largest liquid scintillator apparatus for the detection of stellar collapses and, besides SNO, SuperKamiokande and Amanda, it is a charter member of the SNEWS network, that has become fully operational since July 1st, 2005.

During August 2006 there was the first run of the CNGS project: LVD was fully operative and it detected the first CNGS events.

1 The LVD experiment

1.1 Scientific ground

The Large Volume Detector (LVD), located in the hall A of the INFN Gran Sasso National Laboratory, Italy, is a multipurpose detector consisting of a large volume of liquid scintillator interleaved with limited streamer tubes in a compact geometry (a front view is shown in fig.1). The major purpose of the LVD experiment is the search for neutrinos from Gravitational Stellar Collapses (GSC) in our Galaxy [1].

Indeed, in spite of the lack of a "standard" model of the gravitational collapse of a massive star, the correlated neutrino emission appears to be well established. At the end of its burning phase a massive star ($M > 8M_{\odot}$) explodes into a supernova, originating a neutron star which cools emitting its binding energy $E_B \sim 3{\cdot}10^{53}$ erg mostly in neutrinos. The largest part of this energy, almost equipartitioned among neutrino and antineutrino species, is emitted in the cooling phase: $E_{\bar{\nu}_e} \sim E_{\nu_e} \sim E_{\nu_x} \sim E_B/6$ (where ν_x denotes generically $\nu_\mu, \bar{\nu}_\mu, \nu_\tau, \bar{\nu}_\tau$ flavors). The energy spectra are approximatively a Fermi-Dirac distribution, with different mean temperatures, since ν_e, $\bar{\nu}_e$ and ν_x have different couplings with the stellar matter: $T_{\nu_e} < T_{\bar{\nu}_e} < T_{\nu_x}$.

Figure 1: *Front view of the LVD detector in the hall A of the Gran Sasso National Laboratory, INFN.*

LVD is able to detect $\bar{\nu}_e$ interactions with protons in the scintillator, which give the main signal of supernova neutrinos, with a very good signature. Moreover, it can detect ν_e

through the elastic scattering reactions with electrons, $(\nu_e + \bar{\nu}_e)$ through charged current interactions with the carbon nuclei of the scintillator, and it is also sensitive to neutrinos of all flavors detectable through neutral currents reactions with the carbon nuclei. The iron support structure of the detector can also act as a target for electron neutrinos and antineutrinos. The products of the interaction can exit iron and be detected in the liquid scintillator. The amount of neutrino-iron interaction can be as high as about 20% of the total number of interactions. The signal observable in LVD, in different reactions and due to different kinds of neutrinos, besides providing astrophysical informations on the nature of the collapse, is sensitive to intrinsic ν properties, as oscillation of massive neutrinos and can give an important contribution to define some of the neutrino oscillation properties still missing.

1.2 The detector

The LVD experiment has been in operation since 1992, under different increasing configurations. During 2001 the final upgrade took place: LVD became fully operational, with an active scintillator mass $M = 1000$ t.

LVD consists of an array of 840 scintillator counters, 1.5 m^3 each, arranged in a compact and modular geometry; each of them is viewed on the top by three photomultipliers (visible in fig. 2). Up to 2004, before a re-calibration of the full detector, the counters were divided in two subsets: the external ones (43%), operated at energy threshold $\mathcal{E}_h \simeq 7$ MeV, and inner ones (57%), better shielded from rock radioactivity and operated at $\mathcal{E}_h \simeq 4$ MeV. After the re-calibration (which, started in 2004, ended during 2005) all the counters are operated at a common threshold, $\mathcal{E}_h \simeq 5$ MeV.

Figure 2: *Top view of the LVD detector in the hall A of the Gran Sasso National Laboratory, INFN.*

To tag the delayed γ pulse due to n-capture, all counters are equipped with an additional discrimination channel, set at a lower threshold, $\mathcal{E}_l \simeq 1$ MeV.

Other relevant features of the detector are: (i) good event localization and muon tagging;
(ii) accurate absolute and relative timing: $\Delta t_{abs} = 1\,\mu$s, $\Delta t_{rel} = 12.5$ ns;
(iii) energy resolution: $\sigma_E/E = 0.07 + 0.23 \cdot (E/\mathrm{MeV})^{-0.5}$;
(iv) very high duty cycle, i.e. $> 99.5\%$ in the last five years;
(v) fast event recognition.

1.3 Supernova neutrino interactions in LVD

The observable neutrino reactions in the LVD scintillator are:

(1) $\bar{\nu}_e p, e^+ n$, (physical threshold $E_{\bar{\nu}_e} > 1.8\ MeV$) observed through a prompt signal from e^+ above threshold $\mathcal{E}_h$ (detectable energy $E_d \simeq E_{\bar{\nu}_e} - 1.8$ MeV $+2m_e c^2$), followed by the signal from the $np, d\gamma$ capture ($E_\gamma = 2.2$ MeV), above $\mathcal{E}_l$ and with a mean delay $\Delta t \simeq 180\ \mu$s.

(2) $\nu_e\ ^{12}$C,^{12}N e^-, (physical threshold $E_{\nu_e} > 17.3\ MeV$) observed through two signals: the prompt one due to the e^- above $\mathcal{E}_h$ ($E_d \simeq E_{\nu_e} - 17.3$ MeV) followed by the signal, above $\mathcal{E}_h$, from the β^+ decay of ^{12}N (mean life $\tau = 15.9$ ms).

(3) $\bar{\nu}_e\ ^{12}$C,^{12}B e$^+$, (physical threshold $E_{\bar{\nu}_e} > 14.4\ MeV$) observed through two signals: the prompt one due to the e^+ ($E_d \simeq E_{\bar{\nu}_e} - 14.4\,\text{MeV} + 2m_e c^2$) followed by the signal from the β^- decay of ^{12}B (mean life $\tau = 29.4$ ms). As for reaction *(2)*, the second signal is detected above the threshold $\mathcal{E}_h$.

(4) $\overset{(-)}{\nu}_\ell\ ^{12}$C, $\overset{(-)}{\nu}_\ell\ ^{12}$C* ($\ell = e, \mu, \tau$), (physical threshold $E_\nu > 15.1\ MeV$), whose signature is the monochromatic photon from carbon de-excitation ($E_\gamma = 15.1$ MeV), above $\mathcal{E}_h$.

(5) $\overset{(-)}{\nu}_\ell\ e^-$, $\overset{(-)}{\nu}_\ell\ e^-$, which yields a single signal, above $\mathcal{E}_h$, due to the recoil electron.

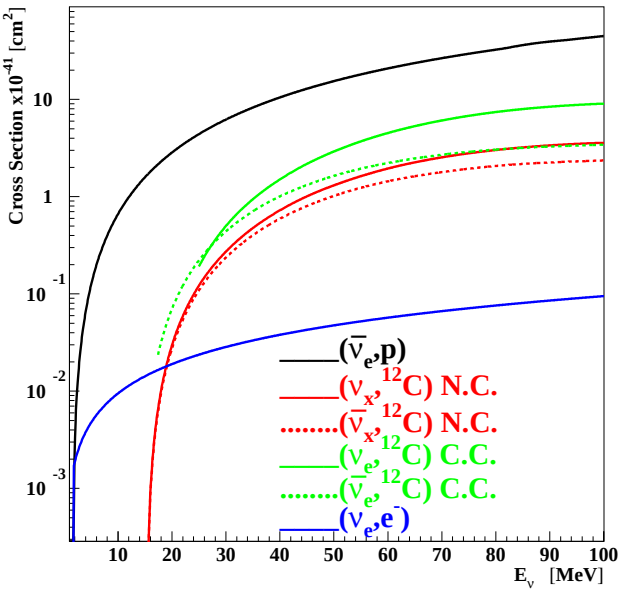

Figure 3: *Cross section behavior for the different neutrino reactions observable in the LVD scintillator.*

The LVD detector is supported by an iron structure made basically by two components: the tank (mean thickness: 0.4 cm), containing the scintillator, and the "portatank" (mean thickness: 1.5 cm) hosting a cluster of 8 tanks. The higher energy part of the ν flux can thus be detected also with the $\nu(\bar{\nu})$Fe interaction, resulting in an electron (positron) that may exit the iron and release energy in the scintillator. The reactions of interest are the following:

(6) $\nu_e\ ^{56}$Fe,^{56}Co e^-. The mass difference between the nuclei is $\Delta_{m_n} = m_n^{\text{Co}} - m_n^{\text{Fe}} = 4.055$ MeV, the first Co allowed state being at 3.589 MeV. Other higher energy allowed states are present in ^{56}Co: considering $E_{e^-}^{\text{kin}} = E_{\nu_e} - \Delta_{m_n} - E_{\text{level}} - m_e$ MeV, where E_{level} is the energy difference between the excitation level and the ground state level, this can take values: $3.589, 4.589, 7.589, 10.589\ MeV$. The efficiency for electron and gammas (also produced in the interaction) to reach the scintillator with energy higher than $\mathcal{E}_h$ is greater than 20% for $E_\nu > 30$ MeV and grows up to 70% for $E_\nu > 100$ MeV. On average, the detectable electron energy is $E_d \simeq 0.45 \times E_\nu$.

(7) $\bar{\nu}_e$ ^{56}Fe,^{56}Mn e^+, the energy threshold and the efficiency are very similar to those of reaction *(6)*.

The number of all the possible targets present in the LVD detector is listed in table 1.

Table 1: Number of targets in the LVD detector.

Target Type	Contained in	Mass	Number of targets
Free protons	Liquid Scintillator	1000 t	$9.34\ 10^{31}$
Electrons	LS	1000 t	$3.47\ 10^{32}$
C Nuclei	LS	1000 t	$4.23\ 10^{31}$
Fe Nuclei	Support Structure	900 t	$9.71\ 10^{30}$

1.4 Effects of neutrino oscillations in the SN signal

There are many experimental works suggesting neutrino conversion among flavors in the recent few years, through the study of atmospheric, solar, reactor and accelerator neutrinos. The interpretation of all these phenomena in terms of neutrino oscillations is rather robust, because it is able to include all the experimental data (except the "not yet confirmed" LSND signal).

In the standard three flavor scenario, six parameters must be determined by oscillation experiments: 3 mixing angles ($\theta_{\rm sol}$, θ_{13}, $\theta_{\rm atm}$), 2 squared mass differences ($\Delta m^2_{\rm sol}$ and $\Delta m^2_{\rm atm}$) and 1 CP-violation phase δ. A recent analysis of all the available experimental data constrains the "atmospheric" and "solar" parameters to be in the following 99% $C.L.$ ranges:

$\Delta m^2_{\rm sol}$ $(7.2 \div 8.9)\, 10^{-5}$ eV^2

$|\Delta m^2_{\rm atm}|$ $(1.7 \div 3.3)\, 10^{-3}$ eV^2

$\theta_{\rm sol}$ $30^\circ < \theta_{\rm sol} < 38^\circ$

$\theta_{\rm atm}$ $36^\circ < \theta_{\rm atm} < 54^\circ$

However the other parameters are not completely determined: the θ_{13} mixing angle is only upper limited, mainly by the Chooz experiment data ($\sin^2\theta_{13} < 3.\ 10^{-2}$ at the 99% $C.L.$), the sign of $\Delta m^2_{\rm atm}$ (that fixes the so–called mass hierarchy) is completely unknown, as well as the CP–violation phase δ.

Because of the wide range of matter density in the stellar envelope, a supernova explosion represents a unique scenario for further study of the neutrino oscillation mixing matrix. Indeed neutrinos can cross two resonance density layers and therefore the resulting possible mixing scenarios are different from the solar ones. The emerging neutrino spectra are sensitive to the sign of $\Delta m^2_{\rm atm}$ and to the value of θ_{13}.

We will show how neutrino oscillations affect the signal detected by LVD and also evaluate the impact on the signal of the astrophysical parameters of the supernova explosion mechanism, such as the total energy emitted in neutrinos, the star distance, the neutrino–sphere temperatures and the partition of the energy among the neutrino flavors. Preliminary results have been presented previously in [10] [11] [12].

For a normal mass hierarchy (NH) scheme, ν (not $\bar{\nu}$) cross two resonance layers: one at higher density (H), which corresponds to $\Delta m^2_{\rm atm}, U^2_{e3}$, and the other at lower density (L), corresponding to $\Delta m^2_{\rm sol}, U^2_{e2}$. For inverted mass hierarchy (IH), transitions at the higher

density layer occur in the $\bar{\nu}$ sector. Given the energy range of SN ν (up to ~ 100 MeV) and considering a star density profile $\rho \propto 1/r^3$, the adiabaticity condition is always satisfied at the L resonance for any LMA solution, while at the H resonance, this depends on the value of U^2_{e3}. When $U^2_{e3} \geq 5{\cdot}10^{-4}$ the conversion is completely adiabatic, meaning that the flip probability between two adjacent mass eigenstates is null ($P_h = 0$). In the adiabatic case and NH, the $\bar{\nu}_e$ produced in the SN core arrive at Earth as ν_1, and they have a high ($U^2_{e1} \simeq cos^2\theta_{12} \simeq 0.7$) probability to be detected as $\bar{\nu}_e$. On the other hand, the original $\bar{\nu}_x$ arrive at Earth as ν_2 and ν_3 and are detected as $\bar{\nu}_e$ with probability $U^2_{e2} \simeq sin^2\theta_{12}$.

The oscillations scheme can be summarized as:
$F_e = P_h U^2_{e2} F^0_e + (1 - P_h U^2_{e2}) F^0_x$ and
$F_{\bar{e}} = U^2_{e1} F^0_{\bar{e}} + U^2_{e2} F^0_{\bar{x}}$ for normal hierarchy;
$F_e = U^2_{e2} F^0_e + U^2_{e1} F^0_x$ and
$F_{\bar{e}} = P_h U^2_{e1} F^0_{\bar{e}} + (1 - P_h U^2_{e1}) F^0_{\bar{x}}$ for inverted hierarchy,
where F^0_{any} are the original neutrino fluxes in the star and F_{any} are the observed ν fluxes. One can notice that, in the antineutrino channel, the non adiabatic ($P_h = 1$), IH case, is equivalent to the NH case (which does not depend on adiabaticity).

With respect to the astrophysical parameters, we assumed a galactic supernova explosion at a typical distance of $D = 10$ kpc, parametrized with a pure Fermi–Dirac energy spectrum ($\eta = 0$) with a total energy $E_b = 3 \cdot 10^{53}$ erg and perfect energy equipartition $f_{\nu_e} = f_{\bar{\nu}_e} = f_{\nu_x} = 1/6$; we fixed $T_{\nu_x}/T_{\bar{\nu}_e} = 1.5$, $T_{\nu_e}/T_{\bar{\nu}_e} = 0.8$ and $T_{\bar{\nu}_e} = 5$ MeV.

For the chosen supernova parameters, it results that the expected number of events and their energy spectrum depend on the unknown oscillation parameters: the mass hierarchy and the value of θ_{13}.

In particular, the inverse beta decay interactions ($\bar{\nu}_e p, e^+ n$) are highly sensitive to the mass hierarchy: for adiabatic transition, the number of events increases of $\sim 25\%$ in the IH case, with respect to the NH one, since the detected $\bar{\nu}_e$ completely come from the higher energy ν_x. The mean energy of the detected positrons is correspondingly increased.

The total number of ($\nu_e + \bar{\nu}_e$) CC interaction with ^{12}C nuclei is highly increased taking into account neutrino oscillations, because of their high energy threshold. For adiabatic transition the expected number of events is higher than the non adiabatic one, because at least one specie (between ν_e or $\bar{\nu}_e$) comes significantly from the original and higher–energy ν_x in the star. However, if it is not possible to discriminate between ν_e and $\bar{\nu}_e$, the normal and inverted hierarchy cases present similar results. Indeed, in the NH (IH) case, the increase in ν_e ($\bar{\nu}_e$) is compensated by a decrease in $\bar{\nu}_e$ (ν_e).

The neutrino interactions with the iron of the support structure, which are studied in details in this work, are also incread by the oscillations. The efficiency for the detection of the produced charged leptons and gammas in the active part of the detector has been calculated with a full simulation of the apparatus. The contribution of ($\nu_e + \bar{\nu}_e$) Fe interactions can be as high as 15% of the total number of events (in the adiabatic NH case) and they contribute mostly to the high energy part of the spectrum.

With respect to the previous detection channels, the number of NC interactions with ^{12}C nuclei does not depend on oscillations. In principle they could be used as a reference to identify the ν_x–sphere temperature. However, this is partly limited by the unknowledge of the other astrophysical parameters.

In conclusion, for our choice of the astrophysical parameters, the expected signal of

neutrinos in the LVD detector from a supernova core collapse greatly benefits of the neutrino oscillation mechanism, practically in all the possible detection channels, especially if the transition is adiabatic and the hierarchy inverted (since in LVD the most relevand signal is given by $\bar{\nu}_e$).

The expected number of events in the various LVD detection channels and in the different oscillation scenarios are shown in table 2.

Table 2: Expected results in the various LVD detection channels and in the mean energy of the detected $\bar{\nu}_e$ p events.

	No Oscillation	Non Adiabatic	Adiabatic NH	Adiabatic IH
$\bar{\nu}_e$ p	346.	391.		494.
$\langle E_{\bar{\nu}_e} \rangle$ in $\bar{\nu}_e$ p	25. MeV	30. MeV		37. MeV
CC with ^{12}C	8.	22.	29.	27.
CC with ^{56}Fe	22.	72.	95.	92.
NC with ^{12}C	27			

However, being aware of the fact that the astrophysical parameters of the supernova mechanism are up to now not well defined, we performed the same calculations using different values of them. The resulting differences are in fact important; they are mainly due to the poor theoretical knowledge of the physics of the gravitational collapse. This will be hopefully improved after the occurence and detection of the next galactic supernova, to which the LVD experiment can give a significant contribution.

2 LVD and its experimental activity in 2006

2.1 Supernova physics

2.1.1 Monitoring the Galaxy

LVD has been continuously monitoring the Galaxy since 1992 in the search for neutrino bursts from GSC [1].

[1] The results of this search have been periodically updated and published in the ICRC Proceedings, since 1993 until 2005. [3, 4, 5, 6, 7, 8, 9]

Its active mass has been progressively increased from about 330 t in 1992 to 1000 t in 2001, always guaranteeing a sensitivity to gravitational stellar collapses up to distances $d = 20$ kpc from the Earth, even in the case of the lowest ν-sphere temperature.

In fig. 4 we show the duty cycle of the experiment during the last 6 years. Considering just the last year (2006) the average duty cycle was 99.93% and the average active mass in the same period 940 t.

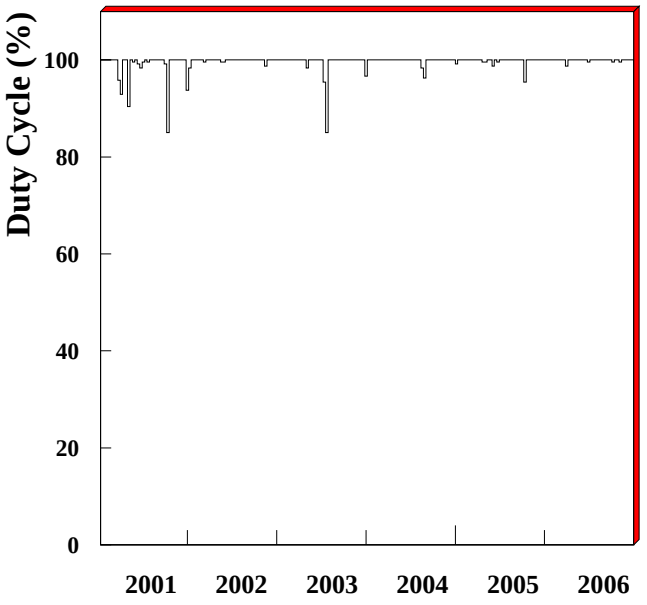

Figure 4: LVD duty cycle during the last six years of data acquisition.

All events are processed on the base of their time sequence, searching for cluster not compatible with a poissonian fluctuation of the background. A first selection consists in rejecting the crossing muon events and accepting only those with energy in the $[7-100]$ MeV range. After this selection cut we obtain a very stable counting rate $f_b = 0.3$ Hz. Each cluster is identified by its multiplicity m and its duration Δt (up to 200 s): the imitation frequency Fim (that is the frequency that a particular cluster (m,Δt) is due to a poissonian fluctuation of the background f_b) is then calculated. The interesting candidates (those with $Fim < 1$ ev/year) undergo several consistency checks: (i) the topological distribution of pulses inside the detector has to be uniform; (ii) their energy spectrum is checked against the background spectrum and (iii) the time distribution of the delayed low energy pulses (due to the 2.2 MeV gamma from the neutron capture) must follow an exponential law.
No significant signal has been registered by LVD during 14 years of data acquisition. Since the LVD sensitivity is higher than expected from GSC models (even if the source is at a distance of 20 kpc and for soft neutrino energy spectra) we can conclude that no gravitational stellar collapse has occurred in the Galaxy in the whole period of observation: the resulting upper limit to the rate of GSC, updated to 2006, at 90% C.L. is 0.18 events/yr.

2.1.2 SNEWS

The SNEWS (SuperNova Early Warning System) [13, 14] project is an international collaboration including several experiments sensitive to a core-collpase supernova neutrino

signal in the Galaxy and neighbour. The goal of SNEWS is to provide the astronomical community with a prompt and confident alert of the occurrence of a Galactic supernova event, generated by the coincidence of two or more active detectors. In addition the collaboration is engaged in cooperative work, such as the downtime coordination and inter-experiment timing verification, designed to optimize the global sensitivity to a supernova signal. A dedicated process waits for alarm datagrams from the experiments' clients, and provides an alert if there is a coincidence within a specified time window (10 seconds for normal running). In July 2005, after a few years of tuning, the charter members of SNEWS (i.e., LVD, Super-K and SNO[2]) together with the newly joined Amanda/IceCube, started the effective operation of the network, which means that the alert is really sent to the list subscribers, in the case of an at least two-fold coincidence (see *http://snews.bnl.gov* to get your own SN alert !).
Up to now, no inter-experiment coincidence, real or accidental, has ever occurred (except during a special high rate test mode), nor any core collapse event been detected within the lifetimes of the currently active experiments.

2.2 CNGS beam monitor

The Cern Neutrinos to Gran Sasso (CNGS) project aims to produce a high energy, wide band ν_μ beam at Cern and send it towards the INFN Gran Sasso National Laboratory (LNGS). Its main goal is the observation of the ν_τ appearance, through neutrino flavour oscillation, by the Opera experiment.

As proven in [15], due to its large area and active mass, LVD can act as a very useful beam monitor, detecting the interaction of neutrinos inside the detector and the muons generated by the ν interaction in the rock upstream the detector.

2.2.1 The CNGS beam

The information about the CNGS beam characteristics are taken by the LHCLOG_CNGS_OPERA database (hereafter DB) [16]. Two main quantities are relevant for each proton extraction:

- the UTC time of the spill (in ns),
- the number of extracted protons on target (p.o.t.) [3].

The CNGS beam started its first run of operation on 18^{th} August, 2006 (first spill at 11:31:54.072 UTC) and finished on 30^{th} August (last spill at 03:30:04.872 UTC). In the following we will refer to this first run as Run1. The total number of protons delivered against the graphite target is 7.59 10^{17}. The beam intensity per each spill is shown in figure 5. It started with an average intensity of 1.38 10^{13} p.o.t. per spill until 23^{rd} August; then there was a predefined stop called "Machine Development" (MD). On 25^{th} August the run restarted with a slightly higher intensity of 1.64 10^{13} p.o.t. per spill, on average.

[2] Actually the SNO experiment is stopped and under decommissioning

[3] Due to some known problems (see [17]) it happened that for some extraction there was only the UTC time or only the number of p.o.t. . In the following we will consider only those extraction where both the informations were present.

The time structure of the CNGS beam is characterized by two extractions, 10.5 μs long, separated by 50 ms; this pattern is repeated each CNGS cycle, whose duration can change: during Run1 there were two main repetition cycles: 16.8 s and 22.8 s.

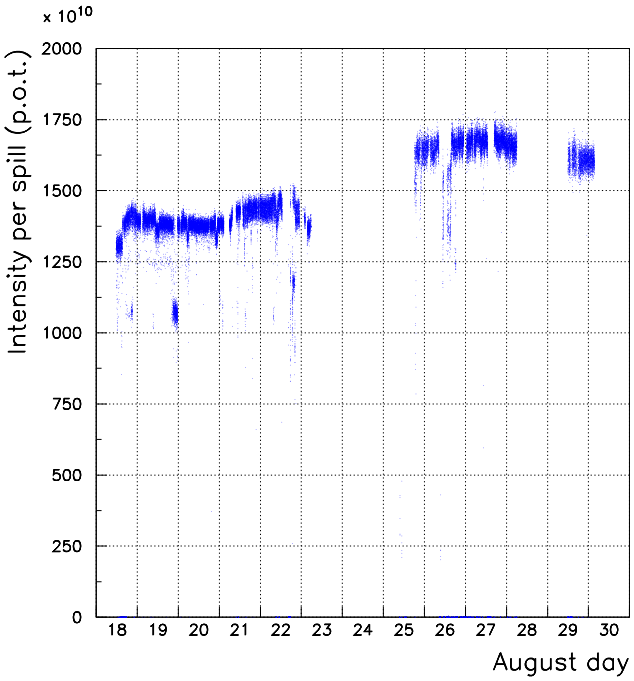

Figure 5: Beam intensity (in protons on target) per each spill of Run1.

2.2.2 MC simulation of the expected events

The CNGS events in LVD can be subdivided into two main categories:

- ν_μ charged current (CC) interactions in the rock upstream the LNGS; they produce a muon that can reach LVD and be detected,
- ν_μ CC and neutral current (NC) interactions in the material (liquid scintillator and iron of the support structure) of LVD.

We developed a full Montecarlo simulation that includes the generation of the neutrino interaction products, the propagation of the muon in the Gran Sasso rock and the response of the LVD detector. The details of the simulation were described in [15]; however, with respect to that paper, some modifications were done with up–to–date informations. In particular we now use the CNGS flux calculated in 2005 by the Fluka group [18] and the neutrino cross section NUX-FLUKA [19]. There are also some modifications in the detector: there are actually 7 active levels of scintillation counters instead of the 8 previously considered, and the energy threshold for the definition of a CNGS event is now 100 MeV instead of 200 MeV.

The resulting number of expected events, at the nominal intensity 4.5 10^{19} p.o.t./y is 32160/y, equivalent to 7.147 10^{-16} events per p.o.t. (considering 200 effective days per year it corresponds to $\sim$ 160 CNGS events per day): 78% are muons from the rock, 17% are CC interactions in the detector and 5% are NC.

During Run1 the total number of p.o.t. was 7.59 10^{17}, thus 542 events are expected in LVD.

2.2.3 CNGS detected events

The LVD events are filtered using a very loose selection cut: we require to have at least one scintillation counter with an energy release larger that 100 MeV. The resulting rate is quite stable, with an average value of 0.37 Hz, see figure 6.

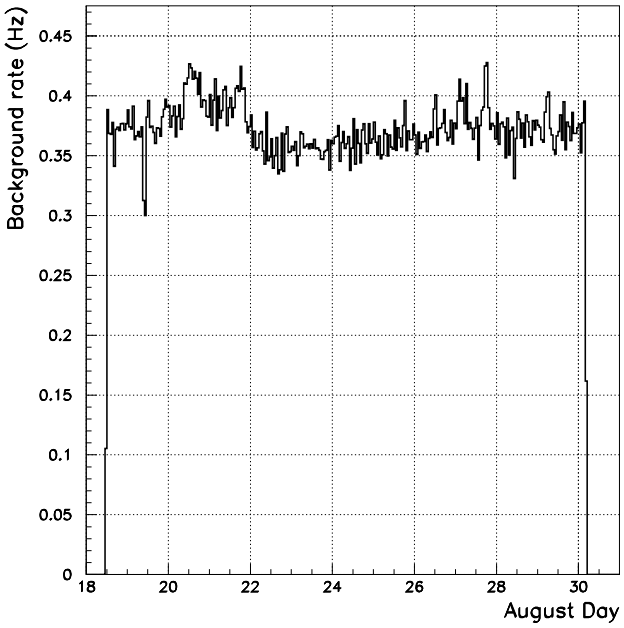

Figure 6: Background rate of events during Run1. These events present at least one scintillation counter with an energy release larger than 100 MeV.

Among this sample the first selection criteria is based on the coincidence of the LVD event time with the beam spill time written in the DB. Two main corrections have been done: the neutrino time of flight from Cern to the LNGS (2.440 ms) and the propagation of the GPS time signal from the outside laboratories to slave clocks in the underground hall (42116, 42064 and 42041 ns respectively for tower 1, 2 and 3), measured in July, 2006 together with the other experiments at LNGS [20].

During Run1 there were some additional time shifts between the LNGS time and the UTC time written in the DB: from the beginning until 18^{th} 16:00 it was +100 μs, then

+10 μs until 22^{nd} 9:00 and -2 ms until 23^{rd} 5:30. After the MD there was no additional bias.

After applying all these corrections, we search for the CNGS events in the interval $[-15, +25]$ μs around the start time of the beam spill. In this way 569 events are selected; their distribution in the time window is shown in figure 7.

The four events with time difference between -13 and -8μs occured on 19^{th} August when there was a failure in the LNGS master clock. The second master was switched on and a time shift of about 10 μs was present. Thus those events are considered in the analysis.

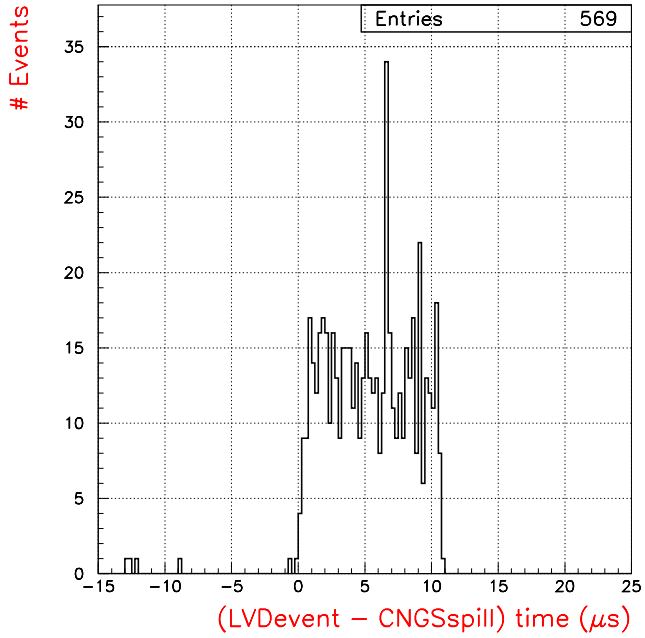

Figure 7: Distribution of the detection time of the 569 CNGS events, with respect to the initial time of the beam spill.

In figure 8 (left) we show the comparison between the expected and detected event rate per each day of data acquisition; in figure 8 (right) the comparison of the integral number of events, hour by hour, is shown. Given the presently limited statistics, the agreement is good.

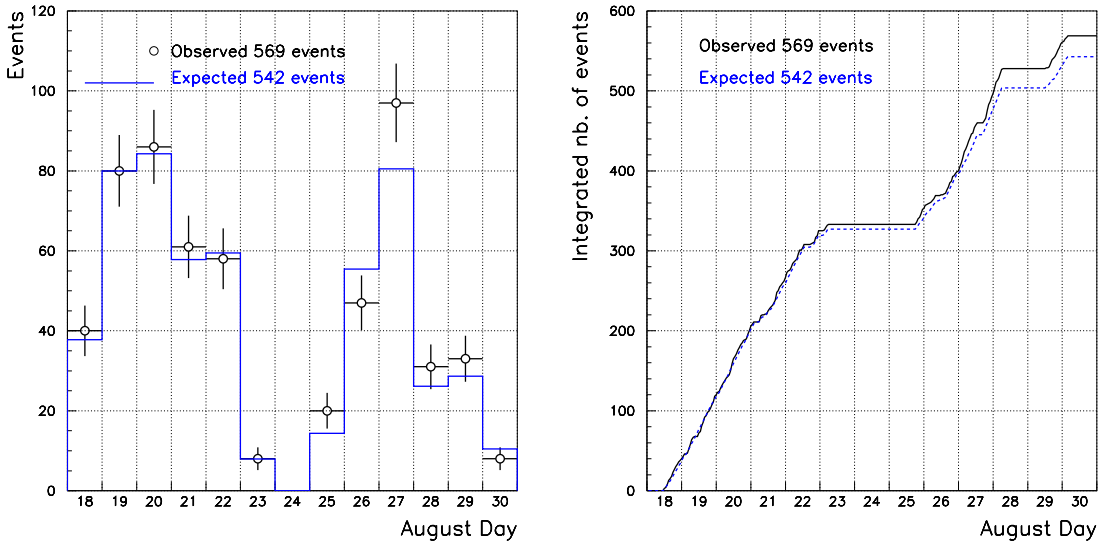

Figure 8: Comparison between the expected and detected number of events during Run1. In the *left* panel there is the number of events per day: observed (black circles) and expected (blue line). In the *right* one the integrated number of events: observed (black solid line) and expected (blue dashed line).

Two examples of typical CNGS events in LVD are shown in figure 9 (muon from the rock) and 10 (neutrino interaction inside the detector).

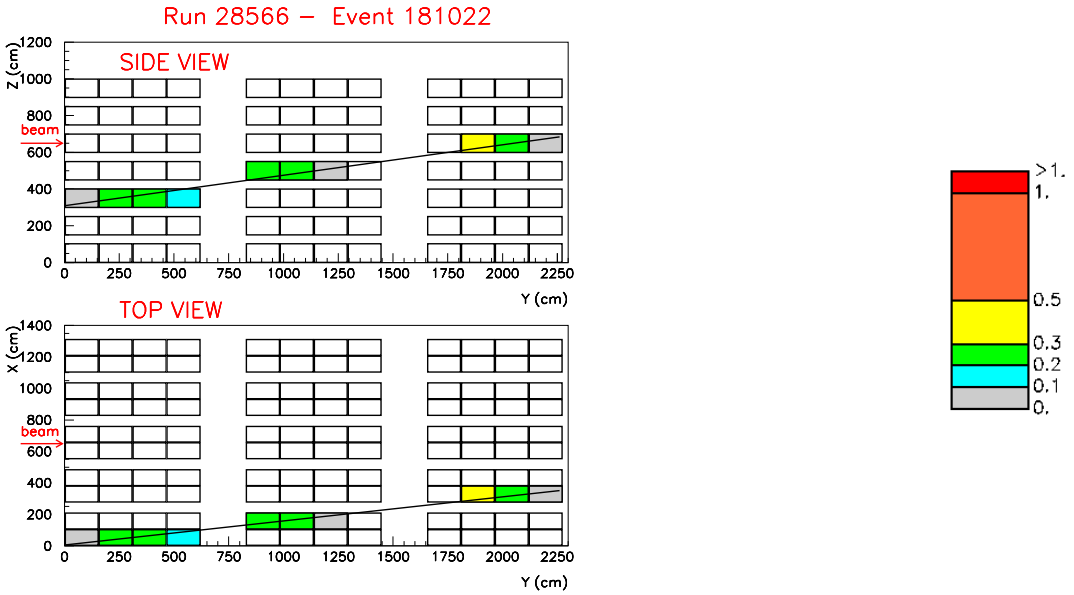

Figure 9: Display of a CNGS events: typical charged current interaction in the rock upstream LVD, producing a muons that go through the detector. The colours represent the amount of energy released in the scintillation counters; the legenda is expressed in GeV. The black straight line is the result of a linear fit to the hit counters.

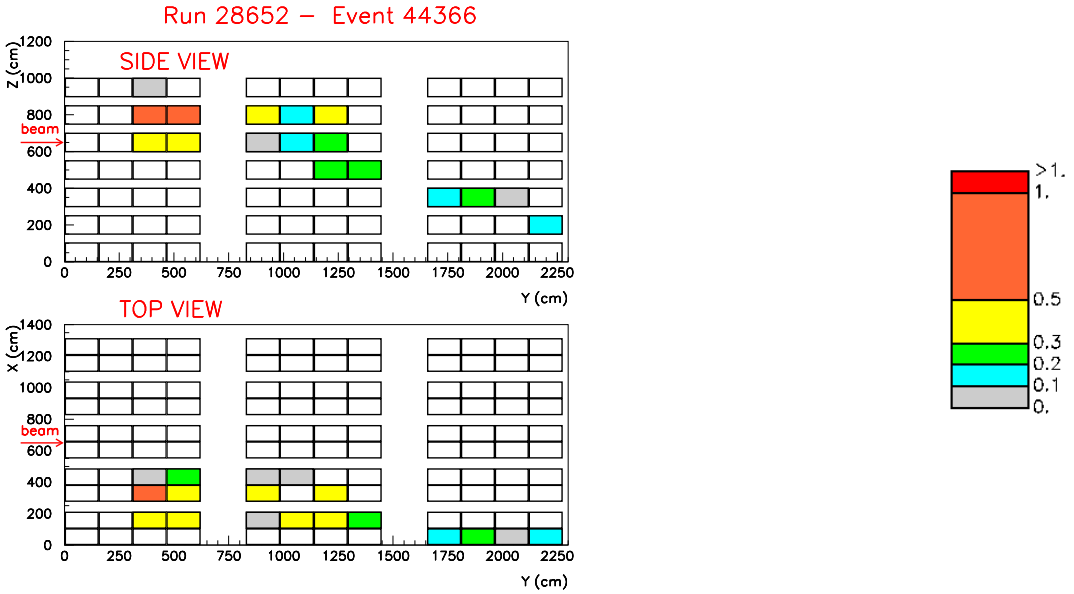

Figure 10: Display of a CNGS events: neutrino interaction inside the LVD detector. The colours represent the amount of energy released in the scintillation counters; the legenda is expressed in GeV.

Comparison with the MC simulation

In the following we show the comparison between the CNGS detected events and the results of our MC simulation, normalized to the same number of events. In figure 11 we show the distribution of the number of scintillation counters hit per each event, with an energy threshold of 10 MeV. In figure 12 the total amount of energy detected by the scintillation counters is displayed. These two histograms are normalized to the total sample of 569 detected events.

In order to select the events generated in the rock, producing a penetrating muon inside the detector, we perform the muon track reconstruction with a linear fit to the centers of the hit scintillation counters. Requiring at least 3 hit counters and a good χ^2 (probability larger than 1% in both the *TOP* and *SIDE* projections) we select 319 events. From the MC simulation we estimate that, using this selection cut, the efficiency to detect "muons from the rock" is about 80% and the contamination of "internal events" is low (less than 5%). For this selected sample of events we can reconstruct the muon direction and compare it with the expectation from the reconstruction of MC events. The results are shown for the angle between the muon and the main axis of the hall A: its projections in the *SIDE* and *TOP* view of the detector are in figure 13 and 14 respectively.

The events are almost horizontal and the main part of them are reconstructed exactely at 0° because of the discreteness of the scintillation counters (cross section 1×1 m^2). In the *TOP* view the beam is parallel to the hall A axis, while in the *SIDE* view the beam "comes out" from the floor with an angle of 3.2°, as seen in figure 13. The agreement of the data and the MC simulation is very good in both the projections.

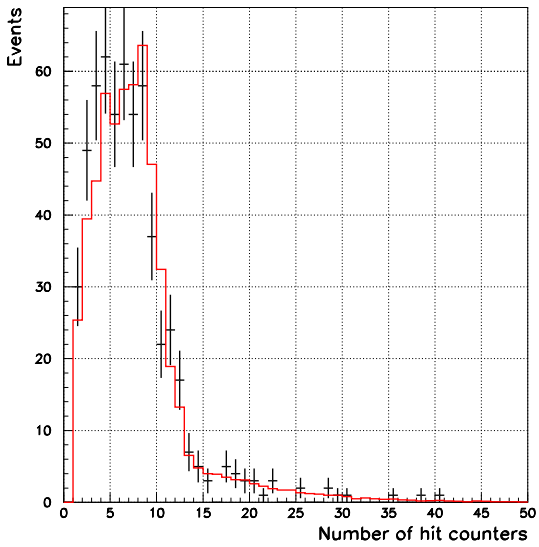

Figure 11: Distribution of the number of scintillation counters hit per each CNGS event: comparison between the data (black crosses) and MC simulation (red line).

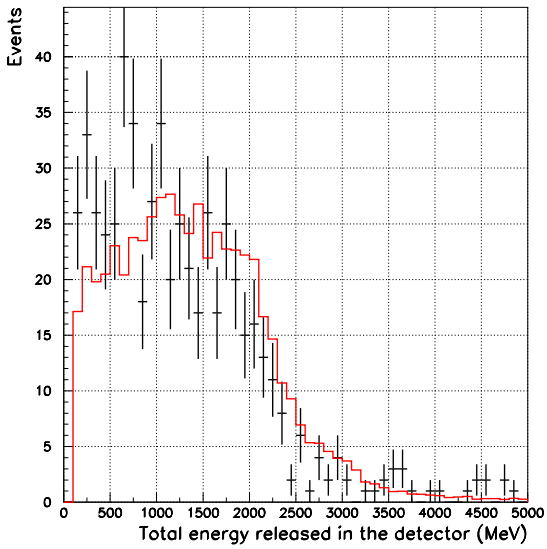

Figure 12: Distribution of the total energy detected in the apparatus per each CNGS event: comparison between the data (black crosses) and MC simulation (red line).

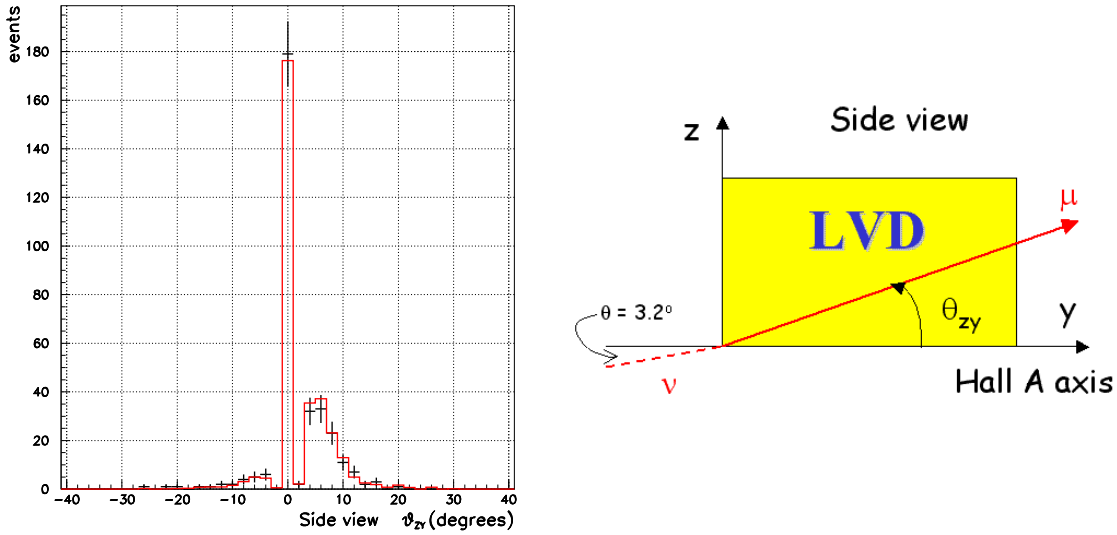

Figure 13: Distribution of the "side" projection of the angle between the reconstructed muon track and the main axis of the LNGS hall: comparison between the data (black crosses) and MC simulation (red line). In the right picture there is a description of the considered angle θ_{zy}.

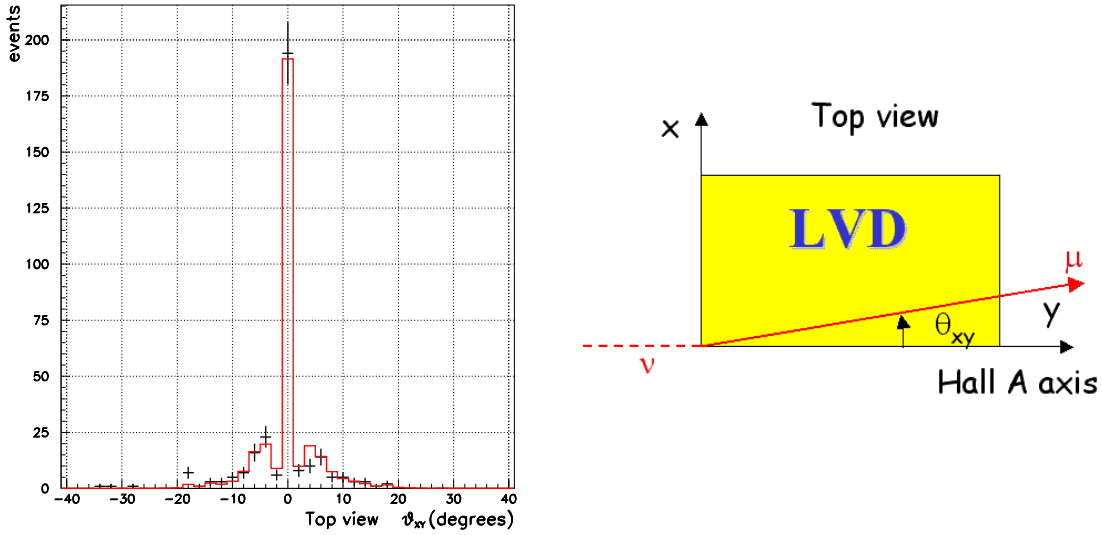

Figure 14: Distribution of the "top" projection of the angle between the reconstructed muon track and the main axis of the LNGS hall: comparison between the data (black crosses) and MC simulation (red line). In the right picture there is a description of the considered angle θ_{xy}.

Background

The background is estimated considering the rate of events shown in figure 6 among which the CNGS events are searched for, with an average value of 0.37 Hz. We remind that the time window where we search for the events around the beam spill time is 40 μs wide, and the number of useful spills in the DB is 51581. Thus the number of events due to the background, during Run1, is

$$N_{bkg} = 0.37\ Hz \times 40\ \mu s \times 51581 = 0.764$$

practically negligible.

2.2.4 Summary

We presented the results of the first events detected by the LVD detector in coincidence with the CNGS beam. The first run of the CNGS beam was started in August 2006, with an overall number of 7.6 10^{17} protons delivered on the target. The LVD detector was fully operative during the whole run, with an average active mass of 950 t.

LVD can detect the CNGS neutrinos through the observation of penetrating muons originated by ν_μ CC interactions in the rock upstream the LNGS and through internal CC and NC neutrino interactions.

The expected number of events, as predicted by our Montecarlo simulation, is 542. We searched for the CNGS events by looking at the time coincidence with the beam spill time; the number of detected events is 569.

There is a good agreement, between the detected events and the MC simulation, in the distribution of the number of hit counters, the total energy released in the apparatus and the direction of the reconstructed muons.

We estimate that the number of events due to the background is lower than one in the whole Run1 time.

Thus, this first run of the CNGS beam confirmed that, as it was proposed in [15], LVD can act as a very useful CNGS beam monitor.

3 List of publications in 2006

- *Study of muon-induced neutron production, propagation and energy spectrum with the LVD detector at LNGS*,
  Nuovo Cim. **29** C, 345 (2006).

- *LVD highlights*,
  Proceedings of the Vulcano Workshop 2006 *"Frontier Objects in Astrophysics and Particle Physics"*, F. Giovannelli & G. Mannocchi (eds.), Italian Physical Society, Editrice Compositori, Bologna, Italy (in press).
  `hep-ex/0608061`

- *Study of the effect of neutrino oscillations on the supernova neutrino signal in the LVD detector*,
  Accepted for publication in Astroparticle Physics (in press).
  doi:10.1016/j.astropartphys.2006.11.004
  `hep-ph/0609305`

- *Low energy background measurements with the LVD*,
  Proceedings of the 9^{th} International Conference on Topics in Astroparticle and Underground Physics (TAUP),
  Journal of Physics: Conference Series **39**, 278 (2006).

References

[1] LVD Collaboration, Il Nuovo Cimento **A105** (1992) 1793

[2] A. Strumia, F. Vissani, `astro-ph/0302055`.

[3] LVD Collaboration, 23th ICRC Conf.Proc.,HE 5.1.1,Vol.4,468,1993

[4] LVD Collaboration, 24th ICRC Conf.Proc., HE 5.3.6,Vol.1,1035,1995

[5] LVD Collaboration, 25th ICRC Conf.Proc., HE 4.1.12,1997

[6] LVD Collaboration, 26th ICRC Conf.Proc., HE 4.2.08,Vol.2,223,1999

[7] LVD Collaboration, 27th ICRC Conf.Proc., HE230,1093,2001

[8] LVD Collaboration, 28th ICRC Conf.Proc., HE2.3,1333,2003

[9] LVD Collaboration, 29th ICRC Conf. Proc., OG2.5, 2005

[10] LVD Collaboration, Nucl. Phys. B Proc. Sup. 110 (2002) pp 410-413, astro-ph/0112312

[11] A. Zichichi, *The most powerful scintillator supernova neutrino detector*, talk presented at the symposium *LVD: the First Ten Years*, LNGS, 28-29 October, 2002).

[12] LVD Collaboration, 28th ICRC Conf.Proc., HE2.3,1297,2003

[13] http://hep.bu.edu/∼snnet/

[14] P. Antonioli et al., New J. Phys., 6 (2004) 114

[15] M. Aglietta et al., *CNGS beam monitor with the LVD detector*, Nuclear Instruments and Methods in Physics Research **A 516**, 96 (2004).

[16] C. Roderick, LHC LOGGING - CNGS-OPERA gateway database user guide, https://edms.cern.ch/file/750206/1/LHCLOG_CNGS_OPERA_GW_DB_GUIDE.pdf.

[17] D. Autiero, private communication. See also his presentation at the Gran Sasso seminar "First events from CNGS", January 2007, available in http://www.lngs.infn.it in the seminar web page.

[18] A. Ferrari et al., *An updated Monte Carlo calculation of the CNGS neutrino beam*, CERN-AB-Note-2006-038, EDMS No. 745389.
Fluxes available in http://www.mi.infn.it/∼psala/Icarus/cngs.html

[19] G. Battistoni et al., *The FLUKA nuclear cascade model applied to neutrino interactions*, Proceedings of NUINT'02, December 2002, University of California, Irvine, USA.
Available online at http://nuint.ps.uci.edu/proceedings/sala.pdf

[20] D. Autiero et al., *Measurement of the fibre delays for the GPS signal underground distribution*, internal note, (2006).

OPERA

R. Acquafredda[24], N. Agafonova[18], M. Ambrosio[24], A. Anokhina[21], S. Aoki[15], A. Ariga[23], L. Arrabito[17], D. Autiero[17], A. Badertscher[37], A. Bergnoli[28], F. Bersani Greggio[9], M. Besnier[2], M. Beyer[30], S. Bondil-Blin[27], K. Borer[5], J. Boucrot[27], V. Boyarkin[18], C. Bozza[31], R. Brugnera[28], S. Buontempo[24], Y. Caffari[17], J. E. Campagne[27], B. Carlus[17], E. Carrara[28], A. Cazes[9], L. Chaussard[17], M. Chernyavsky[20], V. Chiarella[9], N. Chon-Sen[33], A. Chukanov[8], R. Ciesielski[28], L. Consiglio[6], M. Cozzi[6], F. Dal Corso[28], N. D'Ambrosio[3], J. Damet[2], G. De Lellis[24], Y. Déclais[17], T. Descombes[17], M. De Serio[4], F. Di Capua[24], D. Di Ferdinando[6], A. Di Giovanni[16], N. Di Marco[16], C. Di Troia[9], S. Dmitrievski[8], M. Dracos[33], D. Duchesneau[2], B. Dulach[9], S. Dusini[28], J. Ebert[12], R. Enikeev[18], A. Ereditato[5], L. S. Esposito[3], C. Fanin[28], J. Favier[2], G. Felici[9], T. Ferber[12], L. Fournier[2], A. Franceschi[9], D. Frekers[22], T. Fukuda[23], C. Fukushima[10], V. I. Galkin[21], V. A. Galkin[26], R. Gallet[2], A. Garfagnini[28], G. Gaudiot[33], G. Giacomelli[6], O. Giarmana[17], M. Giorgini[6], L. Girard[17], C. Girerd[17], C. Goellnitz[12], J. Goldberg[11], Y. Gornoushkin[8], G. Grella[31], F. Grianti[9], C. Guerin[17], M. Guler[1], C. Gustavino[3], C. Hagner[12], T. Hamane[2], T. Hara[15], M. Hauger[25], M. Hess[5], K. Hoshino[23], M. Ieva[4], M. Incurvati[9], K. Jakovcic[36], J. Janicsko Csathy[25], B. Janutta[12], C. Jollet[33], F. Juget[25], M. Kazuyama[23], S. H. Kim[13], M. Kimura[10], J. Knuesel[5], K. Kodama[14], D. Kolev[32], M. Komatsu[23], U. Kose[1], A. Krasnoperov[8], I. Kreslo[5], Z. Krumstein[8], I. Laktineh[17], C. de La Taille[27], T. Le Flour[2], S. Lieunard[2], A. Ljubicic[36], A. Longhin[28], A. Malgin[18], K. Manai[34], G. Mandrioli[6], U. Mantello[28], A. Marotta[24], J. Marteau[17], G. Martin-Chassard[27], V. Matveev[18], M. Messina[5], L. Meyer[5], S. Micanovic[36], P. Migliozzi[24], S. Miyamoto[23], P. Monacelli[16], I. Monteiro[2], K. Morishima[23], U. Moser[5], M. T. Muciaccia[4], P. Mugnier[2], N. Naganawa[23], M. Nakamura[23], T. Nakano[23], T. Napolitano[9], M. Natsume[23], K. Niwa[23], Y. Nonoyama[23], A. Nozdrin[8], S. Ogawa[10], A. Olchevski[8], D. Orlandi[3], D. Ossetski[26], A. Paoloni[9], B. D Park[23], I. G. Park[13], A. Pastore[4], L. Patrizii[6], L. Pellegrino[9], H. Pessard[2], V. Pilipenko[22], C. Pistillo[5], N. Polukhina[20], M. Pozzato[6], K. Pretzl[5], P. Publichenko[21], L. Raux[27], J. P. Repellin[27], T. Roganova[21], G. Romano[31], G. Rosa[29], A. Rubbia[37], V. Ryasny[18], O. Ryazhskaya[18], D. Ryzhikov[26], A. Sadovski[8], C. Sanelli[9], O. Sato[23], Y. Sato[35], V. Saveliev[26], N. Savvinov[5], G. Sazhina[21], A. Schembri[29], W. Schmidt Parzefall[12], H. Schroeder[30], H. U. Schütz[5], L. Scotto Lavina[24], J. Sewing[12], H. Shibuya[10], S. Simone[4], M. Sioli[6], C. Sirignano[31], G. Sirri[6], J. S. Song[13], R. Spaeti[5], M. Spinetti[9], L. Stanco[28], N. Starkov[20], M. Stipcevic[36], P. Strolin[24], V. Sugonyaev[28], S. Takahashi[23], V. Tereschenko[8], F. Terranova[9], I. Tezuka[35], V. Tioukov[24], I. Tikhomirov[19], P. Tolun[1], T. Toshito[23], V. Tsarev[20], R. Tsenov[32], U. Ugolino[24], N. Ushida[14], G. Van Beek[7], V. Verguilov[32], P. Vilain[7], L. Votano[9], J. L. Vuilleumier[25],

T. Waelchli[5], R. Waldi[30], M. Weber[5], G. Wilquet[7], B. Wonsak[12] R. Wurth[30], J. Wurtz[33], V. Yakushev[18], C. S. Yoon[13], Y. Zaitsev[19], I. Zamboni[36] and R. Zimmermann[12].

1. METU-Middle East Technical University, TR-06531 Ankara, Turkey
2. LAPP, Université de Savoie, CNRS/IN2P3, 74941 Annecy-le-Vieux, France
3. Laboratori Nazionali del Gran Sasso dell'INFN, 67010 Assergi (L'Aquila), Italy
4. Dipartimento di Fisica dell'Università di Bari and INFN, 70126 Bari, Italy
5. University of Bern, CH-3012 Bern, Switzerland
6. Dipartimento di Fisica dell'Università di Bologna and INFN, 40127 Bologna, Italy
7. IIHE-Inter-University Institute for High Energies, Université Libre de Bruxelles, B-1050 Brussels, Belgium
8. JINR-Joint Institute for Nuclear Research, 141980 Dubna, Russia
9. Laboratori Nazionali di Frascati dell'INFN, 00044 Frascati (Roma), Italy
10. Toho University, 274-8510 Funabashi, Japan
11. Department of Physics, Technion, 32000 Haifa, Israel
12. Hamburg University, 22043 Hamburg, Germany
13. Gyeongsang National University, 900 Gazwa-dong, Jinju 660-300, Korea
14. Aichi University of Education, 448 Kariya (Aichi-Ken), Japan
15. Kobe University, 657 Kobe, Japan
16. Dipartimento di Fisica dell'Università dell'Aquila and INFN, 67100 L'Aquila, Italy
17. IPNL, Université Claude Bernard Lyon 1, CNRS/IN2P3, 69622 Villeurbanne, France
18. INR-Institute for Nuclear Research of the Russian Academy of Sciences, 117312 Moscow, Russia
19. ITEP-Institute for Theoretical and Experimental Physics, 117259 Moscow, Russia
20. LPI-Lebedev Physical Institute of the Russian Academy of Sciences, 117924 Moscow, Russia
21. SINP MSU-Skobeltsyn Institute of Nuclear Physics of Moscow State University, 119992 Moscow, Russia
22. University of Münster, 48149 Münster, Germany
23. Nagoya University, 464-01 Nagoya, Japan
24. Dipartimento di Fisica dell'Università Federico II di Napoli and INFN, 80125 Napoli, Italy
25. Université de Neuchâtel, CH 2000 Neuchâtel, Switzerland
26. Obninsk State University, Institute of Nuclear Power Engineering, 249020 Obninsk, Russia
27. LAL, Université Paris-Sud 11, CNRS/IN2P3, 91898 Orsay, France
28. Dipartimento di Fisica dell'Università di Padova and INFN, 35131 Padova, Italy
29. Dipartimento di Fisica dell'Università di Roma "La Sapienza" and INFN, 00185 Roma, Italy
30. Fachbereich Physik der Universität Rostock, 18051 Rostock, Germany
31. Dipartimento di Fisica dell'Università di Salerno and INFN, 84084 Fisciano, Salerno, Italy
32. Faculty of Physics, Sofia University "St. Kliment Ohridski", 1000 Sofia, Bulgaria
33. IPHC, Université Louis Pasteur, CNRS/IN2P3, 67037 Strasbourg, France
34. UPNHE-Unité de de Physique Nucléaire et des Hautes Energies, 1060 Tunis, Tunisia
35. Utsunomiya University, 320 Tochigi-Ken, Utsunomiya, Japan
36. IRB-Rudjer Boskovic Institute, 10002 Zagreb, Croatia
37. ETH-Eidgenössische Technische Hochschulen Zürich, CH-8092 Zurich, Switzerland

Abstract

The OPERA neutrino detector is designed to perform the first detection of neutrino oscillations in appearance mode, through the study of $\nu_\mu \to \nu_\tau$ oscillations. The apparatus consists of a lead/emulsion-film target complemented by electronic detectors. It is placed along the high-energy CERN to LNGS beam (CNGS) in Hall C of Gran Sasso Underground Laboratory, 730 km away from the neutrino source. In August 2006 a first run with CNGS neutrinos was successfully conducted. A first sample of neutrino events was collected, statistically consistent with the integrated beam intensity. After a brief description of the beam and of the various sub-detectors, we report on the achievements obtained during 2006, presenting the first data and the status of the detector and the needed infrastructures.

1 Introduction

The solution of the long-standing solar and atmospheric neutrino puzzles has come from the hypothesis of neutrino oscillations. This implies that neutrinos have non vanishing and not degenerate masses, and that their flavor eigenstates involved in weak interaction processes are a superposition of their mass eigenstates.

Several key experiments conducted in the last decades with solar neutrinos, and with atmospheric, reactor and accelerator neutrinos, have contributed to build-up our present understanding of neutrino mixing. Atmospheric neutrino oscillations, in particular, have been studied by the Super-Kamiokande, Kamiokande, MACRO and SOUDAN2 experiments. Long baseline experiments confirmed the oscillation hypothesis with accelerator neutrinos: K2K in Japan and MINOS in the USA. The CHOOZ and Palo Verde reactor experiments excluded the $\nu_\mu \to \nu_e$ channel as the dominant one in the atmospheric sector.

However, the direct appearance of a different neutrino flavor is still an important open issue. Long-baseline accelerator neutrino beams can be used to probe the atmospheric neutrino signal and confirm the preferred solution of $\nu_\mu \to \nu_\tau$ oscillations. In this case, the beam energy should be large enough to produce the heavy τ lepton. This is one of the main goals of the OPERA experiment that uses the long baseline (L=730 km) CNGS neutrino beam from CERN to LNGS. The challenge of the experiment is to measure the appearance of ν_τ from ν_μ oscillations. This requires the detection of the short-lived τ lepton ($c\tau = 87.11$ μm) with high efficiency and low background. The τ is identified by the detection of its characteristic decay topologies, in one prong (electron, muon or hadron) or in three-prongs. The τ track is measured with a large-mass sampling-calorimeter made of 1 mm thick lead plates (absorber material) inter-spaced with thin emulsion films (high-accuracy tracking devices).

The OPERA detector is made of two identical Super Modules each consisting of a target section of about 900 ton made of lead/emulsion-film modules (bricks), of a scintillator tracker detector, needed to pre-localize neutrino interactions within the target, and of a muon spectrometer.

The construction of the CNGS beam has been recently completed and a first run took place in August 2006 with good performance of the facility. First data were collected by the OPERA detector still without bricks installed, yielding a preliminary measurement of the beam features along with the collection of a number of neutrino interactions (319) consistent with the integrated beam intensity of 7.6×10^{17} protons on target (p.o.t.). The OPERA experiment operated very satisfactorily during the run.

2 The CNGS beam and the OPERA experiment

The CNGS neutrino beam was designed and optimized for the study of $\nu_\mu \to \nu_\tau$ oscillations in appearance mode, by maximizing the number of charged current (CC) ν_τ interactions at the LNGS site. A 400 GeV proton beam is extracted from the CERN SPS in 10.5 μs short pulses with design intensity of 2.4×10^{13} p.o.t. per pulse. The proton beam is transported through the transfer line TT41 to the CNGS target T40. The target consists of a series of thin graphite rods. Secondary pions and kaons of positive charge

produced in the target are focused into a parallel beam by a system of two magnetic lenses, called horn and reflector. A 1,000 m long decay-pipe allows the pions and kaons to decay into muon-neutrinos and muons. The remaining hadrons (protons, pions, kaons) are absorbed by an iron beam-dump. The muons are monitored by two sets of detectors downstream of the dump; they measure the muon intensity, the beam profile and its center. Further downstream the muons are absorbed in the rock while neutrinos continue their travel toward Gran Sasso.

The average neutrino energy at the LNGS location is ~ 17 GeV. The $\bar{\nu}_\mu$ contamination is $\sim 4\%$, the ν_e and $\bar{\nu}_e$ contaminations are lower than 1%, while the number of prompt ν_τ from D_s decay is negligible. The average L/E_ν ratio is 43 km/GeV. Due to the earth curvature neutrinos from CERN enter the LNGS halls with an angle of about 3° with respect to the horizontal plane.

Assuming a CNGS beam intensity of 4.5×10^{19} p.o.t. per year and a five year run about 31,000 CC plus neutral current (NC) neutrino events will be collected by OPERA from interactions in the lead-emulsion target. Out of them 95 (214) CC ν_τ interactions are expected for oscillation parameter values $\Delta m^2_{23} = 2 \times 10^{-3}$ eV^2 (3×10^{-3} eV^2) and $\sin^2 2\theta_{23}=1$. Taking into account the overall τ detection efficiency the experiment should gather 10-15 signal events with a background of less than one event.

In the following, we give a brief description of the main components of the OPERA detector.

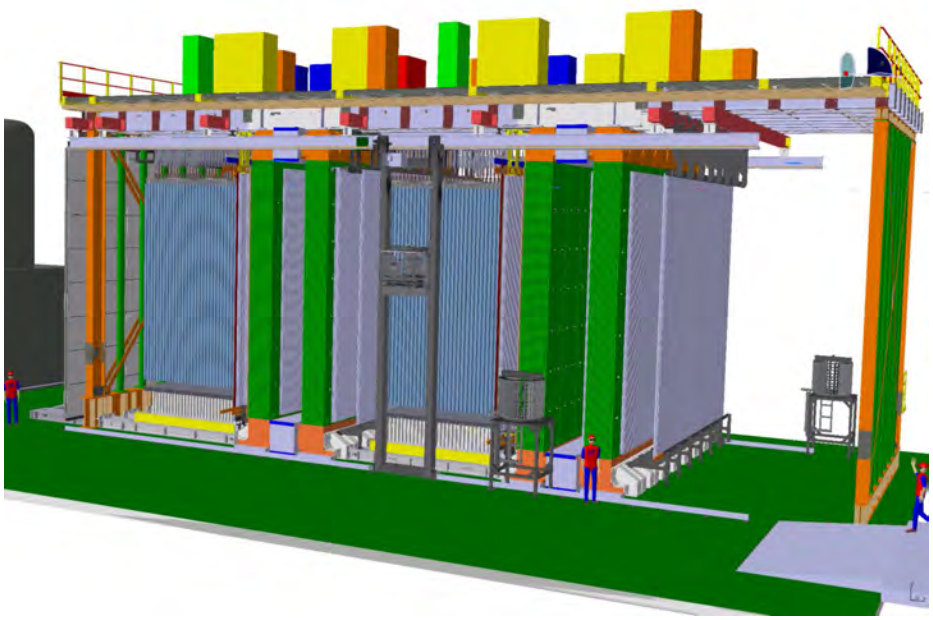

Figure 1: Schematic drawing of the OPERA detector at LNGS.

Each of the two Super Modules (SM1 and SM2) consists of 103,168 lead/emulsion bricks arranged in 31 target planes (Fig. 1), each one followed by two scintillator planes with an effective granularity of 2.6×2.6 cm^2. These planes serve as trigger devices and

allow selecting the brick containing a neutrino interaction. A muon spectrometer at the downstream end of each SM allows to measure the muon charge and momentum. A large size anti-coincidence detector placed in front of SM1 allows to veto (or tag) interactions occurring in the material and in the rock upstream of the target.

The construction of the experiment started in Spring 2003. The first instrumented magnet was completed in May 2004 together with the first half of the target support structure. The second magnet was completed in the beginning of 2005. In Spring 2006 all scintillator planes were installed. The brick production started in October 2006 with the aim of completing the full target for the high-intensity run of 2007.

The run of August 2006 was conducted with electronic detectors only, taking neutrino interactions in the rock upstream of the detector, in the passive material of the mechanical structure and in the iron of the spectrometers. In addition, the information from a tracking plane made of pairs of emulsion films (Changeable Sheets, CS) was used to study the association between emulsion-film segments with tracks reconstructed in the Target Tracker (TT). Fig. 2 shows a photograph of the detector in the underground Hall C of LNGS as it was during the neutrino run.

Figure 2: Photograph of OPERA in the LNGS Hall C.

2.1 The electronic detectors

The construction in Strasbourg and the installation in the LNGS underground laboratory of the OPERA Target Tracker, responsible to indicate the right lead/emulsion brick to extract from the detector target, has finished in May 2006. The commissioning of the detector has continued up to the end of the same year. The Target Tracker is composed by 62 walls, each one associated with one brick wall. Each Target Tracker wall contains four horizontal and for vertical modules defining a sensitive area of about 7x7 m^2. The Target Tracker modules enclose 64 scintillator strips readout by Wave Length Shifting fibers and multianode Hamamatsu photomultipliers. For the whole Target Tracker (496 modules), 992 photomultipliers, 31200 AMCRYS-H scintillator strips and about 300 km Kuraray WLS fiber have been used. During the first data taking period in August and October, the Target Tracker was fully operational. A big number of cosmic rays has been recorded since the end of the Target Tracker installation. These cosmic rays are used for alignment testing and m.i.p. detection efficiency evaluation. It has been verified that the Target Tracker detection efficiency was higher than 98%, as expected by the calibration tests done during the module construction

Muon identification and charge measurement are needed for the study of the muonic τ-decay channel and for the suppression of the background from the decay of charmed particles, featuring the same topology. Each muon spectrometer consists of a bipolar magnet made of two iron arms for a total weight of 990 ton. The measured magnetic field intensity is 1.52 T. The OPERA magnets have been commissioned in spring 2006 and were fully operative during the first CNGS run. In February, the power supplies of the magnets were delivered at Gran Sasso after completion of tests at firm. They were subsequently installed in the top platform of the experiment and connected to the driving coils by means of flexible cables. The magnets have been switched on for the first time in March using a temporary cooling system. During the physics run, Magnet 1 was operated very smoothly (100% lifetime) while several power interruptions were observed in Magnet 2. The problem was traced to the power supply regulator and has been solved by the supplier in September 2006. The two arms of magnets are interleaved with vertical, 8 m long drift-tube planes (PT) for the precise measurement of the muon-track bending. Planes of Resistive Plates Chambers (RPC's) are inserted between the iron plates of the arms, providing a coarse tracking inside the magnet, range measurement of the stopping particles and a calorimetric analysis of hadrons.

In order to measure the muon momenta and determine their sign with high accuracy, the Precision Tracker (PT) is built of thin walled aluminum tubes with 38 mm outer diameter and 8 m length. Each of the $\sim$ 10,000 tubes has a central sense wire of 45 μm diameter. They can provide a spatial resolution better than 300 μm. Each spectrometer is equipped with six fourfold layers of tubes. By end of December 2006, 82% (162 modules) of the total PT were produced, wired and successfully tested in Hamburg. The wire tension, the dark current and the leakage rate are within the specifications. 130 of the produced modules are already installed in the OPERA detector, named planes HPT 1 to 8. Thus the complete 1st and 1/3 of the 2nd spectrometer have been mechanically installed and successfully tested.

All electronics components of the PT are produced and successfully tested. Further-

more, half of the HV boards, the preamp boards, the support boards, the trigger boards and the TDCs are installed and successfully operated in SM1.

The slow control for the PT, using a new industrial standard system of the company Beckhoff, is developed, some improvements are ongoing. The gas system is ready for SM 1 and SM 2. The first two stations (SM1) are successfully operated since august 2006. The commissioning of the installed planes is ongoing. All the electronics components of PT were successfully operated. Since November the new developed trigger system was installed and commissioned. For each SM three independent trigger stations are installed to identify muons from beam neutrinos but also to be sensitive to stopping muons from beam and cosmic rays. The overall alignment of HPT 1 to 6, using the new reference system, was better than 500 μm, which is within the requirement. During the commissioning phase several data were taken and analyzed. The reached resolution is better than 500 μm. This value will be improved by including all alignment results.

RPC's identify penetrating muons and measure their charge and momentum in an independent way with respect to the PT. They consist of electrode plates made of 2 mm thick plastic laminate of high resistivity painted with graphite. Induced pulses are collected on two pickup strip planes made of copper strips glued on plastic foils placed on each side of the detector. The number of individual RPC's is 924 for a total detector area of 3,080 m^2. The total number of digital channels is about 25,000, one for each of the 2.6 cm (vertical) and 3.5 cm (horizontal) wide strips.

In order to solve ambiguities in the track spatial-reconstruction each of the two drift-tube planes of the PT upstream of the dipole magnet is complemented by an RPC plane with two 42.6° crossed strip-layers called XPC's. RPC's and XPC's give a precise timing signal to the PT's.

Finally, a detector made of glass RPC's is placed in front of the first Super Module, acting as a veto system for interactions occurring in the upstream rock. The veto detector was not yet operational for the August 2006 run but was installed later in 2006.

OPERA has a low data rate from events due to neutrino interactions well localized in time, in correlation with the CNGS beam spill. The synchronization with the spill is done offline via GPS. The detector remains sensitive during the inter-spill time and runs in a trigger-less mode. Events detected out of the beam spill (cosmic-ray muons, background from environmental radioactivity, dark counts) are used for monitoring. The global DAQ is built as a standard Ethernet network whose 1,147 nodes are the Ethernet Controller Mezzanines plugged on controller boards interfaced to each sub-detector specific front-end electronics. A general 10 ns clock synchronized with the local GPS is distributed to all mezzanines in order to insert a time stamp to each data block. The event building is performed by sorting individual subdetector data by their time stamps.

2.2 Emulsion films, bricks and related facilities

An R&D collaboration between the Fuji Company and the Nagoya group allowed the large scale production of the emulsion films needed for the experiment (more than 12 million individual films) fulfilling the requirements of uniformity of response and of production, time stability, sensitivity, schedule and cost. The main peculiarity of the emulsion films used in high energy physics compared to normal photographic films is the relatively large

thickness of the sensitive layers ($\sim$ 44 μm) placed on both sides of a 205 μm thick plastic base.

A target brick consists of 56 lead plates of 1 mm thickness and 57 emulsion films. The plate material is a lead alloy with a small calcium content to improve its mechanical properties. The transverse dimensions of a brick are 12.7 $\times$ 10.2 cm^2 and the thickness along the beam direction is 7.5 cm (about 10 radiation lengths). The bricks are housed in support structures placed between consecutive TT walls.

In order to reduce the emulsion scanning load the use of Changeable Sheets, successfully applied in the CERN CHORUS experiment, was extended to OPERA. CS doublets are attached to the downstream face of each brick and can be removed without opening the brick. Charged particles from a neutrino interaction in the brick cross the CS and produce a trigger in the TT scintillators. Following this trigger the brick is extracted and the CS developed underground and analyzed in the scanning facility at LNGS (Fig. 3). The information of the CS is used for a precise prediction of the position of the tracks in the most downstream films of the brick, hence guiding the so-called scan-back vertex-finding procedure.

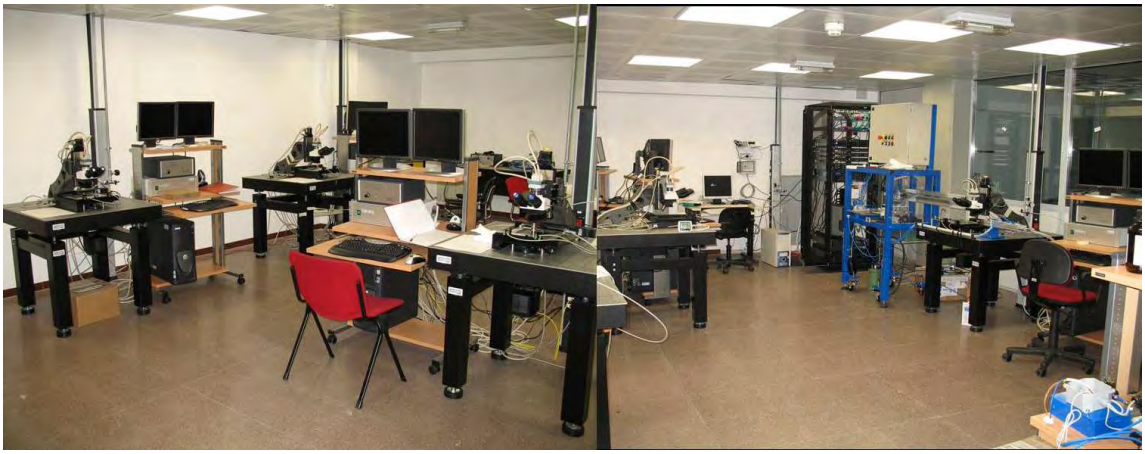

Figure 3: The OPERA Scanning Station in the outside Laboratory. During 2006 the installation of 6 microscopes with computer control, has been completed. The microscopes will be mainly used for the scanning of the changeable sheets to look for tracks of charged particles validating the occurrence of a neutrino interaction in the corresponding brick.

The hit brick finding is one of the most critical operations for the success of the experiment, since one aims at high efficiency and purity in detecting the brick containing the neutrino interaction vertex. This requires the combination of adequate precision of the TT, precise extrapolation and high track finding efficiency in the CS scanning procedure. During the neutrino run of August 2006 a successful test of the whole procedure was performed by using an emulsion detector plane consisting of a matrix of 15 $\times$ 20 individual CS doublets with overall transverse dimensions of 158 $\times$ 256 cm^2 inserted in one of the SM2 target planes.

The construction of more than 200,000 bricks for the neutrino target is accomplished by an automatic machine, the Brick Assembly Machine (BAM) operating underground in

order to minimize the number of background tracks from cosmic-rays and environmental radiation.The BAM has been mounted during 2006 in a specially constructed site in the underground laboratory and has started the brick production (Fig. 4). Two Brick Manipulating Systems (BMS) have been mounted during last year on both lateral sides of the detector. They will fill the target walls with the bricks produced by the BAM, position the bricks in the target walls and also extract those bricks containing neutrino interactions during runs. BMS commissioning has started in 2006 (around 4000 bricks have been inserted up to February 2007).

Figure 4: The piling/pressing station of the Brick Assembly Machine (BAM) in the underground laboratory. It consists of 6 anthropomorphic robots which have to assembly the bricks alternating emulsion and PB sheets. The final brick production rate should reach the value of 1000 bricks/day.

While running the experiment, after the analysis of their CS doublets, bricks with neutrino events are brought to the LNGS external laboratory, exposed for several hours to cosmic-ray muons for film alignment and then disassembled. The films are developed with an automatic system in parallel processing chains. In 2006 the large Laboratory for emulsion plate development, was arranged close to its final shape, and the first real-case bricks extracted after the CNGS pilot runs were successfully processed therein.

The Laboratory, designed to be hosted in the new building recently open to users at the surface LNGS site, is at close internal path from the Cosmic ray exposure pit (40 cm Fe shielding). Apart from complementary equipment, it includes: 1) A Chemical Plant with large-scale equipment for filtering, thermal control and demineralization of large volumes of water, as a solvent of chemicals and for final plate washing; large volume tanks for numerically controlled preparation of the chemicals needed for the emulsion development and fixation; intermediate tanks and pipelines to service the development lines; differentiated collection and exhaustion of wasted solutions out to large external tanks. 2) An Automated development system, hosted in large safelight darkrooms, with

Figure 5: Partial view of the emulsion development laboratory realized during 2006 in the new LAB1 building. Three of six computer controlled chains of development are shown in the picture and are already working, the other three are in completion phase.

six independent lines, running in parallel, (see Fig. 5) with a sequence of automatically refilled and step-timed tanks, locally controlled by PLCs.

The expected number of bricks extracted per running-day with the full target installed and CNGS nominal intensity is about 30. The large emulsion surface to be scanned requires fast automatic microscopes continuously running at a speed of $\sim$ 20 cm^2 film surface per hour. This requirement has been met after R&D studies conducted using two different approaches by some of the European groups of the Collaboration and by the Japanese groups.

3 The 2006 runs with CNGS neutrinos

The first shot of the extracted proton beam onto the CNGS target was made on 11 July. A low intensity run with neutrinos took then place from 18 to 30 August 2006 with a total integrated intensity of 7.6×10^{17} p.o.t.. The beam had been active for a time equivalent to about 5 days. The low intensity was partly due to the chosen SPS cycle and to the intensity of the spill that was 55% of the nominal value during the first part of the run and 70% during the second part.

The GPS clock used to synchronize the CERN accelerators and OPERA had been fine-tuned before the start of data-taking. At CERN the current pulse of the kicker magnet used for the beam extraction from the SPS to the TT41 line was time-tagged by a GPS unit with absolute time (UTC) calibration. An analogous GPS at the LNGS site provided the UTC timing signal to OPERA. The resulting accuracy in the time synchronization between CERN and OPERA timing systems was better than 100 ns. However, during the first days of the run a time offset of 100 μs was observed due to problems in adjusting

the time tagging of the kicker pulse. This offset was eventually reduced to 600 ns.

The OPERA detector started collecting neutrino interactions from the very first beam spills with nearly all electronic detectors successfully operating. Altogether, 319 neutrino events, with an estimated 5% systematic uncertainty, were taken by OPERA during the August run. This is consistent with the 300 expected events for the given integrated intensity of 7.6×10^{17} p.o.t.. The analysis of the CNGS data conducted at CERN and the comparison with simulations is in progress. Once completed, we expect to reach a 20% systematic error on the prediction of the number of muon events from neutrino interactions in the rock. This error is due to uncertainties in the neutrino flux prediction, in the cross-section and in the muon transport in the rock.

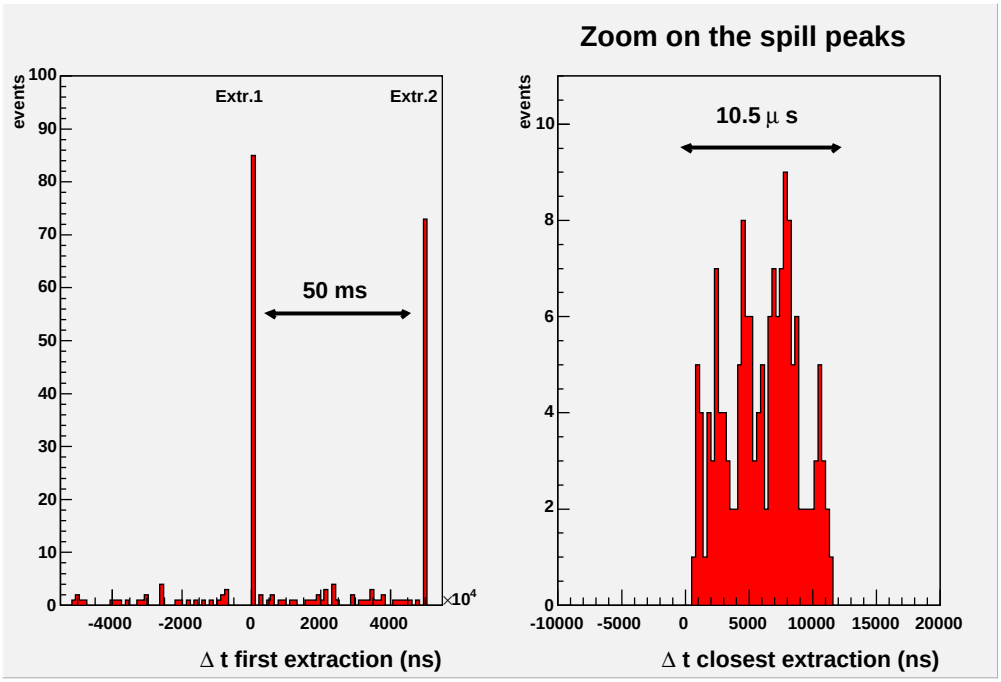

Figure 6: Time distribution of events collected in the neutrino run. The event time difference with respect to the closest extraction is shown in the right histogram.

The event analysis was performed in two ways. In the first one the event timing information was treated as a basic selection tool, since the time window of beam events is well sized in a 10.5 μs interval, while the uniform cosmic-ray background corresponded to 10^{-4} of the collected statistics (Fig. 6). The second analysis dealt with the reconstruction of track-like events disregarding timing information. Neutrino events are classified as: 1) CC neutrino interactions in the rock upstream of the detector or in the material present in the hall leading to a penetrating muon track (Fig. 7, top-left); 2) CC and NC neutrino interactions in the target material (Fig. 7, top-right and bottom-right) and CC interactions in the iron of the spectrometers (Fig. 7, bottom-left).

The θ angular distribution with respect to the horizontal axis obtained by selecting single-track events is shown in Fig. 8. Events were selected with a minimum number of 6 layers of fired RPC's in each spectrometer. In the same Figure, the distribution of

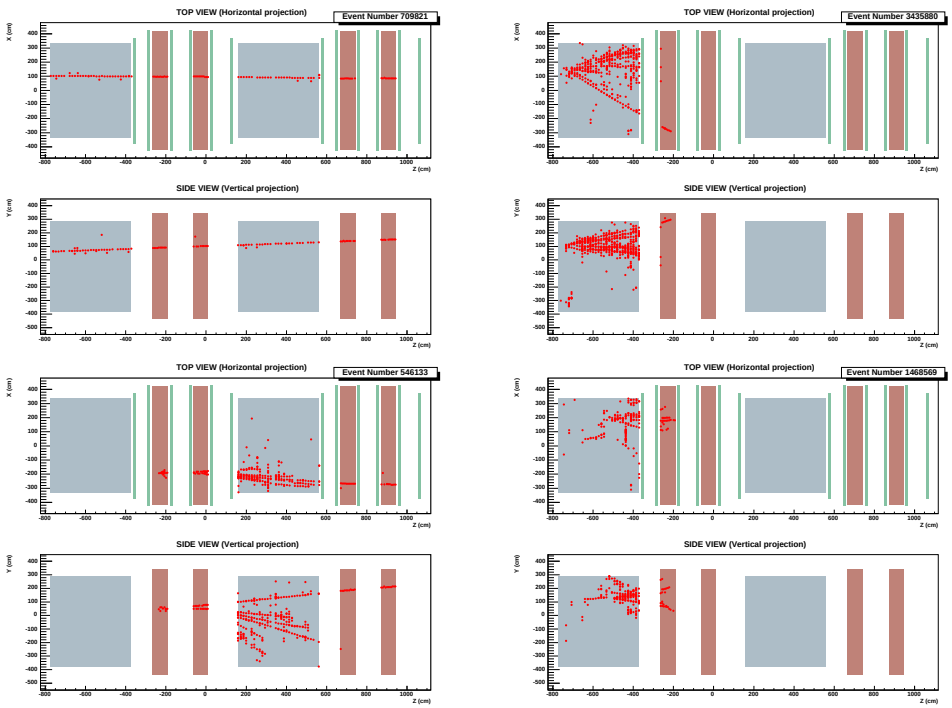

Figure 7: Display of neutrino events from the CNGS run. For each event the top and side views are shown, respectively. The SM targets are indicated in blue, the spectrometers in light brown, TT and RPC hits in red. See the text for event classification.

simulated cosmic-ray muons is also shown. The comparison between experimental data and Monte Carlo events proved the beam-induced nature of the muons in the peak around the horizontal direction. By counting events selected with topological criteria we found $\sim 10\%$ of the events corresponding to beam spill data missing in the CERN database. A Gaussian fit to the θ angle of the events on-time with the beam (shown in the inset of Fig. 8) yielded a mean muon angle of $3.4 \pm 0.3^{\circ}$ in agreement with the value of 3.3° expected for neutrinos originating from CERN and traveling under the earth surface to the LNGS underground halls. The systematic error on θ was evaluated to be 3% by applying different track reconstruction models.

Concerning the analysis of the CS detector, 9 muons produced by neutrino interactions in the rock surrounding the detector crossed the CS plane surface. 5 muon tracks predicted by the electronic detectors were found by scanning the emulsion films. The reasons of inefficiency can be traced-back to the tight cuts applied in this preliminary analysis and in the significant decrease of the fiducial volume. In fact, the dead space between adjacent emulsion films was $\sim 10\%$ and the scanning was only performed up to 3 mm from the film edge, bringing the overall dead space to $\sim 20\%$. However, the test proved the capability in passing from the centimeter scale of the electronic tracker resolution to the micrometric resolution of nuclear emulsions. The angular difference between predicted and found tracks is better than 10 mrad, largely dominated by the electronic detector resolution. Fig. 9 shows the display of one of the 6 reconstructed events.

In October two weeks of CNGS beam were foreseen. The expected integrated intensity

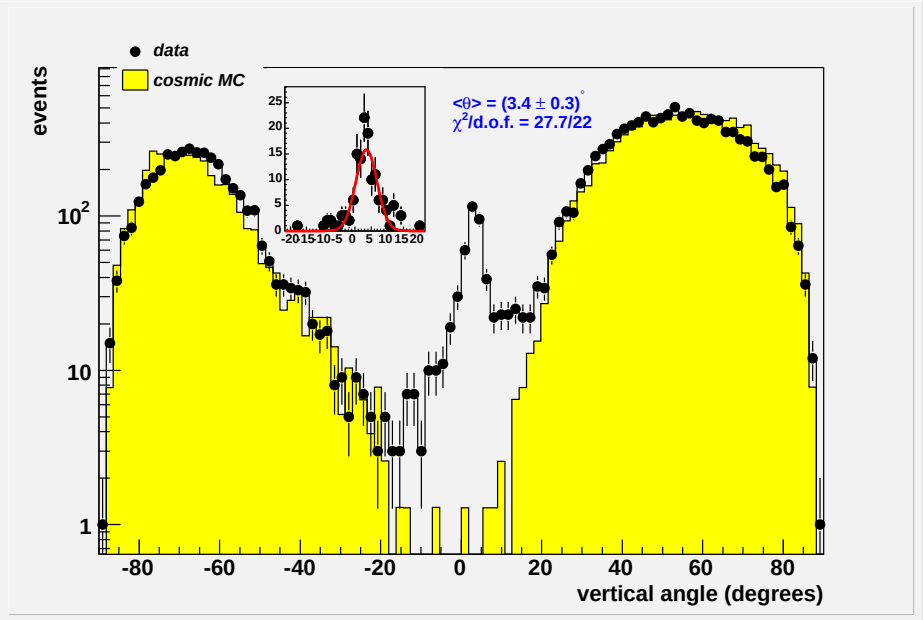

Figure 8: Angular distribution of beam-induced and cosmic-muon events taken with the electronic detectors (black points). The histogram indicates the predictions from cosmic-ray simulations. The inset shows the angular distribution of on-time beam events.

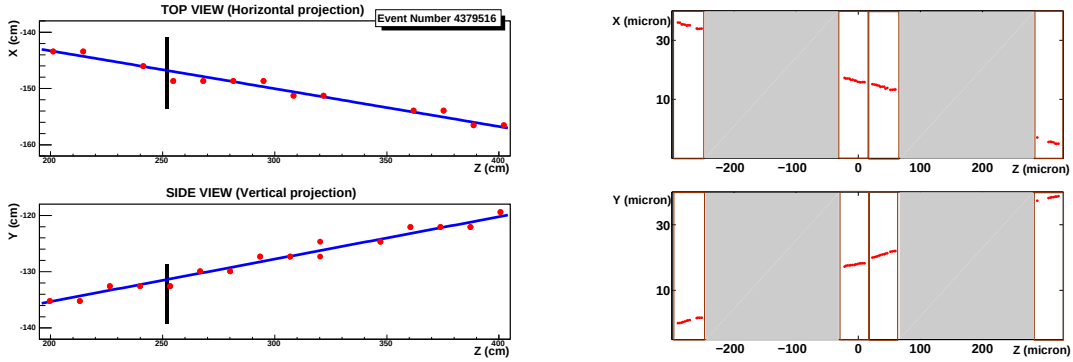

Figure 9: Left: display of one event with the muon passing through the CS detector plane. Only hits of the electronic detectors close to the CS plane are shown; the vertical segment indicates the position of the CS doublet intercepted by the track. Right: display of the corresponding 4 micro-tracks reconstructed in the CS doublet.

was around 1.6×10^{18} p.o.t. with a SPS supercycle containing three short CNGS cycles similar to the single cycle of the August run. After some hours the SPS was successfully brought to operate in the new timing configuration, but unfortunately the run lasted only 25 hours. The beam had to be suspended because of a serious water leak which occurred in the cooling system of the reflector downstream of the beryllium target. The failure could not be directly inspected and repaired because of the high local radiation. It will be repaired at the beginning of 2007 before the next CNGS run foreseen in Summer 2007. The total integrated beam intensity collected in this short run was very low and only 19

beam events were collected, mainly corresponding to CC interaction in the rock. In this run the OPERA target was containing around 1000 bricks but only one rock muon passed through one of those bricks. This event has been reconstructed both in the changeable sheets and in the brick. In the meantime the Brick assembling Machine is being finally commissioned to reach a brick production speed near to the design value (1000 bricks/day) in order fill all the detector target within one year.

List of Publications

1. T. Nakamura *et al.*, "The Opera Film: New Nuclear Emulsion For Large-Scale, High-Precision Experiments," Nucl. Instrum. Meth. A **556**, 80 (2006).

2. R. Zimmermann *et al.*, "The precision tracker of the OPERA detector," Nucl. Instrum. Meth. A **555**, 435 (2005) [Erratum-ibid. A **557**, 690 (2006)].

3. V. Tyukov, I. Kreslo, Y. Petukhov and G. Sirri, "The FEDRA Framework for emulsion data reconstruction and analysis in the OPERA experiment," Nucl. Instrum. Meth. A **559**, 103 (2006).

4. L. Arrabito *et al.*, "Hardware performance of a scanning system for high speed analysis of nuclear emulsions," Nucl. Instrum. Meth. A **568** (2006) 578 [arXiv:physics/0604043].

5. R. Acquafredda *et al.*, "First events from the CNGS neutrino beam detected in the OPERA experiment," New J. Phys. **8** (2006) 303 [arXiv:hep-ex/0611023].

THEORY GROUP

Members of the group: R. Aloisio, Z. Berezhiani, V. Berezinsky, V. Caracciolo, P. Ciarcelluti, M.L. Costantini, G. Di Carlo, A. Grillo, E. Luzio, F. Nesti, L. Pilo, N. Rossi, A.S. Sakharov, F. Vissani.

The activity of research is organized in the four working groups FA51, GS51, PI12, PI21 that are generically denoted as IS (from "Iniziative Specifiche") and concerned four main areas: astroparticle physics (mainly FA51), phenomenology of Planck scale (GS51), computer simulations of gauge theories (PI12), particle physics phenomenology (mainly PI21), also in collaboration with experimental groups. The activities of the theory group for 2006 are described below.

1 Astroparticle Physics (FA51)

The Astroparticle Physics group of LNGS in 2006 included R. Aloisio, V. Berezinsky, M.L. Costantini, F. Vissani and visitors V. Dokuchaev (Institute for Nuclear Research, Moscow), Yu. Eroshenko (Institute for Nuclear Research, Moscow), B. Hnatyk (Lviv University, Ukraine), S. Grigorieva (Institute for Nuclear Research, Moscow) and A. Gazizov (Stepanov Institute of Physics, Minsk, Belarus). The group worked in close collaboration with A. Vilenkin (Tufts University, USA), M. Kachelrieß (MPI, Munich), P. Blasi (Arcetri Observatory, Firenze), G. Senjanović (ICTP, Trieste), A. Strumia (Pisa University) and others.

Scientific work

The main field of the work is astroparticle physics, including neutrino oscillations, massive neutrinos, ultra high energy cosmic rays, and high energy neutrino and gamma astrophysics. We work also in particle physics, including the fermion masses in supersymetric and non-supersymmetric SO(10).

Conferences, seminars and other activities

R.Aloisio works as the scientific secretary of the LNGS scientific committee.

R.Aloisio works (together with C.Cattadori) as the organizer of the LNGS general seminars.

R.Alosio presented two invited talks at "Workshop on Exotic Physics with Neutrino Telescopes", Uppsala, Sweden, September 2006 and at "6th Rencontre du Vietnam, Challenges in Particles Astrophysics", Hanoi, Vietnam, August 2006.

V.Berezinsky works as an editor of Int. Journal "Astroparticle Physics".

V.Berezinsky presented three invited talks at 13th Lomonosov Conference (Moscow), Astroparticle conference (Daijon, Korea) and COSPAR meeting (Beijing, China) and gave lectures at IDAPP school in Ferrara.

V.Berezinsky worked as the member of Int. Advisory Committee of Neutrino -2006 Conference (USA).

F.Vissani gave lectures on neutrino oscillations and extensions of the standard model at the University of L'Aquila, in the PhD courses in Catania (LNS) and Milano.

F. Vissani presented four invited talks at the "International Workshop on Cryogenic Liquid Detectors for Future Particle Physics" (March, Gran Sasso), at "Vulcano Workshop 2006: Frontier Objects in Astrophysics and Particle Physics" (May, Vulcano-ME), at "LHC days in Split" (October, Split) and at the "CHIPP Workshop on neutrino physics" (October, Bern).

Journal, proceedings and preprints in 2006

[1] R. Aloisio, V. Berezinsky, M. Kachelriess
ON THE STATUS OF SUPERHEAVY DARK MATTER
Phys.Rev. D74 (2006) 023516 (astro-ph/0604311).

[2] R. Aloisio, V. Berezinsky, P. Blasi, A. Gazizov, S. Grigorieva, B. Hnatyk
A DIP IN THE UHECR SPECTRUM AND THE TRANSITION FROM GALACTIC TO EXTRAGALACTIC COSMIC RAYS.
Astropart.Phys. 27 (2007) 76 (astro-ph/0608219).

[3] R. Aloisio
TRANSITION FROM GALACTIC TO EXTRA-GALACTIC COSMIC RAYS
J.Phys.Conf.Ser. 39 (2006) 416.

[4] V. Berezinsky
DIP IN UHECR AND TRANSITION FROM GALACTIC TO EXTRA-GALACTIC COSMIC RAYS
Proceedings of Yamada Conference 2006.

[5] V. Berezinsky, V. Dokuchaev, Y. Eroshenko
DESTRUCTION OF SMALL-SCALE DARK MATTER CLUMPS IN THE HIERARCHICAL STRUCTURES AND GALAXIES
Phys.Rev. D73 (2006) 063504.

[6] V. Berezinsky, A. Z. Gazizov
DIFFUSION OF COSMIC RAYS IN EXPANDING UNIVERSE. (I)
Astrophys.J. 643 (2006) 8.

[7] V. Berezinsky, A. Gazizov, M. Kachelrieß
SECOND DIP AS A SIGNATURE OF ULTRAHIGH ENERGY PROTON INTERACTIONS WITH COSMIC MICROWAVE BACKGROUND RADIATION
Phys.Rev.Lett. 97 (2006) 231101.

[8] V. Berezinsky, V. Dokuchaev, Y. Eroshenko
ANISOTROPY OF DARK MATTER ANNIHILATION WITH RESPECT TO THE GALACTIC PLANE
astro-ph/0612733.

[9] F. Vissani
NEUTRINOS FROM SUPERNOVA REMNANTS AFTER THE FIRST H.E.S.S. OBSERVATIONS
astro-ph/0609575.

[10] N.Yu.Agafonova *et al.* (F.Vissani)
STUDY OF THE EFFECT OF NEUTRINO OSCILLATIONS ON THE SUPERNOVA NEUTRINO SIGNAL IN THE LVD DETECTOR
hep-ph/0609305.

[11] M.L. Costantini, A. Ianni, G. Pagliaroli, F. Vissani
IS THERE A PROBLEM WITH LOW ENERGY SN1987A NEUTRINOS?
astro-ph/0608399.

[12] F. Vissani
NEUTRINOS FROM GALACTIC SOURCES OF COSMIC RAYS WITH KNOWN γ-RAY SPECTRA.
Astropart.Phys.26:310-313,2006.

[13] NEUTRINO MASSES AND MIXINGS AND...
A. Strumia, F. Vissani
Review regularly updated on web, hep-ph/0606054.

[14] B. Bajc, A. Melfo, G. Senjanovic, F. Vissani
FERMION MASS RELATIONS IN A SUPERSYMMETRIC SO(10) THEORY
AIP Conf.Proc.805:152-157,2006.

[15] G. Battistoni, A. Ferrari, C. Rubbia, P.R. Sala, F. Vissani
ATMOSPHERIC NEUTRINOS IN A LARGE LIQUID ARGON DETECTOR
hep-ph/0604182.

[16] B. Bajc, A. Melfo, G. Senjanovic, F. Vissani
FERMION MASS RELATIONS AND THE STRUCTURE OF THE LIGHT HIGGS IN A SUPERSYMMETRIC SO(10) THEORY
Phys.Lett.B634:272-277,2006.

[17] B. Bajc, A. Melfo, G. Senjanovic, F. Vissani
YUKAWA SECTOR IN NON-SUPERSYMMETRIC RENORMALIZABLE SO(10)
Phys.Rev. D73 (2006) 055001.

2 Phenomenology of Planck Scale (GS51)

The members of the Phenomenology of Planck Scale (GS51) are R. Aloisio, A. Grillo (national coordinator of GS51) and E. Luzio, and they worked in

close collaboration with the TS node of GS51–in particular with S. Liberati (SISSA)–and with F. Mendez (Santiago University), formerly postdoc fellow in Gran Sasso and now professor at Santiago University, Chile.

The description of this activity follows:

Since a few years it emerged the realization that it is conceivable that effects of Planck scale physics,generally believed to follow from Quantum Gravity, could be phenomenologically testable. Moreover, although a Quantum Gravity theory is still far from being formulated and there are in fact several approaches to it, there are indications that a non trivial space-time structure will be relevant nearby the Planck scale. This structure could lead to phenomena which will be therefore characteristic of quantum gravity. Some of the proposed ideas are: loss of quantum coherence or state collapse, QG imprint on initial cosmological perturbations, extra dimensions and low-scale QG, deviations from Newton's law, black holes produced in colliders,and Planck-scale deviations from classical spacetime symmetries, such as CPT and Lorentz invariance (LI).

This research initiative aims to clarify the theoretical framework of these testable effects of Planck scale physics, focusing primarily on the issues relevant for the fate of classical symmetries at the Planck scale, and at the same time to explore all the opportunities that planned astrophysics observatories and cosmology studies may provide for testing/falsifying such Planck-scale effects.

The Gran Sasso section of GS51 has continued a systematic approach to Double Special Relativity in Space-Time. Although the Formulation of DSR in momentum space is satisfactory, the real phenomenological consequences cannot be fully discussed without a space-time (which is where experiments are performed) formulation. This formulation has to emerge if any as a semiclassical limit of Quantum Gravity, and there are some interesting indications in this sense. In 2005-2006 we have continued and extended the collaboration with the TS group, in particular S. Liberati and with F. Mendez on the interpretation of DSR's as a measurement problem. It has been shown that this connection is in fact emerging, at least with simplifiyng hypoteses, from the necessary averaging of QG fluctuations done in interpreting properties of semiclassical (from QG point of view) particles.

Journal, proceedings and preprints in 2006

[1] R. Aloisio, A.Galante, A.F. Grillo, S.Liberati, E. Luzio, F.Mendez
DEFORMED SPECIAL RELATIVITY AS AN EFFECTIVE THEORY OF MEASUREMENTS ON QUANTUM GRAVITATIONAL BACKGROUNDS
Phys.Rev. D73 (2006) 04520

[2] R. Aloisio, A.Galante, A.F. Grillo, S.Liberati, E. Luzio, F.Mendez
MODIFIED SPECIAL RELATIVITY ON A FLUCTUATING SPACETIME
Phys.Rev. D74 (2006) 085017

3 Computer Simulations of Gauge Theories (PI12)

The members of the Computer Simulations of Gauge Theories group (PI12) are Giuseppe Di Carlo and Angelo Galante, and worked in close collaboration with Vicente Azcoiti, Eduardo Follana, Victor Laliena (University of Zaragoza), with partial support of INFN-MEC agreement. Our activity during 2006 mainly regarded:

Non-zero baryon density QCD We have introduced a new variant of the well known Hasenfraz-Karsch action that allows some step forward toward the determination of the critical line in the Temperature-Baryon density plane. A study in three dimensional Gross-Neveu model and a detailed analysis of 4 Flavours QCD has produced exciting results. We have further developed our methodology with the inclusion of a reweighting technique that allows us to perform safer extrapolations toward the physical point; a completely new set of simulation data for the 4 flavour model has been produced and the analysis is in progress.

Models with θ-term in the action Using the methods we have introduced in the last years continue this study with the simulation of other models

with topological terms, in particular CP^N and SU(2) gauge. Our recent interest has been focused on the CP^1 model; our analysis shows the existence of a line of second order phase transition points at $\theta = \pi$ for intermediate coupling constant β, with critical exponents varying continuously along the line.

Results

A study of the deconfining phase transition of 4 Flavours QCD, extended in the Temperature-Chemical potential plane up to values of the quark chemical potential as large as 270 MeV, has been carried out; the resulting paper that reports on the above results has been published in Nucl. Phys. B. The analysis of the data for the reweighting procedure is on the way.

The analysis of the phase structure of the CP^1 model has been completed and a paper entitled "Critical Behavior of CP^1 at $\theta = \pi$, Haldane's Conjecture and the Universality Class" has been submitted for publication.

4 Particle Physics Phenomenology (PI21)

The activity of the group, which included Z. Berezhiani, P. Ciarcelluti, F. Nesti, L. Pilo and N. Rossi, was mainly devoted to different problems of particle phenomenology and its applications to astrophysics and cosmology.

The following results can be mentioned.

Z. Berezhiani and F. Nesti suggested a supersymmetric $SO(10)$ model with a flavour symmetry $SU(3)$. The mass matrices of all fermion types (up and down quarks, charged leptons and neutrinos) appear in the form of combinations of three symmetric rank-1 matrices common for all types of fermions, with different coefficients that are successive powers of small parameters related to each-other by $SO(10)$ symmetry properties. The model perfectly describes the mass and mixing patterns for the quarks and leptons, dangerous D=5 operators for the proton decay are naturally suppressed and flavour-changing supersymmetric effects are under control.

Z. Berezhiani in collaboration with P. Chankowski, A. Falkowski and S. Pokorski (Warsaw) suggested a mechanism for the Higgs potential stability against the "little hierarchy" problem. In this model the potential of the

MSSM Higgs doublets is doubly protected: by supersymmetry and by an accidental global symmetry, as far as the Higgses appear as pseudo-Goldstone modes of the spontaneoulsy broken extra global symmetry.

Z. Berezhiani in collaboration with L. Bento (Lisbon) discussed the phenomenological implications of the neutron (n) oscillation into the mirror neutron (n'), a hypothetical particle from a parallel mirror world, exactly degenerate in mass with the neutron but sterile to normal matter. It was shown that the present experimental data allow a maximal $n - n'$ oscillation in vacuum with a characteristic time τ much shorter than the neutron lifetime, in fact as small as 1 sec, which corresponds to a mass mixing $\delta m = \tau^{-1} \sim 10^{-15}$ eV between n and n' states. This phenomenon may manifest in neutron disappearance and regeneration experiments perfectly accessible to present experimental capabilities and may also have interesting astrophysical consequences, in particular it could help the propagation of ultra high energy cosmic rays at cosmological distances without substantial energy loses.

Participation in conferences and schools

Z. Berezhiani participated 2nd Int. Conf. on 'The Dark Side of the Universe' DSU 2006, Madrid, Spain, 20-22 June 2006: invited talk "Marriage between the baryonic and dark matters"

Z. Berezhiani participated Int. Conf. 'CFNUL 30 Years', Lisbon, Portrugal, 23-25 June 2006: invited talk "On the origin of observable matter, dark matter and ultra high energy cosmic rays"

Z. Berezhiani, F. Nesti, L. Pilo and N. Rossi participated 1st Galileo Institute 'New Directions Beyond the Standard Model in Field and String Theory', Florence, Italy, 1 May - 30 June 2006: Z. Berezhiani has delivered a seminar on "Parallel mirror sector"

F. Nesti participated 14th Int. Seminar on High Energy Physics "Quarks 2006", St. Petersburg, Russia, 19-25 May 2006: invited talk "Fermion masses at intermetiate tanbeta: unification of Yukawa determinants"

Z. Berezhiani, F. Nesti, L. Pilo and N. Rossi participated in organization of 11th Gran Sasso Summer Institute "Frontiers in Astroparticle Physics", Assergi, Italy, 11-28 July 2006: lectures of Z. Berezhiani "Mirror World: ori-

gin of visible/dark matter" and F. Nesti "Supersymmetric chance for proton decay" were delivered

Z. Berezhiani, F. Nesti, L. Pilo and P. Ciarcelluti participated 2nd Galileo Institute 'Astroparticle and Cosmology', Florence, Italy, 28 Aug. - 30 Sept. 2006: Z. Berezhiani has delivered a seminar on "Origin of the baryon and dark matter components in the universe"

Journal, proceedings and preprints in 2006

[1] Z. Berezhiani, P.H. Chankowski, A. Falkowski, S. Pokorski,
DOUBLE PROTECTION OF THE HIGGS POTENTIAL IN A SUPERSYMMETRIC LITTLE HIGGS MODEL
Phys. Rev. Lett. **96**, 031801 (2006).

[2] Z. Berezhiani, L. Bento,
NEUTRON - MIRROR NEUTRON OSCILLATIONS: HOW FAST MIGHT THEY BE?
Phys. Rev. Lett. **96**, 081801 (2006).

[3] Z. Berezhiani, L. Bento,
FAST NEUTRON - MIRROR NEUTRON OSCILLATION AND ULTRA HIGH ENERGY COSMIC RAYS
Phys. Lett. **B 635**, 253-259 (2006).

[4] Z. Berezhiani, F. Nesti,
SUPERSYMMETRIC SO(10) FOR FERMION MASSES AND MIXINGS: RANK-1 STRUCTURES OF FLAVOR
JHEP **0603**, 041 (2006).

[5] Z. Berezhiani, F. Nesti, L. Pilo
SOFT SUSY BREAKING CONTRIBUTIONS TO PROTON DECAY
JHEP **0610**, 030 (2006).

[6] Z. Berezhiani, S. Cassisi, P. Ciarcelluti, A. Pietrinferni,
EVOLUTIONARY AND STRUCTURAL PROPERTIES OF MIRROR STAR MACHOS
Astropart. Phys. **24**, 495-510 (2006).

[7] A. Drago, G. Pagliara, Z. Berezhiani
SHORT GRAVITATIONAL WAVE BURSTS INDUCED BY R-MODE SPIN-DOWN OF HYBRID STARS
Astron. & Astrophys. **445**, 1053-1060 (2006).

[8] Z. Berezhiani,
MARRIAGE BETWEEN THE BARYONIC AND DARK MATTERS
hep-ph/0612371; AIP Conf. Proc. **878**, 195-204 (2006).

[9] F. Nesti,
FERMION MASSES AT INTERMEDIATE TANβ: UNIFICATION OF YUKAWA DETERMINANTS,
hep-ph/0610307

The WArP Programme

R. Acciarri[f], B. Baibussinov[g], M. Baldo-Ceolin[g], P. Benetti[a], F. Calaprice[d], E. Calligarich[a], M. Cambiaghi[a], F. Carbonara[b], F. Cavanna[f], S. Centro[g], A.G. Cocco[b], F. Di Pompeo[f], G. Fiorillo[b], C. Galbiati[d], V. Gallo[b], L. Grandi[a], A. Ianni[c], G. Mangano[b], G. Meng[g], C. Montanari[a], O. Palamara[c], L. Pandola[c], F. Pietropaolo[g], G.L. Raselli[a], M. Rossella[a], C. Rubbia[a], A.M. Szelc[e], S. Ventura[g] and C. Vignoli[a]

[a] Dipartimento di Fisica Nucleare e Teorica, INFN and University of Pavia, Italy
[b] Dipartimento di Scienze Fisiche, INFN and University Federico II, Napoli, Italy
[c] Laboratori Nazionali del Gran Sasso dellINFN, Assergi (AQ), Italy
[d] Department of Physics, Princeton University, Princeton, New Jersey, USA
[e] Instytut Fizyki Jadrowej PAN, Krakow, Poland
[f] Dipartimento di Fisica, INFN and University of LAquila, Italy
[g] Dipartimento di Fisica, INFN and University of Padova, Italy
(WArP Collaboration)

Abstract

The WArP programme in LNGS is summarized together with the most recent achievements. The short and long term planning is discussed in view of the WIMP search theoretical predictions.

1 General considerations.

There is very strong evidence that a large fraction of the matter in the Universe is dark and that galaxies are immersed in a dark halo, which out-weights the visible component. The nature of Dark Matter is one of the fundamental puzzles in astrophysics today. From astrophysical considerations we know that the density of matter is $\Omega_m = 0.27 \pm 0.04$. Non-baryonic Dark Matter (NBDM) must be present, since the gravitational density is apparently much larger than the contribution from the Big Bang Nucleo-Synthesis, $\Omega_b = 0.044 \pm 0.004$. The existence of Dark matter can be considered as a confirmed result because of its gravitational effects. The open question is its presence of an electroweak coupling to ordinary matter, which would permit the direct observation on Earth of such a missing component of cosmic matter.

The search for SUSY particles is one of the most central problems of LHC and an almost necessity in elementary particle physics. The fact that such particles can also account for the cold NBDM is either a big coincidence or a big hint. In the context of such minimal SUSY models, the Lightest Super Symmetric (LSP) particle is supposed to be stable because of the so called R-symmetry. It could then be a neutral Majorana fermion of mass $M > 20 GeV/c^2$, the experimental lower limit from LEP.

A major effort is under way in order to produce such particles with LHC at CERN. If SUSY is discovered in the future, in order to have cosmological relevance, at least one neutral particle must be sufficiently stable to be cosmologically active today. Therefore a corresponding, parallel effort should be pursued by non accelerator experiments, in order to detect them directly in Nature, also in view of the fact that their abundance in the Universe should be such as to account for about one order of magnitude more mass than ordinary matter!

A direct detection of the existence of relic WIMP in an underground laboratory may rely on the observation of the tiny recoils produced in ordinary matter by the elastic scattering reaction on target nuclei with the subsequent recoiling nucleus, mediated by weak interactions (neutrino-like). Evidently the specific signature of these events as recorded by the detector must be such as to isolate nuclear recoil events from the much more abundant background due to natural radioactivity and other cosmic ray and solar neutrino events. Since Ω_{DM} is known, the number of particles can be roughly estimated once the mass of the elementary particle is given. For instance, for a mass of $100 GeV/c^2$, the flux on earth is about $10^6 p/cm^2/s$, about six orders of magnitude smaller than the one of solar neutrinos.

It must be noted, however, that any sufficiently heavy relic particle will behave as CDM and a host of more exotic possibilities have been suggested. Hypothetical WIMPs, whether SUSY or otherwise, could be crossing Earth with galactic velocity of the order of $\beta \approx 10^{-3}$, presumably with an approximately Maxwellian distribution, eventually truncated at the escape velocity from the Galaxy.

This very small, neutrino like, interaction cross section makes WIMP-nucleus scattering a very rare event. Just like the case of SUSY at LHC, such a rate is not easily predicted, since it depends on many variables which are poorly defined like for instance: the halo model, the nature of the WIMP (cross section), their survival probability from the Big Bang (related to R-violation), the features of the nuclear target (atomic number, spin...),

and so on. In practice, uncertainties may encompass many orders of magnitude, although the minimal SUSY leaves open the optimistic possibility of very significant rates. For instance the present limits of WIMP detection of several experiments, including WARP, are already mapping some segments of the SUSY plot that LHC is planning to explore.

Recent measurements of the g - 2 of the muon suggest an upper limit for the LSP mass $M < 800 GeV/c^2$ at a 2σ confidence level. Therefore it may be possible that even the lowest laying SUSY / LSP remains undetectable at the LHC. Instead, in the case of relic events, the differential energy spectrum of nuclear recoils from elastic WIMP reaction, neglecting nuclear form factors, is generally expected to be a smoothly decreasing exponential function of the recoil kinetic energy. The simple kinematics of the elastic scattering of WIMPs on (much lighter) target nuclei implies that the average kinetic energy of the nuclear recoils is proportional to the WIMP kinetic energy. *More specifically, the recoils average speed is about twice the galactic speed of the WIMP, independently of the WIMP mass. Therefore, in contrast to LHC experiments, there is no strict kinematical limit to the mass of the WIMP, provided it maintains, as expected, galactic speeds.*

In order to estimate the range of values for an hypothetical SUSY/WIMP cross sections, we report in Figure 1 a recent paper with predictions for CMSSM by R. Trotta et al. (astro-ph/0609126). Any definitive search must reach an ultimate sensitivity that is several orders of magnitudes higher than the one of the presently published results. To achieve such a goal, both sensitive mass and background discrimination should be incremented by many orders of magnitude. This is the reason of the conceptual advances and technological developments we have been concentrating over the last decades and the creation of a new line of dark matter detectors based on noble cryogenic liquids.

2 The WArP experimental programme.

The most sensitive searches for massive WIMP have been traditionally performed with the help of cryogenic detectors in the milli-K range (EDELWEISS, CDMS, etc.). An alternative technology based on noble liquids (Xe, Ar +) at much more conventional temperatures has been developed originally by us as a spin-off of the ICARUS programmes.

Both technologies are capable of an apriori comparable WIMP counting rate for a given active mass and recoil threshold. The interest in using pure noble liquids at standard temperature ($90K$ for liquid Argon) is that larger active masses, ultimately of many tons, can be easily instrumented.

Our pioneering work in the nineties developed both in Pavia and at CERN was based on the concept of liquid Xenon, with the simultaneous detection of scintillation and ionization signals from the heavy ionizing elastic recoils from WIMP at an appropriate threshold of about $20 \div 30 keV$.

Later on, we have replaced Xenon with Argon for many reasons, the most relevant being the very high discrimination power between e/γ signals and elastic recoils generated both by hypothetical WIMP and/or by neutron recoils (acting as strongly interacting WIMP). *Presently the remarkable e/γ rejection limit of one part in 10^{-8} has been attained,* and we are confident that it might be even further improved. These developments have now evolved into the WARP programme (Wimp Argon programme), intended to actually

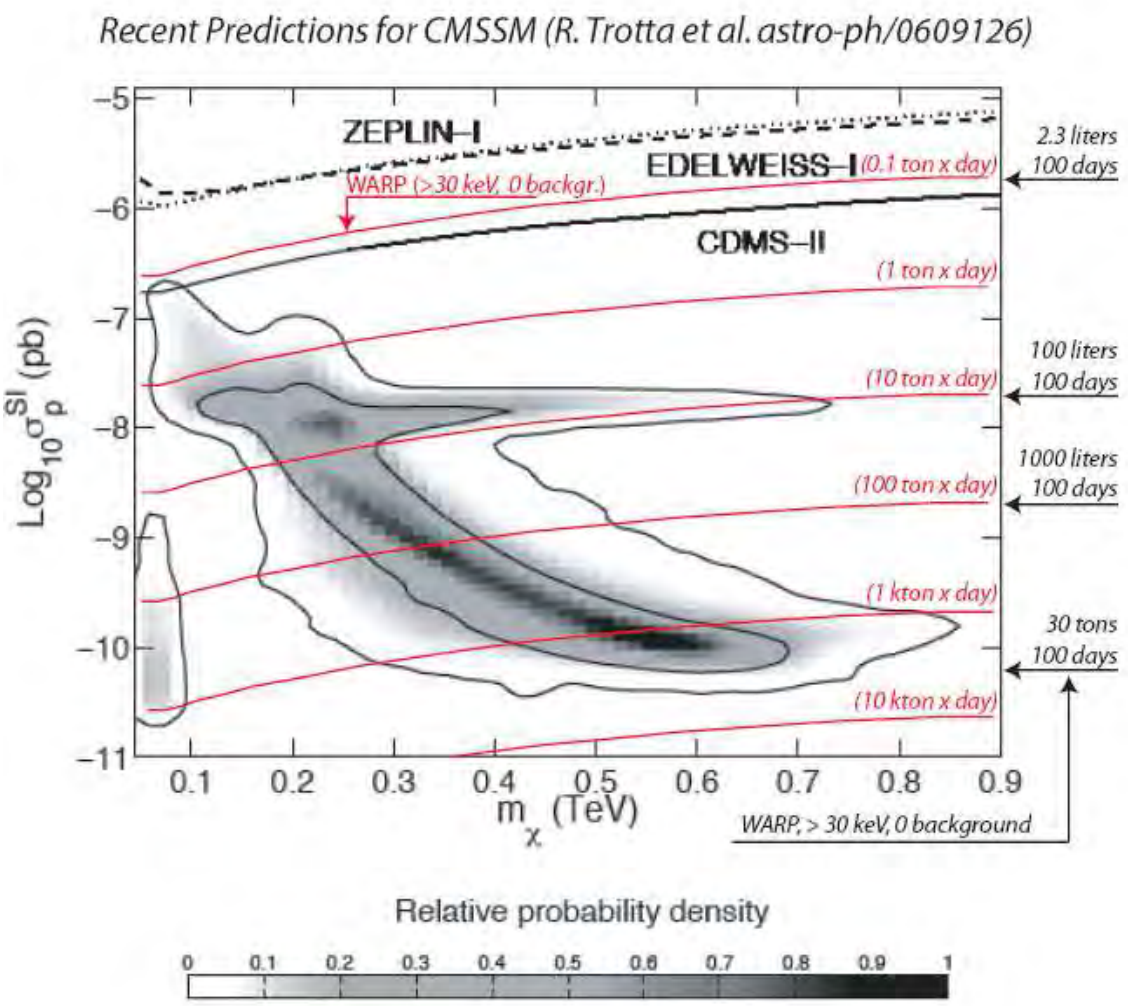

Figure 1: The 2-dimensional probability density in the neutralino mass and spin independent cross section plane in the CMSSM with the contours containing 68% and 95% probability also marked. Current 90% experimental upper limits are also shown. A large fraction of the high probability region lies just below current constraints and it will be probed by the next generation of dark matter searches.

search for Cold Dark Matter in the form WIMP's at the LNGS.

The cryogenic noble liquid detector, such as Argon, unlike an ordinary scintillator, permits the simultaneous detection of both ionisation and scintillation. These particles may produce via weak interactions nuclear recoils in the energy range $20 - 80keV$.

When a particle interacts in the liquid region excitation and ionization occur: *the ratio of primary scintillation over secondary ionization signal and the shape of the primary scintillation depend on the kind of particle producing excitation and ionization.* The detector consists on a double phase (liquid with above gas) cryogenic container in which both the primary scintillation light and the drifted electron signal, also converted into light by a multiplying grid, are recorded. Three simultaneous criteria are used to discriminate potential WIMP recoils from e/γ backgrounds:

1. Simultaneous detection of prompt scintillation and drift time-delayed ionisation in Liquid Argon: pulse height ratio strongly dependent from columnar recombination of ionizing track.

2. Pulse shape discrimination of primary scintillation: wide separation in rise times between fast ($\approx 10ns$) and slow ($\approx 1.6\mu s$) components of the emitted UV light.

3. Precise 3D reconstruction of the event position: additional rejection of multiple neutron recoils and gamma background.

The programme at the LNGS consists of 4 phases which are fully approved and funded and a 5th phase under consideration:

1. A small (2.3 l) bi-phase chamber tested first in Pavia and since 2004 at LNGS, firstly without and later with passive neutron shield. In this phase, ordinary Argon has been deliberately used with a high background rate, which has permitted to explore the very high rejection rates in a relatively short time. A paper with the details of the method has been submitted to Astroparticle Physics (preprint in astro-ph/0701286). An early limit on WIMP has been given, comparable to the one of EDELWEISS.

2. A main background, due to the ^{39}Ar natural contamination[1] will be strongly reduced ($\approx 1/100$) with the help of isotopic purification of Argon. This should improve the sensitivity in the (2.3 l) bi-phase chamber by about an order of magnitude, bringing the level to the CDMS result. Commercial amounts of depleted Ar have been produced by a commercial manufacturer and data taking with the 2.3 l chamber is expected to start in March 2007.

3. A new, larger detector with a 100 l bi-phase chamber is under construction and it will be operational at LNGS by summer 2007. The main new features are: (a) localization of the centroid of the ionization signal, permitting the three dimensional location of the event to better than 1 cm; (b) a large, 4π active, hermetic anticoincidence ($\approx 8ton$ of LAr) to further reduce the presence of neutrons and γ.

[1] A paper will appear soon on NIM A with a recent measurement of the ^{39}Ar activity in natural argon made by us with the 2.3 l chamber in LNGS (preprint in astro-ph/0603131).

4. The sensitive volume of the detector may be later extended to $1ton$ with minor modifications, which will keep the main setup unchanged, including the outer active anticoincidence, depending on the background level attained during phase 3.

5. An even greater sensitive volume, of the order of $> 10tons$ is presently under consideration. However, such a large extrapolation from the present detectors at this stage is still strongly dependent on the progress associated to phases 3 and 4.

In conclusion :

- Liquid Argon at 89 K has been proven to be a unique target for WIMP searches, because of its high sensitivity to signals and its superior background rejection capabilities.

- Many years of effort have firmly established this new technology, now being implemented underground in the WARP 100lt detector.

- Identification of e/γ signals and of elastic atomic recoils at unprecedented levels, established with the 2.3-liter prototype programme, intentionally designed as high background detector.

- The 140-kg detector, ready by summer 2007, will bring a further upgrade on light yield. Background will be further minimized. We expect a big step in sensitivity for WIMP Dark Matter Searches.

- Mass upgrade to $1ton$ as soon as possible, an implicit next step.

LAr is a mature technology, ultimately capable of very massive detectors with a relatively low cost (see ICARUS present experience with a $600ton$ detector). A very large ultimate detector with $> 30tons$ could be readily constructed at the LNGS. It is already at the level of conceptual design, the main open question to be perfected in phases 2-4 being a background rejection sufficient to separate out the potential signal. Such a large sensitive mass is necessary in order to cover the entire set of options predicted by SUSY/WIMP. We believe that at the present state of the art, cryogenic detectors are the most suited for such very large masses.

The experiment is funded, by INFN (LNGS, lAquila, Napoli, Padova and Pavia), by NSF (Princeton) and by the Polish Academy of Sciences (Krakow).

A relatively small but very active team is presently sufficient in order to realize the detector of a few hundred liters. But a wider international collaboration is welcome to extend the activities in phases 4 and 5.

The XENON10 Dark Matter Experiment

J. Angle[a], E. Aprile[b,*], F. Arneodo[c], L. Baudis[d], A. Bernstein[e], A. Bolozdynya[f], L. Coelho[g], C.E. Dahl[h], L. DeViveiros[i], A. Ferella[c], L. Fernandes[g], S. Fiorucci[i], R.J. Gaitskell[i], K.L. Giboni[b], R. Gomez[j], R. Hasty[k], L. Kastens[k], J. Kwong[h], J.A.M. Lopes[g], N. Madden[e], A. Manalaysay[a], A. Manzur[k], D. McKinsey[k], M.E. Monzani[b], K. Ni[k], U. Oberlack[j], J. Orboeck[d], G. Plante[b], R. Santorelli[b], J. Santos[g], P. Shagin[j], T. Shutt[f], P. Sorensen[i], S. Schulte[d], C. Winant[e] and M. Yamashita[b]

[a] Department of Physics, University of Florida, Gainesville, FL 32611, USA
[b] Department of Physics, Columbia University, New York, NY 10027, USA
[c] Gran Sasso National Laboratory, Assergi, L'Aquila, 67010, Italy
[d] Department of Physics, RWTH Aachen University, Aachen, 52074, Germany
[e] Lawrence Livermore National Laboratory, 7000 East Ave., Livermore, CA 94550, USA
[f] Department of Physics, Case Western Reserve University, Cleveland, OH 44106, USA
[g] Department of Physics, University of Coimbra, R. Larga, 3004-516, Coimbra, Portugal
[h] Department of Physics, Princeton University, Prineton, NJ 08544, USA
[i] Department of Physics, Brown University, Providence, RI 02912, USA
[j] Department of Physics, Rice University, Houston, TX 77251, USA
[k] Department of Physics, Yale University, New Haven, CT 06511, USA

[*] Spokesperson

Abstract

XENON10 is a new direct dark matter detection experiment using liquid Xenon as target for weakly interacting, massive particles (WIMPs). A dual-phase (liquid/gas) time projection chamber with 15 kg fiducial mass has been installed in the Gran Sasso Underground Laboratory in March 2006. The detector was moved in its final location, inside a low-background shield, in July 2006. After initial performance tests with various calibration sources, the science data run started on August 24, 2006. The detector has been running stably since then, and a full analysis of approximately 100 live days of WIMP search data is now in progress.

1 Introduction

The goal of XENON [1] is to search for interactions of massive, cold dark matter particles in liquid xenon. The motivation of this search comes from our current understanding of the universe. Over the last ten years, a variety of cosmological observations, from the primordial abundance of light elements, to the study of large scale structure, to the observations of high redshift supernovae, to the detailed mapping of anisotropy of the cosmic microwave background, have led to the construction of a so-called concordance model of cosmology. In this model, the universe is made of $\sim$4% baryons which constitute the ordinary matter, $\sim$23% nonbaryonic dark matter and $\sim$73% dark energy [2]. Understanding the nature of dark matter poses a significant challenge to astrophysics. The solution may involve new particles with masses and cross sections characteristic of the electroweak scale. Such Weakly Interactive Massive Particles (WIMPs), which would have been in thermal equilibrium with quarks and leptons in the hot early universe and decoupled when they were non-relativistic, represent a generic class of dark matter candidates [3, 4]. If WIMPs are the dark matter, their density in the Milky Way halo may allow them to be detected in laboratory experiments by looking for the nuclear recoils produced in elastic WIMPnuclei collisions [5]. A WIMP with a typical mass between 10 GeV and 10 TeV will deposit a nuclear recoil energy below 100 keV in a terrestrial detector. The expected rates are determined by the WIMP-nucleus cross section and by their density and velocity distribution in the vicinity of the solar system [4]. Direct-detection experiments, in particular CDMS II [6, 7], CRESST [8], EDELWEISS [9], ZEPLIN II [10] and WARP [11], are beginning to significantly constrain the WIMP-nucleon scattering cross section and, for the first time, start to probe the parameter space which is predicted by supersymmetric extensions to the Standard Model (recent reviews can be found in [12, 13, 14]). While it is clear that cryogenic experiments such as CDMS are still leading the field, detectors based on liquid noble elements (Ar, Xe) are rapidly evolving and are already catching up in sensitivity. Liquid argon (LAr) and xenon (LXe) have excellent properties as dark matter targets. They are intrinsic scintillators, with high scintillation (λ = 128 nm for Ar, λ = 175 nm for Xe) and ionization yields. They are available in large quantities (with LAr being much cheaper) and can be purified to 1 ppt (part per trillion)-levels. Scintillation in LAr and LXe is produced by the formation of excimer states, which are bound states of ion-atom systems. If a high electric field ($\sim$1 kV/cm) is applied, ionization electrons can also be detected, either directly or through the secondary process of proportional scintillation. Measuring both the primary scintillation signal and a secondary process yields a method of discriminating between electron and nuclear recoils. In LAr, an additional differentiation, namely the time difference between the decay of the singlet and triplet excited states (6 ns versus 1.6 μs) is being used. An advantage of LXe is its high density (3 g/cm^3), which provides self-shielding and allows for compact detectors, and the high atomic number (Z=54, A=131.3), which is favorable for scalar WIMP-nucleus interactions. Moreover, since natural Xe has two isotopes with spin (^{129}Xe,^{131}Xe, at the combined level of almost 50% abundance), a liquid Xenon detector is susceptible for both coherent and axial-vector WIMP-nucleus couplings.

2 The XENON10 Experiment

XENON10 is a new direct dark matter search experiment with the aim of observing the small energy released after a WIMP scatters off a xenon nucleus [1]. The simultaneous detection of ionization and scintillation in a liquid xenon (LXe) 3D position sensitive time projection chamber (TPC) allows to distinguish nuclear recoils (as produced by WIMPs and neutrons) from the dominant electron recoil background (as originated from photon and electron interactions) [15, 16]. The detector has been transported from the Nevis Laboratory at Columbia University to Gran Sasso in March 2006 and has been installed in its low-background shield in mid July 2006. It has been taking data continuously and very stably since then, with a total approximately 100 live days of WIMP search data accumulated.

2.1 Main results from the XENON R&D activity

The R&D for the XENON experiment started in September 2002. Using a variety of prototypes from a few hundred grams to several kg, the collaboration has carried out many measurements from which we have learnt a great deal about the physics of LXe irradiated by electrons and Xe ions of energy as low as a few keV.

The two most important accomplishments from the R&D program are the measurements of the scintillation efficiency and charge yield for low energy Xe recoils, shown in figure 1. The scintillation efficiency for nuclear recoils (NR) in the low energy range of interest to a dark matter search was measured for the first time using a small detector with very high light collection provided by two Hamamatsu compact PMTs immersed in the liquid. The detector, built by Columbia, was exposed to MeV neutrons, using the Van der Graff available at Nevis Lab. A separate detector, operated in dual phase, was subsequently designed and built for a measurement of the ionization yield of Xe recoils produced by an AmBe neutron source. The ionization yield, defined as the ratio of charge (S2) and light (S1), shown in figure 1 (right) versus recoil energy, quantifies the capability of LXe to differentiate NR from electron recoils (ER), down to 10 keVr. The same measurement was performed at CWRU, with a similar detector. The two measurements agree on the large charge yield of nuclear recoils in LXe and the weak field dependence. The CWRU group has continued to optimize the small detector, achieving lower energy threshold and better resolution [17]. The data from these small prototypes (with no position sensitivity) point to a rejection power of 99% for 50% NR acceptance, less than what was originally assumed for LXe. These results are now published [15, 16].

2.2 The XENON10 Detector

XENON10 is a dual phase time projection chamber (TPC) filled with 22 kg of ultra pure LXe. The active volume is defined by a Teflon cylinder with an inner diameter of 20 cm and a height of 15 cm for a total active mass of 15 kg of LXe. The TPC is equipped with four wire meshes, two in the liquid and two in the gas. The bottom mesh serves as cathode and the next one, positioned just below the liquid level, together with a series of field shaping rings, form the 15 cm drift region. The two last meshes, together with the

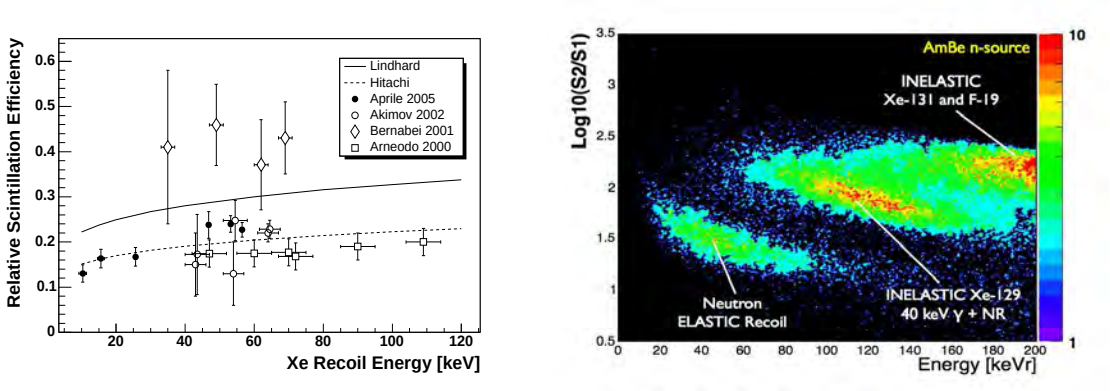

Figure 1: (left) Scintillation efficiency for low energy nuclear recoils relative to that of gamma rays. (right) Ionization yield vs recoil energy, measured in the Columbia dual phase detector irradiated with an AmBe neutron source.

one below the liquid level, serve to define the gas proportional scintillation region.

Custom-made cylindrical capacitors are installed to monitor the liquid level. The active volume is viewed by 89 Hamamatsu R8520-06-Al 1" square PMTs. The bottom array of 41 PMTs is located below the cathode, fully immersed in LXe, to detect the direct scintillation light. The ionization electrons produced in the liquid are drifted towards the liquid surface by the 1 kV/cm electric field (a custom HV feedthrough provides the HV to the cathode) and extracted into the gas phase where they emit proportional scintillation light. Simulations have guided the optimization of the electrostatic fields in the liquid and gas regions. The 48 PMTs of the top array, in the gas, are used to detect this proportional signal.

Images of the top and bottom PMT arrays are shown in figure 2: the top array is assembled in the "diving bell" which was designed to keep the liquid level constant. The

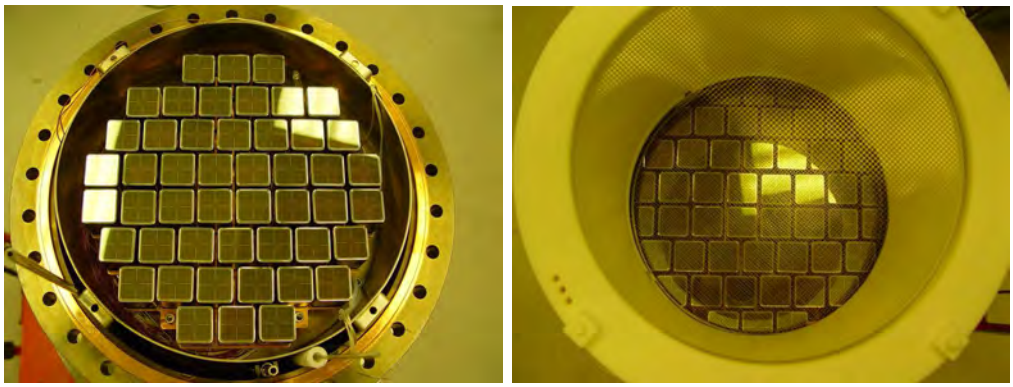

Figure 2: (left) The top PMT array and (right) the bottom PMT array: the meshes and the Teflon cylinder are clearly visible.

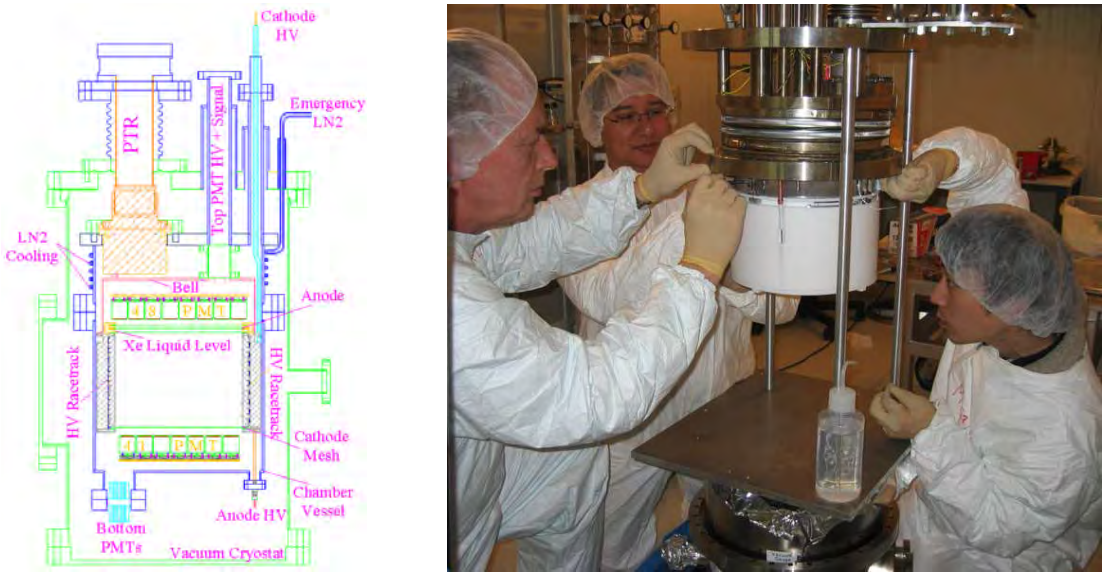

Figure 3: (left) Schematics of he XENON10 TPC and (right) work on the detector assembly at LNGS (March 2006).

Teflon/metal HV feedthrough and the level meter are also visible. The HV bases, attached to the PMTs, are built on a Cirlex substrate with surface mount components. A typical low energy gamma event detected by XENON10 PMTs is shown in figure 4 (right). The time separation between two pulses of direct and proportional light, (maximum 75 μs determined by the 15 cm drift and the 2mm/μs electron drift velocity) provides the event depth of interaction in the liquid (or z-coordinate). The XENON10 electronics readout is based on 100 MHz FADCs.

The Pulse Tube Refrigerator (PTR) used in XENON10 has been pivotal for the success of this detector. The unit, especially designed for LXe temperature, is mounted on the cryostat top flange, directly in contact with the Xe gas. The 90 W maximum cooling power delivered to the detector is PID controlled. It is sufficient to liquefy the xenon gas during filling and to maintain the liquid temperature. With this system we have been able to achieve the level of long term stability and reliability required for a dark matter experiment. Figure 4 (left) shows the remarkably stable pressure ($\Delta P < 0.006$ atm) and temperature ($\Delta T < 0.005$°C) values of XENON10 as monitored by the Slow Control System for over three months. Under such stable conditions the fluctuation of PMT gains is $< 2\%$.

High purity of the LXe is an essential requirement for a TPC like XENON10, with a drift over 15 cm. The purity must be preserved at all time during the detector operation in order to ensure stable performance. We have fulfilled this requirement by continuous gas circulation through a high temperature getter. The electron lifetime inferred from recent data is (1.8 ± 0.4) ms, corresponding to $\ll 1$ ppb (O_2 equivalent) purity.

The detector is contained in a low-background shield, featuring 20 cm of lead (Pb) and 20 cm of Polyethylene. The design with inner Pb to suppress the gamma background

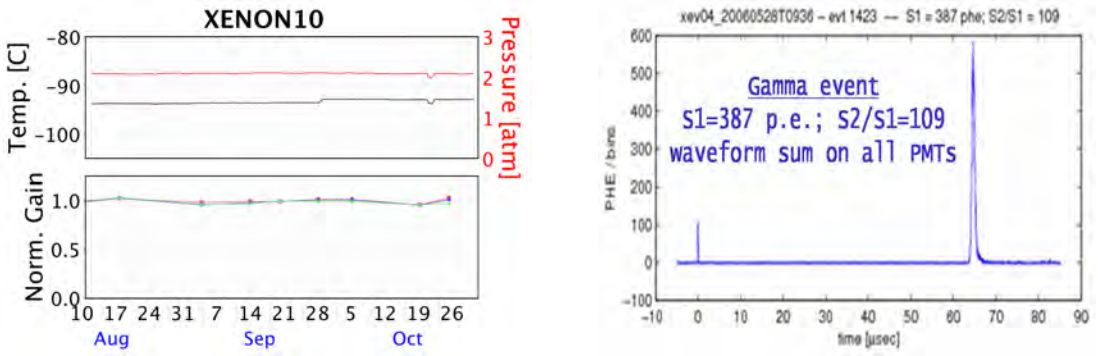

Figure 4: (left) XENON10 detector's pressure, temperature and PMT gains during operation; (right) total waveform for a typical gamma event

and outer PE to moderates the neutrons, was optimized with MonteCarlos. Substantial contributions to the design and installation of the shield were provided by the LNGS engineering service. The heavy structure (1.6 tons of PE and 34 tons of Pb) is fixed in place on 5 sides. One side slides sideways on rails carrying a section of the shielding materials and the detector with it. The shield construction was completed by the middle of July 2006 and the detector with all its subsystems were moved in the final location assigned to XENON at LNGS.

Figure 5: The XENON10 lead/poly shield, before (left) and after (right) the detector installation.

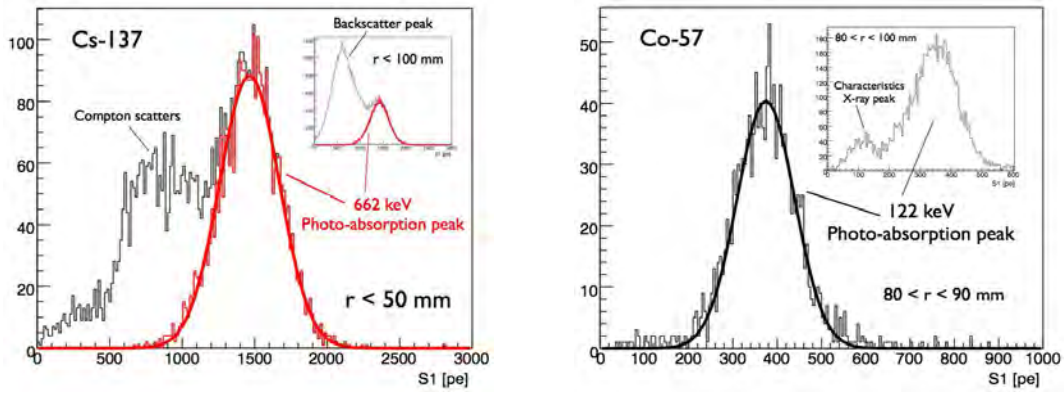

Figure 6: (left) S1 scintillation spectrum from a ^{137}Cs calibration. The light yield for the 662 keV photo-absorption peak is 2.2 p.e./keV. (right) S1 scintillation spectrum from a ^{57}Co calibration. The light yield for the 122 keV photo-absorption peak is 3.1 p.e./keV.

2.3 Calibration of the XENON10 detector

The XENON10 detector underwent an extensive calibration program, based on the use of gamma (^{57}Co, ^{137}Cs) and neutron (AmBe) calibration sources, as well as neutron-activated Xenon (^{131m}Xe,^{129m}Xe). To achieve a minimum impact on WIMP search exposure time, the passive lead and polyethylene shields were designed to allow insertion of external, encapsulated sources without exposing the detector cavity to outside, radon-contaminated air.

The light yield in XENON10 depends on event energy and position. Measurement of this yield has been carried out with gamma sources. As shown in figure 6 (left), in the bulk region ($r < 5$ cm), the 662 keV photo-absorption peak of ^{137}Cs gives an average light yield of 1464 photo-electrons (2.2 p.e./keV) and a sigma of 205 p.e. (14%). The light yield does not change substantially (less than 5%) for $r < 9$ cm. Figure 6 (right) shows a scintillation light spectrum from a ^{57}Co calibration, after drift time corrections. For r between 8 and 9 cm, the average light yield for 122 keV gamma rays is 374 p.e. (3.1 p.e./keV), with a resolution of 17% (σ). The higher light yield from the 122 keV gamma rays is partly due to the different electron-ion recombination contributions for different energy gamma rays in LXe [18]. The inset in figure 4 shows the characteristic X-ray peak due to K-shell electrons (30 keV). While the 122 keV gamma rays interacting in the LXe outside of the Teflon are easily absorbed in this region, the 30 keV X-rays enter into the detector's sensitive volume and can be used to monitor the stability of the detector's light yield over time.

On December 1, 2006, the XENON10 detector was calibrated with an encapsulated AmBe neutron source with an activity of 200 neutrons/s. Such a calibration allows to determine the predicted WIMP signal region as well as the detectors ability to distinguish between nuclear and electron recoils down to its energy threshold. The energy threshold was determined to be at ~10 keV nuclear recoil energy (keVr) with a light yield of 0.7 photo-electrons/keVr. In figure 7 (left) we show a data versus Monte Carlo comparison

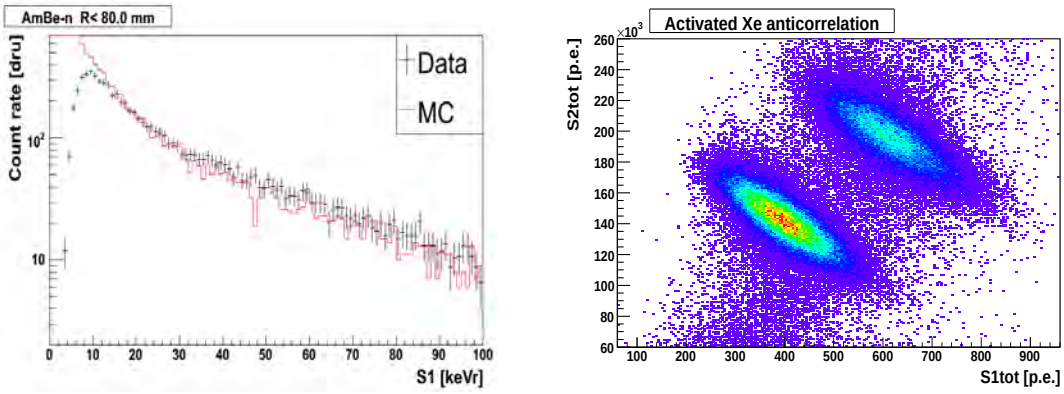

Figure 7: (left) A data versus MC comparison of the energy spectrum of elastic nuclear recoils in XENON10. (right) S2 versus S1 signal for neutron-activated Xenon data: the gamma lines at 164 keV and 236 keV are clearly visible.

of the energy spectrum of elastic nuclear recoils in LXe. We note the good agreement between the data and the Monte Carlo above ∼10 keVr.

At the time of this writing a small amount of neutron activated xenon gas was added to the XENON10 detector. Two xenon meta-stable states, ^{131m}Xe and ^{129m}Xe decay emitting 164 keV and 236 keV gamma rays with half-lives of 11.8 days and 8.9 days, respectively. These photons allow for a more uniform energy and position calibration across the LXe active volume. Figure 7 (right) shows a preliminary S2 versus S1 plot for a subset of the activated Xe data: the two gamma lines and the anti-correlation between the S1 and the S2 signals are clearly visible.

2.4 XENON10 Dark Matter Search

The overall raw event rate in XENON10, including events in the LXe outside the sensitive volume, is shown in figure 8 (black curve). The reduction of this rate, by removing events interacting in the passive LXe which surrounds the sensitive volume, amounts to three orders of magnitude and is also shown (red curve). This rate can be further reduced by a factor of 2 by applying a 5 cm radial cut (green curve).

Monte Carlo simulations, using the GEANT4 software package, were carried out to understand the background sources in XENON10. As shown in figure 8 (right), the measured background can be explained by the radioactivity in the PMTs, the stainless steel used in the detector and cryostat, and the signal and high voltage ceramic feedthroughs. In this simulation the activity of the PMTs is taken from the measurement of a sample of 14 PMTs counted with the very sensitive HPGe detector operated at the Gran Sasso Low Background facility.

The statistics of the dark matter search data accumulated to-date amount to approximately 100 days of live time with a 15 kg sensitive volume. Figure 9 (left) shows a plot of $\log_{10}$(S2/S1) as a function of energy for 22.2 live days, giving a total exposure of 38 kg d after cuts. The magenta and green lines corresponds to the centroid of the elec-

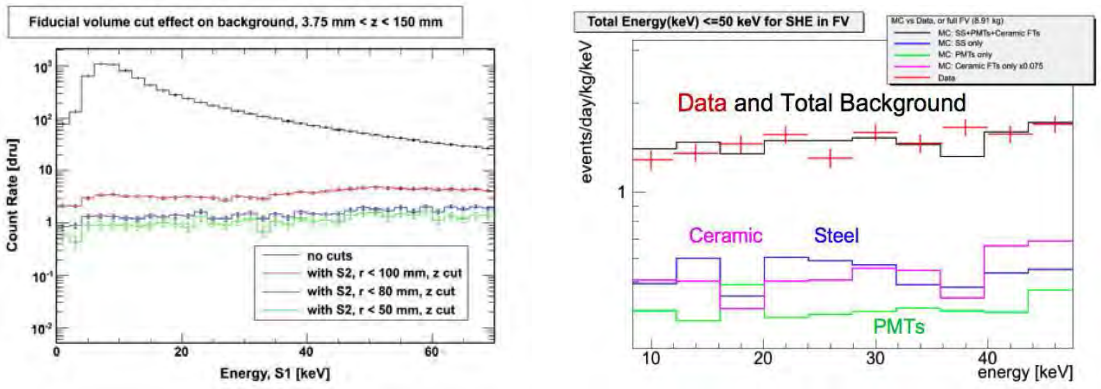

Figure 8: (left) Background energy spectrum in XENON10, before and after different fiducial volume cuts. (right) Comparison of XENON10 background data with Monte Carlo background data from radioactivity in the PMTs, Ceramic and Stainless Steel detector components.

tron and nuclear recoil bands respectively. In the energy region 3-16 keVee (10-40 keVr), zero events are observed in the 50% acceptance window of the nuclear recoil band. In the region above 16 keVee energy, we observed few events in the NR band. Our current understanding is that these events are double scatter events, with one interaction in a passive region and one in the fiducial volume. Since no S2 signal is observed for scatters in a passive region, then the additional S1 signal from the passive region results in a smaller $\log_{10}$(S2/S1) ratio. We are currently testing this hypothesis with Monte Carlo simulations and comparison with calibration data, and are planning to block the passive Xenon regions for the S1 light signal for an upgraded XENON10 version.

We are in the process of analyzing the complete science dataset, whereby we have blinded about two-thirds of the total WIMP search data. We are developing the data quality and physics cuts, and are testing their efficiencies on calibration and non-blinded WIMP search data. We expect that the existing configuration can probe WIMP-nucleon cross sections down to $\sim 10^{-7}$ pb for coherent WIMP-nuclei interactions. Concomitantly, we are preparing an upgrade of the XENON10 detector. Modest changes, such as the replacement of ceramic feedthroughs with lower activity ones, already in hand, the replacement of the stainless steel vessel with a vessel madeof OFHC Copper, along with the low PMT activity as recently measured, would reduce the expected background to 0.1events/keV/kg/day, one order of magnitude below the current level. We also expect that operation of the detector at a higher drift field will improve the nuclear versus electron recoil discrimination, and that optically masking the dead Xenon regions will decrease the number of potential leakage events. If lower backgrounds and a higher discrimination can be achieved, XENON10 could reach a WIMP-nucleon sensitivity of 2×10^{-7} pb by the end of 2007, as shown in figure 9 (right).

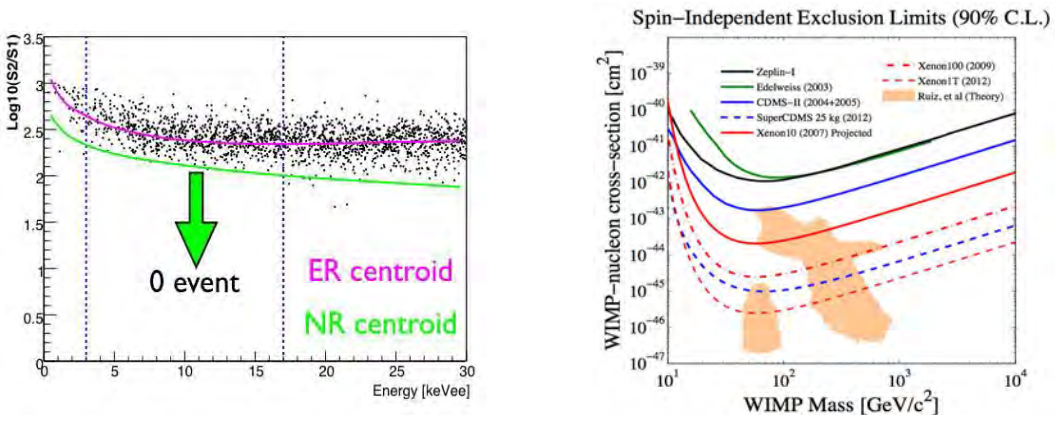

Figure 9: (left) XENON10 ionization yield versus energy plot. The magenta and green lines correspond to the centroids of the ER and the NR bands respectively. (right) Predicted XENON10 WIMP-nucleon sensitivity.

3 Acknowledgements

This work was funded by NSF Grants No. PHY-03-02646 and No. PHY-04-00596, the CAREER Grant No. PHY-0542066, the DOE Grant No. DE-FG02-91ER40688, by the Volkswagen Foundation (Germany) and by the FCT Grant No POCI/FIS/60534/2004 (Portugal). We would like to thank the LNGS/INFN staff, engineers and scientists for their continuous help and support.

4 List of Publications during 2006

1. E Aprile *et al.*, "Simultaneous Measurement of Ionization and Scintillation from Nuclear Recoils in Liquid Xenon for a Dark Matter Experiment"', Phys. Rev. Lett. **97**, (2006) 081302.

2. K. Ni, E. Aprile, K.L. Giboni, P. Majewski and M. Yamashita, "Gamma Ray Spectroscopy with Scintillation Light in Liquid Xenon", JINST **1** (2006) P09004.

3. T. Shutt, C.E. Dahl, J. Kwong, A. Bolozdynya and P. Brusov, "Performance and fundamental processes at low energy in a two-phase liquid xenon dark matter detector", submitted to Nucl. Instrum. Meth. **A**, astro-ph/0608137.

4. E. Aprile *et al.*, "The XENON dark matter search: Status of XENON10," J. Phys. Conf. Ser. **39** (2006) 107.

5. L. Baudis, "Dark Matter Searches", Int. J. Mod. Phys. **A 21** (2006) 1925-1937.

6. E. Aprile, L. Baudis, B. Cabrera, "Search for Weakly Interacting Massive Particles with CDMS and XENON", J. Phys. Conf. Ser. **60** (2007) 58-65.

7. J. Angle *et al.*, "3D position sensitive XeTPC for dark matter search", to appear in the Proceedings of 7th UCLA Symposium on Sources and Detection of Dark Matter and Dark Energy in the Universe, February 2006, astro-ph/0609714.
8. K. Ni and L. Baudis, "Direct Dark Matter Searches with CDMS and XENON", to appear in the Proceedings of 36th COSPAR Scientific Assembly, Beijing, China, July 2006, astro-ph/0611124.
9. M. Yamashita, "XENON", to appear in the Proceedings of 6th International Workshop on the Identification of Dark Matter, Rhodes, Greece, September 2006.
10. P. Sorensen, "Backgrounds and Threshold of XENON10 Dark Matter Experiment", to appear in the Proceedings of 6th International Workshop on the Identification of Dark Matter, Rhodes, Greece, September 2006.

References

[1] E. Aprile *et al.* (XENON Collaboration), New Astr. Rev. **49** (2005) 289.

[2] D.N. Spergel *et al.*, Astrophys. J. Suppl. **148** (2003) 175.

[3] B.W. Lee and S. Weinberg, Phys. Rev. Lett. **39** (1977) 165.

[4] G. Jungman, M. Kamionkowski and K. Griest, Phys. Rep. **267** (1996) 195.

[5] M. W. Goodman and E. Witten, Phys. Rev. **D 31** (1985) 3059.

[6] D. S. Akerib *et al.* (CDMS Collaboration), Phys. Rev. Lett. **96** (2006) 011302.

[7] D. S. Akerib *et al.* (CDMS Collaboration), Phys. Rev. **D 73** (2006) 011102.

[8] G. Angloher *et al.* (CRESST Collaboration), Astropart. Phys. **23** (2005) 325.

[9] A. Benoit *et al.* (EDELWEISS Collaboration), Phys. Lett. **B 545** (2002) 43.

[10] G. J. Alner *et al.* (ZEPLIN-II Collaboration), astro-ph/0701858.

[11] P. Benetti *et al.* (WARP Collaboration), astro-ph/0701286.

[12] G. Chardin in "Cryogenic Particle Detection", editor C. Enss, Springer, Heidelberg, (2005).

[13] R.J. Gaitskell, Ann. Rev. Nucl. Part. Sci. **54** (2004) 315.

[14] L. Baudis, Int. J. Mod. Phys. **A 21** (2006) 1925.

[15] E. Aprile *et al.*, Phys. Rev. **D 72** (2005) 072006.

[16] E. Aprile *et al.*, Phys. Rev. Lett. **97** (2006) 081303.

[17] T. Shutt, C.E. Dahl, J. Kwong, A. Bolozdynya and P. Brusov, astro-ph/0608137.

[18] M. Yamashita *et al.*, Nucl. Instrum. Meth. **A 535** (2004) 692.

ERMES. Monitoring of radon in geogas at the Gran Sasso National Laboratory

Wolfango Plastino[a,b], Gideon Steinitz[c], Naama Gazit-Yaari[d], Gaetano De Luca[e], Gustavo Haquin[d]

[a] Department of Physics, University of Roma Tre, Rome (Italy)
[b] National Institute for Nuclear Physics, Section of Roma Tre, Rome (Italy)
[c] Geological Survey of Israel, Jerusalem (Israel)
[d] Soreq Nuclear Research Center, Yavne (Israel)
[e] National Institute for Geophysics and Volcanology, Rome (Italy)

Abstract

In the framework of the research project ERMES (Environmental Radioactivity Monitoring for Earth Sciences) radon in air was systematically measured in two sites at the Gran Sasso National Laboratory (GSNL), with a sampling period of 15 minutes. Utilizing both alpha and gamma-ray spectrometers systematic and recurring radon signals were recorded. The occurrence of these signals in a deep low background facility provided information on the time variation of the local environmental radioactivity and possible link with deformation processes of tectonic interest. Then, it emphasized the GSNL as a high priority location for performing advanced investigations of these geophysical phenomena.

1 Introduction

The exploratory monitoring of radon in the geogas environment of the laboratory was started in October 2005. This activity extended radon measurements and monitoring in the local hydrologic system, conducted in the laboratory since 1996 [1, 2].

Chemical-physical groundwater and geogas monitoring have been performed in seismic areas to estimate the possible correlations between the spatial-temporal variations and deformation phenomena of tectonic interest. The transport of radon through microfractures or the crustal gas fluxes along active faults are the possible sources. Nevertheless, the non-tectonic factors have an important role, so it is very important to define correctly the geological, hydrogeological settings of the measurement site to discriminate the

variations induced by tectonic phenomena only. Another important aim is to test continuously the stability and reliability of the monitoring system using several checks during the measurement time.

The goal of the present investigation was to determine whether radon signals in geogas do occur in the GSNL, and identifying the nature of such variations for understanding radon as a geophysical tracer.

2 Experimental setup

Radon monitoring was performed in two sites along the service tunnels at the GSNL (figure 1). The sites are separated from the service tunnels by a metal partitions and tight doors. The site n. 1 is characterized by limestone and marl. The site n.2 is similar to n. 1 with a concrete lining.

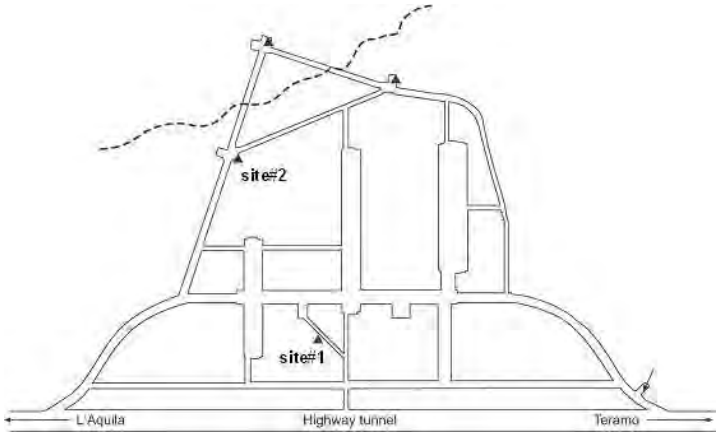

Figure 1: The map of GSNL. Radon measurements in geogas were conducted mainly in site n. 1 and also in site n. 2. Both sites are located in service tunnels.

Radon measurements were performed utilizing alpha and gamma detectors. Two 2"X2" NaI detectors (PM-11 detector, ROTEM Inc., Israel) were placed at site n. 1. Also, the measurement of radon by alpha radiation was performed with a calibrated AlphaGUARD system (Genitron Ltd). Ancillary environmental parameters (P, T, RH) were recorded by the AlphaGUARD system. Integration times were set to 15 minutes for the gamma-ray spectrometers and 10 minutes for the alpha system.

3 Results

An initial test (phase I) for temporal variation of radon in geogas was made using an AlphaGUARD detector system equipped also for the measurement of ancillary atmospheric parameters.

Monitoring results showed that the temperature and humidity levels were very stable over time. Small variations in temperature ($\leq$0.5 °C) were probably reflecting temperature variations in the tunnel (figure 2).

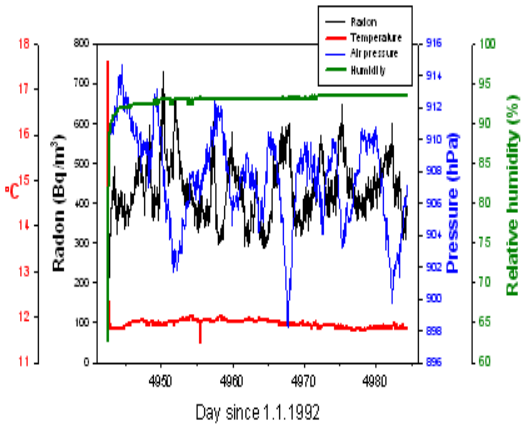

Figure 2: Time series of radon (using an alpha detector) in geogas at site n. 1 and local environmental parameters (pressure, temperature, relative humidity).

Two PM-11 gamma sensors were installed at the site n. 1 (phase II) and an Alpha-GUARD system with the environmental sensors was also operated (figure 3). The count rate of both gamma sensors was similar, and the systematic difference among them can be attributed to a slight difference in sensitivity and/or due to their slightly differing positions or calibration. A very high concordance was observed among the time series of the two gamma-ray spectrometers, and among these and the time series of the alpha detector (figure 3).

Limited radon monitoring started at site n. 2 after day 5151 (phase III), using the alpha detector system. The overall level of radon at site n. 2 was lower (50%) and the temporal fluctuations were barely visible. This difference between the two sites can be attributed to the extensive concrete lining and the relatively minor rock exposure at site n.2.

4 Discussion

The concordant signals measured at site n. 1 utilizing two independent detector systems reflects the higher radon content in the air of the isolated site, which is in contact with the geogas system of the locally exposed rock surface. Anyway, the origin of the radon signals in geogas observed at LNGS must be further investigated, including the attribution to transport mechanisms of radon in a closed environment.

Recent research of subsurface radon phenomena utilizing high time-resolution monitoring and analysis of long time series indicates that signals in geogas rather reflect hitherto

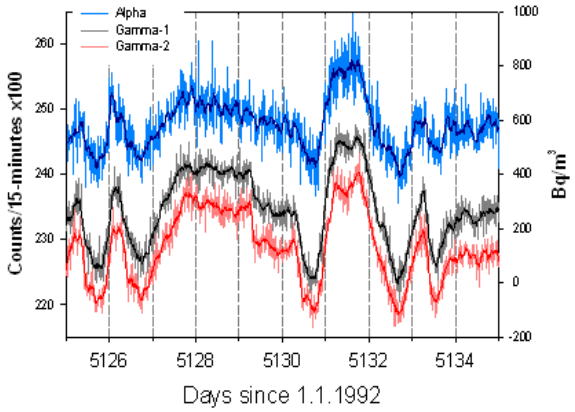

Figure 3: A 10-day detail of the time series exhibiting the concordance of the measurements among the three sensors. The concordance is further manifested by de-noising each time series using a 9-point sliding average (shown as solid lines).

unidentified geophysical processes. Then, investigations about the relation of the radon signals in the groundwater and associated geogas system should be perfomed.

The phenomena observed at GSNL, and the criteria and reasoning behind the assertion made as to the driving mechanism(s) were similar to the situation observed on radon signals occurrences in geogas at other places, where a comparable set of features are observed and similar considerations were made [3, 4].

5 Conclusions

The results obtained to date enable to set recommendations for further research. These recommendations were based and related to geological and geophysical situation of GSNL, and its environmental conditions. The primary immediate topics to be addressed were:

- setting a geophysical baseline by obtaining long, continuous high-time resolution time series of radon, to track eventual long term variations and to enable advanced data processing;

- initiating a local spatial array of measurements in order to obtain the 2D-time and 3D-time variations of the radon;

- integrating the activities with other geophysical measurements to enable better interpretation of the phenomena.

Acknowledgements This activity was performed in the frame of ILIAS-TARI project ERMES-Radon at LNGS (P2005-02-LNGS). We thank Prof. Eugenio Coccia, the Director of Gran Sasso National Laboratory (INFN), and especially Dr Nicola Ferrari for his kind and precious collaboration. Also, the authors are grateful to Mr. Uri Malik for the preparation of the analytical gamma system and Ms. Oksana Piatibratova for the

organization and reduction of the data.

References

[1] W. Plastino and F. Bella, 2001. Radon groundwater monitoring at underground laboratories of Gran Sasso (Italy). Geophysical Research Letters, 28/14, 2675-2678.

[2] W. Plastino, 2006. Monitoring of geochemical and geophysical parameters in the Gran Sasso aquifer, Radionuclides in the Environment, Elsevier, 335-342.

[3] G. Steinitz, Z. B., Begin and N. Gazit-Yaari, 2003. A statistically significant relation between radon flux and weak earthquakes in the Dead Sea Rift Valley, Geology, 31, 505-508.

[4] G. Steinitz, M. C., Martn, N., Gazit-Yaari, M. L., Quesada, J., de la Nuez, R., Casillas, U., Malik and Z. B. Begin, 2006. Multi-day radon signals with a radioactive decay limb occurrence and geophysical significance, Applied Radiation and Isotopes, 64/4, 520-524.

GIGS. The Interferometric Station at LNGS

Antonella Amoruso[a,b], Luca Crescentini[a,b,c]

[a] Dip.to di Fisica Univ. di Salerno, Salerno - Italy
[b] INFN - Gruppo collegato di Salerno, Salerno - Italy
[c] Spokeperson

Abstract

Since several years two Michelson-type laser interferometers, operating as geodetic extensometers, are working at LNGS. Until 1999 one interferometer measured difference in extension between the two baselines in an equal-arm configuration, since then two independent unequal-arm interferometers are monitoring extension along the two orthogonal directions, striking N66E and N24W. Both instruments are unequal-arm Michelson interferometers, using a 90-m long measurement arm and a <40-cm long reference arm, and sharing the same stabilized HeNe laser source.

1 Activity

In June 2005 data acquisition was stopped because of the laser tube failure. We decided to spend the inevitable long dead time before restarting acquisition to improve the electro-optical set-up in order to make the instrument easier to be managed, less expensive, and thus easier to be duplicated elsewhere. Improvement of the instruments encountered technical logistic administrative problems (in part still holding) thus requiring much longer time than expected. This report is consequently restricted to a short technical description of the new instrumental set-up.

As regards the laser source, instead of changing the laser tube we preferred to acquire a new laser head equipped with a fiber optic output. This improvement avoids re-aligning of all the optical components in case of substitution of the laser tube.

As regards the electro-optical set-up, until 2005 each reference arm included a transverse-field electro-optical phase modulator. The two complementary outputs of each interferometer where used as input signals for a control system acting on the optical length of the phase modulator in order to maintain a fixed phase delay, around 45°, between the reference and the measurement beams. In order to extend the dinamic range of the instrument, limited by the maximum voltage that can act on the electro-optical modulator, a reset circuit had been included, capable of changing the optical length of the phase modulator by $\pm\lambda$, each time the path length difference reaches $\mp\lambda/2$. Voltage applied

to the phase modulator was sampled at 800 Hz by a 12-bit digital-to-analog converter. Each datum consisted of two numers, the former related to the voltage applied to the phase modulator, and the latter related to the number of resets since the acquisition started. Both sequencies of numbers were digitally filtered using a linear nonrecursive filter, decimated at 5 Hz, and recorded.

Such a configuration allowed recording data at any frequency, after applying a proper low-pass digital filter to the two above mentioned sequencies of numbers. This feature of the apparatus was particularly useful in the past, when local storage of huge amount of data was a difficult task. But it required expensive electro-optical components, a very accurate optical alignment and electronic adjustment, and an occasionally careful data pre-analysis to correct for wrong reset counting. Thus we decided to test a simpler electro-optical configuration where the reference arm only included what required to get two quadrature signals at one output for each interferometer (the other output is no more used, see e.g. *Crescentini and Amoruso, Rev. Scient. Instrum.,* **67***, 3044-3046, 1996*) i. e. a polarizer and a quarter-wave retarder plate, and external optics do not include Faraday rotators any more. Also electronics is now much more simple, consisting only in what necessary to measure light intensity at the photodiodes. As a drawback, phase is no more linearly related to the ADC output, which can not be simply low-passed and decimated before storage. Real time conversion from light intensity to phase (i. e., strain) is not possible, because instabilities of dc level and amplitude of the interference signal, and phase lag fluctuations between the quadrature signals ask for nonlinear fitting of the Lissajous' figure given by few hours of quadrature data. Quadrature signals are sampled and stored at 600 Hz, to avoid artificial mixing of frequencies due to nonlinearity. Intensity-to-phase conversion is accomplished on stored signals when needed.

A small-size prototype has been built and tested at the Physics Department of the University of Salerno during spring 2006. The Gran Sasso geodetic interferometers have been equipped with the new electro-optical system in June 2006. Data acquisition is in progress since November 2006. Unfortunately, technical (laser source and vacuum system malfunction) logistic (heavy water infiltration inside the control room) administrative (long delays in funds availability) problems (in part still holding) have not yet allowed reaching expected instrumental performances completely. Nevertheless, management of the instruments and data appears much simpler than in the past, without degradation of retrieved strain.

2 Acknowledgments

We are very grateful to F. Tronca and C. Fischione for their help, and personnel of the Workshop Service and the Electronics Laboratory for their valuable work. The Gran Sasso geodetic interferometers are supported through an Accordo di Programma between INFN and Istituto Nazionale di Geofisica e Vulcanologia.

TELLUS. Ground deformations and their effects in the near-Earth Space

V. Sgrigna [a], A.Buzzi[a], L. Conti [a], M.Parrot[b], J.L.Pinçon[b], C.Stagni[a], D.Zilpimiani[c]

a Dipartimento di Fisica "E. Amaldi", Universitá e Sezione INFN Roma Tre- Italy.

b LPCE/CNRS, 3A Avenue de la Recherche, 45071 Orlans Cedex 2, France.

c Institute of Geophysics, Georgian Academy of Sciences (GAS) and National Space Agency, Tbilisi, Republic of Georgia.

Abstract

This report describes the activities carried out by the TELLUS team during 2006. These activities have been continuing those concerning ground aseismic creep strain events, observed by the TELLUS tilt network installed inside the LNGS, the ESPERIA space mission project planned and designed for studying Earth-near-Earth space interactions, the particle detector ARINA within the PAMELA mission and the ALTCRIS-EGLE experiment on board the International Space Station. During 2006, the research activity of the TELLUS group consisted of 1) the analysis of DEMETER data looking for a possible correlation between seismic activity and electromagnetic (EM) perturbations in the topside ionosphere, 2) the design and construction of electric and magnetic sensors for measurements of EM fields in space.

1 Introduction

Within the DEMETER Guest investigator program by CNES (French Space Agency), the TELLUS team has been involved in the study of electromagnetic (EM) and particle data collected by the polar DEMETER satellite mission, which is still flying (the end of the mission is scheduled for 2008) . The study is focused to search in the topside ionosphere possible time and space correlations between medium/large earthquakes (EQs) and anomalous whistler-waves detected by DEMETER.
In recent times, ionospheric and magnetospheric perturbations constituted by radiation belt particle precipitations, variations of temperature and density of ionic and electronic components of ionospheric plasma, as well as electric and magnetic field fluctuations, have been detected on board of Low-Earth-Orbit (LEO) satellites. Observations aim at reconciling these phenomena not only with solar or atmospheric effects but also with

Earth natural and anthropogenic activities. The former are associated with natural disaster as EQs, while the latter are constituted by power line harmonic radiation (PLHR), VLF transmitters, and HF broadcasting stations. Physical mechanisms underlying all these phenomena are not yet well-known, but one of the most fascinating applications is the so-called seismo-electromagnetic emissions (SEME). It consists of EM emissions (EME) in a large frequency band (from DC to a few tens of MHz), which may cause ionospheric perturbations as a consequence of the EQ preparation and occurrence. The idea is that EM fields generated by seismic sources in the seismogenic layer of the upper lithosphere, are transmitted into the near Earth's space, before, during, and after an EQ. These emissions can be detected on board of LEO satellites together with EME-waves produced by human activities. The privileged zone for investigating these phenomena appears to be the ionosphere-magnetosphere transition zone. What is lacking is the demonstration of a causal relationship with explained physical processes and looking for a correlation between data gathered simultaneously and continuously by space observations and ground-based measurements. In contrast to ground experiments, satellite missions cover most seismic zones of the Earth, and statistical studies become meaningful because of the much larger number of recorded events. DEMETER is the first satellite devoted and optimized to study the correlation between seismo- electromagnetic phenomena and iono-magnetospheric perturbations.
Within the framework of the MIUR program PRIN 2005 , the TELLUS laboratory research team has developed an innovative instrumentation for simultaneous investigations of electric and magnetic field perturbations in space optimized to carry out measurements of seismo-electromagnetic and geophysical natural phenomena.

2 TELLUS-DEMETER collaboration data analysis

On 29 June 2004, the French Space Agency (CNES) launched the micro-satellite DEMETER (Detection of Electro-Magnetic Emissions Transmitted from Earthquake Regions) (Parrot et al., 2006). The satellite is based on the Myriade platform and is specifically devoted to EM and particle studies. Scientific objectives are to search ionospheric disturbances related to seismo-electromagnetic effects and to anthropogenic activities. Demeter is entirely devoted to these observations, through i) continuous data collection, ii) in the appropriate frequency ranges, and iii) in the different components of the EM field. The satellite performs a polar orbit, at an altitude of 715 km, and works continuously in two modes: a survey mode in which EM data are recorded at a low bit-rate (spectrograms are computed), and a burst mode during which waveforms are recorded at several kHz. The time and space locations of one or the other of the two modes are determined as a function of the ground and seismic target. In figure 1 are reported the Myriade platform performances and a list of the parameters measured by Demeter.

A three-axis magnetic search-coil instrument (IMSC), four electrical sensors (ICE), two Langmuir probes (ISL), a plasma analyzer (IAP), an energetic particle detector (IDP) and an electronic unit (BANT) constitute the Demeter scientific multi-instrument payload. For magnetic cleaness, the IMSC magnetometer is set at the end of a 1.9m expanding boom, while ICE probes are set at the end of four 4m expanding booms. One can see this

Orbit	• Low earth orbit • DEMETER : 710 km, SSO
Pointing	• Earth pointing (DEMETER) • Sun or inertial pointing
Stabilisation	• 3 axis. • Typical accuracy: Coarse mode < 5° Fine mode < 0,1 ° • Stability: < 3'/s.
Telemetry Telecommand	• CCSDS, convolutionnal & R- S coding. • S -Band Transmission. • Useful TM rate: 400 kbits/s. • Useful TC rate: 20 kbit/s.
Localisation	• Doppler measurement • Accuracy: 1 km (LEO), 10 km (GTO).
Date	• Ground synchronization. • On board accuracy: < 0,5 s.
Power	• Steerable sun generator • AsGa solar cells(200 W EOL) • Li Ion battery: 14 Ah • Payload: around 70 W permanent.
Weight *Propulsion*	• Total: 130 kg. • Payload weight: 50 kg. • *Hydrazine, Δv : 80 m/s* • *4 thrusters 1 N*
High rate TM	• *X-Band emitter 16,8 Mbits/s* • *Memory : 8 Gbits (Flash)*
GPS	• *Topstar 3000*

▪ Frequency range, B	10 Hz - 17 kHz
▪ Frequency range, E	DC – 3,5 MHz
▪ Sensibility B :	2 10^{-5} nT $Hz^{-1/2}$ at 1 kHz
▪ Sensibility E :	0.2 µV $Hz^{-1/2}$ at 500 kHz
▪ Particles: Electrons :	30 keV - 10 MeV
▪ Ionic density:	5 10^{2} - 5 10^{6} ions/cm^{3}
▪ Ionic temperature:	1000 K - 5000 K
▪ Ionic composition:	H^{+}, He^{+}, O^{+}, NO^{+}
▪ Electron density:	10^{2} - 5 10^{6} cm-3
▪ Electron temperature:	500 K - 3000 K

Figure 1: Myriade platform performances and DEMETER Measured Parameters.

boom configuration in figure 2.

Figure 2: Picture of the Demeter satellite in flight with its deployed booms and sensors.

The general layout of the satellite is given in figure 3.

Within the DEMETER guest investigator program, the TELLUS team has studied the effect of seismicity on the whistlers-waves propagation. Following a previous work (Hayakawa et al., 1993) based on whistler data detected by ground based observatories, which has suggested the influence of seismic activity on the occurrence of anomalous whistlers of high dispersion parameter, the TELLUS team has investigated the spatial and temporal correlation between earthquakes and whistlers phenomena using the DEMETER space data. This is the first study on the topic based on satellite observations. At this

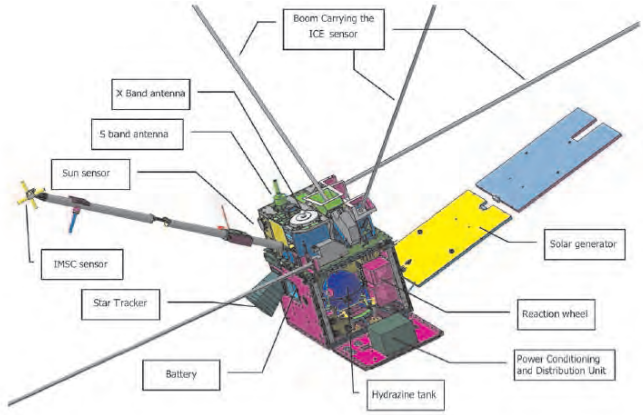

Figure 3: Layout of the Demeter satellite.

purpose it has been studied how whistlers generated near the EQ magnetic field line and propagating along it can be perturbed by seismic activity. In the following, are detailed cuts applied to data in order to select EQs and whistlers populations to be compared. A special software (WHIMAP) has been developed to construct the DEMETER whistler database, which includes time, position, whistler data and geomagnetic activity indices information. By the USGS database an ad hoc catalogue of medium and strong earthquakes has been built including magnitude and epicenter, magnetic field line data, McIlwain L-parameter and conjugate coordinates of the geomagnetic point. Whistler waves and EQ events to be compered have been selected with an original method of analysis applying several cuts. To know the geographic regions sensitive to seismic activity have been determined the coordinates of points belonging to the projection on the Earth's surface of EQ magnetic field lines defined as follows (fig.4), and along this magnetic field line a narrow region of DEMETER observations have been selected and compared with seismic phenomena. For each earthquake have been calculated the geographic coordinates of the projection to the Earth surface of the magnetic field line, which footprints are the EQ epicenter and the EQ geomagnetic conjugate point(CP), respectively (fig. 4). Two correlation estimators have been identified and, to check the stability of results, the significance of their spatial and temporal distributions have been investigated, as a function of distance, time, geomagnetic condition, whistler dispersion, EQ magnitude, geomagnetic latitude, spatial distribution and local time dependence.

At this purpose, two variables have been introduced in the study and defined as follows:

$$\Delta w_\sigma(lat, long, t) = \frac{w(lat, long, t) - < w(lat, long, t) >_{|cell,1month}}{\sigma(lat, long, t)|_{cell,1month}} \quad (1)$$

$$hcum_{ratio}(lat, long, t) = \frac{hcum(w(lat, long, t))}{hcum(< w(lat, long, t) >_{|cell,1month})} \quad (2)$$

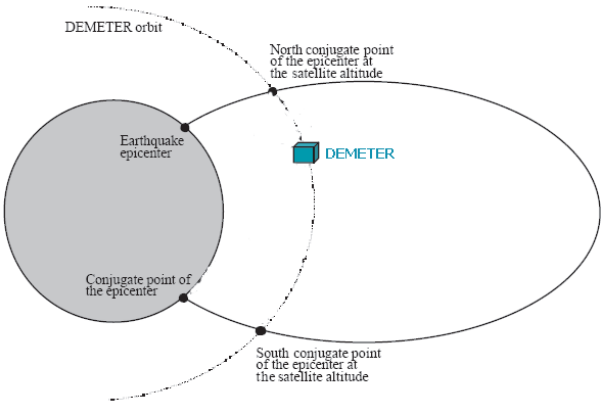

Figure 4: Schematic illustration of an EQ magnetic field line, up the EQ conjugate point CP. Also the intersection points between the EQ field line and Demeter orbit are shown.

First variable represents the standard score number of whistlers as a function of latitude, longitude and time, where σ is the standard deviation. Second variable is the cumulative function of number of whistlers calculated at the observation point and normalized to the cumulative function of number of whistlers calculated at mean value. hcum(w) (also called the cumulative density function (CDF)) is related to the discrete probability *P(w)* as follows:

$$hcum(w_0) = P(w \leq w_0) = \sum_{0}^{w_0} P(w) \tag{3}$$

Δw_σ and $hcum_{ratio}$ have been calculated for each dispersion value of whistlers data detected by DEMETER. The value of each variable has been calculated separately for day or night times and it has been normalized to the monthly mean value of observations. Geographic distributions of the above-mentioned variables for each geographic cell of 10^o in latitude and 4^o in longitude, and for each month of data, have been constructed for the whole period May 25, 2005-April 30, 2006.

In this statistical analysis we have only considered the propagation of whistlers along the EQ magnetic field lines by selecting whistlers detected inside an interval of $\pm 2^o$ degrees in geocentric longitude along each EQ magnetic field line. Moreover, whistler data are accepted for the analysis only when the geocentric latitude of Demeter (λ_D) is within the inequality

$$[\lambda_{CP} \leq \lambda_D \leq \lambda_{EQ}]_{alongtheEQfieldline} \tag{4}$$

for EQs occurring in the Northern magnetic Hemisphere, and

$$[\lambda_{EQ} \leq \lambda_D \leq \lambda_{CP}]_{alongtheEQfieldline} \tag{5}$$

for EQs occurring in the Southern geomagnetic Hemisphere. In addition to these whistlers selection criteria, based on the whistlers observation position, with respect to the projection of EQ magnetic field line on the Earth's surface, a further cut based on time was applied to data. In particular, only whistlers detected in a time window of +/- 48 hours, centered on the time of origin of the selected EQs, were taken into account. Whistlers selected in this way were classified as a function of parameters: Δt and $nmld$. $\Delta t = T_D - T_{EQ}$ is the difference between the time of satellite data and the time of earthquake; $nmld$ is the distance between the magnetic latitude of the EQ and the whistler data detection point, normalized to the length of the EQ magnetic field line, that is:

$$nmld = \frac{latmag_{Demeter} - latmag_{EQ}}{latmag_{CP} - latmag_{EQ}} \tag{6}$$

where, denominator indicates the difference in magnetic latitude between CP and EQ. $nmld$ values close to 0 indicate whistlers collected close to EQs. On the contrary, nmld values close to 1, correspond to whistlers collected close to CPs, independently from the EQ geomagnetic latitude and the length of the EQ appropriate field line.

The analysis has been performed by gathering whistlers data into three different groups of whistler dispersion coefficient values D, as follows: low D (classes 0-6), medium D (classes 7-12) and high D (classes 13-18), corresponding to $0s^{1/2} < D < 10s^{1/2}$, $10s^{1/2} < D < 40s^{1/2}$, $40s^{1/2} < D < 202s^{1/2}$, respectively. Plots for Δw_σ and $hcum_{ratio}$ averaged over whistlers classes in these three D intervals are reported in figures 5 and 6. Plots of $hcum_{ratio}$ for D classes (13-18) during daytime show two bands near $nmld \simeq 0$ and $nmld \simeq 1$, which indicate a high fluctuation of number of anomalous whistlers with respect to the spatial and temporal mean value.

We stress that Δw_σ maps are more noisy than $hcum_{ratio}$ ones, and that the two above-mentioned bands of anomalous whistler signals appear only for highest whistler dispersion values. The existence of these two bands of anomalous signals in the $hcum_{ratio}$ maps is in agreement with results of ground-based observations by *Hayakawa et al.,* [1993], who pointed out the existence of an anomalous increment of whistlers with high dispersion value in coincidence with the EQ occurrence.

The existence of such two bands close to the EQ and CP regions could indicate that seismic activity influences the whistler propagation mainly for highest whistler dispersion coefficient values. On the contrary, no dependence is observed versus Δt, indicating that any possible anomalous signal associated with EQs can not be catalogued as pre-seismic, co-seismic, or post-seismic one, but only associated with a time window around a seismic event as a whole. Even if this study is over preliminary, the existence of the two bands could indicate the existence of a fluctuation in the number of whistlers with high D values induced by seismic activity near the EQ epicenter and its CP.

3 TELLUS electric and magnetic field probes

During 2006 we also planned to design and build a device to detect electric and magnetic fields in the frequency band ULF-HF. Aim of the project is to develop an engineer-

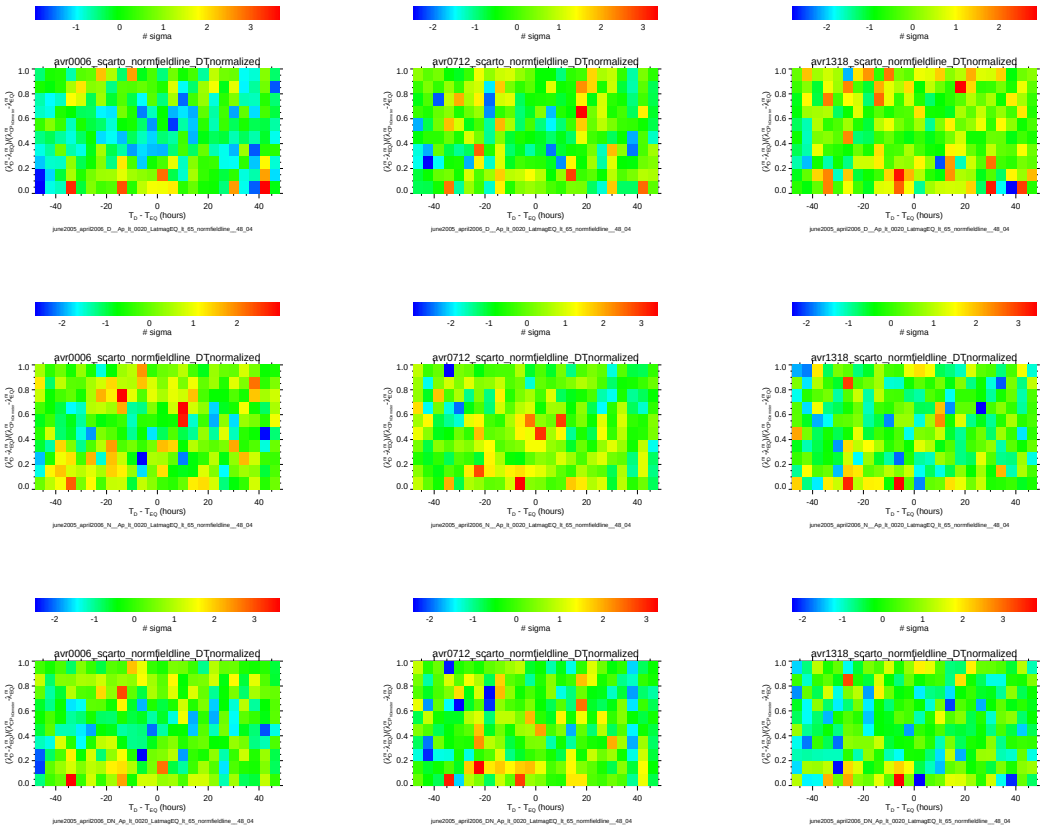

a) b) c)

Figure 5: Δw_σ v.s *nmld* and Δt averaged over whistler coefficient dispersion classes from 00 to 06 a), 07 to 12 b), 13 to 18 c) during Daytime (top), Nighttime(center), Nighttime+Daytime (bottom).

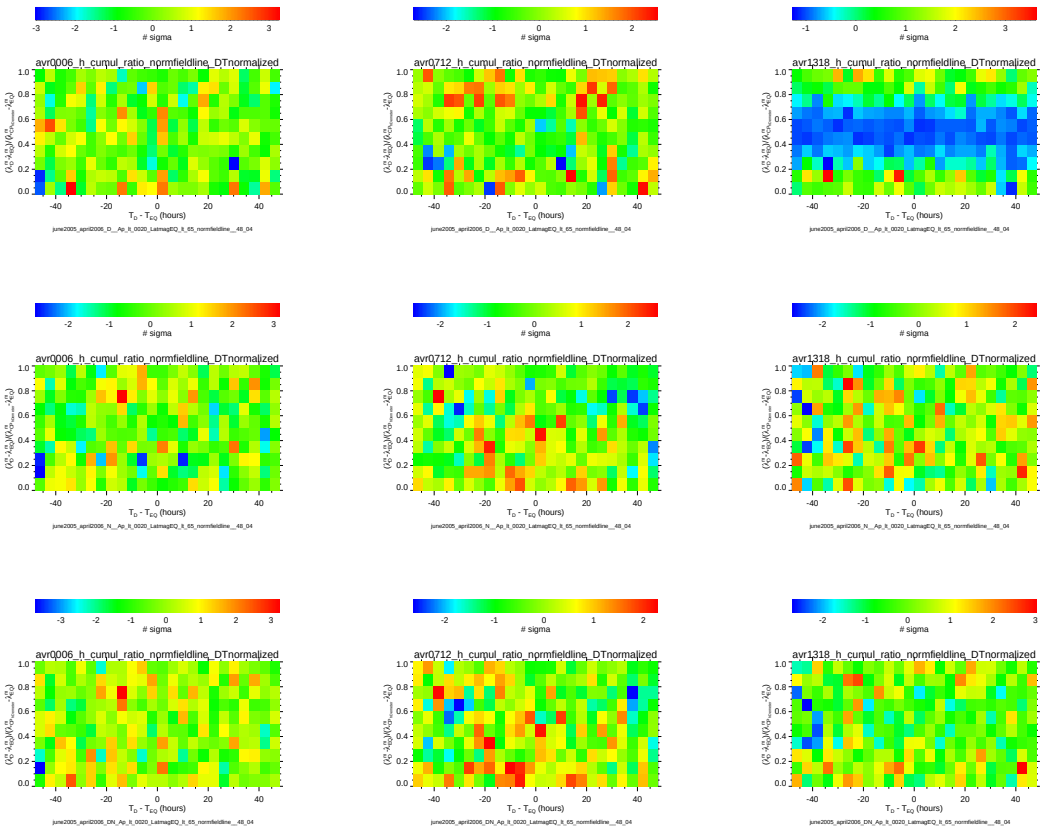

a) b) c)

Figure 6: $hcum_{ratio}$ v.s $nmld$ and Δt averaged over whistler coefficient dispersion classes from 00 to 06 a), 07 to 12 b), 13 to 18 c) during Daytime (top), Nighttime(center), Nighttime+Daytime (bottom).

ing model of this instrumentation with characteristics suitable for possible application in space, finalized to the monitoring of EM perturbations in the topside ionosphere to correlate them with EME signals of terrestrial origin (seismic and anthropogenic ones). Then, it has been built a prototype of a high sensitivity,low consumption (300 mW for

Basic technical specifications of the EGLE probe MH	
Frequency band of receiver signals	0.5 ÷ 50000 Hz
Shape of transfer function	linear – flat
Type of output	Symmetrical
Transformation factor at both output terminals:	
▪ **at linear part (0.5 – 5 Hz)**	f*4 mV/(nT*Hz)
▪ **at flat part (5 – 50000 Hz)**	20 mV/nT
Transformation factor error:	
▪ **at flat part of band pass without edges**	≤ ±0.25 dB
▪ **at flat part band pass edges**	≤ 3 dB
Magnetic noise level, $pT*Hz^{-1/2}$:	
▪ **at 5 Hz**	≤ 0.4
▪ **at 100 Hz**	≤ 0.02
▪ **at 5 kHz**	≤ 0.004
▪ **at 50 kHz**	≤ 0.02
Nominal output load	≤ 200 pF ≥ 50 kΩ
Power supply voltage	± (15 ± 0.2) V
Power consumption	300 mW
Temperature range of operation	-30° C ÷ $+50^{\circ}$ C
Outer dimensions (without prominent parts)	l = 400 mm d = 32 mm
Length of the output cable	0.7 m
Weight	≤ 320 g

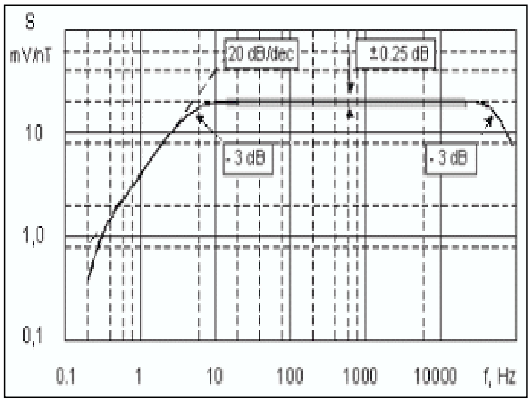

Figure 7: Main characteristics of the search-coil magnetometer.

each sensor), broad-band (0.5Hz ÷50 kHz), low-weight (≃330 g for each sensor) tri-axial search-coil magnetometer. Each sensor is constituted by an induction coil with a high magnetic permeability core of amorphous material. The sensor has also a pre-amplifier inside. In the same year 2006, the TELLUS team has also developed a spherical probe

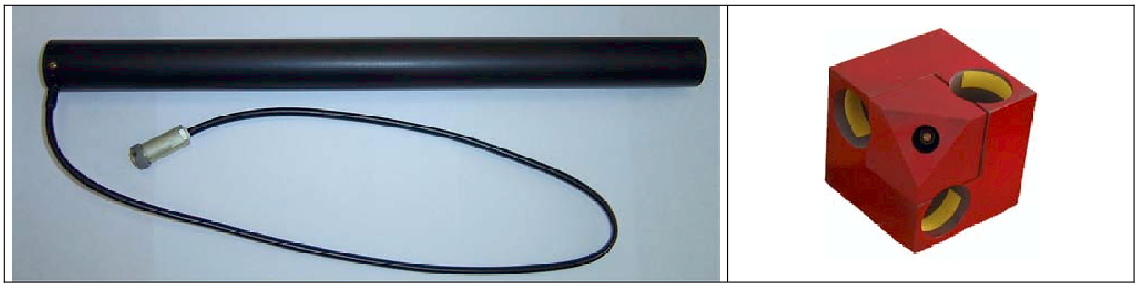

Figure 8: Search-coil sensor (left) and support for the tri-axial search-coil magnetometer (right).

for electric field measurement in space in the frequency range from DC to 10MHz. The electrode contains inside a pre-amplifier. Within this framework, the TELLUS research

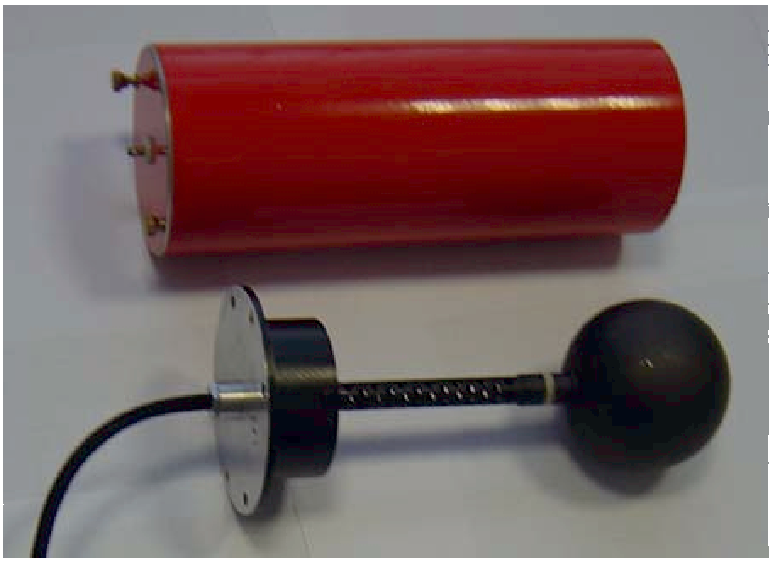

Figure 9: Electric field probe

activity has been carried out in collaboration with the Institute of Geophysics of the Georgian Academy of Sciences and the Lviv Centre of the Institute of Space Research of the National Academy of Sciences of Ukraine.

4 Conclusions

Although some aspects in the distribution of DEMETER whistler dispersion classes have to be clarified, it has been observed that for high whistler coefficient dispersion values, the number of whistlers close to EQs and EQ conjugated points exhibits a greater increase than those detected in average in the same zone. On the contrary, this result does not allow to associate anomalous signals to pre-seismic, co-seismic, and post-seismic periods.

Results must be validated by extending the time window used in the analysis and refining selection criteria. The analysis is still in progress in order to confirm and improve the quality of results obtained up to now.

Within the framework of the MIUR program PRIN 2005, the TELLUS research team has developed a tri-axial search coil magnetometer and an electric field probe suitable for measurements in space on board of LEO satellites. The corresponding data acquisition system optimized to carry out measurements of seismo-electromagnetic and geophysical natural phenomena is under study.

5 List of Publications

1. Buzzi, A., Conti, L., Galper, A. M., Koldashov, S.V., Malvezzi, V., Murashov, A.M., Picozza, P., Scrimaglio, R., Sgrigna, V., Stagni, L., 2006. *Seismo-electromagnetic emissions*, Proc. NATO Adv. Study Institute on "Sprites, Elves and Intense Lightning Discharges", Edited by M. Fullekrug, E.A. Mareev and M.J. Rycroft, Published by Springer, vol. 225, pp. 388-389, 2006. (NATO Science Series II: Mathematics, Physics and Chemistry- vol.225. ISBN-10 1-4020-4628-6 (PB)).

2. Parrot, M., Buzzi, A., Santolik, O., Berthelier, J.J., Sauvaud, J.A., Lebreton, J.P., 2006. *New observations of electromagnetic harmonic ELF emissions in the ionosphere by the DEMETER satellite during large magnetic storms*, J. Geophys. Res., 111, A08301, doi: 10.1029/2005JA011583, 2006.

3. Sgrigna, V., A. Buzzi, L. Conti, P. Picozza, C. Stagni, D. Zilpimiani, 2006. *The ESPERIA satellite project for detecting seismic-associated effects in the topside ionosphere. First instrumental tests in space*, Earth Planets and Space, accepted in press.

4. Sgrigna, V., Altamura, F., Ascani, S., Battiston, R., Bencardino, R., Blasko, S., Buzzi, A., Casolino, M., Conti, L., Lucidi, S., Minori, M., Papi, A., Picozza, P., Rossi, S., Stagni, C., Zilpimiani, 2006. *The EGLE space experiment onboard the ISS*, Microgravity and Sci. Technology, submitted 2006.

5. Sgrigna, V., 2006. *The EGLE space experiment onboard the ISS*, ESA Meeting "Science on European Soyuz Missions to the ISS (2001-2005)", Toledo, Spain, 27-30 June 2006, Splinter Session: Life and Physical Sciences, Human Physiology, Splinter room: Technology.

6. Conti, L., Buzzi, A., Picozza, P., Ronchetti, S., Sgrigna, V., Stagni, C., Zilpimiani, D., 2006. *Seismo-induced electromagnetic and particle perturbations in space*, International Symposium DEMETER, Toulose, France, June 14-16, 2006.

7. Sgrigna, V., 2006. *The ESPERIA satellite project for detecting seismo-associated effects in the topside ionosphere*, ISRS 2006 PORSEC, Joint Conference of International Symposium on Remote Sensing and Pacific Ocean Remote Sensing conference. Session Natural Hazards. Busan (Korea), 7-10 November, 2006 (Invited).

8. Parrot, M., Buzzi, A., Santolik, O., Berthelier, J.J., Sauvaud, J.A., Lebreton, J.P., 2006. *New observations of electromagnetic harmonic ELF emissions in the ionosphere by the DEMETER satellite during large magnetic storms* (Solicited), European Geosciences Union (EGU) General assembly, 2006, Vienna, Austria, 2-7 April 2006; Geophysical Research Abstracts, vol 8, 01643, 2006.

9. Buzzi, A., Parrot, M., Sauvaud, J.A., 2006. *Precipitation of particles by intense electromagnetic waves during magnetic storms.* International Symposium DEMETER, Toulose, France, 14-16 June, 2006.

References

[1] Hayakawa M., T. Yoshino, and V.A. Morgounov, 1993. *On the possible influence of seismic activity on the propagation of magnetospheric whistlers at low latitudes*, Phys. Earth Planet. Int., 77, pp. 97-108.

[2] Parrot, M., Benoist, D., Berthelier, J.J., Blecki, J., Chapuis, Y., Colin, F., Elie, F., Fergeau, P., Lagoutte, D., Lefeuvre, F., Legendre, C., Leveque, M., Pincon, J.L., Poirier, B., Seran, H.C., Zamora, P., *The magnetic field experiment IMSC and its data processing onboard DEMETER: scientific objectives, description and first results.* Planet. Space Sci., this issue, 2006.

UNDERSEIS - Underground Seismic Array

C. Fischione[a], M. Martini[a], G. Saccorotti[c], R. Scarpa[a,b], F. Tronca[a]

[a] Osservatorio Vesuviano, I.N.G.V. - Napoli, Italy
[b] Dipartimento di Fisica, Universit`a di Salerno - Baronissi (SA), Italy
[c] I.N.G.V. - Sez. Pisa, Italy

Abstract

This report describes a geophysical instrument under installation in the underground physics laboratories of Gran Sasso (LNGS-INFN), located in the seismic zone of central Apennines, Italy. This instrument is aimed to monitor seismic radiation with very high sensitivity; it is a small aperture seismic array composed by 20 three-components short period seismometers (Mark L4C-3D).

1 Introduction

The physics of earthquakes is based on the measurements of radiated seismic waves and ground displacement associated with this phenomena. The inertial pendulum is the oldest and most diffused instrument used to measure the main features of seismic waves. The advantages of this instrument are the simplicity of the theory, the high sensitivity, the robust design and the simple calibration methods, in spite of the quite reduced frequency band and linearity (Wielandt, 1983). Other instruments based on different physical principles, such as strainmeters and gyroscopes, are only partially used by seismologists (Benioff, 1935; Farrell, 1969; Aki and Richards, 1980). Networks of short period seismometers are as far the most diffused system to monitor local and regional seismicity (Lee and Stewart, 1981). Broad-band instruments make up a powerful system to study the details of seismic sources and also to study large earthquakes at global scale (Lee and Wallace, 1995). Strainmeters and tiltmeters (Agnew, 1986) are used to study the lower frequencies radiated from seismic sources and allow to detect slow earthquakes and strain steps (i.e. anelastic deformations around seismic sources). Moreover arrays of seismometers and accelerometers are used to study the Earth structure at global, regional and local scale (Green, 1965; Kedrov and Ovtchinnikov, 1990; Mikkeltveit, 1985), earthquake source process (Spudich and Oppenheimer, 1986; Goldstein and Archuleta, 1991), nuclear underground explosions (Bolt, 1976; Chouet, 1996) and, more recently, for the analysis of complex signals associated to the volcanic activity (see f.i. Goldstein and Chouet, 1994;

Chouet et al., 1997; Almendros et al., 1991). The main advantage of the seismic arrays consists in their ability to detect small signals through multichannel waveform stacking (Capon, 1969). The area is interested by relevant seismicity associated with the mainly distensive tectonics affecting the Apennines since the late Pliocene (D'Agostino et al., 2001; Galadini et al., 2003). The last large historical event is the 1915, $M_S = 6.8$ Fucino earthquake, which caused about 32000 casualties, recently modelled by a normal fault striking along the Apennines (Amoruso et al., 1998). In addition, swarms of low- to moderate-size earthquakes occur quite frequently, the most recent on 1992, 1994 and 1996 (De Luca et al., 2000). This massif is intersecting a main seismogenetic fault where the occurrence of slow earthquakes has been recently detected through two wide-band geodetic laser interferometers (Crescentini et al., 1999; Amoruso et al., 2002). This quite relevant rate of seismicity, joint to the low-noise conditions and site response associated to the underground setting, make the Gran Sasso underground laboratories an ideal site for high-resolution seismic observations (De Luca et al., 1998).

2 The Underground Seismic Array

A seismic array is a set of seismographs distributed over an area of the Earth's surface at spacing narrow enough so that the signal waveform may be correlated between adjacent seismometers (Aki and Richards, 1980).

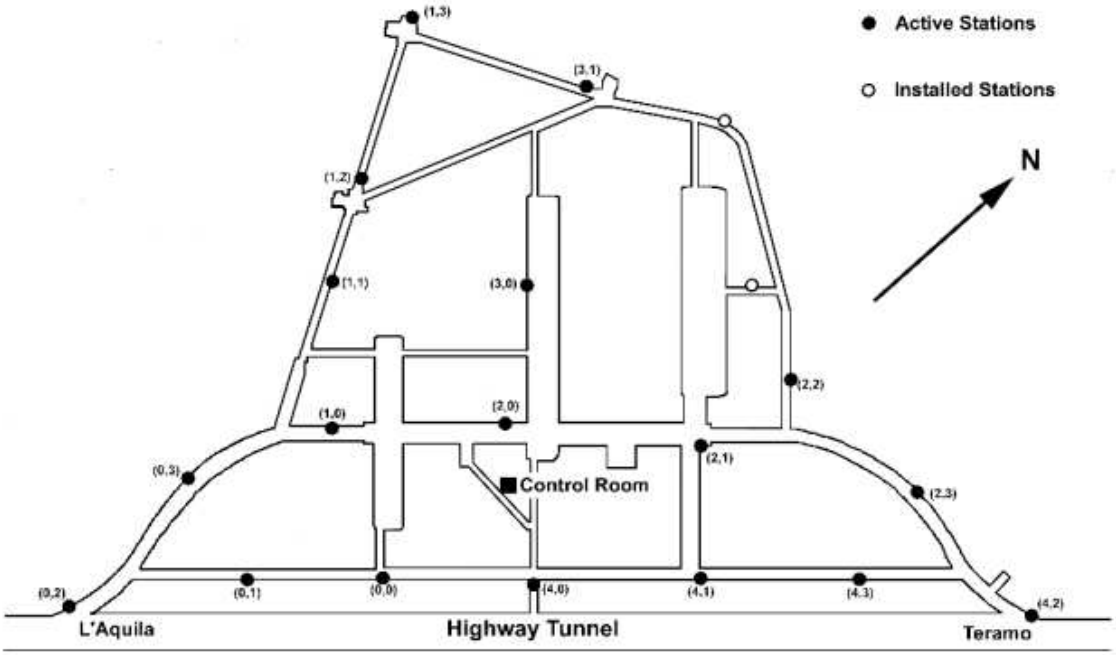

Figure 1: Map of the Underground Seismic Array. The notation (n,m) shows the line number (n) and the station number (m).

The design of the UNDERSEIS hardware and software components began on the late 90's; over the following years, major upgrades were developed under a technological effort jointly carried out by engineers from the University of Granada (Spain), University of L'Aquila (now the team moved to the University of Salerno), and INGV - Osservatorio Vesuviano. The array become fully operative since May, 2002. In its present configuration, it consists of 19 elements, each equipped with a MARK Product L4C-3D, 1 Hz, 3-component seismometer. The average sensor spacing is on the order of 90 m, and the largest distance among sensors is about 400 m. Seismic signals are digitized locally at each individual seismometer with a dynamic range of 24 bits and sampling frequency of 100 Hz. Data synchronization is achieved via a Master Oscillator which transmit the UTC synchronized pulses from an atomic clock to the different ADC boards. The synchronized data packets are then sent via serial cable connection to a set of five nodal PCs, which are in turn connected via an Ethernet network to a central data server and an on-line processor (Scarpa et al., 2004).

2.1 Array performance. MUSIC algorythm response on synthetic data

In order to evaluate the MUSIC algorythm (Schmidt, 1986) capability to reconstruct real slowness data with the configuration of the UNDERSEIS array, we run MUSIC on some sets of synthetic data, proceeding as described below.

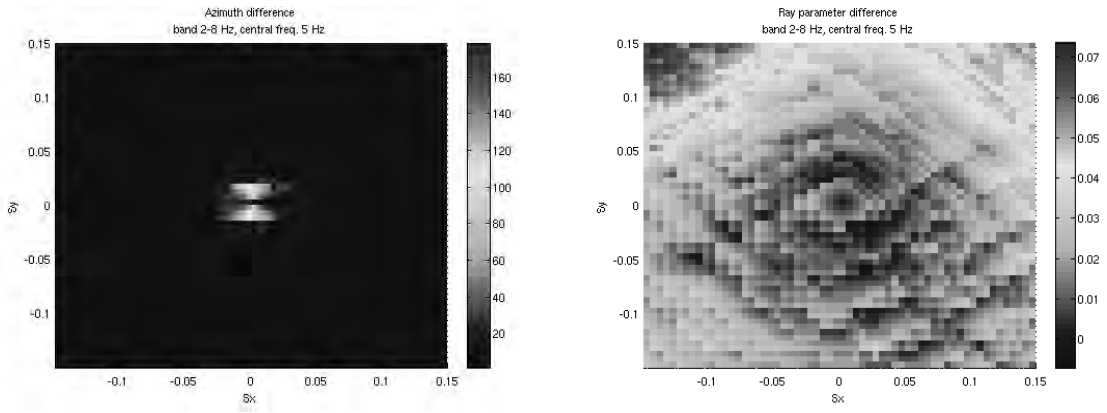

Figure 2: Discrepancies between original and recalculated azimuth (left) and ray-parameter (right).

As first step, we choose a real wave (P arrival) in a window of 0.5 sec, compiled the station list including the station coordinates and defined a grid of slowness values (S_x and S_y). Then, we duplicated the wave for every array station (19) and time-shifted it, according to station coordinates and to a the first pair of S_x and S_y values, so creating a synthetic set of waves. After that, we repeated the procedure iteratively in order to have a set of synthetics for every pair of slowness values present in the grid. Once prepared, we used the synthetics as input of MUSIC algorhythm compared the outputted Ray-

parameter and Azimuth values with that derived from the S_x and S_y values used to generate the synthetics. Different tests were done. The results can be resumed in the Fig. 2 which represents err(az) vs (S_x, S_y) and err(RayP) vs (S_x, S_y), for a set of synthetics generated on a slowness grid ranging from $-0.15\frac{s}{km}$ to $0.15\frac{s}{km}$ with a step of $0.05\frac{s}{km}$. The signals were filtered in the 2-8 Hz band. The results are quite clear: as we can expect, the difference between original and recalculated azimuth values raises at significant values for low slowness values. This is the case of earthquakes with depth much greater than epicentral distance. Under these circumstances, seismic rays impinge at the array with steep incidence angles, and the apparent velocity reaches very high values.

3 Data analysis

3.1 Automatic data selection and storage procedure

An automatic data selection c-shell script was written. This script runs on a dedicated Linux calculator at LNGS. The script works as follows:

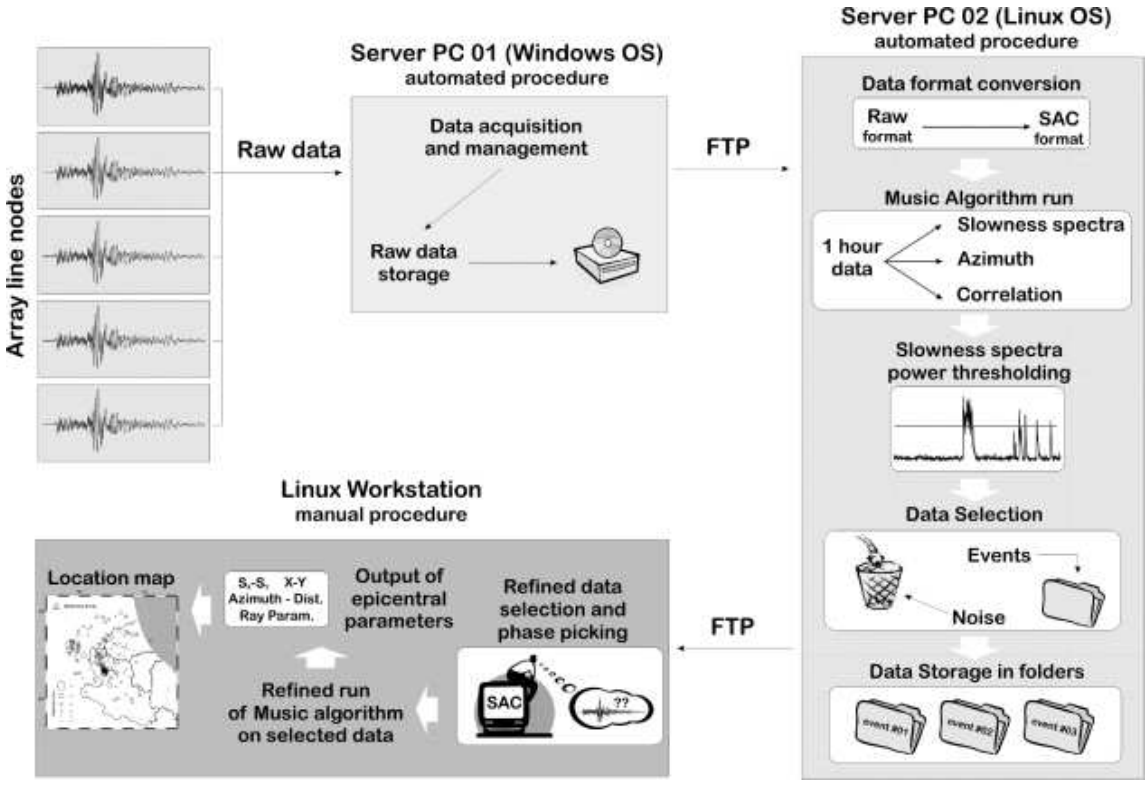

Figure 3: Block scheme of the data selection, storage and refined analysis procedure.

1. ten minutes after every hour change (that is few minutes after the array server closes the hourly data recording files), the scripts connects to the array server and downloads all the files related to the correctly working stations;

2. it converts these files in SAC format;

3. it runs the MUSIC (multiple signal correlation analysis) algorithm, computing the slowness spectra, the propagation azimuth of the wave field and the correlation parameters for the just converted files. MUSIC is run on 2 s sliding (with 50% overlapping) time windows. The slowness search grid varies from -0.5 to 0.5 $\frac{s}{km}$ with a 0.02 $\frac{s}{km}$ step in both x and y direction;

4. it runs a procedure for the thresholding of the slowness spectra power;

5. if there are any peaks, an info text file is written, the SAC data files are windowed on the correlation peak (50 s before and 100 s after the peak) in order to include the earthquake, and saved them as new files in a new directory (Fig. 3).

After the automatic data selection and storage, we perform a refined analysis as follows. Every selected event is checked and phase-picked manually by an operator. Then MUSIC is run again using a small and finer slowness search grid (-0.24 to 0.24 $\frac{s}{km}$ with a 0.004 $\frac{s}{km}$ step in both x and y direction). This method allows us for a robust and precise estimation of the direction-of-arrival of plane waves crossing the array. Measurements of propagation azimuths and S-P delay times were then used to evaluate reliable epicentral locations.

3.2 Epicentral distance and magnitude estimation

After peaking P and S arrival times, we conducted the epicentral distance (in km) estimation using the empirical formula $dist = (S - P) \cdot k$, where k is the factor used to convert S-P delay times to epicentral distance (Wadati diagram). The k parameter is computed using a set of 50 events of known epicentral location (data from INGV bulletin). The dist parameter was calculated from epicentre coordinates and $S - P$ delay times were measured with SAC for all the 50 events considered, which were then plotted on a delay time-distance picture and fitted with a linear function thus obtaining a reasonable estimate of the k parameter, giving us the value of $k = 6.7$ (Fig. 4). An empirical magnitude scale for the array site has been established using the duration-magnitude formula: $M = B \cdot \log_{10} d + A$. The A and B parameters were computed using about 50 events of known magnitude between a minimum value of 1 and a maximum value of 5 (data from INGV bulletin) recorded by the array. The d parameter (event duration) was measured with SAC. These events were then plotted on a duration-magnitude picture and fitted with a logarithmic function (linear regression) in order to obtain a reasonable estimate of the A and B parameters which were evaluated as $A = -1.467$ and $B = 2.415$ (Fig. 5).

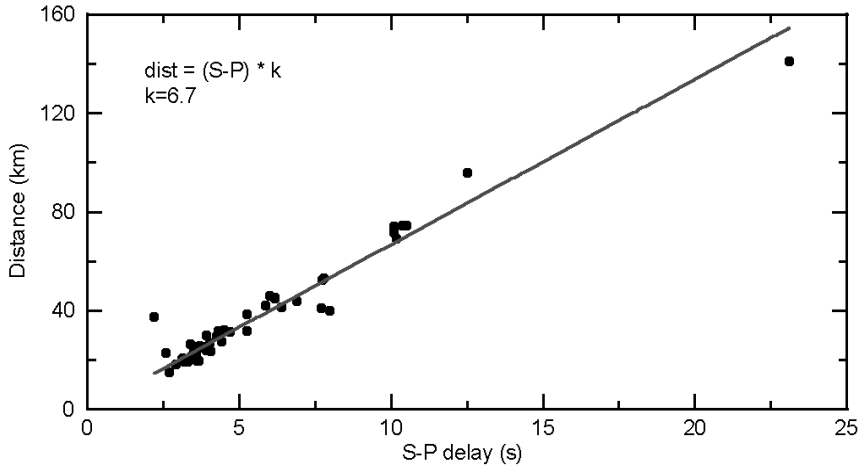

Figure 4: Empirical estimation of the k parameter to be used to convert $S - P$ delay times to epicentral distance.

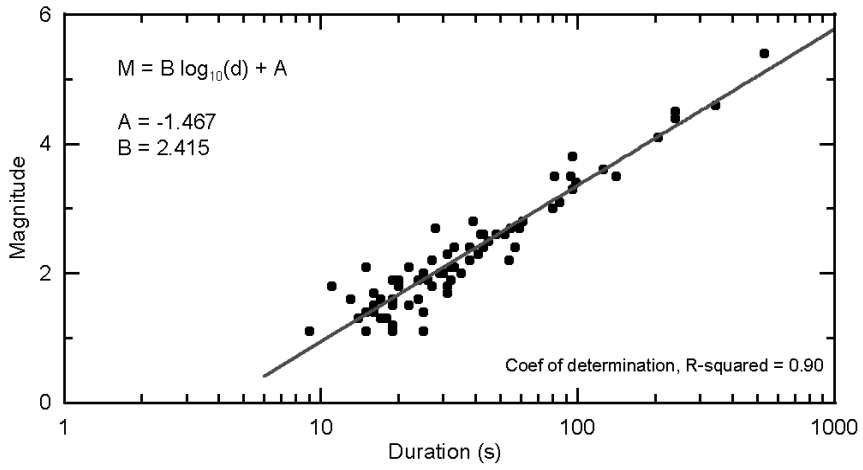

Figure 5: Empirical estimation of the A and B parameters to be used in the magnitude calculation formula.

3.3 Latest regional seismicity

Fig. 6 shows the regional seismicity from August 2005 to July 2006. The events were selected by the automatic procedure and located with the refined analysis described above. These events depicts a microearthquake distribution consistent with the last years regional seismicity. Most of the seismicity is located north from the UNDERSEIS array, in the area interested by the swarms occurred in 1994 and in 1996 (see De Luca et al., 2000). The UNDERSEIS is capable for retrieving, due to its sensitivity, a consistent picture of the seismic activity along the Central Apennines, which one of the high potential

seismogenetic region of Italy. The continuous recording of signals at the UNDERSEIS is moreover able to reveal the possible existence of other signals of tectonic origin, related to the "silent" fault creeping, already discovered in the area by Crescentini et al. (1997) and to the deep tremor observations reported in the last years for several seismic active regions in the world (see Obara K., 2002; Rogers and Dragert, 2003; La Rocca et al., 2005; Nadeau and Dolenc, 2005).

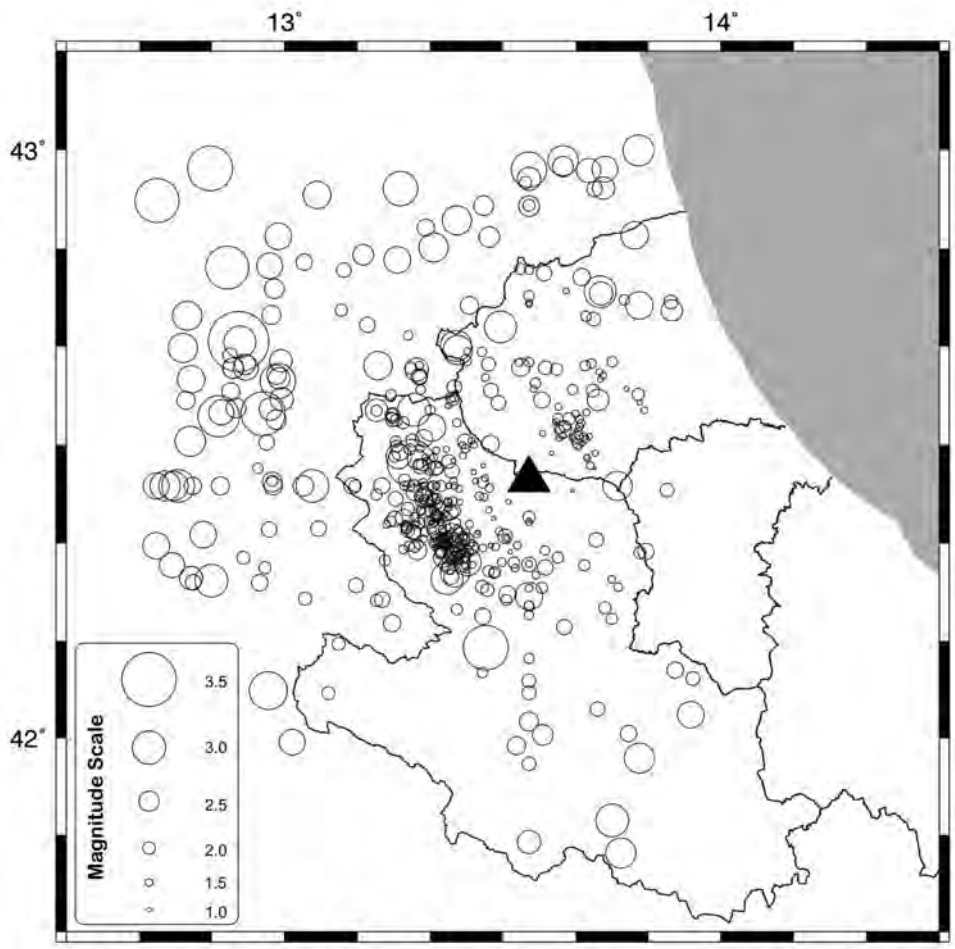

Figure 6: Local seismicity as recorded and located by UNDERSEIS array during the August 2005 - July 2006 period.

3.4 Systematic anomalies in the measurements with multichannel analysis

An interesting remark concernes the systematic character of disagreement between the azimuth angles measured with the multichannel analysis and those estimated with the

RSNC localization. In effect, the multichannel measurements show both positive and negative anomalies. The first occur for azimuths included in the range of $-40°$ and $30°$; the second occur in the range of $270°$ and $320°$. At first view, this observation can be interpreted assuming a lateral discontinuity of velocity, with NE-SW orientation. In order to verify this hypotesis, the disagreements between the azimuth angles estimated with the RSNC localizations and those expected with a simple two-dimensional earth model, where the geometry of the seismic radii have been obtained by means of Snell law, have been computed (see Fig. 7, left side). Approximately it has been verified that the shown anomalies could be explained supposing a lateral discontinuity of velocity located around 10 km NW respect of UNDERSEIS array, oriented along the NE-SW direction with an azimuth angle of $45°$, $V1 < V2$ and $\frac{V2}{V1} = 2.0$ (see Fig. 7, right side).

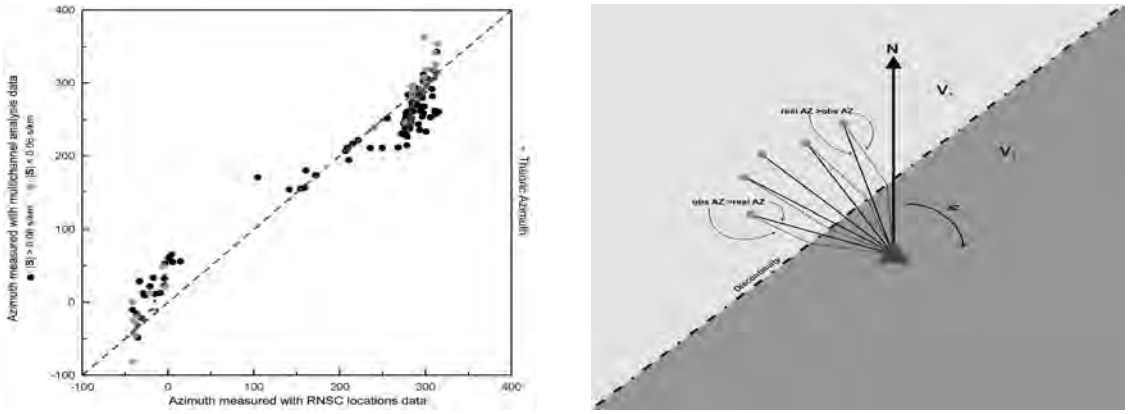

Figure 7: Disagreements between the azimuth angles estimated with the RSNC localizations and those expected with a simple two-dimensional earth model (left) and supposed lateral discontinuity of velocity (right).

3.5 Conclusions

The Gran Sasso Underground Seismic Array provides a very unique monitoring system to investigate the seismic activity of central Apennines and in particular of Gran Sasso massif and the entire region of Abruzzo. The array position inside the LNGS assures a very low detection threshold ($M = 1.0$) with a very high signal-to-noise ratio. The array can be used to depict a map of the current seismic activity, using automatic procedures. This system provides important information about the structure of seismic wave velocities nearby the array and along the seismogenetic zone. The described analysis confirmes that the Gran Sasso Underground Seismic Array resolution allows the real time analysis of middle-low intensity seismicity. These capabilities open new outlooks to define seismogenetic structures, to minutely study unhomogeneities of earth's crust and the process in extensive seismic sources.

4 Acknowledgements

The financial support from Consorzio Gran Sasso and Laboratori Nazionali del Gran Sasso made possibile the realization of the seismic array. We acknowledge E. Bellotti and E. Boschi for support and stimulation. This work has been realized in the framework of the program agreement between Istituto Nazionale di Geofisica - Osservatorio Vesuviano and Istituto Nazionale di Fisica Nucleare - Laboratori Nazionali del Gran Sasso. We aknowledge also the financial support from MIUR-PRIN2005 project $\ll$*Analisi e modellistica dei processi sismici e deformativi nell'Appennino centrale*$\gg$.

5 List of Publications

1. G. Saccorotti, B. Di Lieto, F. Tronca, C. Fischione, R. Scarpa, R. Muscente. *Performances of the UNDERground SEISmic array for the analysis of seismicity in central Italy.* Annals of Geophysics, Vol. 49, number 4/5, August/October 2006.

2. Fischione C., Tronca F., Saccorotti G., Scarpa R. *Recent seismicity in central Italy as observed by the Gran Sasso Underground Seismic Array.* EGU General Assembly 2006, Vienna, Austria, April, 2-7, 2006, EGU06-A-04310; SM1-1WE5P-0435.

3. Fischione C., Tronca F., Saccorotti G., Scarpa R. *Sismicità recente nell'Italia centrale osservata dall'antenna sismica sotterranea del Gran Sasso.* 25° Convegno Nazionale G.N.G.T.S. (Gruppo Nazionale di Geofisica della Terra Solida), Roma, Italy, November, 28-30, 2006.

References

[1] Agnew D. C., 1986. *Strainmeters and tiltmeters.* Rev. Geophys. 24, 579-624.

[2] Aki K. and Richards P., 1980. *Quantitative seismology: Theory and methods.* Freeman, San Francisco, California, 932 pp.

[3] Aki K., Christoffersson A. and Husebye E. S., 1977. *Determination of the three dimensional seismic structure of the lithosphere.* J. Geophys. Res. 82, 277-296.

[4] Benioff H., 1935. *A linear strain seismographs.* Bull. Seism. Soc. Am. 25, 283-309.

[5] Bolt B. A., 1976. *Nuclear explosions and earthquakes. The parted veil.* Freeman, San Francisco.

[6] Capon J., 1969. *High resolution frequency-wavenumber spectrum analysis.* Proc. IEEE 57, 1408-1418.

[7] Chouet B., 1996. *New methods and future trends in seismological volcano monitoring.* In "Monitoring and mitigation of volcano hazards", R. Scarpa and R. Tilling (Eds.), Springer-Verlag, New York.

[8] Chouet B., G. Saccorotti, M. Martini, P. Dawson, G. De Luca, G. Milana and R. Scarpa (1997). *Source and path effects in the wavefields of tremar and explosions at Stromboli Volcano, Italy.* J. Geophys. Res., 102, 15,129-15,150.

[9] De Luca G., Scarpa R., Del Pezzo E. and Simini M., 1997. *Shallow structure of Mt. Vesuvius volcano, Italy, from seismic array analysis.* Geophys. Res. Lett. 24,481-484.

[10] De Luca G., Del Pezzo E., Di Luccio F., Margheriti L., Milana G. and Scarpa R., 1998. *Site response study in Abruzzo (centraI Italy): underground array versus surface stations.* J. Seismol., 2, 223-226.

[11] Farrell W. E., 1969. *A gyroscopic seismometer: measurements during the Borrego earthquake.* Bull. Seism. Soc. Am. 59, 1239-1245.

[12] Green Jr., Frosh B. A. and Romney C. F., 1965. *Principles of an experimental large aperture seismic array.* Proc. IEEE 53, 1821-1833.

[13] Kedrov O. K. and V. M. Ovtchinnikov, 1990. *An on-line analysis system for three component seismic data: method and preliminary results.* Bull. Seism. Soc. Am. 80, 2053-2071.

[14] Lee W. H. K. and Stewart S. W., 1981. *Principles and applications of microearthquake networks.* Academic Press, New York, 293 pp.

[15] Lay T. and Wallace T. C., 1995. *Modern Global Seismology.* Academic Press, New York, 517 pp.

[16] Mikkeltveit S., 1985. *A new regional array in Norway: design, work and results from analysis of data from a provisional installation, in The Vela Program.* A twenty- Five Review of Basic Research, edited by U. A. Kerr (Defence Advanced Research Project Agency), 546-553.

[17] Milana G., Barba S., Del Pezzo E. and Zambonelli E., 1996. *Site response from ambient noise measurements: new perspectives from an array study in CentraI Italy.* Bull. Seism. Soc. Am. 86, 1-9.

[18] Schmidt R. O., 1986. *Multiple emitter location and signal parameter estimation.* IEEE Trans Antennas Propagation 34, 276-280.

[19] Wielandt E., 1983. *Design principles of electronic inertial seismometers.* In H. Kanamori and E. Boschi (Eds.) "Earthquakes: Observation, Theory and Interpretation". Proc. Int. School of Phys. "E. Fermi", North Holland, Amsterdam.

[20] R. Scarpa, R. Muscente, F. Tronca, C. Fischione, P. Rotella, M. Abril, G. Alguacil, W. De Cesare, M. Martini, 2004. *UNDERSEIS - Underground Seismic Array.* Seis. Res. Lett. Vol. 75, number 4, July/August 2004.

[21] Fischione C., Martini M., Tronca F., Saccorotti G., Scarpa R., 2003, 2004, 2005. *UNDERSEIS - Underground Seismic Array.* Annual Reports, I.N.F.N., Laboratori Nazionali del Gran Sasso, Italy.

THE PIERRE AUGER COSMIC RAY OBSERVATORY

F. Arneodo[a], P.L. Ghia[a,b], A.F. Grillo[a], M. Iarlori[c], C. Macolino[c], S. Parlati[a], S. Petrera[c], V. Rizi[c], F. Salamida[c]
for the Auger Collaboration*

[a] LNGS-INFN - Italy
[b] INAF - Italy
[c] Universita' dell' Aquila - Italy

Abstract

The southern site of the Pierre Auger Cosmic Ray Observatory (PAO) is in the final part of commissioning, and already taking data as the largest cosmic ray experiment in the world, in Malargüe (Argentina).

Making profit of the experience in experiments at Gran Sasso entirely (EAS-Top) or partially (MACRO) devoted to Cosmic Ray Physics, a group from Gran Sasso/L' Aquila University is part of PAO with responsibilities both in the experiment set-up and monitoring, as well as in the analysis. The status of the experiment and of the Gran Sasso/L' Aquila group is here reported.

1 Introduction

The Pierre Auger Observatory has been designed to study ultra high energy cosmic rays with unprecedented statistics and to solve the cosmic ray puzzle. In fact, after about 100 years from their discovery, cosmic rays have not yet lost their interest as there are still open questions: sources, acceleration mechanisms, propagation and composition, especially for the energies around 10^{20}eV. At these energies, cosmic rays are expected to interact with the cosmic microwave background, and lose their energy. This effect, known as the *"GZK cutoff"*, limits the maximum distance the ultra high energy cosmic rays can traverse to about 50 Mpc.

The Observatory consists of two twin sites, one in each hemisphere, in order to reach a full sky coverage. The locations are Malargüe in Mendoza province (Argentina) and Lamar in Colorado (USA), respectively for the southern and northern sites. Each site will be instrumented with an array of surface detectors overlooked by a group of fluorescence

*The complete author list of the Pierre Auger Observatory can be found at http://www.auger.org/admin/ICRC_2005_Author_List.pdf

telescopes. The Auger Observatory is the first Hybrid detector employing two different techniques (charged particles at surface and fluorescence light emitted in the atmosphere) to observe Extensive Air Showers (EAS); the hybrid detection technique provides the most powerful way to control the systematic uncertainties in the determination of energy scale and arrival directions.
The surface array is similar to the Haverah Park one that operated for twenty years[1]. The fluorescence detector is similar to the one used for the first time in the Fly's Eye experiment[2]. Both fluorescence and array detectors are able to measure primary energy, mass and arrival direction.
The ground array measures the lateral and temporal distribution of shower particles at ground level, while the fluorescence detector follows the entire shower development in the atmosphere.
Southern Auger site is located in Pampa Amarilla (Argentina) at about 1400 m a.s.l. spread over a 3000 km^2 area, between latitudes from 35.0° to 35.3° S and longitudes from 68.9° and 69.4° W. This area is being instrumented with 1600 water Čerenkov tanks spaced 1.5 km and 4 fluorescence "eyes" overlooking the array. Each eye is composed of 6 telescopes, each one with a field of view of 30°x30°; telescopes have been settled in such a way that they overlook the entire area occupied by the Surface Array.
The main characteristics of the experiment are:

great aperture: its large detection area permits to detect in one year about 6000 events with energy above $10^{19}eV$ and about 60 events above $10^{20}eV$, so that a very large statistics can be obtained

total sky coverage: with two observatories, in both hemispheres, large scale anisotropies can be determined

hybrid technique: both detection techniques minimize uncertainties in the EAS energy and geometrical parameters determination

Pierre Auger Observatory will be soon able to solve the major questions about high energy cosmic rays such as:

- the energy spectrum in the region of the GZK cutoff
- observation of possible compact sources of the high energy cosmic rays
- possibly estimation of the intergalactic magnetic field
- large and small scale anisotropies
- mass composition in the region of GZK cutoff
- high-energy neutrino interactions in atmosphere

The Gran Sasso/L'Aquila group is active both in the management of the experiment, both concerning the surface (SD) and fluorescence (FD) detectors, as well as in the analysis of the data. In particular we can indicate the following activities:

- monitoring of the efficiencies of the SD and computation of the acceptance in various trigger conditions.
- Study of the Hybrid (*i.e.* SD+FD) aperture and energy spectrum.
- Monitoring of the atmospheric transparency (in particular the aereosol content) through the use of a dedicated Raman LIDAR, entirely built in collaboration from Gran Sasso and L' Aquila.

The group, in collaboration with the Computer Group at LNGS and the Lecce Auger group, takes care of the national Auger Computing Cluster, and collaborates with the LNGS theoretical group, in particular V. Berezinsky and R. Aloisio.

2 The water Cherenkov detector

The Pierre Auger Observatory surface detector (SD) array samples the shower particles at the ground level by 1600 Cherenkov water tanks (1.2 m. height and 10 m^2 cross section) having a 1500 m. spacing between each other. The shower particles at the ground level are mainly γ's, electrons and muons with mean energies below 10 MeV for γ's and electrons and 1 GeV for muons. When impinging on the water tanks, electrons and muons emit Cherenkov radiation. The γ rays are converted by Compton scattering and pair production into relativistic electrons similarly emitting Cherenkov radiation. The produced light is detected by three large 9" photomultiplier tubes (Photonis XP1805/D1 PMT) viewing the water tank from the top. The shower front extends typically over several microseconds and its intensity varies strongly as a function of the distance from the shower core. In order to reconstruct the shower, the signals from different detectors are to be correlated in time. Information on the nature of incident particles has to be extracted from the signal shape and the energy is inferred from the signal density at about 1000 m. from the shower core. A local intelligence is required for trigger, data acquisition and monitoring. Moreover, the electronics is powered by solar energy limited to 10 W per detector station, it is implemented in a non-laboratory environment, and it has to be reliable over 20 years. Following these requirements, the PMT signals are processed and digitized locally before being sent to the central data acquisition system (CDAS) hosted in Pierre Auger Observatory main building.

Each detector station has a two level trigger, memory buffers for temporary data storage and a slow control module for monitoring. The time information is obtained from the Global Positioning Satellite (GPS) system.

Figure 1: The XP1805/D1 photomultiplier and the dedicated two outputs, last dynode amplified base.

This local software processing is performed by the station micro-controller.
The amount of light registered by each tube varies from a few photoelectrons, for tanks

far away from the shower core, to more than 10^5 photoelectrons for tanks close to the core. In order to fully cover this large dynamic range (15bit), a PMT base with two outputs, anode and amplified last dynode (A=32), has been developed.

2.1 Shifts, maintenance and commissioning

Significative contributions from our local group are related to SD detectors calibration and monitoring, muon decay investigation, saturated signal recovery and detector response. Our local group is also involved in the deployment and maintenance shifts of the SD, beside the commissioning of the deployed detectors:

- Deployment: this means to coordinate and participate to the installation of the detectors. The key step is the installation of the electronics kits on each SD tank. The operation is, on the average, quite straightforward, and in normal conditions can be carried out routinely by the Malarg¨ue local technical staff. Nevertheless some grade of control must be kept by the scientist on shift, in order to choose the better order of deployment and to check on the routine operations, whose minimal error can be source of big troubles in the future.

- Maintenance. This means to "cure" the occasional troubles of detector in the field. Normally the troubles can be cured with the replacement of one PMT or the electronics, but such operations, although simple in themselves, must be kept to a minimum, in order not to overload the local technical staff and not to interfere with the DAQ. Therefore a strict diagnostic and intervention planning is mandatory. We have set up a web accessible database which keeps track of all the failures or problems of the detectors in the field and of their behavior after the intervention. This instrument is precious for the shifter(s) and allows a quick overview of the current problems and an easy planning of the interventions. Moreover, we are testing hardware and software which can help the work on the array, easing the navigation in the field. Namely, we are testing a PocketPC, military standards, equipped with Windows Mobile, a GPS receiver and the OziExplorer navigation software. The memory of this device can easily accomodate for the detailed map of the entire experiment (1600 waypoints!), allowing the staff on shift to reach any part of the field, and with the possibility of keeping in memory also the output of the failures database. We also started investigating the possibility to interface directly the PocketPC with the "Local Station" (the PowerPC CPU onboard the SD, runing OS9), in order to use this device also for the installation and quick diagnostic of the SD electronics.

- Commissioning. Our local group, in collaboration with the IPNO (France) one has been involved in the commissioning of SD stations from the point of view of the PMTs and related electronics. The commissioning of the stations (PMTSs) must indeed be seen as a process of authorization to perform a defined duty or task. Once a tank (PMT) is commissioned it means that it is in fit condition for use, and can be used safely for trigger, signal measurement, and event reconstruction. We have thus identified tank (PMTs) parameters and criteria to apply, which beside allowing the debugging of each station and each PMT, will provide quality cuts to be applied on

each tank (PMT), in a certain period of data taking. The parameters of interest are for examples the mean values and the dispersion of the dynode and anode baselines for each PMT, of the local station triggers, of the muon peak and area. In general, the distribution of the mean values (over a certain period) of these parameters will allow us to set tolerances, the individual mean values themselves will allow us to identify problematic tanks (PMTs), while the dispersion of the parameters will give us hints on the tank (PMT) stability. A systematic study on all the tanks taking data in the field is on-going.

2.2 Triggers and acceptance

- The trigger. The local group, in collaboration with the Torino one, has given important contributions to one of the main analysis tasks, namely the definition of the triggers of the surface detector and the calculation of the associated aperture [1, 2, 3]. This involves defining different levels of triggers, forming a hierarchy including i) two triggers at the single tank level (T1 and T2), ii) one online trigger at the global observatory level (T3), iii) an offline trigger selecting real physical events (i.e. real cosmic-ray-induced showers) and thus rejecting the background (T4), and iv) a final offline trigger selecting high-quality events, ensuring an accurate reconstruction of the parameters of the incident particle.
  Within this frame, our group has had the responsability of the analysis task related to event selection, where significant efforts were made to define the trigger chain that would be best adapted to the precise measurement of the cosmic-ray energy spectrum and angular distribution at ultra-high energy. By introducing a Time-over-Threshold (ToT) trigger at the T2 level, we were able to characterize extensive air showers of energies as low as a few 10^{17} eV, with almost perfect rejection of the background. A coincidence of 3 tanks passing the ToT trigger was indeed shown to guarantee that the signal is associated with a real shower (T4 level), and this criterion was even found to be a sufficient and necessary condition applicable to all showers that can be reconstructed by the Auger detector, at zenith angles lower than 60°. This important contribution has made possible for the Pierre Auger surface detector to decrease dramatically the energy threshold with respect to the original proposal, thus allowing the study of cosmic rays not only at the highest observed energies but also in the interesting energy region around 10^{18} eV, where the transition between galactic and extra-galactic primaries is expected.
  In addition to providing a clear identification of the events of interest, the above-mentioned criterion of space-time coincidence of 3 ToT triggers also allows one to use a simple, reliable method to calculate the acceptance of the surface array as a function of the energy and arrival direction of the incoming particle. This is obtained from a simple tool that was introduced by the IPN-Orsay group (Paris), in close collaboration with our group, namely the Lateral Trigger Probability, or LTP function, giving the trigger probability of a given tank as a function of its distance to the shower core.

By simple statistics one can then identify the shower core positions on the ground that lead to a non-zero probability of detection, and by simple integration over the array surface, one obtains the effective detection area as a function of energy, zenith angle and particle type. Fig.2 shows the detection efficiency as a function of energy obtained by integration on angles (from 0 to 60 for iron and proton primary. A further integration over angles gives the instantaneous aperture of the whole array, which finally gives the global exposure achieved by the detector over a given period of time, taking into account its continuous growth as well as occasional tank or system failures.

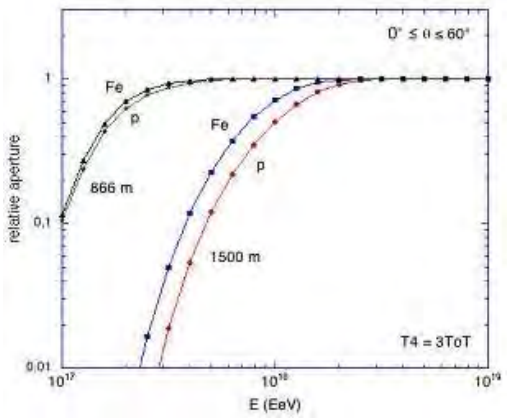

Figure 2: Detection efficiency as a function of energy.

- The acceptance. At full trigger efficiency (i.e., above 3 10^{18} eV), the aperture of the surface detector is purely geometrical. The choice of a quality trigger (T5) based on strict hexagons (i.e., the highest-signal station must be surrounded by a full hexagon of working tanks), allows us to simply exploit the regularity of the array: the aperture of any array configuration is obtained as a multiple of the aperture of the elemental hexagon cell ($a_{cell} = 4.59$ km^2 sr, for $\theta < 60°$).
  To calculate the integrated exposure over a given period of time, one finally has to count the number of cell-seconds. The array configuration changes occasionally: these changes are monitored second by second. For each new configuration the number of elemental hexagons, N_{cell}, is computed and the exposure incremented by $N_{cell} \cdot a_{cell} \cdot \Delta t$, where Δt is the duration of the configuration. These informations however are based on the performances of the individual stations only, and not on the status of the data taking: to take into account dead times (hidden or not) our group, in collaboration with the CBPF one , has studied an empirical method based on the study of the distribution in the arrival times of the events, under the reasonable hypothesis that they follow a Poisson distribution. The output of this study is a list of "bad" periods (i.e., those not to be used both in the determination of the number of observed events and in the computation of the exposure) which are now officially used by the collaboration.

3 Amospheric Monitoring: the Raman Lidar

Primary cosmic ray energy determination, from the fluorescence detector data, is possible if the right number of fluorescence photons produced by the shower particles is known, so that the determination of the fluorescence light transmission in the atmosphere becomes

necessary. For this purpose, many atmospheric monitoring apparatuses have been employed on the Surface Array area and in particular the Raman Lidar (LIght Detection And Ranging). It is able to retrieve the parameter which is directly involved in the description of the light transmission in air, due to aerosols, defined as:

$$VAOD(r; r_0) = \int_{r_0}^{r} \alpha_{aer}(r\prime)dr\prime \tag{1}$$

where $\alpha(r)$ is the atmospheric extinction coefficient and so VAOD(r) represents minus the natural logarithm of the transmission due to aerosols in the range interval between r and r$\prime$.
Raman Lidar technique is based upon the detection of backscattered photons from the atmosphere by Raman scattering, that is at a different wavelength from the incident radiation[[5]].
The equation which describes the number of photons detected is:

$$N(\lambda_0, r) = \frac{K}{r^2} \cdot OV(r) \cdot N_0^{\lambda_0} T_{mol}^{\lambda_0}(r) T_{aer}^{\lambda_0}(r) T_{abs}^{\lambda_0}(r) [\beta_{Raman}] \frac{d\Omega}{4\pi} T_{mol}^{\lambda_i}(r) T_{aer}^{\lambda_i}(r) T_{abs}^{\lambda_i}(r) \tag{2}$$

A great advantage of the Raman technique respect to other atmospheric monitoring systems is the fact that the number of photons detected doesn't depend from the aerosol backscattering term, so that in principle no assumption has to be made.
The Raman Lidar system has been updated during March 2006, with the goal of optimizing the laser operations and for a better performance of the Raman Lidar vertical sounding at short range. In particular a new telescope has been installed and the laser was placed inside the lidar shelter, with a steering mirror which deviates vertically the beam through an optical window(see figure 3).

Figure 3: The present Raman Lidar telescope on the top of the Lidar shelter in Los Leones and the new laser configuration inside the shelter, firing to the steering mirror.

The system is formed by a transmitter, a receiver and a detector box. The transmitter is a Nd:YAG laser which fires at 355 nm, at the frequency of 20 Hz and energy about

10 mJ; the receiver is constituted by a telescope which points to the zenith, with a parabolic mirror of 50 cm diameter and 150 cm focal length. Backscattered light from the atmosphere is detected from the telescope and reflected into a optical fiber which ends into the detector box. Detector box was equipped with three photomultipliers, so that Rayleigh and Raman (N_2 at 374 nm and O_2 at 387 nm) backscattered photons are detected separately.
The Raman cross section is $\approx$ 4orders of magnitude smaller than the elastic (rayleigh) one. Therefore the laser has to be operated at a power too large for the FD, and as a consequence, Raman DAQ is performed 40 min before and 20 minutes afterthe staring of the fluorescence detector acquisition. Data are analyzed on line and stored remotely in the Gran Sasso Laboratory Auger cluster, where an offline analysis is authomatically performed.[4]. We perform an analysis of Raman data in order to calculate values of VAOD(r) at r=3 km, because it is the range value at which VAOD(r) is expected to become constant bacause it is assumed that above 3 km no more aerosol are present in the atmosphere. Nights with values of VAOD(3 km) less than 0.05 are considered as "clear atmosphere nights".
Up to now we have followed two directions for the analysis. One is the traditional VAOD computation from the Nitrogen channel (a few VAOD curves are enclose, see figure 4). VAOD estimation is obtained from

$$T_{aer} = exp[-VAOD(r)] \tag{3}$$

where T_{aer} is the aerosol transmission, obtained from the detected signal $S^{\lambda}(r)$ as

$$ln(T^{\lambda}_{aer}(r)) = ln\frac{S^{\lambda}(r)r^2}{2 \cdot K \cdot OV(r) \cdot \beta^{\lambda_i}_{Raman}(r) \cdot T^2_{mol,\lambda_0}(\frac{\lambda_0}{\lambda})^4(\frac{\lambda}{\lambda_0})^q} \tag{4}$$

In principle the value of the esponent q can be retrieved if both Raman signal (from

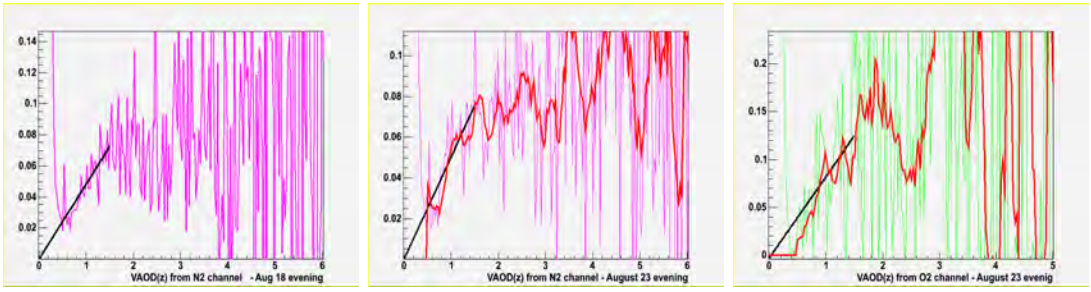

Figure 4: VAOD curves obtained from the nitrogen channel and the oxigen channel(the last one). The Oxigen channel contains much more noise than the other one, so VAOD retrieval is much more affected by errors.

N_2 and O_2) are considered; this value, in fact, describes the scaling of the Raman transmission with wavelenght. Anyway in our analysis we made the assumption for q=1 and considered only the nitrogen scattered photons. The signal detected is multiplied by the

range squared and then divided by the molecular density and the Rayleigh cross section at scattering angle of 180°. What we obtain is, therefore, the aerosol transmission multiplied by an unknown constant represented by the product of the detector efficiencies, the Raman backscattering cross section and the nitrogen percentage in air. This multiplicative constant can be removed imposing that VAOD(0)=0 where we consider tha range 0 as the corresponding altitude of the Raman Lidar site. The second direction uses the so-

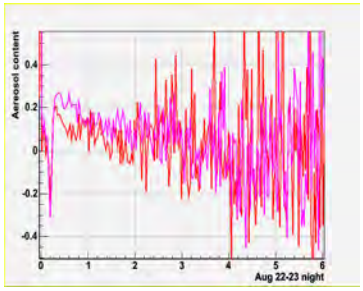

Figure 5: Backscatter Ratio obtained for the night of August, 22nd(red line) and 23rd(rose line).

called Backscatter Ratio, namely the ratio of the elastic/nitrogen channels, corrected for (small) atmospheric effects. In this quantity instrumental effects such as an incomplete overlap, misalignment,defocusing, etc. largely cancel. The BSR properly normalized is proportional to the aerosol content in the Planetary Boundary Layer: comparing data taken in different moments it is easy to follow the evolution of the PBL, as reported in figure5.

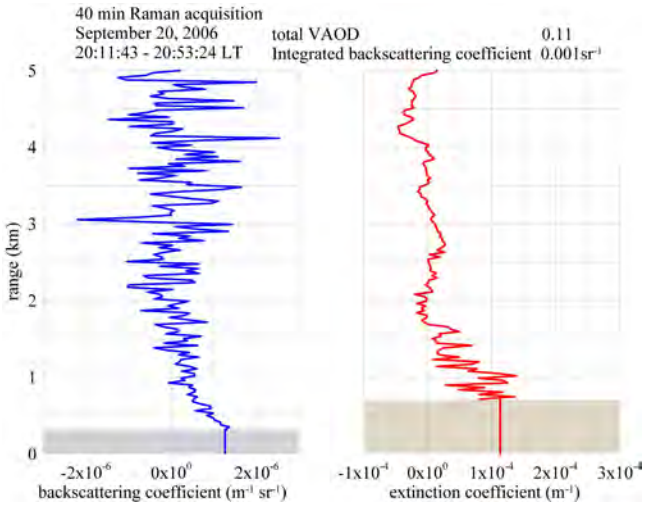

Figure 6: The aerosol extinction coeffcient from the N_2 signal on the left and the backscatter coefficient from the backscatter ratio of N_2/elastic signal.

A complete comparison of the results from the elastic and inelastic nitrogen channels

is reported (as an example for the evening of September 20, 2006), fig.6. Comparing α and β, it is possible to speculate about the typical dimension of the aerosols, lower α/β ratio means larger aerosols; looking at the structure of the α and β vertical profiles one can have an idea of the vertical extent of the Planetary Boundary Layer and for this case il lasts up to about 1.5 km above the Lidar site (the shaded areas indicate a range of altitudes inaccessible to the Lidar sounding:not full optical overlap between laser and receiver telescope). This analysis will be easily implemented as a routinely feature.

4 Hybrid Detector Aperture

Aperture is an important piece for the cosmic ray flux calculation. The flux of cosmic rays J as a function of energy is defined as:

$$J(E) \;=\; \frac{1}{\Delta E}\frac{N^D(E)}{\mathcal{A}(E)T}; \tag{5}$$

where $N^D(E)$ is the number of detected in the energy bin E, $A(E)$ is the energy dependent aperture of the detector, T is the is the total running time of the detector and ΔE is the width of the energy bin E. The product $\mathcal{A}(E)T$ is usually referred to as the exposure, $\mathcal{E}(E)$.

The aperture in eq.5 can be expressed as:

$$\mathcal{A}(E) = \int_\Omega \int_{A_{gen}} \varepsilon \mathrm{d}S\ \cos\theta\ \mathrm{d}\Omega = \int_\Omega S_{eff}\ \mathrm{d}\Omega; \tag{6}$$

where $\mathrm{d}\Omega = \sin\theta \mathrm{d}\theta \mathrm{d}\phi$ and Ω are respectively the differential and total solid angles. ϕ goes from 0 to 2π and θ from 0 to a maximum angle, usually around 60°. More inclined showers ($\theta > 60^\circ$) need to be treated separately, as the Earth curvature influence the event reconstruction efficiency[6].

The detection efficiency ε is the product of the trigger efficiency ε_{trg} and reconstruction efficiency ε_{rec}:

$$\varepsilon_{trg} \times \varepsilon_{rec}; \tag{7}$$

where ε_{trg} is the ratio between triggered events and the number of showers hitting the ground and ε_{rec} is the ratio between reconstructed events and triggered showers including the analysis cuts needed to prevent reconstruction failures.

Using the equation 6 to express the aperture and assuming negligible the dependence of trigger efficiency on angles, we obtain:

$$\mathcal{A}(E) \;=\; \pi(1-\cos^2\theta_{max})\ \overline{S}_{eff}; \tag{8}$$

For $\theta_{max} = 60^\circ$, $\pi(1-\cos^2\theta_{max}) \;\simeq\; 2.36\ sr$ and $\overline{S}_{eff}$ is the effective area averaged over solid angle. Obviously the aperture energy dependence is entirely derived from $\overline{S}_{eff}$.

4.1 Aperture and Exposure Calculation

In Auger the aperture calculation is obtained generating simulation data sets and calculating, for each core position of the shower, the ratio of triggered to generated events. Each simulation data set depends on many parameters: energy and mass of the primary and atmospheric parameters.

The main dependence of aperture is energy; the mass and atmosphere are considered as secondary parameters to compare the apertures with different values of these parameters (e.g. proton and iron nuclei, typical "clean" and "dirty" atmospheres).

Since hybrid aperture is concerned, we have to keep in mind that, for a given simulation data set, the aperture value is affected by the actual SD and FD configurations. The aperture at a given time, that is at a given detector configuration, is the so called "instantaneous hybrid aperture".

The SD configuration is mainly determined by the actual list of "active" stations. It depends on the current status of the stations in the field as well as on their DAQ status. The FD status depends primarily on the telescope optical configurations: these are changing since new hardware is added during construction (e.g new telescopes, new corrector ring lenses), but also since these can change for hardware failures and/or controls (e.g Moon or lightnings in the field of view). As detector change, also the trigger response changes and consequently also the instantaneous aperture should be recalculated.

However if the detector configurations changes, the cosmic ray flux given in (5) has to be rewritten as:

$$J(E) \;=\; \frac{1}{\Delta E}\frac{1}{n}\sum_{i=1}^{n}\frac{N_i^D}{\mathcal{A}_i(E)\Delta T_i}; \tag{9}$$

where the index i labels the different configurations (n in total), $\mathcal{A}_i(E)$ is the aperture of the detector and ΔT_i is the running time of the detector in the ith configuration.

In Auger the SD configurations are continously changing following the actual list of "active" tanks, but they are easy to be handled, since the response of each tank affects a small region (of the order of 1 km^2) around its position and this reflects directly onto the local trigger efficiency. On the contrary, a change of the FD configuration reflects on a wide region and then one needs the evaluation of the whole trigger efficiency map for each configuration occurring during data taking. Moreover the calculation of the whole detector aperture, requires the concurrence of maps from different eyes for all the occurring combinations.

The Fluorescence detector in its final status is composed by $N = 6 \times 4$ independent telescopes. Since each telescope has three possible status (0, 1 or 2) the number of possible configurations is $4{\times}3^6 = 2916$.

From our analysis[7] we evaluated the number of different optical configurations, actually occurring: they are about 150 for each eye[1]. They are obviously much less than the maximum, but the number is still very high. In principle the aperture of the detector should be evaluated, through a dedicated simulation, for each of them.

[1]In the period from 25 September 2003 up to 3 May 2006: 160 for Los Leones, 152 for Los Morados and 130 for Coihueco.

However we can notice that the value of the flux in each configuration is an independent measure of the same physical quantity. Thus the flux $J(E)$ can be calculated as the weighted mean of fluxes in the various configurations. Using the exposure $\mathcal{E}_i(E) = \mathcal{A}_i(E)\Delta T_i$ as the i-th weight we obtain:

$$\overline{J}(E) \;=\; \frac{\sum_{i=1}^{n} J_i(E)\;\mathcal{E}_i(E)}{\sum_{i=1}^{n}\mathcal{E}_i(E)} = \frac{1}{\Delta E}\frac{\sum_{i=1}^{n} N_i^D}{\sum_{i=1}^{n}\mathcal{E}_i(E)} = \frac{1}{\Delta E}\frac{N^D}{\mathcal{E}(E)} \tag{10}$$

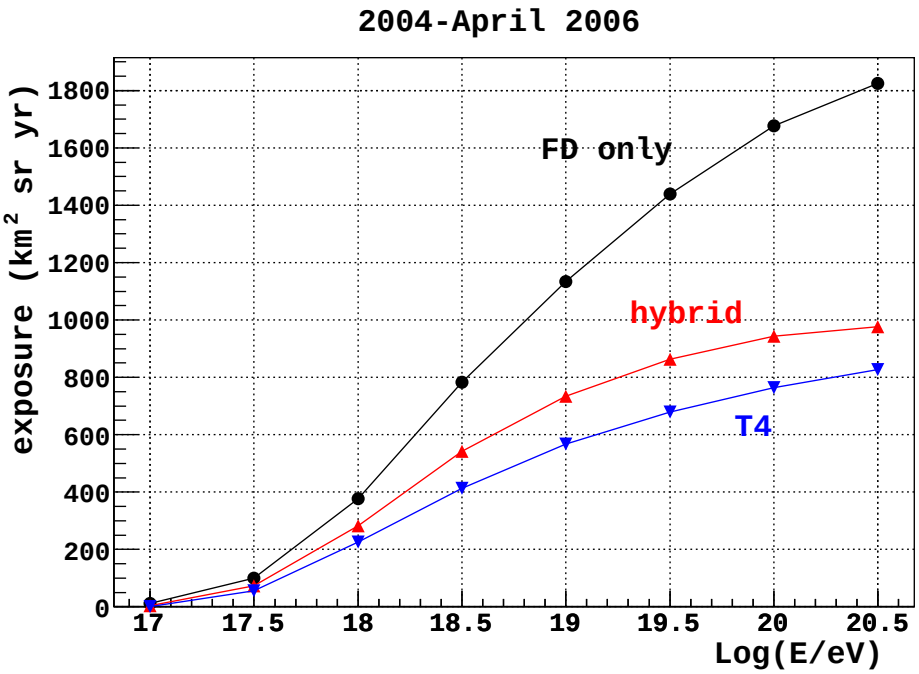

Figure 7: Exposure $\mathcal{E}$ as a function of energy in the range 10^{17} eV and $10^{20.5}$ eV for three trigger levels: "FD only" (black circles), "hybrid" (red upward triangles) and "Reconstruction" (blue downward triangles). It has been calculated considering the period between January 2004 and April 2006.

Therefore to calculate the flux at a given energy one should know the overall exposure at that energy as a sum of the individual exposures at the different time intervals ΔT_i.

On the other hand, if we call $\overline{\mathcal{A}}(E)$ the average aperture in a solar time interval ΔT including all the previous "active" periods ΔT_i, we have for the exposure:

$$\mathcal{E}(E) \;=\; \sum_{i=1}^{n}\mathcal{A}_i(E)\Delta T_i = \overline{\mathcal{A}}(E)\Delta T. \tag{11}$$

Therefore one should simulate a sample of events which reproduces the exact conditions of the experiment (with their actual sequencing of the configurations) and evaluate

the exposure as the average aperture times the total solar time interval ("end-to-end" exposure).

In figure 7 the exposures at FD trigger, Hybrid trigger and reconstruction[8] levels are shown. The "FD-only" exposure does not correspond to any real case. It has only to be considered for reference as the maximum achievable if all SD stations would have been active in the field during the data taking period.

The value of exposure grows with time as expected. It shows a change in the slope (March 2005) due to the starting of data acquisition operations in Los Morados fluorescence building as it is clear from figure 8.

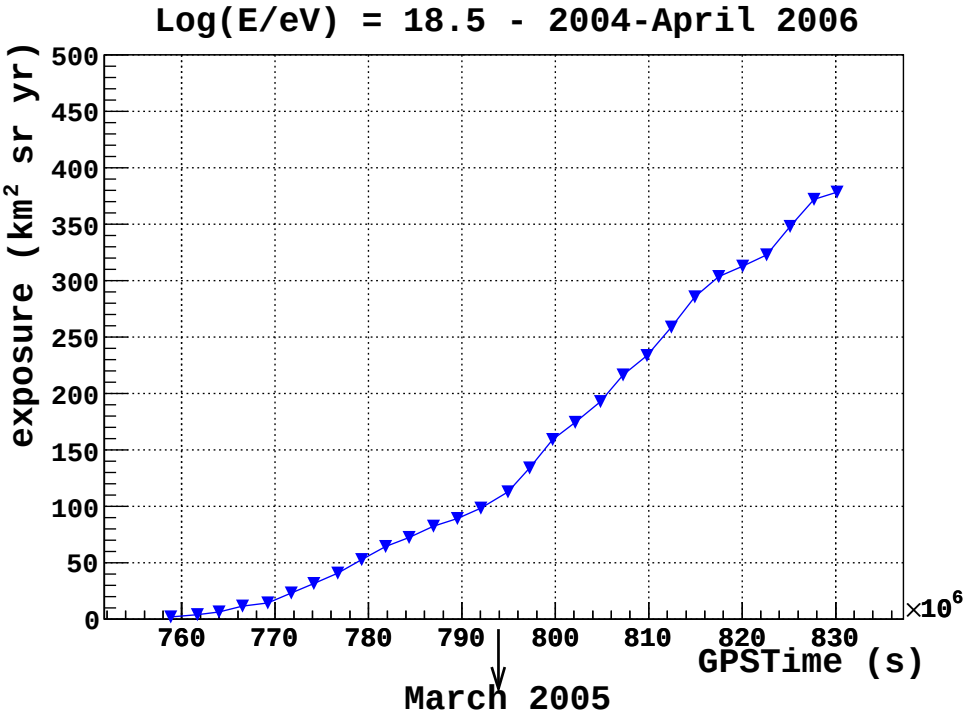

Figure 8: Reconstruction exposure as a function of time for $Log(E/eV) = 18.5$. The value of exposure grows with time as expected. The change in the slope (March 2005) is due to the starting of data acquisition operations in Los Morados fluorescence building.

5 List of Publications

1. First cosmic-ray grapes ripen in Argentina: Results and progress of the Pierre Auger Observatory. By Pierre Auger Collaboration (M. Prouza for the collaboration). 2006. 5pp. Prepared for CIPANP 2006: 9th Conference on the Intersections of Particle and Nuclear Physics, Westin Rio Mar Beach, Puerto Rico, 30 May - 3 Jun 2006. Published in AIP Conf.Proc.870:181-185,2006. Also in *Rio Grande 2006, Intersections of particle and nuclear physics* 181-185

2. Status and first results of the largest UHECR Observatory. By Pierre Auger Collaboration (E. Zas for the collaboration). 2006. Prepared for International Conference on Interconnection between High Energy Physics and Astroparticle Physics: From Colliders to Cosmic Rays, Prague, Czech Republic, 7-13 Sep 2005. Published in Czech.J.Phys.56:A231-A240,2006.

3. Physics Results of the Pierre Auger Observatory. By Pierre Auger Collaboration (Veronique Van Elewyck for the collaboration). Dec 2006. 10pp. Prepared for International School of Cosmics Ray Astrophysics (ISCRA) 15th Course: Astrophysics at Ultra-High Energies, Erice, Sicily, Italy, 20-27 Jun 2006. e-Print Archive: astro-ph/0612731

4. The Pierre Auger observatory - status and first results. By Pierre Auger Collaboration (L. Nellen for the collaboration). 2006. 11pp. Prepared for 10th Mexican Workshop on Particles and Fields, Morella, Michoacan, Mexico, 7-12 Nov 2005. Published in AIP Conf.Proc.857:100-110,2006. Also in *Morelia 2005, Particles and fields* 100-110

5. The Lidar System of the Pierre Auger Observatory. S.Y. BenZvi et al. Sep 2006. 28pp. Submitted to Nucl.Instrum.Meth.A e-Print Archive: astro-ph/0609063

6. First results from the Pierre Auger Observatory. By Pierre Auger Collaboration (Ronald C. Shellard for the collaboration). Sep 2006. 10pp. Published in Braz.J.Phys. 36:1184-1193,2006. e-Print Archive: astro-ph/0609060

7. Status and recent results of the Pierre Auger Observatory. By Pierre Auger Collaboration (Serguei Vorobiov for the collaboration). Aug 2006. 8pp. Prepared for International Cosmic Ray Workshop (ICRW Tien-Shan 2006), Almaty City, Kazakhstan, 25-27 Aug 2006. e-Print Archive: astro-ph/0608576

8. Cosmic Rays at the Highest Energies: First Data from the Pierre Auger Observatory. By Pierre Auger Collaboration (Karl-Heinz Kampert for the collaboration). Aug 2006. 13pp. Presented at International Symposium on Heavy Ion Physics 2006 (ISHIP 2006), Frankfurt, Germany, 3-6 Apr 2006. Submitted to Int.J.Mod.Phys.E e-Print Archive: astro-ph/0608136

9. The Fluorescence Detector of the Pierre Auger Observatory: A Calorimeter for UHECR. Bianca Keilhauer (Karlsruhe U., EKP & Pierre Auger Observ.) . Aug 2006. To appear in the proceedings of 12th International Conference on Calorimetry in High Energy Physics (CALOR 06), Chicago, Illinois, 5-9 Jun 2006. Published in AIP Conf.Proc.867:175-182,2006. Also in *Chicago 2006, Calorimetry in high energy physics* 175-182 e-Print Archive: astro-ph/0608074

10. Hybrid Detection of UHECR with the Pierre Auger Observatory. By Pierre Auger Collaboration (Miguel Mostafa for the collaboration). Aug 2006. Presented at Vulcano Workshop 2006: Frontier Objects in Astrophysics and Particle Physics, Vulcano, Italy, 22-27 May 2006. e-Print Archive: astro-ph/0608005

11. Propagation and distribution on the sky of the ultra high energy cosmic rays within the Pierre Auger Observatory. (In French) Eric Armengaud (Paris U. VII, APC) . May 2006. 220pp. Ph.D.Thesis.

12. Extracting first science measurements from the southern detector of the Pierre Auger observatory. By PIERRE AUGER Collaboration and Lawrence Wiencke Pierre Auger Collaboration (Lawrence Wiencke for the collaboration). Jul 2006. 4pp. To appear in the proceedings of 10th Pisa Meeting on Advanced Detectors: Frontier Detectors for Frontier Physics, La Biodola, Elba, Italy, 21-27 May 2006. e-Print Archive: astro-ph/0607449

13. 16-point discrete Fourier transform based on the Radix-2 FFT algorithm implemented into cyclone FPGA as the UHECR trigger for horizontal air showers in the Pierre Auger Observatory. Z. Szadkowski (Wuppertal U.) . 2006. 8pp. Published in Nucl.Instrum.Meth.A560:309-316,2006.

14. Measuring the lateral distribution of extended air showers with data from the surface detector and hybrid data of the Pierre Auger Observatory. (In German) Talianna Schmidt (Karlsruhe, Forschungszentrum) . FZKA-7231, Jun 2006. 86pp.

15. Enhancing the Pierre Auger Observatory to the 10**17 to 10**18.5-eV Range: Capabilities of an Infill Surface Array. M.C. Medina (CNEA, Buenos Aires) , M.Gomez Berisso, I. Allekotte (Centro Atomico Bariloche) , A. Etchegoyen (CNEA, Buenos Aires) , G.Medina Tanco (Mexico U., ICN) , A.D. Supanitsky (CNEA, Buenos Aires) . Jul 2006. 21pp. Published in Nucl.Instrum.Meth.A566:302-311,2006. e-Print Archive: astro-ph/0607115

16. Recent results from the Pierre Auger Observatory. By AUGER Collaboration (Andreas Zech for the collaboration). May 2006. 6pp. To appear in the proceedings of 41st Rencontres de Moriond on Electroweak Interactions and Unified Theories, La Thuile, Aosta Valley, Italy, 11-18 Mar 2006. e-Print Archive: astro-ph/0605344

17. Status of the Southern Pierre Auger observatory. By Auger Collaboration (M. Kleifges for the collaboration). 2006. 5pp. Prepared for 9th Topical Seminar on Innovative Particle and Radiation Detectors (Siena 2004), Siena, Italy, 23-26 May 2004. Published in Nucl.Phys.Proc.Suppl.150:181-185,2006. Also in *Siena 2004, Innovative particle and radiation detectors* 181-185

18. The first scientific results from the pierre auger observatory. By Pierre Auger Collaboration (Tokonatsu Yamamoto for the collaboration). Jan 2006. 4pp. To appear in the proceedings of Particles and Nuclei International Conference (PANIC 05), Santa Fe, New Mexico, 24-28 Oct 2005. Published in AIP Conf.Proc.842:1016-1018,2006. Also in *Santa Fe 2005, Particles and nuclei* 1016-1018 e-Print Archive: astro-ph/0601035

References

[1] E. Armengaud, P. Ghia, C. Lachaud *Study of the Auger SD event rate stability and (T,P) modulations*, GAP note 2006-028

[2] Carla Bonifazi and Piera Luisa Ghia *Selection of data periods and calculation of the SD geometrical acceptance*, GAP note 2006-101

[3] I.Lhenry-Yvon, J.Aublin, P. Ghia *Using the Relative Balance of the signals of the 3 PMTS in a tank*, GAP note 2006-036

[4] V.Rizi et al.: *The Raman Lidar Receiver at Pierre Auger Observatory:Installation and Hardware Tests*;
Auger Tech. Note GAP-2006-015.

[5] S.Y.BenZvi et al.: *The Lidar System of the Pierre Auger Observatory*;
Sep 2006. 28pp. Submitted to Nucl.Instrum.Meth.A.

[6] P.Billoir, O.Deligny, A.Letessier-Selvon: *A Complete Procedure for the Reconstruction of Inclined Air Showers*;
Auger Tech. Note GAP-2003-003.

[7] S.Petrera, F.Salamida: *Selection of data for the Auger FD analysis: the RunSel database*;
Auger Tech. Note GAP-2007-001.

[8] S.Petrera, F.Salamida: *An end-to-end calculation of the Auger hybrid aperture*;
Auger Tech. Note GAP-2007-002.

MIDIX
Soft X-rays microradiography

A. Reale[a], G. Tomassetti[a], L. Palladino[a], A. Poma[a], A. Tucci[a] , A. Ritucci[a], L. Reale[a], T.Limongi[a], F.Flora[b], R.M.Montereali[b], A. Lai[b], L. Mancini[c] , G. Tromba[c], A.Balerna[d], G. Cinque,[d] A. Ya.Faenov[e], T..Pikuz[e], J. Kaiser[f], M.Fanelli[g], F.Ruggieri[g], M.Francucci[h], P.Gaudio[h], S.Martellucci[h], M.Richetta[h]

[a] Faculty of Science,University of l'Aquila , g.c. to LNGS-INFN,Coppito,L'Aquila,Italy
[b]Enea,UTS FIS Dip Innovazione,Settore Fisica Applicata, CRE- Frascati,Frascati,Italy
[c]Sincrotrone Trieste SpcA,strada statale 14 in Area Scientific Park,Basovizza,Trieste,Italy
[d]LNF,Laboratorio DAFNE-Luce,INFN,Frascati,Roma,Italy
[e] MISDC of VNIIFTRI , Mendeleevo, Moskow Region, Russia
[f] Institut of Physical Engineering, Brno University of Technology, Brno, Czech.Republic
[g] Dipartimento di Chimica,Ing.Chimica e Materiali, University of L'Aquila, Coppito, Aquila, Italy
[h]Dipartimento Ingegneria dell'Impresa, Università di Tor Vergata, Roma, Italy

Abstract

The aim of this experiment has been the detection by soft X-ray microradiography ,of metal accumulated in vegetal tissues and their localization in specific hyperaccumulation sites in leaves or roots.Data were collected, in absorption or phase contrast conditions and processed using dual energy analysis, that is subtracting the X ray images of the samples above and below the K,L,M absorption edges .We also compared this method to other techniques, such as simple microradiography by point-like sources as plasma laser X-ray sources or LIBS technique.

For dual energy measurements , data were collected at ELETTRA SYRMEP beamline in Trieste and at the DAFNE-LUCE X-ray beamline in Frascati . For simple absorption measurements we used the plasma laser source Hercules at ENEA and the plasma-laser source of Tor Vergata.

Because this experiment,for the first time, is reported in this 2006 LNGS Annual Report , some of the more relevant previous results are also reported .

1-Introduction

The main goal of the MIDIX experiment is the determination of the accumulation sites of metal pollutants like Cu,Cd,Pb,..in plant parts as leaves, roots, or their sections, by some X-ray imaging techniques such as dual energy X-ray differential microradiography,in phase-contrast

or absorption microradiography conditions and tomography.. The dual energy microradiography is achieved by exposing (at the right distance, according to the sample thickness , the requested magnification etc) the sample to an X-ray beam, above and below the absorption edge of the metal considered, and subtracting the two images, in order to get the contribution of the metal alone, and, looking at the differential image, to identify the sites where the metal has been accumulated in the sample.
In fact, MIDIX is an elemental microanalysis experiment, using synchrotron radiation, or other sources, to obtain microradiographies of biological samples as X-rays images at energies near the absorption edges of the polluting elements to be identified. In this way the spatial distribution of elements in the sample can be visualized, and ,in special cases, the surface density quantitatively measured.
This investigation is useful in order to control the metal pollution in plants, which can be dangerous for humans through the food chain, and also in the determination of specific bioaccumulation sites in plants, which could be selected accordingly for the phytoremediation of polluted soils.

2 - Experimental procedures

2.1 - General remarks

As we anticipated in the introduction, we performed the experiment using various X–ray sources, such as the SYRMEP beamline of ELETTRA-Trieste, where dual energy experiments were possible in direct absorption or phase contrast conditions, and the DAFNE-Luce soft X-ray beamline at the Frascati National Laboratories of INFN.
Some other measurements have been made with 'point-like' sources and getting an image of the sample, where the contrast was given by the metal concentration in the environment matrix. Thus measurements were doneusing the Hercules plasma source at CR-ENEAin Frascati or the plasma source of Tor Vergata University. Not only microradiographies were collected ; also in the spectral range of the so-called "water window" (2.3-4.4 nm) snapshot microscopic images of living samples were taken on PMMA photoresists, which were observed, after development, by the Atomic Force Microscope in L'Aquila. More recently, a novel detector developed at CR-ENEA has been utilized, (based on X-ray excitation of color centers in a LiF crystal), which presents some advantages because its high resolution and easier observation of the image.

2.2 - Measurements at the ELETTRA SYRMEP beamline

The metal which have been considered in our experiments are Cu, Pb, Ag, Cd, Mo.
Pb is a well known pollutant that represents a high health risk because of the possibility to be transferred to living organisms (and so to the food-chain) through fresh water or vegetables.
We started measurements at the SYRMEP beamline of the ELETTRA synchrotron in Trieste. The beamline provides, at a distance of about 24 m from the source, a monochromatic, laminar-section X-ray beam with a maximum area of about 160 x 6 mm^2.
The monochromator, that covers the entire angular acceptance of the beamline, is based on double Si (111) crystals working in Bragg configuration. The useful energy range is 8.3 - 35 keV. The intrinsic energy resolution of the monochromator is about $2x10^{-3}$ because of the natural divergence of the beam. Typical flux measured at the sample position at 17 keV, at 2 GeV, with a stored beam of 300 mA, is about 1.6×10^8 ph/mm^2 s.

The detector used was a water cooled CCD camera (Photonic Science X-ray Hystar, 2048 x 2024 full frame, 16 bit, pixel size = 14 µm, field of view 28 x 28 mm^2).
In the case of absorption radiography (Fig. 1), the sample is illuminated by a monochromatic hard X-ray beam, and a position-sensitive detector is set at a distance *d*, typically between a few cm and a few m from the specimen.
We report here,from already published data (see ref), some results,concerning the evidence of accumulation of Pb pollutant in the veins of leaves of Heliantus annuus treated for ten days with a solution of 10 mM PbAcetate.

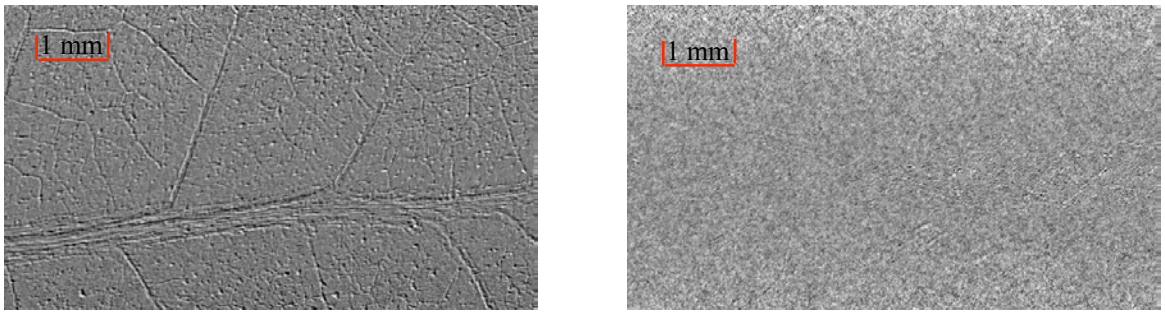

a) **b)**

Fig 1: Pb detection by dual energy (13.150 – 12.975 keV) imaging at d=168cm in *Helianthus annuus* leaf, 10 mM PbAc treated (a), compared with untreated control sample (b).

Micro-tomography planar radiographs of a root (of Dyplotaxis erucoides grown in 2% $CuSO_4$ solution) are shown in Fig.2.

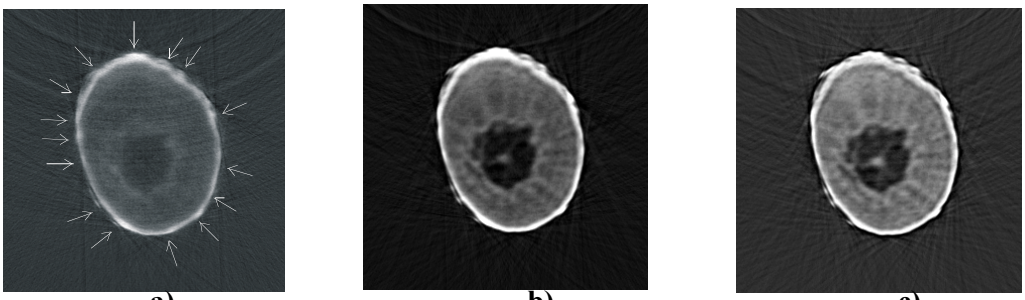

a) **b)** **c)**

Fig.2:Micro-tomography planar radiographs of a root of Dyplotaxis erucoides grown in 2% $CuSO_4$ solution. Figure a) b) and c) shows the slice image taken above and below the Cu K-edge and the difference, respectively. The white arrows indicate the location of the Cu accumulation.

Fig. 3 shows the results on the 3D reconstruction of a root of Dyplotaxis erucoides grown in 2% $CuSO_4$ solution.

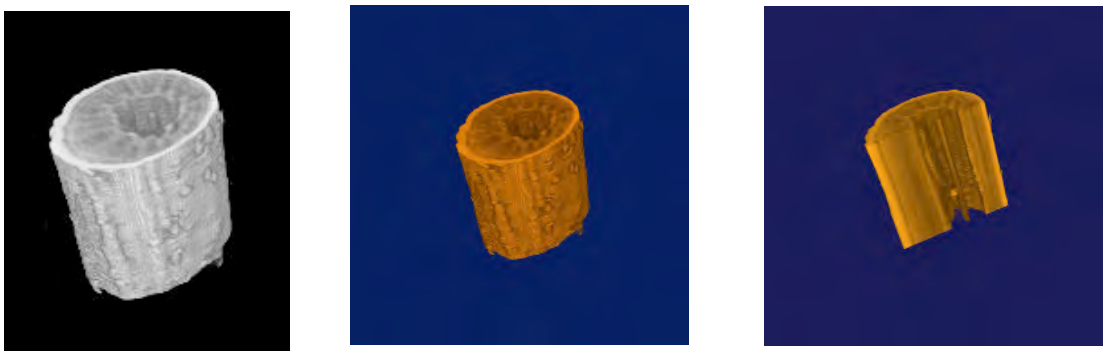

Fig. 3. 3D reconstruction of a root of Dyplotaxis erucoides grown in 2% $CuSO_4$ solution.

As an other example, on Figure 4 a few slices as the results on the tomography investigation of the root part of *Helianthus annuus* sample are presented.

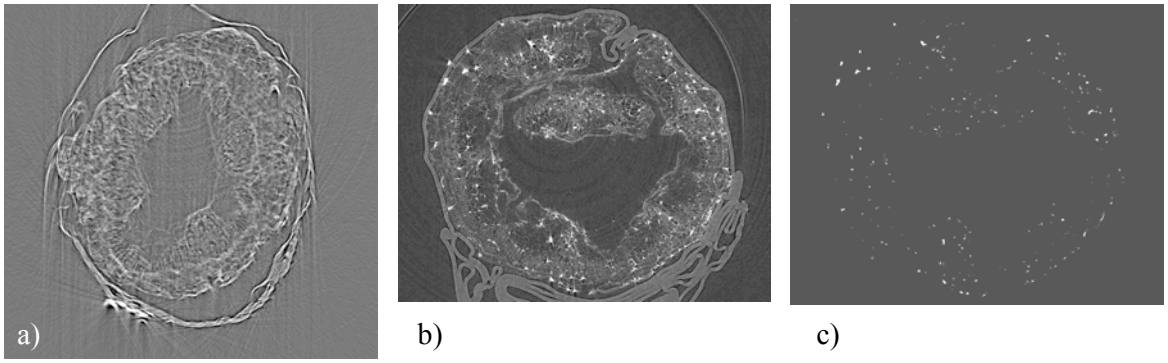

Figure 3. Slices of the Helianthus annuus root section. a) control (untreated) sample exposed to radiation of energy 13.15 keV, b) treated sample (1 day, 10 mM of PbAc) exposed to radiation of energy 13.15 keV; c) the map of the Pb deposition in this treated sample, obtained by dual energy measurements (13.15 keV – 12.975 keV).

2.3-Measurements at the DAFNE –LUCE beam line

The soft X-ray beam-line at the DAFNE storage ring uses a wiggler source and a double-crystal fixed-exit monochromator, with an useful energy range 1 - 3 keV. The DAFNE double storage ring collider for electrons and positrons in these experiments was operated with electron beam energy of 0.51 GeV and a mean electron current I >1 A. The X-ray monochromator, equipped with a pair of Ge(111) crystals, in the “boomerang” geometry was

used to ensure a fixed exit mode while scanning the whole energy range. The energy resolution of the monochromator is about 0.6 eV at 1.5 keV.
As a detector a CCD camera (Princeton Instruments, PI-SX:2048) with 2048 x 2048 imaging array and 13.5 μm x 13.5 μm pixel size was utilized. More details on the soft X-ray beamline can be found for example in (Burattini et al., 2004)
The sample studied were leaves and roots of *Zea Mais* and of *Pisum sativum* from plants grown in hydroponics culture and artificially doped with lead acetate at different concentrations.
At the age of two months the small plants were treated with three different solutions of the lead acetate, that is 0.1 mM, 1 mM and 10 mM, and also a control sample was prepared.
After the time of the treatment the leaves from either the control or the treated samples were collected, let them air-dry and kept in a paper holder.
The X-ray dual-energy microradiography was performed on the samples at the Pb M-edge and at S K-edge. The S and Pb are not present in the sample as free elements, but in molecules where they are bonded with some other elements. For mapping the distribution of these elements within the sample, it is important to measure the shift in absorption edges due these bonds.
The Pb M-edge and the S K-edge for X-ray absorption measurements were controlled, for energy calibration in transmission mode, using a $NiSO_4$ and PbAc solutions
The first utilization of the soft X-rays beamline at the DAFNE synchrotron light source for mapping the intake of sulfur and lead in vegetal tissues will be reportedin a forthcoming paper Dual-energy X-ray micro-radiography was used to investigate the natural sulfur content in dried *Zea Mais* and *Pisum sativum* leaf and root samples and to monitor the lead pollutant intake by these samples. The lead was added in controlled doses to the hydroponic medium of laboratory-controlled samples of vegetal species.
In order to prove the results obtained by the non-destructive X-ray radiography analysis at the soft X-ray beamline of DAFNE storage ring, after these measurements the lead content of the sample was determined by a standard chemical analysis utilizing AAS. The quantitative results of the chemical analysis are in good agreement with our X-ray dual-energy analysis.
Actually the limit to proceed with the experiment was in the restrictions in the use of the DAFNE-LUCE beam, only available as a parasitic use of the machine, because the storage ring was in first priority dedicated to high energy experiments. This has meant too often that a run of measurements had to be suddenly stopped, giving away the collection of data which was going on.
Because of what we said above and of the initial delay of the firm in delivering the dedicated X ray chamber planned for the MIDIX project,only recently ready, all the runs in DAFNE have been done using an auxiliary chamber and we are still processing the microradiographies that have been collected.

2.4 - X RAY microradiography using a laser plasma source

The leaf samples of similar morphology and same mass per unit of surface within a few percent (~3.8 mg/cm^2), with a controlled Cd or Pb content, were irradiated by a soft X-ray radiation produced by a laser plasma source with a cadmium or lead target, respectively. A high power table-top excimer laser (*Hercules*) has been employed to create this appropriate X-ray source. This laser, manufactured by ENEA, Frascati, is a discharge pumped XeCl system emitting

radiation at λ=380 nm from an active volume 10x5x100 cm^3. Its characteristics are detailed in Bollanti *et al*., 1990.
The visible radiation emitted by the laser created plasma was removed utilizing a 2 μm polypropylene filter coated with 0.4 μm aluminum layer. The samples with different Cd (or Pb) concentration, together with the X-ray sensitive Kodak film RAR 2492 were placed in a vacuum chamber and exposed to X-rays at the same time. The X-ray intensity at the sample position was measured by calibrated pin diode (100-PIN-125). Its value was ~140 nJ/cm^2/shot in the spectral range of 1-1.4 keV (0.8 – 1.35 nm). In order to avoid the absorption of the created radiation by the water content of the leaf, the samples were oven dried.
The gray scale levels of the scanned (CanonScan FS4000US) images were converted into optical density values using both the RAR 2492 film response curve (using Kodak standard film) in the investigated spectral range and the scanner's calibration curve. More detailed description on the detection part of the experimental set-up can be found in (Reale *et al*., 2004). From the obtained values of the optical density it is possible to derive the fluence of the radiation on the leaf sample. Using the derived fluence value and the fluence in the region out of the sample (directly on the film) one can obtain the transmission of the sample. After measuring the transmission of the control (untreated) sample, the surface density *X* (microg/cm^2) can be calculated from

$$\mu X = - \ln T$$

where *T* is the ratio of the transmission of the treated sample with respect to the control sample and μ is the mass absorption coefficient in cm^2/g at the central energy value of the spectrum. The values of μ used in our calculation (at 1.2 keV) were 4050 cm^2/g and 5200 cm^2/g for Pb and Cd, respectively.
Figure 1 shows some typical examples of the microradiographs obtained for Cd and Pb doped leaves. The plant on image Ctrl is the control sample (without treatment). The a), b), c) images represent the treatment with different concentrations of contaminants: 1 mM, 5 mM and 10 mM, respectively. All samples in Fig.1 were grown for ten days in hydroponics solution. On Fig.1 the significant differences on the images of untreated and treated samples are clearly observable.

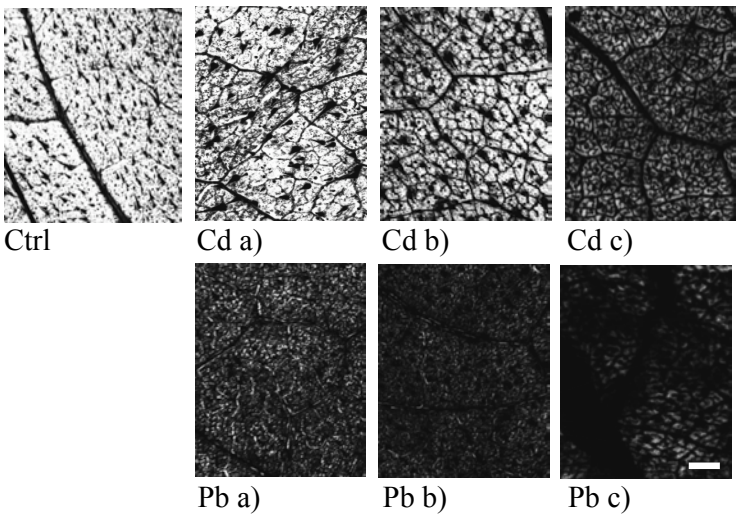

Figure 1. Radiographic images of control (Ctrl) and of 10 days Cd or Pb treated *Helianthus annuus* samples with different concentration of contaminants a) 1 mM b) 5 mM and c) 10 mM. The length of the bar on image Pb c) is 400 μm.

2.4 - LIBS measurements

A third method used for the detection of the metal content of some samples is represented by LIBS (Laser induced Breakdown Spectroscopy) , a recently developed technique wich enables to identify the spectral lines of the various elements, not only metals, present in a sample.
The fs-laser system (Hurricane, Spectra Physics), emitted pulses of around 160 fs in width with an energy (at the sample) of about 100 μJ. The wavelength was 795 nm and the pulse repetition rate of 10 Hz. The radiation was focused onto the surface of leaf samples by a lens of 10 cm focal length and craters of diameters of about 100μm were obtained.
Lateral observations of emission were performed using an Échelle-spectrometer (type: ESA 3000, LLA, Germany) equipped with an intensified charge coupled device (ICCD). The plasma was imaged by a quartz lens (f = 5 cm) on the end of a quartz fiber, which was connected with the Échelle-spectrometer.
In this work we demonstrate spectro-chemical analysis of the leaf samples- doped by Cd - using femtosecond laser. However, in the case of plant leaves it is very difficult to obtain standard material for laser-ablation based techniques (e.g. LIBS or LA-ICP-MS) and at the same time to allow the determination of spatial (and lateral) distribution of elements within individual plant cells or different cell layers.
Fig.6 shows the spectra for Cd treated samples, in which the Cd spectral line has different height if the laser was focussed on a leaf vein or out of it, thus showing the difference in Cd bioaccumulation, but we cannot give a quantitative result for this difference.

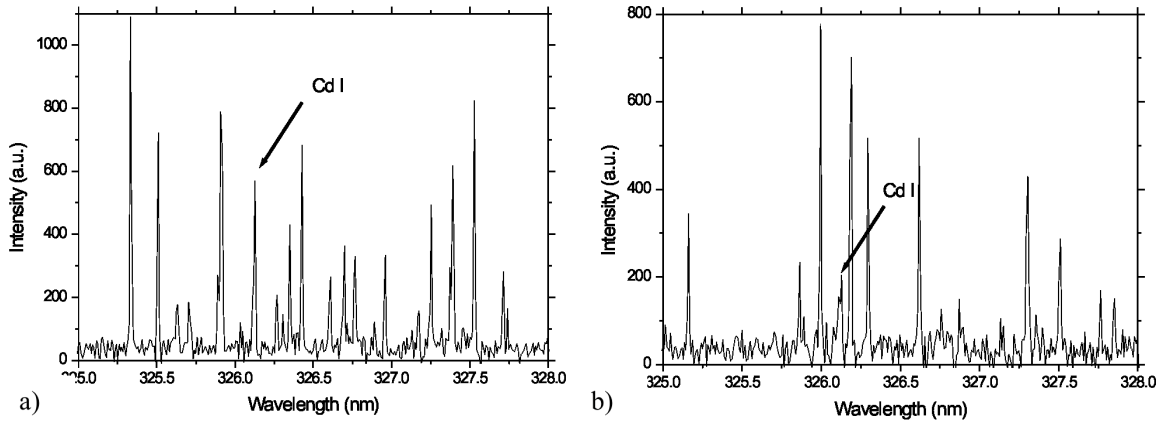

Fig.6: LIBS spectra of 5 days 10 mM CdAc treated *Helianthus annus* leaf sample. The fs-laser was focussed on a leaf vein ed a) on the vein of the leaf and b) about 1mm outside of the vein.

3-CONCLUSIONS

We reported here on three different methods used for mapping accumulation of metals in vegetal tissues; the related advantages of using soft (~ 1 keV) X-ray radiation from laser produced plasma or synchrotron radiation dual-energy micro-radiography have been checked.

If in the next future dedicated time and the planned space along the line will be available at the X ray beamlines ,the measurements will be accomplished with an X-.ray chamber including a spherically bent crystal to focus the X-ray beam to about10- 20 micron spot size .

In this way the experiment will achieve some innovative aspects in comparison to traditional microanalysis**:**

a) possibility of localizing the accumulation sites in biological samples of the trace pollutants with a 10-20 micron resolution-large field size(mm^2) imaging projection microscope as described in the original proposal of the MIDIX experiment

b)possibility of increasing the sensitivity of this measurement down to few ppm, by associating to X-ray imaging the fluorescence detection of the sample using a Si or Li detector located at a large angle with respect to the beam direction;

c) possibility of using the apparatus as a microscope also with plasma sources, as already verified in our previous experiments

The experiments with our LIBS technique are still preliminary and demonstrate that it is possible to perform qualitative analysis of Cd and Pb content and site identification in the leaves**:** Cd and Pb in the *Helianthus annus* are mainly accumulated in veins where they are transported by xylem.

Acknowledgements

The work synthetized in this 2006 Annual Report of LNGS was supported by the Italian National Institute of Nuclear Physics , by the Consorzio di Ricerca Gran Sasso and by the Ministry of Education of Czech Republic (grant MSM0021630508)

References:

1) L.Reale, A.Lai, A,Tucci, A.Poma, A.Faenov, T.Pikuz, F.Flora, L.Spano, T.Limongi, L.Palladino, A.Ritucci, G.Tomassetti,G.Petrocelli, M.Francucci, S.Martellucci - *Differencies in X-ray absorption due to cadmium treatment in Saponaria officinalis leaves* Micr.Res.and Tech. 64, 21-29, 2004

1) J.Kaiser, L.Reale, A.Ritucci, A.Reale, G.Tomassetti, A.Poma, L.Spanò, A.Tucci, A.Faenov, T.Pikuz, *Utilization of the 8.3 – 35 keV synchrotron radiation of the Elettra SYRMEP beamline for mapping the material intake in plants* Je. Mech.Opt.49,235-237, (2004)

1) G. Tomassetti, A. Ritucci, A. Reale, L. Arrizza, F. Flora, R.M. Montereali, A. Faenov, T. Pikuz *Two-Beam Interferometric Encoding of Photoluminescent Gratings in LiF Crystals by High-Brightness Tabletop Soft X-Ray Laser* Applied Physics Letters 85(18) (2004) 4163-4165

3) J. Kaiser, L. Reale, A. Ritucci, G. Tomassetti, A. Poma, L. Spanò, A. Tucci, F. Flora, A. Lai, A. Faenov, T. Pikuz, L. Mancini, G. Tromba, F. Zanini, *Mapping of the metal intake in plants by large field X-ray microradiography and preliminary feasibility studies in microtomography - Eur. Phys. J. D 32, 113 (2005)*

3) G.Baldacchini, S.Bollanti, F.Bonfigli, F.Flora, P.Di Lazzaro, A.Lai, T.Marolo, R.M.Montereali, D.Murra, A.Faenov, T.Pikuz, N.Lisi, G.Tomassetti, A.Reale, L.Reale, A.Ritucci, T.Limongi, L.Palladino, M.Francucci, S.Martellucci, and G.Petrocelli
Soft X-ray submicron imaging detector based on point defects in LiF
Rev.Sci Instr.,76,113104-12 (2005)
4) L.Reale, A. Lai, I. Bellucci, A. Faenov, T. Pikuz, F.Flora, L. Spanò, A. Poma, T. Limongi, L.Palladino, A. Ritucci, G. Tomassetti, G. Petrocelli, S. Martellucci *"Micro-radiography as a tool to detect heavy metal uptake in plants for phytoremediation applications"*
(submitted to Microscopy Research and Technique)
5) L. Reale, A. Lai, A. Faenov, T. Pikuz, F. Flora, T. Limongi, L. Palladino, A. Poma, G. Tomassetti, A. Balerna, G. Cinque. **"***Qualitative detection of Mg content into chlorophyll in a leaf of Hedera helix by using x ray radiation from a laser plasma source"*
(submitted to Microscopy Research and Technique)
6) J.Kaiser, O.Samek, L.Reale, M.Liska, A.Ritucci, G.Tomassetti, A.Reale, A.Poma, A.Tucci, F.Flora, A.Lai, L.Mancini, G.Tromba – *Monitoring of the heavy-metal hyperaccumulation in vegetal tissues by Laser Induced Breakdown Spectroscopy*
Microscopy Research and technique,70:147-153 (2007)

National and International Congresses:

1) F.Flora et al., "*Contact X-ray Microscopy and Microradiography on Lithium Fluoride Detectors*", 8th Int. Conf. on X-ray Microscopy (XRM2005), 26-30/7/2005, Himeji, Japan
2) L.Reale et al."*Detection of heavy metals in various biological samples*"
8th Int. Conf. on X-ray Microscopy (XRM2005), 26-30/7/2005, Himeji, Japan
3) R. M. Montereali, S. Almaviva, S. Bollanti, F. Bonfigli, A. Conti, P. Di Lazzaro, F. Flora, I. Franzini, A. Lai, L. Mezi, D. Murra, A. Pace, A. Santoni, M.A. Vincenti e G. Baldacchini,E. Nichelatti, L. Reale A. Ya. Faenov, T. A. Pikuz
Un rivelatore a lettura ottica basato su film di LiF per l'imaging di radiazione EUV e raggi X molli - 9° Conv. Nazionale Strumentazione e metodi di misura elettroottici
6-Giugno 2006 CR-ENEA Frascati
4) C.Bellecci, M.Francucci, P.Gaudio, S.Martellucci, M.Richetta, A.Faenov, T.Pikuz, S.Bollanti, P.Di Lazzaro, F.Flora, L.Mezi, D.Murra, A.Lai, A.Amodio, T.Limongi, L.Palladino, A.Reale, L.Reale, G.Tomassetti, I.Vullkaj
Radiazione X-soft da sorgente laser plasma:tecniche di microradiografia su film RAR
Convegno SIOF 2006- Firenze
5) C.Bellecci, M.Francucci, P.Gaudio, S.Martellucci, M.Richetta, A.Faenov, T.Pikuz, S.Almaviva, G.Baldacchini, S.Bollanti, F.Bonfigli, P.Di Lazzaro, F.Flora, A.Lai, L.Mezi, R.M.Montereali, D.Murra, A.Pace, A.Amodio, T.Limongi, L.Palladino, A.Reale, L.Reale, G.Tomassetti, M.A.Vincenti, I.Vullkaj
Sorgente laser plasma:microstrutture e microradiografie su cristalli di LiF con raggi X molli - Convegno SIOF 2006- Firenze

WARMX

Giuseppe Tomassetti[a], Armando Reale[a], Antonio Ritucci[a], Paola Zuppella[a], Lorenzo Arrizza[a], Lucia Reale[a], Francesco Flora[b], Luca Mezi[b], Anatoly Ya Faenov[c], Tatiana.Pikuz[c], Josef Kaiser[d]

[a] Dipartimento di Fisica dell'Università dell'Aquila, gc ai LNGS-INFN, Via Vetoio, Coppito (AQ) Italy
[b]ENEA Dip Innov, Fisica Applicata, CRE- Frascati, Frascati, Italy
[c] MISDC of VNIIFTRI, Mendeleevo, Moskow Region, Russia
[d] Institut of Physical Engineering, Faculty of Mechanical Engineering, Brno University of Technology, Czech Republic

Abstract

Recent results regarding the development of a 46.9nm capillary discharge laser are reported: we present the characterization of the laser beam in a given regime of operation and some applications to the processing of a dielectric material. We have also produced photoluminescent patterns of color centers on the surface of Li F crystals , which can be of interest for the production of miniaturized optical devices and soft X ray photolithography.

1-Introduction

In the last years the development of lasers operating at short wavelength, down to the x-ray region (<1nm), has registered a growing interest and significant progresses.
The main objective of this research is to obtain highly coherent x-ray sources of high brilliance and very short duration, by means of compact and low-cost devices, in order to get useful research tools for universities and industrial institutions. Recent experiments at a prototype level demonstrated the advantages of this type of lasers for plasma diagnostics, detectors and X-ray transport devices characterization, materials treatment, and so on.
Many studies have been devoted recently to the improvement of the performances of various soft X-ray laser types: some of them have been obtained by plasma production through the irradiation of metal targets by high power optical or infrared pump lasers , some others by capillary discharge.
The first have the advantage of a higher gain with respect to the second ones: but the direct excitation of plasmas by means of a capillary discharge has the advantage of generating still efficient x-ray lasers, much more cheap and compact. All these lasers mainly utilize electronic transitions between highly excited states of Ne-like or Ni-like ions.
The first clear evidence of laser effect by the capillary discharge technique has been obtained by J.J.Rocca at the Colorado University in 1994, one year before our group began the same research, with the funding of INFN.

2- Experimental procedure

2.1-The capillary laser of l'Aquila Univ. – LNGS group

Our direct discharge capillary laser , has a low divergence **(Fig 1),** a high spatial coherence degree, **(Fig.2).**It is the only one operating in Europe and deserved an invited paper at the 2004 International Conference on X-ray Lasers.

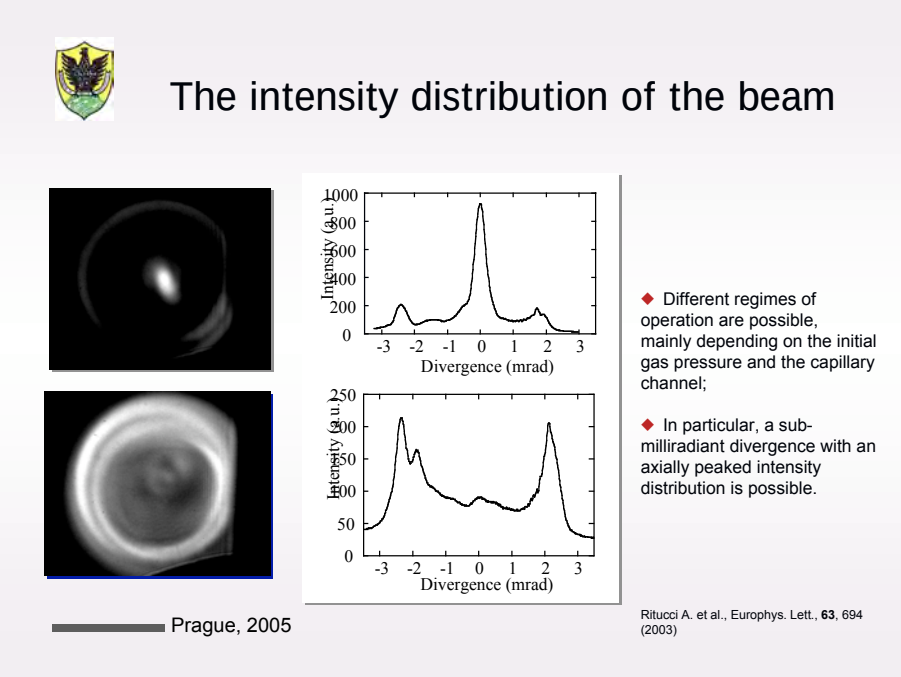

Fig.1

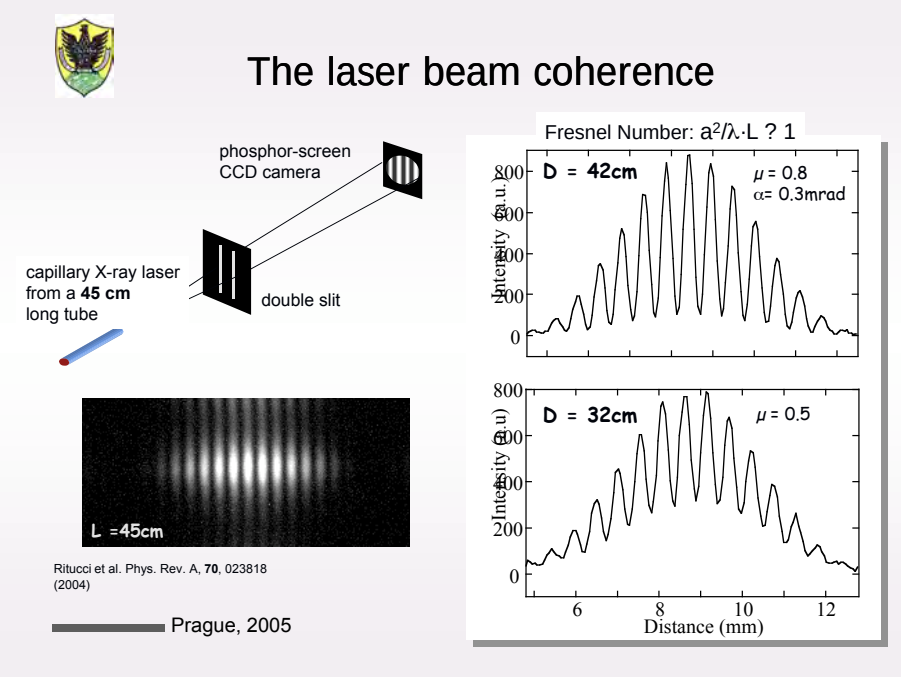

Fig.2

Presently the laser can produce continously many thousand shots at 0.2 hz frequency. Pulses are produced in a highly saturated laser with a capillary length up to 45 cm. The linear increase of exit energy with the capillary length has allowed to extract an average power of 60

microwatt, with energy stability corresponding to a fluctuation less than 5% from shot to shot.It works in a 3p-3s transition of 8 times ionised argon. The active plasma column – density $2.5 \cdot 10^{8}$ cm^{-3}, 70 eV temperature and radial diameter about 300μm- is formed in a fast radial compression (Z-pinch) of the capillary plasma of pure preionized argon, in a 3mm ceramic tube. The gas flows into the capillary maintained at a constant pressure of about 0.5 Torr. A fast exciting current , with a cycle of about 150 ns semiperiod and 20 KA amplitude, produces a plasma and at the same time generates its radial compression. The current comes from a 10nF capacitor, charged at 200 KV and discharged through the capillary tube by a spark-gap in deionised water . The x-ray emitted energy by the capillary is measured by a calibrated photodiode. The single x-ray pulse has 1.2 ns duration, up to 100μJ energy/shot, and 0.5-5 mrad divergence.

3- Applications of the laser

Presently the laser developed by our group is employed in the framework of some collaborations with other research groups, among which the Frascati CR ENEA , for the prototype demonstration of various applications. We quote here some studies which we have taken into consideration.

3.1Set-up of an interferential lithography system with high resolution

Interferential lithography with optical and UV lasers is a technique typically used for writing gratings and periodical patterns on a wide field by means of simple and compact experimental devices.

The use af a soft x-ray laser should have the remarkable advantage to allow a significant reduction of the path of the gratings: in our instance up to 25 nm (half of the length of the radiation utilized).

Applications range from pattern writing for magnetic memories to distributed feedback structures in photonic crystals.Preliminary experiments performed by us on PMMA type photoresists or on LiF crystals allowed so far grating writing up to 100nm path.

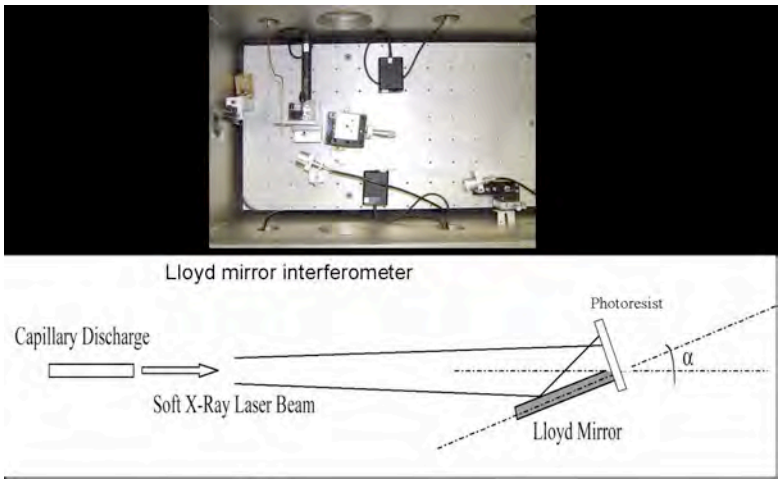

Figura 3- Lloyd mirror as interferometer used in our experiment.

3.2Point defects excitation in crystals

Color centers excitation in alcali halogen crystals may have various applications in photonics, in optic memories production or in X-ray detection. Using this laser our group obtained stable color center F_2 and F_3^+ type excitation in lithium fluoride crystals with various spatial distribution. (**Fig 4**)This excitation, allowed for an X-ray laser, is not allowed for conventional lasers due to the high ionisation potential (10-14eV) of such crystals. Taking advantage of the high spatial coherence of the laser, we impressed on a LiF crystal photoluminescent gratings with up to 200 nm path. These results suggest the possibility of developing a system of holographic writing by means of the X-ray laser for optical memories.

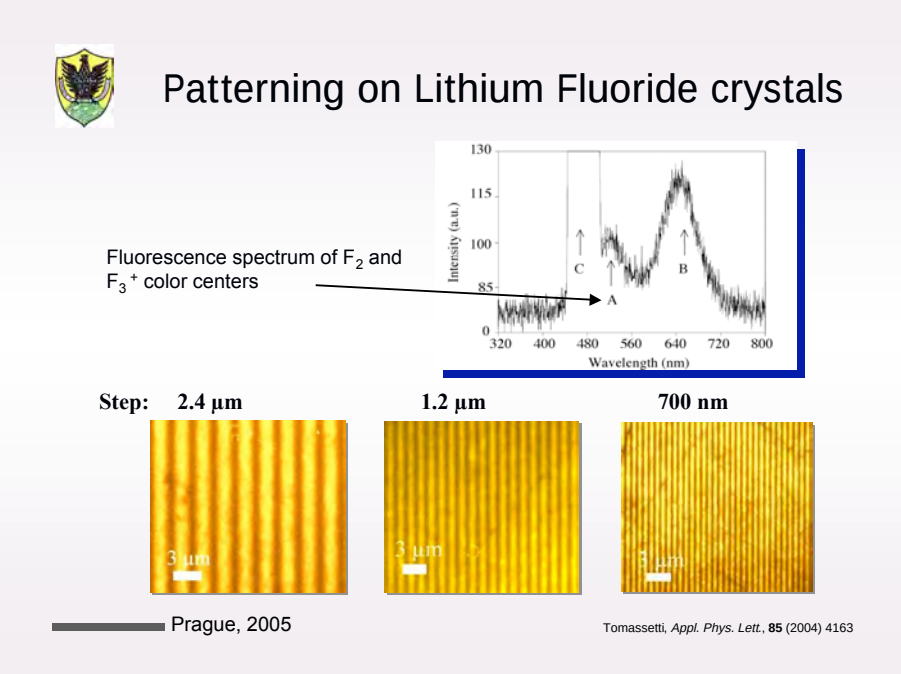

Fig.4

3.3 laser ablation

Laser ablation has many technological applications in material microprocessing, in thin film deposition and in researches on material surfaces. For this reason it is a widely investigated phenomenon in various experimental conditions, particularly by changing the laser parameters. Our group has recently begun some first experimental studies on the ablation induced by soft X-rays laser. We examined first some optical transparent materials (LiF and CaF_2) which present a high soft X-rays absorption. In this study we got the first experimental data on the ablation edges in these materials. (**Fig.4**).

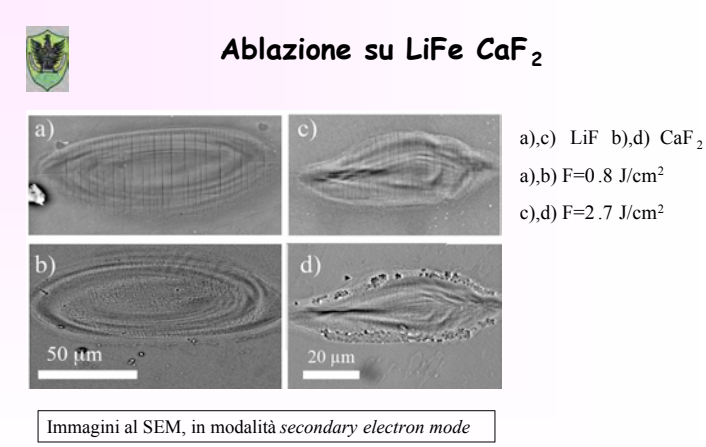

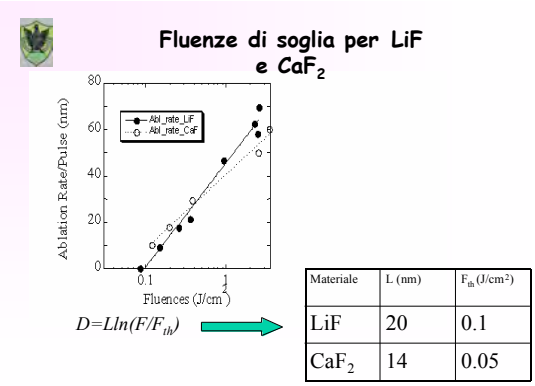

Fig.4

Recently, we have tried the ablation of SiO2, in these images we reports the results:

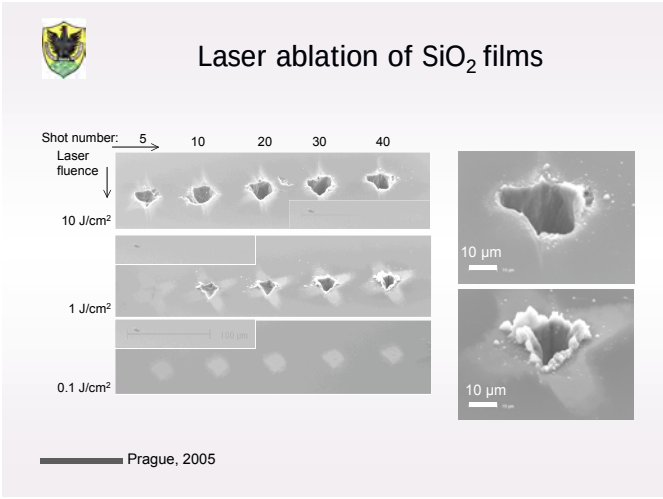

Fig.5

Other works in which the group is involved regard the determination or damage edges of thin films, aimed to the development of ultraintense free electron laser optics (FELS) which will become operative in near future specifically in the region of soft X-rays.

REFERENCES

1)A.Ritucci, G. Tomassetti, A. Reale, L. Arrizza, P. Zuppella, L. Reale, L. Palladino F. Flora, F. Bonfigli, A. Faenov and T. Pikuz, J. Kaiser, J. Nilsen and A. F. Jankowski
Damage and ablation of large bandgap dielectrics induced by a 46.9 nm laser beam
Optics Lett. , Vol. 31,p.68-70, January 1, 2006

2) A.Ritucci, G.Tomassetti, A.Reale, L.Reale, F.Flora, L.Mezi - **Measurement of energy fluctuations of a saturated 46.9 nm Ar laser produced in Z-pinch capillary discharges**
Applied Physics Letters 86,101-106 mar.2005

3) G.Baldacchini, S.Bollanti, F.Bonfigli, F.Flora, P.Di Lazzaro, A.Lai, T.Marolo, R.M.Montereali, D.Murra, A.Faenov, T.Pikuz, N.Lisi, G.Tomassetti, A.Reale, L.Reale, A.Ritucci, T.Limongi, L.Palladino, M.Francucci, S.Martellucci, and G.Petrocelli
Soft X-ray submicron imaging detector based on point defects in LiF
Rev.Sci Instr.,76,113104-12 (2005)